TU Delft

Delft University of Technology

Effect of micro-cracking and self-healing on long-term creep and strength development of concrete

Lyu, Wenjuan

DOI
10.4233/uuid:8389892d-f54c-4a35-ab18-7809f011c1f6

Publication date
2020

Document Version
Final published version

Citation (APA)
Lyu, W. (2020). *Effect of micro-cracking and self-healing on long-term creep and strength development of concrete*. [Dissertation (TU Delft), Delft University of Technology]. https://doi.org/10.4233/uuid:8389892d-f54c-4a35-ab18-7809f011c1f6

Important note
To cite this publication, please use the final published version (if applicable).
Please check the document version above.

Copyright
Other than for strictly personal use, it is not permitted to download, forward or distribute the text or part of it, without the consent of the author(s) and/or copyright holder(s), unless the work is under an open content license such as Creative Commons.

Takedown policy
Please contact us and provide details if you believe this document breaches copyrights.
We will remove access to the work immediately and investigate your claim.

This work is downloaded from Delft University of Technology.
For technical reasons the number of authors shown on this cover page is limited to a maximum of 10.

EFFECT OF MICRO-CRACKING AND SELF-HEALING ON LONG-TERM CREEP AND STRENGTH DEVELOPMENT OF CONCRETE

EFFECT OF MICRO-CRACKING AND SELF-HEALING ON LONG-TERM CREEP AND STRENGTH DEVELOPMENT OF CONCRETE

Proefschrift

ter verkrijging van de graad van doctor
aan de Technische Universiteit Delft,
op gezag van de Rector Magnificus prof. dr. ir. T.H.J.J. van der Hagen,
voorzitter van het College voor Promoties,
in het openbaar te verdedigen op 7 september 2020 om 12:30 uur

door

Wenjuan LYU

Master of Engineering in Bridge and Tunnel Engineering,
Beijing Jiaotong University, P.R.China,
geboren te Shandong, P.R.China.

Dit proefschrift is goedgekeurd door de

Promotor: Prof. dr. ir. K. van Breugel

Samenstelling promotiecommissie:

Rector Magnificus,	voorzitter
Prof. dr. ir. K. van Breugel,	Technische Universiteit Delft
Onafhankelijke leden:	
Prof. dr. ir. H. E. J. G. Schlangen,	Technische Universiteit Delft
Prof. dr. ir. E. A. B. Koenders,	Technische Universität Darmstadt, Duitsland
Prof. dr. F. Benboudjema,	École normale supérieure Paris-Saclay, Frankrijk
Prof. dr. T. Jefferson,	Cardiff University, Verenigd Koninkrijk
Dr. G. Ye,	Technische Universiteit Delft
Dr. ir. T. van Beek,	SKG-IKOB Certificatie BV, Nederland
Prof. dr. ir. L. J. Sluys,	Technische Universiteit Delft, reservelid

Keywords: Long-term creep, micro-cracking, self-healing, strength increase, lattice model

Printed by: Ipskamp Printing

Cover design: Wenjuan Lyu

Copyright © 2020 by Wenjuan Lyu

ISBN 978-94-6366-283-3

An electronic version of this dissertation is available at
http://repository.tudelft.nl/.

To my beloved parents

谨以此献给我最亲爱的父母

CONTENTS

List of Figures xi

List of Tables xix

List of Symbols xxiii

List of Abbreviations xxix

Summary xxxi

Samenvatting xxxiii

1 Introduction 1
- 1.1 Research background . . . 2
- 1.2 Objectives and methodology . . . 3
- 1.3 Scope of this research . . . 4
- 1.4 Research outline . . . 4

2 Behaviour of concrete under sustained load: literature review 7
- 2.1 Introduction . . . 8
- 2.2 Creep of concrete . . . 8
  - 2.2.1 Definition of creep . . . 8
  - 2.2.2 Creep mechanisms . . . 9
  - 2.2.3 Prediction of long-term creep . . . 15
- 2.3 Strength and elasticity of concrete under sustained load . . . 17
- 2.4 Self-healing potential of concrete material . . . 20
- 2.5 Conclusions . . . 25

3 Behaviour of concrete under sustained load: effect of micro-cracking and self-healing 27
- 3.1 Introduction . . . 28
- 3.2 Brook's test on 30-year creep of concrete . . . 28
- 3.3 Strengthening by self-healing concept: basic idea . . . 29
  - 3.3.1 Basic idea . . . 30
  - 3.3.2 Main content of the following sections . . . 30
- 3.4 Self-healing and extra increase in strength of concrete under sustained load . . . 32
  - 3.4.1 Experimental observation of the self-healing phenomenon . . . 32
  - 3.4.2 Numerical simulation of the self-healing phenomenon . . . 34

3.5 Hydration and strength increase triggered by cracks . . . 35
3.5.1 Continuous/normal hydration and strength increase . . . 35
3.5.2 Additional hydration triggered by micro-cracks and extra strength increase . . . 36
3.6 Creep hypothesis . . . 42
3.6.1 Activation energy concept . . . 42
3.6.2 Factors that influence the "real creep" . . . 43
3.7 Modified lattice model: description of the model . . . 44
3.7.1 Incorporation of creep in the lattice model . . . 46
3.7.2 Incorporation of continuous hydration in the lattice model: effect of continuous hydration on creep . . . 47
3.7.3 Incorporation of self-healing in the lattice model: effect of self-healing on creep . . . 47
3.7.4 Summary of the modified lattice model . . . 49
3.8 Preliminary evaluation of modified lattice model . . . 49
3.8.1 Concrete specimen used for evaluation of modified lattice model . . . 49
3.8.2 Values of model parameters . . . 55
3.8.3 Simulation results and discussions . . . 59
3.9 Conclusions . . . 72

4 Interaction between creep, micro-cracking and self-healing in concrete under sustained load: role of water-cement ratio 75
4.1 Introduction . . . 76
4.2 Long-term creep data from Brooks' test . . . 76
4.3 Numerical specimens with w/c=0.50-0.80 . . . 79
4.3.1 Numerical specimens . . . 79
4.3.2 14-day mechanical properties of lattice beams: $f_c(t_0)$ and $E(t_0)$ . . . 79
4.3.3 30-year mechanical properties of lattice beams after continuous hydration . . . 81
4.4 Values of model parameters . . . 83
4.4.1 Empirical ageing factor a for different water-cement ratios . . . 83
4.4.2 Evolution of strength $f_c[\alpha(t)]$ and elastic modulus $E[\alpha(t)]$ of mortar and bond beams resulting from continuous hydration . . . 85
4.4.3 Additional degree of hydration $\triangle\alpha_{add,j}$ of paste adjacent to any crack . . . 86
4.5 Simulation results and discussions . . . 87
4.5.1 Effect of continuous hydration on the long-term creep of concretes: w/c=0.50-0.80 . . . 87
4.5.2 Effect of micro-cracking on the long-term creep and compressive strength of concrete: w/c=0.50-0.80 . . . 90
4.5.3 Effect of self-healing on the long-term creep and compressive strength of concrete: w/c=0.50-0.80 . . . 97
4.6 Conclusions . . . 107

5 Behaviour of lightweight aggregate concrete under sustained load: effect of micro-cracking and self-healing **109**
5.1 Introduction . . . 110
5.2 Brooks' test on creep of concrete with lightweight aggregate . . . 110
5.2.1 General introduction . . . 110
5.2.2 Experimental data of LWAC . . . 111
5.3 Numerical specimens with lightweight aggregate with water-cement ratios of 0.55-0.86 . . . 113
5.3.1 Numerical specimens . . . 113
5.3.2 14-day mechanical properties of lattice beams: $f_c(t_0)$ & $E(t_0)$ . . . 114
5.3.3 30-year mechanical properties of lattice beams after continuous hydration . . . 115
5.4 Values of model parameters . . . 115
5.4.1 Empirical ageing factor a . . . 116
5.4.2 Evolution of strength $f_c[\alpha(t)]$ and elastic modulus $E[\alpha(t)]$ of mortar and bond beams resulting from continuous hydration . . . 117
5.4.3 Additional degree of hydration $\triangle\alpha_{add,j}$ of paste adjacent to any crack . . . 118
5.5 Creep of lightweight aggregate . . . 118
5.6 Simulation results and discussions . . . 120
5.6.1 Effect of continuous hydration on the long-term creep and compressive strength of LWACs: w/c=0.55-0.86 . . . 120
5.6.2 Effect of micro-cracking on the long-term creep and compressive strength of LWACs: w/c=0.55-0.86 . . . 120
5.6.3 Effect of self-healing on the long-term creep and compressive strength of LWACs with water-cement ratios of 0.55-0.86 . . . 126
5.6.4 Final remarks regarding the simulation results . . . 136
5.7 Conclusions . . . 141

6 Retrospection, conclusions and further research **143**
6.1 Retrospection . . . 144
6.2 Conclusions . . . 145
6.3 Contributions of this research . . . 147
6.4 Further research . . . 148

Appendix **151**

A The compaction theory **153**
A.1 General concept . . . 153
A.2 Effective reduction of capillary porosity due to compressive loading . . . 154
A.3 Evaluation of the compaction theory using the experimental data . . . 155

B Effect of continuous hydration and self-healing on creep deformation and failure time of concrete loaded at high stress levels **157**
B.1 Introduction . . . 157
B.2 simulation results . . . 157
B.2.1 Role of continuous hydration . . . 157

B.2.2 Role of self-healing 158

References **161**
References 161

Acknowledgements **177**

Curriculum Vitæ **181**

List of Figures

1.1 Examples of concrete structures: (a) the Pantheon; (b) Fallingwater; (c) Portuguese National Pavilion [1] 2
1.2 The Koror-Babeldaob bridge shortly before collapse [2] 3

2.1 Time-dependent strain in a concrete subjected to a sustained load [3] . . . 9
2.2 Three stages of creep process [4] 10
2.3 Pickett effect in centrically loaded concrete [5] 11
2.4 (a) Typical subsequent humidity distributions in a wall exposed to drying; (b) the corresponding shrinkages at various layers imagined as unrestrained; (c) stresses and cracking caused by the restoration of compatibility [6, 7] 12
2.5 Concrete loaded at different eccentricities [5] 12
2.6 Acoustic emission obtained during a basic creep test (note: first 20 minutes) [8] 13
2.7 Number of acoustic events versus basic creep for different loading levels: (a) 59% loading level; (b) 73% loading level; (c) 80% loading level [9] 14
2.8 Acoustic emission activity during creep tests of mortar (figure above) and concrete (figure below) beams [10] 15
2.9 Confined concrete before and after compaction [11] 19
2.10 Influence of loading duration and tensile stress level on the tensile strength of hardened cement paste. The age at loading is 3 days to 28 days. The increase in strength is described in percentage of the average ultimate tensile stress of the load-free samples (σ is the tensile strength of loaded sample; σ_0 is the tensile strength of load-free sample; τ_1 is age at loading and Vl is stress level) [12] 21
2.11 Artificial cracks in compression and tension and the position of strain gauges in the specimens [12] 21
2.12 Self-healing mechanisms in cementitious materials [13]: (a) Formation of calcium hydroxide or calcium carbonate; (b) Crack blocked by impurities in water or loose concrete particles coming from crack spalling; (c) Further hydration of the unhydrated cement; (d) Swelling of C-S-H due to water absorption. 22
2.13 Schematic diagram of the self-healing of a micro-crack [14] 24

3.1 Effect of continuous hydration, micro-cracking and self-healing on the evolution of compressive strength, strength-stress ratio and creep strain of concrete loaded at t_0 at a constant stress: schematic diagram 31

3.2 BSE image of a crack in Portland cement paste after curing in water for 200 hours [14] 32

3.3 Schematic diagram illustrating the densification of the zone adjacent to crack surface due to absorption of water by bulk cement paste [15] 33

3.4 Schematic diagram illustrating the self-healing mechanism for the extra strength increase in concrete under sustained load: (a) Uncracked porous cement paste; (b) Cracked cement paste (water does into the crack due to capillary suction); (c) Migration of water from the crack into the paste; (d) Dissolution of unhydrated cement grains (uhc), diffusion of the ions to the crack and the pore solution in the paste adjacent to the crack, precipitation of ions in the crack and the paste adjacent to the crack. 33

3.5 Cement paste samples with different crack widths (water-cement ratio=0.50; age=14 days; black=uhc, yellow=inner products, orange=outer products, blue=water; ω=crack width) 34

3.6 Simulated dissolution rate of the unhydrated cement in the samples with different crack widths (water-cement ratio=0.50)[Simulations performed by Jiayi Chen [16]] 35

3.7 Relationship between degree of hydration and strength for a mixture with an arbitrary w/c 36

3.8 Cracked paste specimen and densification of the paste adjacent to the cracks at the end of time step $\triangle t_i$ 37

3.9 Influence of micro-cracks on the overall degree of hydration (conceptual) 38

3.10 Damage degree in two identical paste specimen: small and large damage degree 39

3.11 Crack density in two identical paste specimen: low and high crack density 39

3.12 (a) The reaction products can fill up the crack and there are some left to densify the paste adjacent to the crack; (b) The reaction products can fill up a part of or whole volume of the crack and no reaction products are left to densify the paste adjacent to the crack 42

3.13 Effect of continuous hydration, micro-cracking and self-healing on the creep deformation of concrete loaded at a constant stress (real creep can be calculated with Eq. 3.15) 44

3.14 (left) Regular triangular lattice of beams, (middle) external forces and deformations on a single beam element, and (right) stress-strain relation for an element [17] 44

3.15 Schematics of the generation of meso-structure of concrete 45

3.16 Creep deformation and local axial force of an individual mortar or bond beam (Arrow on the right side means that creep can be tensile or compressive creep, depending on the sign of stress in the beam) 46

3.17 (a) Cement paste with a single crack (j^{th} crack); (b) Three types of beams in the matrix of a lattice network [Note: The lattice network in this figure represents a *paste* sample and it is assumed regular. Later, in the simulations the irregular lattice network will be generated to represent the concrete specimen consisting of mortar, bond and aggregate beams (see Fig. 3.20). The beams, which are connected to the broken beam, can include aggregate beams (see Fig. 3.36). The densification due to self-healing only applies to non-aggregate beams, which are connected to the broken beam.] 48
3.18 Flow chart: modelling procedure 51
3.19 Fuller's curve for aggregate particle size distribution 52
3.20 The meso-structure of the numerical concrete specimen with a water-cement ratio of 0.50 53
3.21 Series-parallel coupling model for the interaction of aggregate and mortar in concrete [18] 55
3.22 Simulated stress-strain curve of the concrete specimen (w/c=0.50; age=14 days) 55
3.23 Simulated stress-strain curve of the concrete specimen (w/c=0.50; age=30 years) 56
3.24 Influence of b and β on the degree of hydration of a mixture with water-cement ratio of 0.50 57
3.25 Calculated compressive strength of mortar beams versus time (Eq. 3.18) . 58
3.26 Compressive strength versus degree of hydration of concrete with a water-cement ratio of 0.50: with back-calculated α_0 and expected α_0 59
3.27 Calculated overall degree of hydration $\alpha(t)$ for the concrete specimen with a water-cement ratio of 0.50 ($b = 0.6$ and $\beta = 0.6$ in Eq. 3.1) 59
3.28 Simulated evolution of compressive strength and stress-strength ratio of the concrete specimen with a water-cement ratio of 0.50 loaded at 14 days at a stress level of 30% of compressive strength: with and without effect of continuous hydration 60
3.29 Simulated creep strains of concrete with a water-cement ratio of 0.50 loaded at 14 days at a stress level of 30% compressive strength: with and without the effect of continuous hydration 61
3.30 Simulated creep strains of concrete with a water-cement ratio of 0.50 loaded at 14 days at a stress level of 30% compressive strength: with and without the effect of micro-cracking 61
3.31 (a) Total number of cracks during the creep process; (b) Percentage of additional deformation caused by micro-cracking [extra deformation by percentage = (deformation with micro-cracking - deformation without micro-cracking) / deformation without micro-cracking]; (c) The extra deformation caused by micro-cracking versus total number of micro-cracks 62
3.32 Maximum crack width of the micro-cracks occurring during the creep process of the concrete specimen with a water-cement ratio of 0.50 63

3.33 Simulated evolution of compressive strength and stress-strength ratio of the concrete specimen with a water-cement ratio of 0.50 loaded at 14 days at a stress level of 30% of compressive strength: with and without the effect of micro-cracking 64
3.34 Simulated 30-year stress-strain curve with and without the effect of micro-cracking 64
3.35 (a) Three types of beams in the lattice network; (b) The areas representing the crack and the concrete adjacent to the crack in the lattice network [Note: The lattice network representing the concrete specimen is irregular (see Fig. 3.20); here for calculating the area of concrete adjacent to the crack it is simplified as regular network.] 65
3.36 The area of concrete adjacent to a bond crack in the lattice network, as shown inside the black frame, contains aggregate phase 65
3.37 Micro-cracks in concrete with a water-cement ratio of 0.50 loaded at a stress of 30% of compressive strength after 30 years (Blue: mortar beams; Red: bond beams) 66
3.38 Three different kinds of beams in the mesh (red beams: broken beams or cracks; dark blue beams: beams which are connected to *one* broken beam; orange beams: overlap beams) 68
3.39 Four cases analysed in the simulations of the effect of self-healing on the long-term creep of concrete with a water-cement ratio of 0.50 69
3.40 Simulated creep strains of the concrete specimen with a water-cement ratio of 0.50 loaded at 14 days at a stress level of 30% of compressive strength: with and without the effect of self-healing 71
3.41 Simulated and experimental compressive strength and stress-strength ratio of the concrete specimen with a water-cement ratio of 0.50 loaded at 14 days at a stress level of 30% of compressive strength: with and without the effect of self-healing 71
3.42 Simulated 30-year stress-strain curve of the loaded concrete specimen with a water-cement ratio of 0.50 72

4.1 Measured creep strains of wet-stored concrete in Brooks' test (constant stress creep test; age at loading is 14 days; loading level is 30% of 14-day compressive strength) [19] 77
4.2 Measured 14-day and 30-year compressive strength of load-free and loaded concretes with water-cement ratios of 0.50-0.80 ($f_c(14d)$ is compressive strength at age of loading (14 days); $f_c(30y_loaded)$ is compressive strength of loaded specimens after 30 years, while $f_c(30y_load\text{-}free)$ is compressive strength of load-free specimens.) [19] 78
4.3 Percentage increase in strength of wet-stored concrete specimens with different water-cement ratios ($f_c(14d)$ is compressive strength at age of loading (14 days); $f_c(30y_loaded)$ is compressive strength of loaded specimens after 30 years, while $f_c(30y_load\text{-}free)$ is compressive strength of load-free specimens.) [19] 78

4.4 Meso-structure of concrete specimens with water-cement ratios of 0.50-0.80 (dimension of specimens: $100 \times 100 mm^2$; percentages volume of aggregate are (a) 40%, (b) 39.7%, (c) 39.5%, (d) 39% and (e) 36%) 79
4.5 Comparison between experimental and simulated 14-day compressive strength and elastic modulus of concretes with water-cement ratios of 0.50-0.80 . . 81
4.6 Simulated stress-strain relationship of concretes with water-cement ratios of 0.50-0.80 (age=14 days) 81
4.7 Comparison between experimental and simulated 30-year compressive strength and elastic modulus of load-free concretes with water-cement ratios of 0.50-0.80 82
4.8 Simulated stress-strain relationships of load-free concretes with water-cement ratios of 0.50-0.80 (age=30 years) 83
4.9 Parameter a_0, n as a function of water-cement ratio (age at loading = 35 days; stress-strength ratio = 0.3; stress is constant) [20, 21] 84
4.10 Calculated compressive strength of mortar beams versus time for the concrete specimens with water-cement ratios of 0.50-0.80 (Eq. 3.18) 86
4.11 Calculated degree of hydration $\alpha(t)$ for the concrete specimens with water-cement ratios of 0.50-0.80 ($b = 0.6$ and $\beta = 0.6$ in Eq. 3.1) 86
4.12 Ultimate degree of hydration α_u and maximum additional overall degree of hydration $\triangle\alpha_{add,tot,max}$ for mixtures with water-cement ratios of 0.50-0.80 87
4.13 Calculated additional degree of hydration of the paste adjacent to any crack, $\triangle\alpha_{add,j}$, for mixtures with water-cement ratios of 0.50-0.80 88
4.14 Simulated compressive strength and stress-strength ratio of the concrete specimens with water-cement ratios of 0.50-0.80 loaded at 14 days at a stress level of 30% of compressive strength: with and without effect of continuous hydration 90
4.15 Simulated creep strains of concrete specimens with water-cement ratios of 0.50-0.80: with and without the effect of continuous hydration (age at loading=14 days; stress level=30% of 14-day compressive strength) 91
4.16 Simulated creep strains with and without the effect of continuous hydration for concrete with a water-cement ratio of 0.54 (age at loading=14 days; stress level=30% of 14-day compressive strength) 91
4.17 Simulated creep strains of concretes with water-cement ratios of 0.50-0.80: with and without the effect of micro-cracking (age at loading=14 days; stress level=30% of 14-day compressive strength) 92
4.18 Simulated creep strains with and without the effect of micro-cracking for concrete with a water-cement ratio of 0.54 (age at loading=14 days; stress level=30% of 14-day compressive strength) 92
4.19 (a) Number of cracks during the creep process; (b) Percentage of additional deformation caused by micro-cracking [extra deformation by percentage = (deformation with micro-cracking - deformation without micro-cracking) / deformation without micro-cracking]; (c) The extra deformation caused by micro-cracking versus total number of micro-cracks 93

4.20 Maximum crack width of the micro-cracks occurring during the creep process of the concrete specimens with water-cement ratios of 0.50-0.80 . . . 94
4.21 Simulated evolution of compressive strength and stress-strength ratio of the concrete specimens with water-cement ratios of 0.50-0.80 loaded at 14 days at a stress level of 30% of compressive strength: with and without the effect of micro-cracking . . . 96
4.22 (a) When $\omega \leq \omega_{cri}$, the crack is filled up with reaction product and some product is left to densify the paste adjacent to the crack; (b) when $\omega > \omega_{cri}$, the crack will *not* be filled up with reaction product and *all* the reaction product produced during the additional hydration is used to densify the paste adjacent to the crack . . . 99
4.23 Simulated creep strains of concrete specimens with water-cement ratios of 0.50-0.80: effect of self-healing (age at loading=14 days; stress level=30% of 14-day compressive strength) . . . 102
4.24 Simulated compressive strength and stress-strength ratio of the concrete specimen with water-cement ratios of 0.50-0.80 loaded at 14 days at a stress level of 30% of compressive strength: with and without the effect of self-healing . . . 104
4.25 Experimental and simulated percentage extra increase in strength after 30 years for concretes with water-cement ratios of 0.50-0.80 (percentage extra increase in strength after 30 years = [30-year compressive strength of loaded concrete - 30-year compressive strength of load-free concrete] / 30-year compressive strength of load-free concrete) . . . 105
4.26 Total number of the beams which are connected to the broken beams ($n_{ac,tot}$), the number of *effective* beams which are connected to the broken beams ($n_{ac,eff}$) and percentage overlap area of the paste adjacent to the cracks (r_{ol}) 106

5.1 Measured creep strains of wet-stored concretes with Lytag aggregates in Brooks' test (constant stress creep test; age at loading is 14 days; loading level is 30% of 14-day compressive strength) [19, 22] . . . 112
5.2 Measured 14-day and 30-year compressive strength of load-free and loaded LWACs with water-cement ratios of 0.55-0.86 (f_c*(14d)* is compressive strength at age of loading (14 days); f_c*(30y_loaded)* is compressive strength of loaded specimens after 30 years, while f_c*(30y_load-free)* is compressive strength of load-free specimens.) [19] . . . 112
5.3 Percentage increase in strength of wet-stored concrete specimens with different water-cement ratios (f_c*(14d)* is compressive strength at age of loading (14 days); f_c*(30y_loaded)* is compressive strength of loaded specimens after 30 years, while f_c*(30y_load-free)* is compressive strength of load-free specimens.) [19] . . . 113
5.4 Meso-structure of LWAC with water-cement ratios of 0.55-0.86 (dimension of specimens: $100 \times 100mm$; percentages volume of aggregate are (a) 40%, (b) 38%, (c) 35% and (d) 32%) . . . 113
5.5 Comparison between experimental and simulated 14-day compressive strength and elastic modulus of LWACs with water-cement ratios of 0.55-0.86 115

5.6 Comparison between experimental and simulated 30-year compressive strength and elastic modulus of load-free LWACs with water-cement ratios of 0.55-0.86 116
5.7 Calculated compressive strength of mortar beams versus time for the LWAC specimens with water-cement ratios of 0.55-0.86 (Eq. 3.18) 117
5.8 Calculated degree of hydration $\alpha(t)$ for LWACs with water-cement ratios of 0.55-0.86 ($b = 0.6$ and $\beta = 0.6$ in Eq. 3.1) 118
5.9 Creep of two sandstones: A, Springhill sandstone and applied stress = 55MPa; B, Wabana sandstone and applied stress = 101MPa [23] 119
5.10 Simulated compressive strength and stress-strength ratio of LWACs with water-cement ratios of 0.55-0.86 loaded at 14 days at a stress level of 30% of compressive strength: with and without effect of continuous hydration 122
5.11 Simulated creep strains of LWACs with water-cement ratios of 0.55-0.86: with and without the effect of continuous hydration (age at loading=14 days; stress level=30% of 14-day compressive strength) 122
5.12 Simulated creep strains with and without the effect of continuous hydration for LWAC with a water-cement ratio of 0.55 (age at loading=14 days; stress level=30% of 14-day compressive strength) 123
5.13 Simulated creep strains of LWACs with water-cement ratios of 0.55-0.86: with and without the effect of micro-cracking (age at loading=14 days; stress level=30% of 14-day compressive strength) 123
5.14 Simulated creep strains with and without the effect of micro-cracking for LWAC with a water-cement ratio of 0.55 (age at loading=14 days; stress level=30% of 14-day compressive strength) 124
5.15 (a) Total number of cracks during the creep process; (b) Percentage of additional deformation caused by micro-cracking [extra deformation by percentage = (deformation with micro-cracking - deformation without micro-cracking) / deformation without micro-cracking]; (c) The extra deformation caused by micro-cracking versus total number of micro-cracks 125
5.16 Simulated micro-cracks in LWAC and NWAC under a stress of 30% of compressive strength after 30 years (Blue: mortar cracks; Red: bond cracks; Magenta: aggregate cracks) 126
5.17 Simulated maximum crack width of the micro-cracks occurring during the creep process of LWACs with water-cement ratios of 0.55-0.86 126
5.18 Simulated compressive strength and stress-strength ratio of LWACs with water-cement ratios of 0.55-0.86 loaded at 14 days at a stress level of 30% of compressive strength: with and without the effect of micro-cracking . . 128
5.19 Three cases for the possibility of the self-healing (closure) of the aggregate cracks 130
5.20 Simulated creep strains of LWACs with water-cement ratios of 0.55-0.86: all the cracks in the aggregate phase are not self-healed (Case 1) 131
5.21 Simulated creep strains of LWACs with water-cement ratios of 0.55-0.86: the aggregate cracks which are close to the ITZ will be self-healed (Case 2) 133
5.22 Simulated creep strains of LWACs with water-cement ratios of 0.55-0.86: all the aggregate cracks are assumed to be self-healed (Case 3) 134

5.23 Simulated compressive strength and stress-strength ratio of LWACs with water-cement ratios of 0.55-0.86 loaded at 14 days at a stress level of 30% of compressive strength: with and without the effect of self-healing 136
5.24 Measured and simulated percentage extra increase in strength after 30 years for LWACs with water-cement ratios of 0.55-0.86 (percentage extra increase in strength after 30 years = [30-year compressive strength of loaded concrete - 30-year compressive strength of load-free concrete] / 30-year compressive strength of load-free concrete) 137
5.25 The rate of experimental and simulated creep strains of LWACs with water-cement ratios of 0.55-0.86 138
5.26 Simulated creep strains of LWACs with water-cement ratios of 0.55-0.86: with the effective empirical ageing factor a_{eff} 140
5.27 Measured and simulated percentage extra increase in strength after 30 years for loaded LWACs with water-cement ratios of 0.55-0.86: before and after correction 141
5.28 Simulated number of micro-cracks in LWACs during the creep process: before and after correction 142

A.1 The evolution of capillary porosity and compressive strength of loaded and load-free concrete over time: schematic diagram 154
A.2 Reduction of volume and capillary porosity of concrete under sustained compressive loading: schematic diagram 155

B.1 Simulated creep strains of the concrete specimen with a water-cement ratio of 0.50 loaded at 14 days at different stress levels: the role of continuous hydration 158
B.2 Number of cracks in the concrete specimen with a water-cement ratio of 0.50 loaded at 14 days at different stress levels 158
B.3 Simulated creep strains of the concrete specimen with a water-cement ratio of 0.50 loaded at 14 days at stress levels 75%-100%: with and without the effect of self-healing 159

LIST OF TABLES

2.1 Comparison between compressive strength of loaded and load-free concrete (age at loading: 7 days; loading duration: 3 days) [24] 17

3.1 Mix design and mechanical properties of specimens with a water-cement ratio of 0.50 [19, 25] 29
3.2 Sum of elastic and creep strain of specimens with a water-cement ratio of 0.50 [19] 29
3.3 Material characteristics of the concrete specimen (taken from Brooks' test [Section 3.2]) 52
3.4 14-day mechanical properties of the mortar, bond and aggregate beams (input for the creep simulations) 53
3.5 30-year mechanical properties of the mortar, bond and aggregate beams (used for the calculations of the parameters in Eq. 3.18 in Section 3.8.2) . . 56
3.6 The values of the parameters for calculating the strength and elastic modulus of the mortar and bond beams in Eq. 3.18 and 3.19 57
3.7 Four cases that will be studied in the simulations for the effect of self-healing on creep and strength (different variations of κ and $\triangle\alpha_{add',j}$) . . . 70

4.1 Mix design, compressive strength and elastic modulus of concrete specimens with water-cement ratios of 0.50-0.80 in Brooks' test [19, 25] 77
4.2 Estimated 14-day mechanical properties of the mortar, bond and aggregate beams for the concrete specimens with water-cement ratios of 0.50-0.80 in order to fit the experimental strength and elastic modulus (input for the creep simulations) 80
4.3 Simulated 14-day compressive strength and elastic modulus of concrete specimens with water-cement ratios of 0.50-0.80 80
4.4 30-year mechanical properties of the mortar, bond and aggregate beams for the load-free concrete specimens with water-cement ratios of 0.50-0.80 (used for the calculations of the parameters in Eq. 3.18) 82
4.5 Simulated 30-year compressive strength and elastic modulus of the load-free concrete specimens with water-cement ratios of 0.50-0.80 82
4.6 Values of the empirical ageing factor a (Eq. 3.17) for concretes with water-cement ratios of 0.50-0.80 loaded at 14 days 85
4.7 The values of the parameters for calculating the strength and elastic modulus of the mortar/bond beams in Eq. 3.18 and 3.19 for the concrete specimens with water-cement ratios of 0.50-0.80 85

4.8 The (reference) degree of hydration after 30 years, α_u, and the maximum total additional degree of hydration $\triangle\alpha_{add,tot,max}$ for mixtures with different water-cement ratios . . . 87
4.9 Values of the additional degree of hydration of the paste adjacent to any crack $\triangle\alpha_{add,j}$ for concretes with water-cement ratios of 0.50-0.80, calculated with Eq. 3.7 . . . 88
4.10 Comparison between simulated 30-year compressive strength with and without the effect of micro-cracking for concretes with water-cement ratios of 0.50-0.80 . . . 94
4.11 Parameters for calculating κ and $\triangle\alpha_{add',j}$ . . . 98
4.12 Values of κ and $\triangle\alpha_{add',j}$ for concretes with water-cement ratios of 0.50-0.80 99
4.13 Values of κ and $\triangle\alpha_{add',j}$ for concrete with a water-cement ratio of 0.80 . . 99
4.14 Experimental and simulated compressive strength of load-free and loaded concrete specimens with water-cement ratios of 0.50-0.80 after 30 years . 105

5.1 Mix design, compressive strength and elastic modulus of concretes with lightweight aggregate (Lytag) [19, 25] . . . 111
5.2 Estimated 14-day mechanical properties of the mortar, bond and aggregate beams of the lattice model for the LWACs with water-cement ratios of 0.55-0.86 in order to fit the experimental strength and elastic modulus (input for the creep simulations) . . . 114
5.3 Simulated 14-day compressive strength and elastic modulus of LWACs with water-cement ratios of 0.55-0.86 . . . 114
5.4 30-year mechanical properties of the mortar, bond and aggregate beams of the lattice model for load-free LWACs with water-cement ratios of 0.55-0.86 115
5.5 Simulated 30-year compressive strength and elastic modulus of load-free LWACs with water-cement ratios of 0.55-0.86 . . . 116
5.6 The values of empirical ageing factor a for LWACs with water-cement ratios of 0.55-0.86 (calculation procedure in Section 4.4.1) . . . 117
5.7 Parameter values for calculating the strength and elastic modulus of the mortar and bond beams in Eq. 3.18 and 3.19 for LWACs with water-cement ratios of 0.55-0.86 . . . 117
5.8 The (reference) degree of hydration after 30 years α_u and the maximum total additional degree of hydration $\triangle\alpha_{add,tot,max}$ for LWACs with water-cement ratios of 0.55-0.86 . . . 118
5.9 Values of the additional degree of hydration of the paste adjacent to any crack, $\triangle\alpha_{add,j}$, for LWACs with water-cement ratios of 0.55-0.86 . . . 119
5.10 Comparison between simulated 30-year compressive strength with and without the effect of micro-cracking for LWACs with water-cement ratios of 0.55-0.86 . . . 128
5.11 Some parameters for calculating κ and $\triangle\alpha_{add',j}$ . . . 129
5.12 Values of κ and $\triangle\alpha_{add',j}$ . . . 129
5.13 Values of κ and $\triangle\alpha_{add',j}$ for LWAC with a water-cement ratio of 0.86 . . . 129
5.14 Measured and simulated compressive strength of load-free and loaded LWACs with water-cement ratios of 0.55-0.86 after 30 years . . . 136

5.15 Effect of absorption of lightweight aggregates on the value of empirical ageing factor a 139
5.16 Measured and simulated compressive strength of load-free and loaded LWACs with water-cement ratios of 0.55-0.86 after 30 years: with the effective empirical ageing factor a_{eff} 141

A.1 Reduction of capillary porosity due to compressive loading (30-year compressive strength of load-free and loaded concrete is 50.6 and 61.2MPa respectively) 155

B.1 Failure time of the concrete specimen with a water-cement ratio of 0.50 loaded at 14 days at different stress levels: the role of continuous hydration 159
B.2 Failure time of the concrete specimen with a water-cement ratio of 0.50 loaded at 14 days at different stress levels 159

LIST OF SYMBOLS

Latin letters:

a	Empirical ageing factor	
a_0	Ageing factor which follows $a_0 = a\sigma$	
a_{eff}	Eeffective empirical ageing factor	
A	Area of cross section of a lattice beam	$[mm^2]$
b	Empirical constant	
C	A constant	
c_1	Material parameter which depend on w/c, cement type, etc.	
c_2	Material parameter which depend on w/c, cement type, etc.	
d	Related to the activation volume	
E	Elastic modulus	[GPa]
E_M	Elastic modulus of mortar	[GPa]
E_A	Elastic modulus of aggregate	[GPa]
E_0	Elastic modulus at time t_0	[GPa]
E_i	Elastic modulus at time t_i	[GPa]
E_{ac}	Elastic modulus of the beams which are connected to the broken beam after self-healing	[GPa]
$E_{ac,i+1}$	Elastic modulus of the beams which are connected to the broken beam at time t_{i+1} after self-healing	[GPa]
E_{hc}	Elastic modulus of the broken beam after self-healing	[GPa]
$E_{hc,i+1}$	Elastic modulus of the broken beam at time t_{i+1} after self-healing	[GPa]
E_{i+1}	Elastic modulus at time t_{i+1}	[GPa]
f_c	Compressive strength	[MPa]
$f_{c,0}$	Compressive strength at time t_0	[MPa]
$f_{c,i+1}$	Compressive strength at time t_{i+1}	[MPa]

$f_{c,max}$	Fictitious maximum strength in case of complete hydration	[MPa]
$f_{cr,i+1}$	Axial force at time t_{i+1} applied to the lattice beam	[N]
$f_{c,ac}$	Compressive strength of the beams which are connected to the broken beam after self-healing	[MPa]
$f_{c,ac,i+1}$	Compressive strength of the beams which are connected to the broken beam at time t_{i+1} after self-healing	[MPa]
$f_{c,hc}$	Compressive strength of the broken beam after self-healing	[MPa]
$f_{c,hc,i+1}$	Compressive strength of the broken beam at time t_{i+1} after self-healing	[MPa]
$f_{c,l}$	Compressive strength of loaded concrete	[MPa]
$f_{c,lf}$	Compressive strength of load-free concrete	[MPa]
$\triangle f_{c,hydr}$	Increase of strength due to the reduction of capillary porosity resulting from the hydration of cement	[MPa]
$\triangle f_{c,compr}$	Increase of strength due to the reduction of capillary porosity resulting from compressive loading	[MPa]
G	Shear modulus	[GPa]
l_1	Length of a lattice beam	[mm]
l_2	Length of the densified zone	[mm]
m	Proportionality factor	
m_{lwa}	Content of lightweight aggregates	$[kg/m^3]$
n	Proportionality factor	
n_i	Number of micro-cracks within $\triangle t_i$	
$n_{ac,tot}$	Total number of the beams which are connected to the broken beams	
$n_{ac,eff}$	Number of *effective* beams which are connected to the broken beams	
n_{ol}	Number of beams in the overlap area	
N	Number of micro-cracks during the creep process	
P	Stress-strength ratio	
p	Capillary porosity	
$\triangle p_{hydr}$	Reduction of capillary porosity due to hydration	
$\triangle p_{compr}$	Reduction of capillary porosity due to compressive loading	

$p_{l,tot}$	Total capillary porosity of loaded concrete	
$\triangle p_{l,tot}$	Total reduction of capillary porosity of loaded concrete	
$p_{lf,tot}$	Total capillary porosity of load-free concrete	
$\triangle p_{lf,tot}$	Total reduction of capillary porosity of load-free concrete	
Q	Activation energy	[J/mol]
q	Considered as a function of $f_c(t_0)$	
R	Gas constant	[8.31 $\mathrm{J \cdot mol^{-1} \cdot K^{-1}}$]
r_{ol}	Percentage overlap area of the paste adjacent to the cracks	[%]
r_p	volume fraction of the paste in concrete	
t	Time	
t_0	Age at loading	
t_{pre}	Predefined time	
$\triangle t_i$	i^{th} time step	
$\triangle t_{i+1}$	$i+1^{th}$ time step	
T	Temperature	[K]
$V_{ac,p,j}$	Volume of the paste adjacent to the jth crack	[mm^2 or mm^3]
$V_{ac,c,j}$	Volume of the concrete adjacent to the jth crack	[mm^2 or mm^3]
$V_{c,j}$	Volume of the jth crack	[mm^2 or mm^3]
V_p	Volume of the paste	[mm^2 or mm^3]
V	Volume of concrete	[mm^2 or mm^3]
V_0	Volume of concrete at age at loading t_0	[mm^2 or mm^3]
$\triangle V_{p,compr}$	Reduction of the volume of the capillary pores due to compressive loading	[mm^2 or mm^3]
$V_{RP,add,j}$	Volume of reaction products produced during the additional hydration of the paste adjacent to the jth crack for self-healing	[mm^2 or mm^3]
$V_{RP,add,j,min}$	Minimum value of $V_{RP,add,j}$	[mm^2 or mm^3]
$V_{hyc,add,j}$	Volume of hydrated cement during the additional hydration of the paste adjacent to the jth crack	[mm^2 or mm^3]
$V_{uhc,0}$	Volume of unhydrated cement at the initial stage	[mm^2 or mm^3]

$V_{uhc,i}$	Volume of unhydrated cement at time t_i	[mm^2 or mm^3]
V_A	Volume of aggregate	[mm^2 or mm^3]
V_M	Volume of mortar	[mm^2 or mm^3]
w/c	Water-cement ratio	
wcr	Water-cement ratio	
wcr_{eff}	Effective water-cement ratio	
wcr_{ref}	Reference water-cement ratio	
$w_{ab,1h}$	Water absorption of lightweight aggregates after 1 hour	
z	Coefficient related to the type of cement	

Greek letters:

α	Degree of hydration	
α_0	Critical degree of hydration below which the strength is zero	
α_l	Degree of hydration of loaded concrete	
α_{lf}	Degree of hydration of load-free concrete	
α_u	Ultimate degree of hydration	
$\alpha_{ref,i}$	Reference degree of hydration at time t_i	
$\alpha_{ref,max}$	Maximum value of $\alpha_{ref,i}$	
$\triangle\alpha_{add,j}$	Additional degree of hydration of the paste adjacent to the jth crack	
$\triangle\alpha_{add',j}$	Effective additional degree of hydration of the paste adjacent to the jth crack	
$\triangle\alpha_{add,i}$	Additional overall degree of hydration of the paste adjacent to n_i cracks	
$\triangle\alpha_{add,tot}$	Total additional overall degree of hydration of the paste adjacent to the cracks	
$\triangle\alpha_{add,tot,max}$	Maximum total additional overall degree of hydration of the paste adjacent to the cracks	
β	Empirical constant	
δ_p	Thickness of the densified paste zone	[mm]

δ_c	Thickness of the densified concrete zone	[mm]
ϵ_{i+1}	Total strain of a lattice beam at time t_{i+1}	[mm/mm]
ϵ_{cr}	Creep strain	[mm/mm]
$\dot{\epsilon}_{cr}$	Creep rate	
$\epsilon_{cr,0}$	Creep strain at time t_0	[mm/mm]
$\epsilon_{cr,i}$	Creep strain at time t_i	[mm/mm]
$\epsilon_{cr,i+1}$	Creep strain at time t_{i+1}	[mm/mm]
ϵ_{cri}	Critical strain	[mm/mm]
ζ	A constant	
κ	Recovery degree of the strength and elastic modulus of the broken beam after self-healing	
λ	Volumetric parameter	
ρ_c	Specific mass of cement	$[kg/m^3]$
ρ_w	Density of water	$[kg/m^3]$
σ	Stress	[MPa]
σ_i	Stress of a lattice beam at time t_i	[MPa]
σ_{i+1}	Stress of a lattice beam at time t_{i+1}	[MPa]
υ	Poisson's ratio	
χ	Volumetric parameter	
ω	Crack width	$[\mu m]$
ω_{max}	Maximum crack width	$[\mu m]$
ω_{cri}	Critical crack width	$[\mu m]$

List of Abbreviations

C-H Portlandite

C-S-H Calcium silicate hydrate

ITZ Interfacial transition zone

NWAC Normal-weight aggregate concrete

NMR Nuclear magnetic resonance

LWAC Lightweight aggregate concrete

SAPs Superabsorbent polymers

UCN Unhydrated cement nuclei

UPV Ultrasonic pulse velocity

w/c Water-cement ratio

μCT x-ray computed microtomography

SUMMARY

When concrete is subjected to sustained load, it first deforms elastically and then continues to deform with time. The stress-induced time-dependent deformation is, by definition, creep. Creep plays an important role in view of the serviceability, durability and sometimes even the safety of concrete structures. Prediction of the long-term creep is still a challenge. Apart from the time-dependent deformation, the microstructure, strength and elasticity of concrete are also continuously changing under sustained load. This will, in turn, have an influence on the creep deformation.

Micro-cracking has been detected experimentally by acoustic emission techniques during creep tests for concrete loaded at different stress levels. It could contribute to both an extra deformation and a reduction in the strength and elasticity. This is somehow contradictory to the experimental observation that there is an extra increase in strength (and elastic modulus) of concrete under sustained load, especially at low and medium stress levels, compared to load-free concrete. There must be another phenomenon during the creep process that "resolves" this contradiction. Despite a few theories which have been proposed in the paste to explain the extra increase in strength of concrete under sustained load, the mechanism behind this phenomenon has not been fully understood yet. Besides, how this extra increase in strength influences the long-term creep deformation has rarely been studied. In this research self-healing is considered as a promising mechanism to explain the extra increase in strength of concrete under sustained load. The main aim of this research is to study the effect of micro-cracking and self-healing on the long-term creep and strength development of concrete under sustained load and to gain a better understanding of the behaviour of concrete under sustained load.

Firstly, an in-house lattice model was modified to take long-term creep into consideration. The activation energy concept was employed to model creep. The self-healing mechanism for the extra increase of the strength of concrete under sustained load, which includes two aspects: self-healing of the cracks and densification of the paste adjacent to the cracks, was proposed and studied with a model for autogenous self-healing. This mechanism was, subsequently, incorporated in the modified lattice model. The effect of continuous hydration, micro-cracking and self-healing on the long-term creep deformation of concrete under sustained load (low stress level) was simulated. The strength after loading was also calculated and compared to the strength of load-free concrete. The simulated results (both deformation and strength) were compared to the experimental data from Brooks' 30-year creep test in order to evaluate the accuracy of the model. A good fit was found between the simulation results and the experimental data. When the self-healing was considered, the creep strain was smaller than that without the effect of self-healing. Besides, an extra increase in strength of concrete under sustained load was obtained.

Secondly, the interaction between creep, micro-cracking and self-healing of con-

cretes with water-cement ratios of 0.50-0.80 under sustained load was studied with the modified lattice model. It was found that the number of micro-cracks at the end of creep process of concrete with a high water-cement ratio is greater than that of concrete with a low water-cement ratio. The additional creep deformation caused by micro-cracking is thus larger for concrete with a high water-cement ratio than for concrete with a low water-cement ratio. The extra increase in strength of concrete with a high water-cement ratio was found to be less than that of concrete with a low water-cement ratio.

Finally, the effect of micro-cracking and self-healing on the long-term creep and strength of lightweight aggregate concrete under sustained load (low stress level) was studied with the modified lattice model. Different from normal-weight aggregate concrete, micro-cracks occurred in the lightweight aggregate phase. This influences the effect of self-healing on creep and strength, since aggregate cracks will not easily be healed. When self-healing only occurred in the paste (not in the aggregates), the creep strain was not becoming less than that without the effect of self-healing and, the extra increase in strength of the loaded concrete was not achieved. This might be because self-healing increases the degree of heterogeneity of lightweight aggregate concrete and exacerbated the stress concentration phenomenon.

SAMENVATTING

Wanneer beton wordt blootgesteld aan permanente belasting, vervormt het eerst elastisch en blijft vervolgens met de tijd vervormen. De tijdsafhankelijke vervorming is, per definitie, kruip. Kruip speelt een belangrijke rol met betrekking tot de bruikbaarheid, duurzaamheid en soms zelfs de veiligheid van betonconstructies. Het voorspellen van kruip op de lange termijn wordt tegenwoordig nog steeds als een uitdaging beschouwd. Afgezien van de tijdsafhankelijke vervorming, veranderen ook de microstructuur en de sterkte en elasticiteit van beton continu onder permanente belasting. En dit zal weer van invloed zijn op de kruip.

Microscheurvorming tijdens een kruiptest voor beton bij verschillende belastingniveaus is experimenteel aangetoond met behulp van akoestische emissietechnieken. Microscheuren kunnen bijdragen aan zowel een extra vervorming als een afname van de sterkte en elasticiteit. Dit lijkt in tegenspraak met de experimentele observatie dat er een extra toename is in sterkte (en elasticiteitsmodulus) van beton onder permanente belasting, vooral bij lage en gemiddelde spanningsniveaus, vergeleken met onbelast beton. Om dit te verklaren moet er sprake zijn van een ander fenomeen. Ofschoon er een aantal theorieën is voorgesteld om de extra toename in sterkte van beton onder permanente belasting te verklaren, is het mechanisme dat hieraan ten grondslag ligt nog niet volledig begrepen. Bovendien is onvoldoende onderzocht hoe deze extra toename in sterkte de langdurige kruipvervorming beïnvloedt. In dit onderzoek wordt het zelfherstellend vermogen beschouwd als een veelbelovend mechanisme om de extra toename in sterkte van beton onder langdurige belasting te verklaren. Het hoofddoel van dit onderzoek is het bestuderen van het effect van microscheurvorming en zelfherstellend vermogen op de lange-termijn kruip van beton onder langdurige belasting en een beter begrip krijgen van het gedrag van beton onder langdurige belasting.

Eerst is een bestaand roostermodel (lattice model) aangepast teneinde de lange-termijn kruip te kunnen modelleren. Hierbij is gebruik gemaakt van het activeringsenergieconcept. Het zelfherstellend mechanisme voor de extra toename van de sterkte van beton onder permanente belasting omvat twee aspecten: herstel van de scheuren en verdichting van de cementsteen direct naast de scheuren. Dit mechanisme is verder onderzocht aan de hand van een model voor autogeen zelfherstel en is vervolgens opgenomen in het gemodificeerde lattice model. Het effect van voortgaande hydratatie, microscheurvorming en zelfherstel op de lange-termijn kruipvervorming van beton onder permanente belasting (lage spanning) is gesimuleerd. De sterkte na de belasting is berekend en vergeleken met de gemeten sterkte van het onbelaste beton. De gesimuleerde resultaten, zowel vervorming als sterkte, zijn vergeleken met de experimentele gegevens van de 30-jaar durende kruiptest van Brooks om de betrouwbaarheid van het model te evalueren. Er werd een goede overeenkomst gevonden tussen de simulatieresultaten en de experimentele gegevens. Rekening houdend met het zelfherstellend vermogen blijkt de kruipvervorming kleiner dan die zonder het effect van het zelfherstellend vermogen.

Daarnaast werd ook een extra toename van de sterkte van beton onder langdurige belasting gevonden.

Vervolgens werd de rol van de water-cement-factor in de wisselwerking tussen kruip, microscheurvorming en zelfherstellend vermogen van beton (w/c=0.50-0.80) onder permanente belasting bestudeerd met het gemodificeerde roostermodel. Het aantal microscheuren aan het einde van het kruipproces in beton met een hogere water-cement-factor bleek groter te zijn dan dat in beton met een lagere water-cement-factor. De extra kruipdeformatie veroorzaakt door microscheuren zal naar verwachting dus groter zijn voor beton met een hogere water-cement-factor dan voor beton met een lagere water-cement factor. De extra toename in sterkte van beton met een hogere water-cement-factor bleek minder te zijn dan die van beton met een lagere water-cement-factor.

Tenslotte werd het gedrag van lichtbeton onder permanente belasting (lage spanning) bestudeerd met het gemodificeerde roostermodel. Anders dan normaalgewicht beton, traden microscheuren op in de lichte toeslagkorrels. Dit beïnvloedt het effect van zelfherstel op kruip en sterkte, omdat microscheuren in toeslagkorrels niet gemakkelijk herstellen. Wanneer zelfherstel alleen in de cementsteen optrad (en niet in de toeslagkorrels), werd de kruipvervorming niet minder dan die zonder het effect van zelfherstel en was er geen sprake van een extra toename in sterkte van het belaste beton. Een mogelijke verklaring hiervoor is dat zelfherstel de mate van heterogeniteit van lichtbeton verhoogt wat leidt tot grotere spanningconcentraties en meer microscheurvorming.

1

INTRODUCTION

Prediction is very difficult,
especially about the future.

Niels Bohr

This chapter presents the background of the research. Then the objectives, scope and methodology and outline of this research are explained.

1

1.1. RESEARCH BACKGROUND

CONCRETE is by far the most widely used building material in the world because of its relatively low price and good availability. It has been used to construct different kinds of structures, including many stunning ones, e.g. the Pantheon in Rome, Italy (Fig. 1.1a), Falling water in Pennsylvania, US (Fig. 1.1b) and Portuguese National Pavilion in Lisbon, Portugal (Fig. 1.1c), and many "down-to-earth" ones, e.g. long-span bridges, high-arch dams, offshore platforms and nuclear power plants (NPPs), etc. These con-

(a)

(b)

(c)

Figure 1.1: Examples of concrete structures: (a) the Pantheon; (b) Fallingwater; (c) Portuguese National Pavilion [1]

crete structures not only serve practical use, but also connote modernity, civilization, and culture. However, the complexity of this material itself plus the complicated ambient and loading conditions have created lots of difficulties in structural design and analysis. Currently, a common problem is that, as service time progresses, structures age, their performance deteriorates and reliability declines, which can have an adverse impact on their return on investment and sometimes even on the national economy as a whole.

Creep is one of the ageing problems, which affects deformation and also stress distribution in materials and structures. Creep can be desirable in reinforced concrete structures as it can promote a better stress distribution. It is undesirable in most cases, however, since it leads to excessive deformation/deflection and loss of prestresses. A critical consideration in design of concrete beams and bridges is the increase in deflection with time due to creep. In eccentrically loaded columns, creep increases the deflection and can lead to buckling. In mass concrete structures, such as dams, on account of differential temperature conditions at interior and surface, creep is harmful and by itself may be a cause of cracking in the interior of dams. Furthermore, in case of a severe accident (loss of cooling agent of the reactor for instance) with NPPs, pressure and temperature will increase in the nuclear vessels. Due to the rapid increase of temperature at the internal surface of the containment, high compressive stresses are generated and the evolution of basic creep will be accelerated, causing an extra loss of prestress. These high stresses, coupled with creep and the effect of elevated temperature, could induce cracking and further leakage of radioactive elements into environment [26].

Creep behaviour is of vital importance when it comes to serviceability and durability of concrete structures. Prediction of long-term creep has been widely investigated and formulated into several empirical models which serve as references for the structural de-

sign. However, making reliable predictions is still a challenge. Take the Koror-Babeldaob bridge in Palau as an example (Fig. 1.2), it collapsed in 1996 due to grossly excessive creep deflections which reached to 1.61m within only 18 years [2, 27, 28]. Apparently the long-term creep deformation was severely underestimated during the design phase. This has kept us thinking about the reasons for the underestimation of creep and what is really happening during the creep phase.

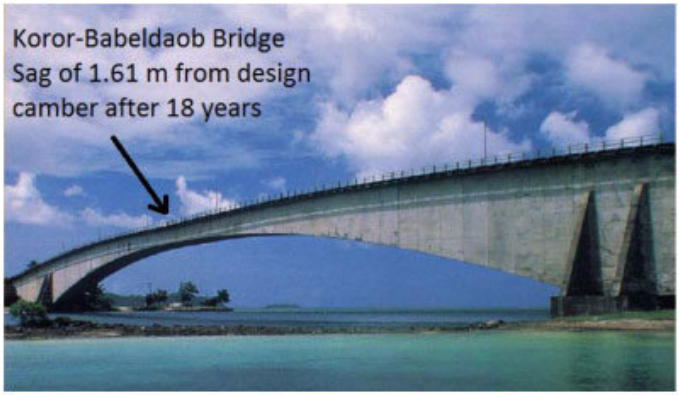

Figure 1.2: The Koror-Babeldaob bridge shortly before collapse [2]

Apart from the relatively complicated mechanisms of creep, it is possible to look at this from the perspective of the interaction between creep and micro-cracking. It has been proved experimentally with the use of acoustic emission techniques that micro-cracks do appear in creeping samples, due to the restraint at the structural or material level, even at stress levels below 40% of the strength [9, 29, 30]. These micro-cracks could contribute to not only the material discontinuity, but also an extra deformation. If the micro-cracks continue to grow, then eventually failure would be inevitable. However, most structures survive in reality. With load levels below 70% strength, no severe failures were observed, but only some bond and mortar cracks have been found in laboratory work [31, 32]. Besides, compressive strength and elastic modulus under sustained compressive loading may increase by a certain amount depending on experimental conditions (stress levels, ambient conditions, etc.) [24, 33, 34]. However, continuous micro-cracking leads to degradation of the mechanical properties of the materials, which seems not consistent with the above observations. Obviously there are some other mechanisms which influence the interaction between creep and micro-cracking and prevent the larger creep deformation, even the failure, to occur. Continuous hydration and self-healing are considered to be potential ones. Understanding and quantifying the effect of micro-cracking and self-healing during the creep process would be helpful for the prediction of long-term creep deformation and also give us a better indication of the mechanical properties of concrete under sustained load.

1.2. OBJECTIVES AND METHODOLOGY

THE main goal of this research is to gain a better understanding on the behaviour of concrete under sustained load and to study the interaction between creep, micro-

cracking and self-healing of concrete under sustained load. The study contains the following sub-objectives:

- To quantify the effect of micro-cracking and self-healing on the long-term (multi-decades) creep deformation of concrete at low stress levels;
- To study the effect of micro-cracking and self-healing on compressive strength of concrete under sustained load;
- To investigate the role of water-cement ratio in the interaction between creep, micro-cracking and self-healing of concrete under sustained load;
- To explore the effect of micro-cracking and self-healing on the long-term creep deformation and strength development of lightweight aggregate concrete under sustained load.

This research is mainly conducted numerically and theoretically. Based on the evidence from literature on results of acoustic emission test and on the enhanced mechanical properties of concrete under sustained load, a new insight is presented for the prediction of long-term creep. Based on it, a theoretical study is performed on the interaction between creep, micro-cracking and self-healing of concrete under long-term sustained load and on the effect of this interaction on the compressive strength. In order to do so, an existing lattice model [17, 35] is modified to take creep into account. Continuous hydration and self-healing mechanism are also inserted into the modified lattice model. The simulations are performed on a three-phase concrete specimen (mortar, bond and aggregate) under sustained compressive load. In order to prove the soundness of the simulations they have been compared with 30-year creep data from Brooks' experiments [19].

1.3. SCOPE OF THIS RESEARCH

CREEP in cementitious materials is a very complex issue. Almost all the internal (e.g. water cement ratios, aggregate distribution, admixtures, etc.) and external parameters (e.g. temperature, humidity, loading and boundary conditions, etc.) have an effect on creep. It is very difficult to predict the long-term creep of concrete taking all variables into consideration. In this study, only creep of concrete stored in water at room temperature (20°C) under sustained compressive loading (constant stress) is focused on. The numerical creep tests are conducted in 2D approach in order to reduce computation time.

1.4. RESEARCH OUTLINE

THE results of the research are given in 6 chapters in this thesis. In Chapter 1, the theoretical background and motivation for the research are given. Chapter 2 gives a critical review on the current study for creep of concrete (parameters needed to be considered in the prediction of creep of concrete). An overview on creep mechanisms and current methods for long-term predictions are firstly presented. Then the development

of strength of concrete under sustained load and the related theories are described. Subsequently, the mechanisms, experiments and simulations for self-healing phenomenon are introduced.

In Chapter 3, a self-healing mechanism for the extra increase in strength of concrete under sustained load is proposed. Creep, continuous hydration and self-healing are then implemented into the lattice model. A concrete sample with a water-cement ratio of 0.50 from Brooks' test [19] is simulated as a three-phase material under a stress of 30% of the 14-day compressive strength in a 2D approach. The soundness of the proposed mechanism is made plausible and the effects of micro-cracking and self-healing on the long-term creep deformation are quantified. The effects on the compressive strength of the concrete specimen under sustained load are also studied.

Water-cement ratio is the most fundamental parameter for the creep of concrete. It plays an important role not only in the creep itself, but also in the micro-cracking and self-healing. In Chapter 4, the interaction between creep, micro-cracking and self-healing of concretes with different water-cement ratios is investigated. The experimental data of concrete specimens with water-cement ratios of 0.50-0.80 from Brooks' test [19] are used to validate the simulations. The effect of micro-cracking and self-healing on the long-term creep of concrete specimens is quantified with the modified lattice model. The compressive strengths after 30 years of loading are calculated and compared to those of load-free concretes.

The property of aggregate (e.g. stiffness, porosity and absorption) has an impact on the creep deformation and stress distributions in concrete. Thus it also affects the micro-cracking and self-healing process. This is studied in Chapter 5. The effect of micro-cracking and self-healing on the long-term creep and strength of lightweight aggregate concrete is investigated using the modified lattice model. The simulated results are compared to the Brooks' experimental data [19, 22].

In Chapter 6, the work in this thesis is summarised. Some conclusions and recommendations are given for further research.

2

BEHAVIOUR OF CONCRETE UNDER SUSTAINED LOAD: LITERATURE REVIEW

The mind is furnished with ideas by experience alone.

John Locke

This chapter gives a thorough review of the behaviour of concrete under sustain load. First, a brief introduction of creep mechanisms is presented, followed by a review of the current state-of-the-art research on the prediction of long-term creep. The strength development of concrete under sustained load is then discussed. In the end the autogenous self-healing phenomenon in cementitious materials is elaborated.

2.1. INTRODUCTION

CONCRETE gradually deforms when subjected to sustained load, including self-weight. This is, by definition, the so-called creep. Creep plays an important role in view of the serviceability, durability and sometimes even the safety of concrete structures. Creep deformations are important in structures subjected to elevated temperatures, such as nuclear power plants (NPPs). It is also important in the design of infrastructures and buildings, such as long-span bridges. According to a database of creep of bridges created by Bažant and his team [36], most bridges exhibit creep deformations higher than expected. This will lead to an increase of maintenance cost and, in rare cases, even to the collapse of structures.

Creep is still a very complex issue. The origin of creep is not fully understood yet. The effect of several factors (e.g. temperature, humidity, hydration and micro-cracking) on creep further contributes to its complexity. This makes it difficult to make reliable creep predictions. On top of that, sustained load deforms concrete and, at the same time, it also continuously changes the microstructure of cement paste and its strength and elasticity. Experimental observations have revealed that concrete becomes stronger (due to compaction or self-healing [37]) at low/medium stress levels or weaker (due to crack propagation [38]) at high stress levels. This will, in return, have an impact on creep deformations. In this chapter, all these aspects with regard to the behaviour of concrete under sustained load are reviewed.

2.2. CREEP OF CONCRETE

SINCE the first publication on creep of reinforced concrete in 1907 [39], creep of concrete has been studied. Numerous experiments, calculations and simulations have been carried out and formulated in valuable reports and publications, including many classic review papers and books [7, 38, 40–43]. These publications give a comprehensive description and analysis of existing creep tests, theories, models and potential problems. The aim of this section is to give a brief survey of the main creep mechanisms proposed over the years. Special attention is paid to the prediction of creep of concrete.

2.2.1. DEFINITION OF CREEP

Creep is defined as a time-dependent deformation under sustained load. On application of a load, an instantaneous elastic strain occurs, followed by a time-dependent deformation. When the load is removed, the elastic strain is fully recovered and then a relatively small portion of the creep deformation is recovered (see Fig. 2.1).

The definition given above seems rather simple and leaves the origin of creep an open question [21]. A considerable number of creep theories has been proposed in an attempt to gain a better understanding of the creep phenomenon of concrete. Concrete is known as a material with continuous changes of its physical and mechanical properties (e.g. due to hydration). These changes might have an effect on the time-dependent deformations under consideration. Since the development of the properties of concrete is influenced by many factors, it is safe to say that these factors play a more or less important role in the current creep theories. Which factor is chiefly responsible for creep is still under discussion. Van Breugel [21] suggested that the discussion on this subject is

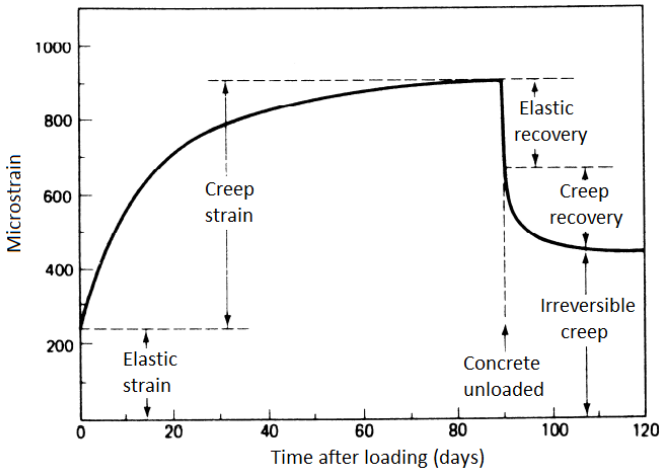

Figure 2.1: Time-dependent strain in a concrete subjected to a sustained load [3]

likely to be less confusing if the creep phenomenon could be traced back to one physical source which is valid for any arbitrary material, i.e. creep could be treated as a pure material property. Additional factors which lead to any changes in the properties or deformations should *not* be considered as the source of creep, but may influence or modify the creep process to a certain extent. Wittmann [43] categorized the physical source of creep as the "real mechanism" for creep and other mechanisms which modify the creep deformation as the "apparent mechanism".

The creep mechanisms are introduced in the next section. Prior to that, some terms regarding creep used in the literatures are specified as follows:

- Basic creep is defined as the creep that occurs under conditions that there is no drying shrinkage or moisture movement between concrete and ambient environment [3].
- Drying creep is, by definition, the additional creep that occurs when the specimen under load is also drying [3].
- Creep coefficient is defined as the ratio of creep strain to elastic coefficient [3].
- Specific creep is defined as creep strain per unit of applied stress [3].
- Three stages of creep process are primary, secondary, and tertiary creep (see Fig. 2.2). The three categories correspond to a decreasing strain rate (primary), approximately constant strain rate (steady state) and increasing strain rate (tertiary) [4].

2.2.2. CREEP MECHANISMS

REAL MECHANISMS

In general, the real creep mechanisms can be subdivided according to the role of water in cementitious materials [44, 45]:

- Delayed elastic theory: the diffusion of capillary water from high- to low-pressure areas;

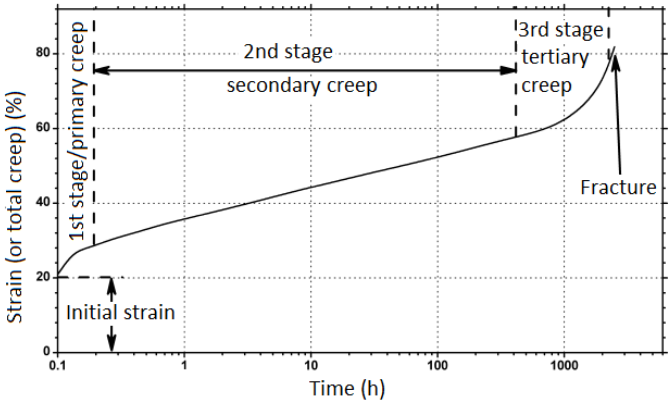

Figure 2.2: Three stages of creep process [4]

- Viscous flow: movements of colloidal particles in the cement gel between the layers of absorbed water;
- Seepage theory: the expulsion and decomposition of interlayer water resulting from the change in the internal vapour pressure.

These proposed mechanisms are judged differently by different authors. Bažant [46] suggested that the main source of creep is the expulsion of absorbed water along the absorbed layers into larger pores. This could explain why completely dried specimens do not exhibit significant creep at low stresses. Feldman [47], on the contrary, claimed that water movement is not the main source for creep. He stated that creep is a result of the gradual crystallization of the layered structure of the cementitious material. According to Klug and Wittmann [48], during the creep process some gel particles are removed from their position of equilibrium. Water molecules only act as a weak bond between these particles. A similar conclusion was drawn by Vandamme and Ulm [49]: creep originates from the rearrangement of C-S-H particles. They did not explicitly consider the role of water. These proposed mechanisms occur at different scales of concrete and play a more or less important role in the overall creep. According to Coutinho [24], the combination of all these mechanisms is most likely the explanation for creep.

APPARENT MECHANISMS

All the aforementioned mechanisms have in common that creep of concrete originates from the cement paste. Any mechanism that leads to the changes in the cement paste influences creep, such as, drying, hydration or micro-cracking, as proposed by some researchers [21, 43]. These mechanisms are the "apparent mechanisms", as introduced in Section 2.2.1.

Concrete exposed to drying conditions exhibits larger creep under sustained load. This is the so-called drying creep or Pickett effect [50], i.e. the excess of creep of a drying specimen over the sum of shrinkage and basic creep (Fig. 2.3). The mechanisms of this additional deformation have been a reason for controversy among researchers. There are two major views on drying creep. The first view is that moisture diffusion

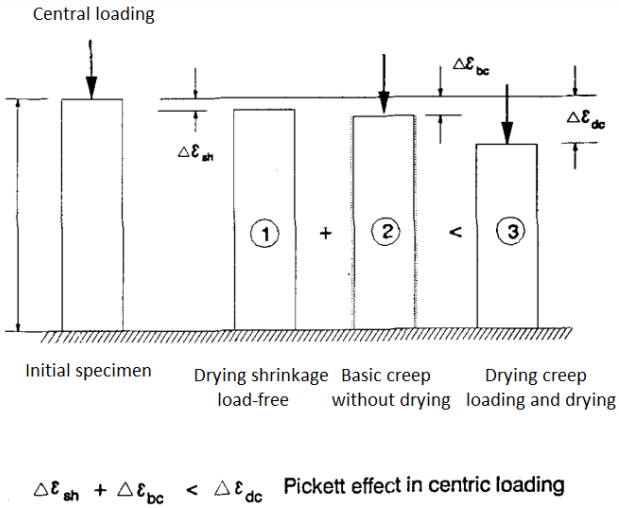

Figure 2.3: Pickett effect in centrically loaded concrete [5]

under drying affects the rate at which the cement gel is deformed under load and promotes the breakage of bonds, which is assumed to be the origin of drying creep [5]. By adopting this view, the authors in [5] attributed drying creep to two sources: micro-cracking and stress-induced shrinkage. Altoubat and Lange [51] developed a new experimental approach to separate the two components of the mechanism of drying creep, i.e. stress-induced shrinkage and micro-cracking. The results showed that the stress-induced shrinkage is a major mechanism of drying creep in both plain and fibre reinforced concrete. The micro-cracking formed a significant portion of drying creep in plain concrete, but was less significant in fibre reinforced concrete. The second view is that drying creep is caused by shrinkage-induced stresses and associated micro-cracking [52]. Drying causes a moisture gradient over the cross section of concrete specimens, resulting in a strain gradient. This will provoke stresses, which will further lead to micro-cracking. This process can be illustrated well by Fig. 2.4 (after [6, 7]). The statement of Pickett [50] "an increase in creep accompanying non-uniform shrinkage or swelling is a natural consequence of the fact that the sustained stress vs. strain curve for concrete is not linear" leads to the assumption that creep may be increased indirectly by shrinkage-induced forces. Gamble [53] found that drying creep was linearly related to simultaneous shrinkage under a wide variety of conditions (e.g. age at loading, drying age and load level). This means that the total time-dependent deformation can be predicted with some confidence based on the basic creep and shrinkage deformation.

The micro-cracking occurs in the surface zone of drying concrete. These cracks will be closed under compressive loading. In the load-free specimens, the micro-cracks remain open during drying. This reduces the observed overall shrinkage, compared to that in the loaded specimens. It was initially thought that this difference in micro-cracking, caused by non-uniform moisture distributions, might be the source of Pickett effect. However, tests from Bažant et al [5], where concrete was loaded under compressive forces of different eccentricities (see Fig. 2.5), showed that the difference in micro-cracking

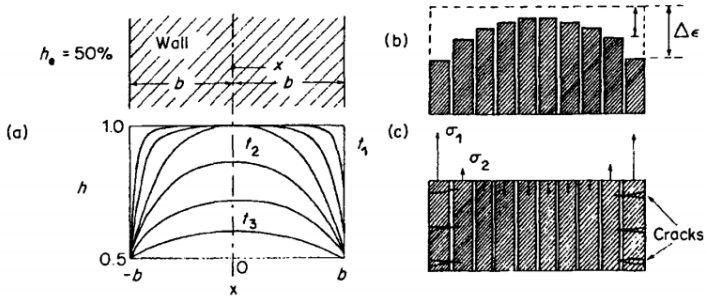

Figure 2.4: (a) Typical subsequent humidity distributions in a wall exposed to drying; (b) the corresponding shrinkages at various layers imagined as unrestrained; (c) stresses and cracking caused by the restoration of compatibility [6, 7]

in loaded and unloaded specimens only plays a minor role in the Pickett effect. Later Bažant et al [54, 55] attributed the Pickett effect to a combination of micro-cracking and changes of microprestress in the bonds or bridges that cross the micropores due to drying. Sinko et al [56] indicated that the theory from Bažant has limitations, since it did not consider water flow along the filled nanopores. Water flow due to drying in the nanopores lowers the underlying energy barrier to shear motion and two pore walls start to slide past one another, which consequently facilities the additional deformation (i.e. Pickett effect).

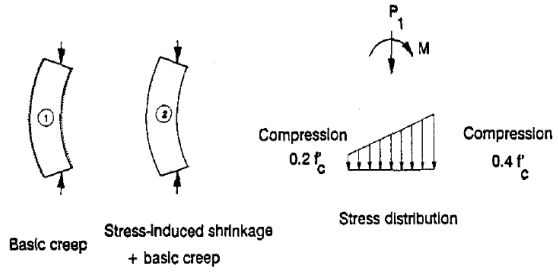

(a) Small eccentricity

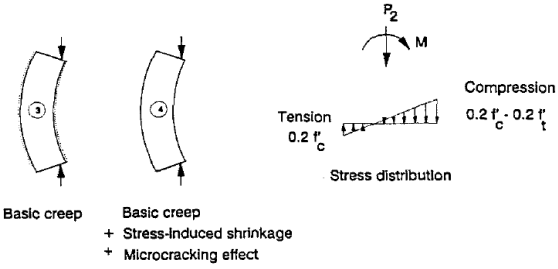

(b) Large eccentricity

Figure 2.5: Concrete loaded at different eccentricities [5]

The typical creep mechanism taking into account the effect of hydration is the solidification theory [57, 58], where the continuously newly formed hydration products can carry the load. This theory was adopted in the model of maturing creep by Lokhorst [44]. Generally, the hydration process gradually comes to an end after a few years. This, together with the fact that the age at loading still has an effect on the creep deformation, suggests that other phenomena, which change the microstructure of cement paste, influence creep. These phenomena could be, for example, viscous shear slips between the opposite walls of the micropores in the hardened cement gel [54, 55], polymerization of silicate phases proposed by Parrott [59], forced hydration by external load [24] (explained in Section 2.3) or the dissolution-diffusion-reprecipitation process [60–62] due to load.

Another phenomenon, which is also considered to affect the creep process, is micro-cracking. Meyers et al [63, 64] concluded that micro-cracking constitutes 10 to 25% of the total creep deformation. With acoustic emission tests, micro-cracking was identified during the creep process under different stress levels [9, 10, 29, 30, 65]. A record of acoustic emissions during a basic creep test is shown in Fig. 2.6. Rossi et al [9, 66] recorded

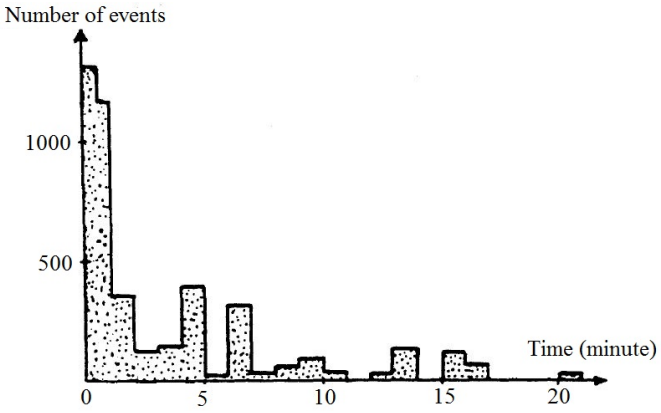

Figure 2.6: Acoustic emission obtained during a basic creep test (note: first 20 minutes) [8]

acoustic emissions during basic creep test under compression at different stress levels (50%-80% of compressive strength at 266 days). It was found that the basic creep strain[1] is linearly proportional to the total number of micro-cracks created in the material, as shown in Fig. 2.7. These micro-cracks were assumed to cross a large number of unhydrated cement grains and also to constitute paths for water transport. Upon the occurrence of micro-cracks, the internal equilibrium is disturbed, which induces the water movement from capillary pores to micro-cracks. Rossi indicated that this has two consequences: 1) the movements of water causes drying of the micro-pores and thus shrinkage, i.e. self-drying, which is considered the reason for the additional strain caused by micro-cracking; 2) the anhydrous cement will react with water and hydration product will be formed in the micro-cracks, i.e. self-healing, which accelerates the kinetics of the

[1] The basic creep strain was classically determined by subtracting from the total strain, the instantaneous elastic strain due to the loading of the specimen and the strain due to the autogenous shrinkage. The authors assumed that the basic creep of concrete was mainly due to micro-cracking which induces additional self-drying shrinkage.

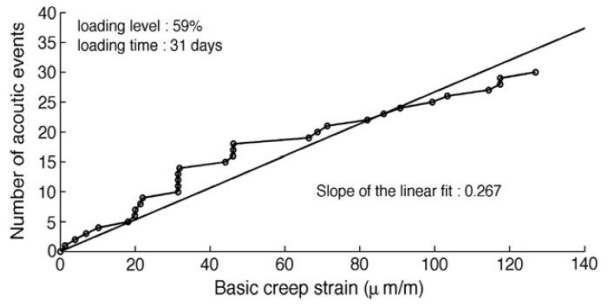

(a)

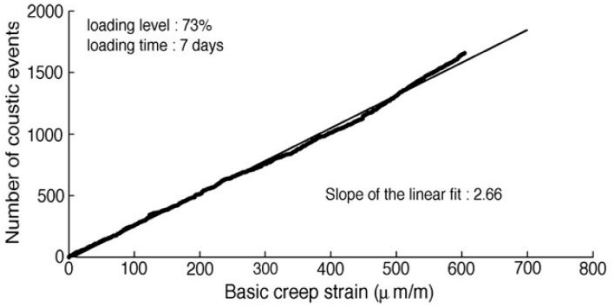

(b)

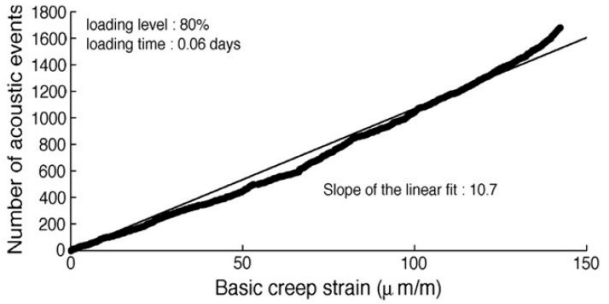

(c)

Figure 2.7: Number of acoustic events versus basic creep for different loading levels: (a) 59% loading level; (b) 73% loading level; (c) 80% loading level [9]

self-drying process. Another consequence which is not elaborated is that: self-healing in the micro-cracks makes material stronger, which might slow down the creep process. In order to quantify the damage mechanism during three stages of creep (see Fig. 2.2), Saliba et al [10, 65] performed flexural creep tests on both mortar and concrete beams at high stress levels (70% and 85% of the flexural strength). The acoustic emission events at several locations in the beams were recorded, as shown in Fig. 2.8. They found that the rate of creep was strongly correlated with the rate of micro-cracking and the creep displacement was proportional to the number of acoustic emission events. The acoustic

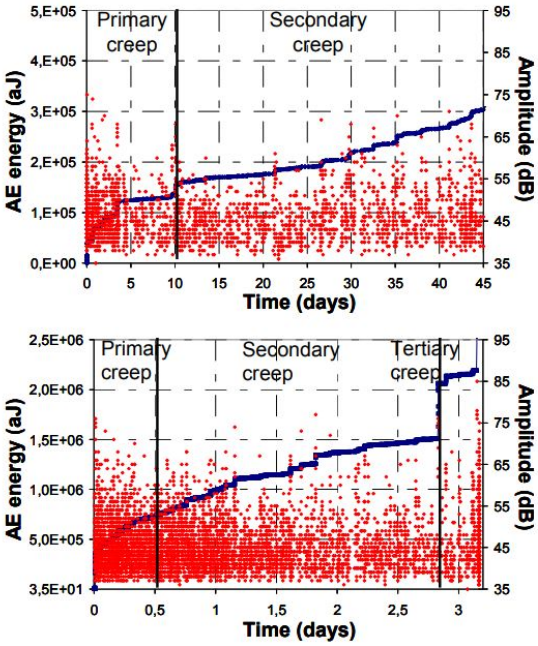

Figure 2.8: Acoustic emission activity during creep tests of mortar (figure above) and concrete (figure below) beams [10]

emission activity differed in the three stages of creep process (see Fig. 2.2). It appeared high during primary stage, but its rate gradually decreased. The rate became more stable during the stage of secondary creep, while the acoustic emission activity increased quickly due to the propagation of micro-cracking in the stage of tertiary creep. Compared with mortar beams, more micro-cracks were recorded in concrete beams, which suggests the important role of aggregate in stress redistribution and crack propagation.

2.2.3. PREDICTION OF LONG-TERM CREEP

Prediction of long-term creep is still a big challenge, since the phenomenon of creep is far from being understood [40]. Many predictive models have been proposed and most of them were derived from empirical data, e.g. mathematical formulations/fitting from limited creep tests. They are widely-used in structural design and analysis. However, the reliability of them is often debatable since large scatters/errors can be found in the predictions. In order to formulate an acceptable predictive model for creep, three practical aspects have been considered:

(1) A mathematical form of the time dependency, e.g. double power law or double-power logarithmic law for basic creep [67, 68];
(2) Input parameters depicting more physical mechanisms (e.g. microprestress solidification theory [54, 55]);
(3) Free parameters, which can be adjusted to make the model fit the existing experimental data [69].

(1) to (3) have been employed in most of the currently-used model codes for creep, such as, ACI Committee 209 Recommendation [70, 71], CEB MC 90-99 [72], GL2000 model [73] and fib model [74]. Model B3 [75] and the most recent model B4 [76], proposed by Bažant, include most of the creep theories including the activation energy concept, diffusion theory, microprestress-solidification theory in the nano-structure. However, they did not really bridge the gap between microstructure changes and the creep behaviour. Moreover, many parameters or formula are still based on the practical experiences or experimental work.

Some researchers suggested that a short-term creep test is helpful to improve the accuracy of the prediction of time-dependent deformations. Mazloom [77] carried out a series of short-term creep tests to estimate the long-term creep of high-strength concrete. He found that for an accurate estimation of long-term deformations of high-strength concrete utilizing the ACI and CEB methods, short-term tests should be performed on the concrete specimens in order to extrapolate long-term strains. Ojdrovic and Zarghamee [78] performed short-time creep tests (time period less than 28 days after load application) on 15cm diameter cylinders. The test results were used to improve the prediction of ultimate creep calculated by Bazant-Panula (BP-KX) [79, 80] and ACI 209 model [71]. By comparing these creep values with the long-term experimental creep data, they found that the coefficient of variation of the adjusted BP-KX and ACI prediction was less than 7%. Brooks [19] stated that the current design methods (or model codes) failed to make good estimations for 30-year creep tests that he carried out. However, these predictions could be improved by measuring the elastic modulus or short-term creep deformation.

Different computational approaches have been developed in order to predict long-term creep deformation [5, 42, 81]:

- One-step approximate solutions, using the age-adjusted effective modulus method;
- Step-by-step solution according to the integral-type creep model based on the principle of superposition;
- Step-by-step solution according to a rate-type creep model based on the Kelvin or Maxwell chain.

The last approach is most popular because the rate-type model can fundamentally take into account the effect of various mix proportions and ambient conditions on ageing and creep, which gives quite good results [40]. Briffaut et al [82] used three Kelvin chains plus one dashpot to model basic creep, considering hydration and temperature effects. They found that three ageing Kelvin units could predict the basic creep for a simple loading history, while a supplementary dashpot is necessary for complex loadings. Hilaire et al [83] simulated micro-diffusion (short-term creep mechanism) using a Kelvin chain; and sliding of C-S-H sheets (long-term creep mechanism) using an isolated dashpot. Gawin et al [84, 85] used the effective stress concept to model the modified microprestress-solidification theory, taking into account the effects of temperature and relative humidity on cement hydration. The microprestress-solidification theory [54, 55] is frequently used for long-term creep simulations. Jirasek and Havlasek [86], however, found that this theory overestimates creep when concrete is subjected to thermal cycles. They reformulated the governing differential equation of microprestress-solidification theory in terms

of viscosity, which leads to a reduction of the number of parameters and an easier identification of them. However, a large deviation still exists between the simulation results and experimental data (1000 days). Maekawa et al [87] presented a multi-scale model for structural performance: DuCOM. It is an integrated computational scheme for life-span simulation of reinforced concrete, taking into account creep and shrinkage. They consider solidification as the main source of long-term creep deformation. Besides, in their original model, the long-term creep were overestimated. The reason, they concluded, was that the parameters representing the viscous flow (simulated by a dashpot) were overestimated.

2.3. STRENGTH AND ELASTICITY OF CONCRETE UNDER SUSTAINED LOAD

SUSTAINED load not only deforms concrete, but also has an effect on the evolution of its strength and elastic modulus. Most experimental observations have shown that the compressive strength and elastic modulus increase when concrete undergoes creep. Coutinho [24] did a series of experiments in 1977 to measure the strength and elastic modulus of concrete with and without sustained load. The compressive strength of concrete loaded at different stress levels (21% to 89% of compressive strength at 7 days) after 3 days was 1.9% to 10.7% higher than that of unloaded specimens (Table 2.1). The

Table 2.1: Comparison between compressive strength of loaded and load-free concrete (age at loading: 7 days; loading duration: 3 days) [24]

Applied stress levels[1]	Compressive strength (MPa)				Relative increase[2] (%)
	After creep test		Free samples		
	Mean value	Standard deviation	Mean value	Standard deviation	
0.21	15.49	5.1	15.20	5.7	1.9
0.48	13.73	4.5	13.24	5.0	3.7
0.68	13.83	3.7	13.14	5.9	5.2
0.89	14.12	4.4	12.75	4.0	10.7

[1] Applied stress levels = fractions of compressive strength at age at loading 7 days;
[2] Relative increase = (strength of loaded concrete - strength of load-free concrete) / strength of load-free concrete.

higher the stress level, the larger the increase in strength of the specimens (loading duration is 3 days). It appeared that the increase in strength reached a certain limit after a certain loading duration. Concrete loaded at an early age exhibited a larger increase in strength than the concrete loaded at a later age at the same stress levels and the same loading period (constant stress tests). Similar results were also found by Hughes and Ash [37], Brooks [19] and Washa and Fluck [34]. From a comparison of concrete and mortar specimens with different mix proportions, Hughes and Ash [37] found that with a higher cement content or larger aggregate size, specimens gained a higher increase in strength. Concrete with a lower aggregate stiffness or a higher water-cement ratio exhibited less increase in strength and elastic modulus, and even a decrease was found in some specimens [19].

As for the tensile strength of concrete loaded with sustained tensile loading, the results are inconsistent. Wittmann and Zaitsev [12] found that the tensile strength increased in concrete under sustained tensile stress up to a certain stress level. However, no obvious increase in the tensile strength of concrete under sustained tensile loading was found by Coutinho [24].

With regards to the increase in compressive strength and elastic modulus of concrete under sustained load, a few mechanisms have been proposed:

(1) Forced hydration by applied load [24]

Coutinho [24] suggested that the increase in strength during the creep process might be due to an additional hydration as a result of the applied load. Thermodynamically speaking, the rate of chemical reactions increases with temperature or pressure. Therefore, the hydration rate should also increase when concrete is exposed to a sustained load. Coutinho stated that this additional hydration due to external loading might be the main source of the irreversible creep, since hydration is irreversible.

However, according to Hughes and Ash [37], the contribution of the forced hydration to the increase in strength might be very small. The hydration rate may accelerate instantaneously at the moment the load is applied, but will not be influenced by loading once the load stabilizes. Bisschop [88] and Tamboue [89] studied the effect of applied stresses on the degree of hydration. Bisschop [88] observed that after 100 days the degree of hydration of the sample[2] loaded at 7 days (stress/strength=0.4) was 2% to 3% lower than that of the load-free sample. This is attributed to a reduced precipitation rate of calcium hydroxide on the stressed surface of pre-existing calcium hydroxide crystals, which has been observed by Bisschop and Dysthe [90], Shtukenberg et al [91] and Sherwood and Ristic [92]. For a sample loaded at an age of 28 days there was no significant reduction in the degree of hydration. He concluded that the effect of applied stress on Portland cement hydration might be negligible. Tamboue [89] applied an external load (30% of compressive strength) on Portland cement paste at the age of 18-30 hours. He observed that 24 out of 36 measurements showed a lower degree of hydration in the first 4 days, compared to the load-free specimens. It is obvious that more tests are needed to eliminate the current inconsistencies of experimental data and so to determine the magnitude of the effect of loading on hydration.

There is another explanation for the effect of pressure on the hydration rate. Under higher pressures, the cement paste will deform to a certain extent. This will "liberate virgin cement grain surfaces and thus stimulate the further hydration" [21]. Further hydration in the crept concrete has been confirmed by experimental observations that the amount of free calcium hydroxide and of chemically and physically bond water is larger than in the load-free sample [24, 88].

(2) Strengthening of cement paste matrix due to compaction or consolidation [37, 65, 88, 93]

[2] Sample was sealed during creep test.

Compaction or consolidation of concrete is a result of a process whereby entrapped air is expelled from freshly poured concrete and aggregate is packed [94, 95]. It is generally perceived that when a material is compressed, its structure will become denser and thus the material may become stronger. This effect would be more pronounced if the material is more coarse or porous. This mechanism has been proposed to explain why the strength of concrete increases under sustained compressive load [12, 37, 88, 96]. Only a few experiments have been performed to study this. Builion et al [11] performed a uniaxial confined compression test on a relatively large concrete sample (confined by a hollow steel tube) and a true hydrostatic test on a smaller mortar sample (the hydrostatic pressure being very high, up to 250MPa). For both tests, the bulk modulus increased and the stiffening effect was observed. The pores were assumed to be crushed progressively and thus the material became tighter and stiffer. The aggregate was observed to be slightly rearranged by the crushing of the mortar phase of the confined concrete sample (Fig. 2.9). No such effect was observed in the unconfined mortar sample. Usually the compaction under normal pressure is explained by the closure of

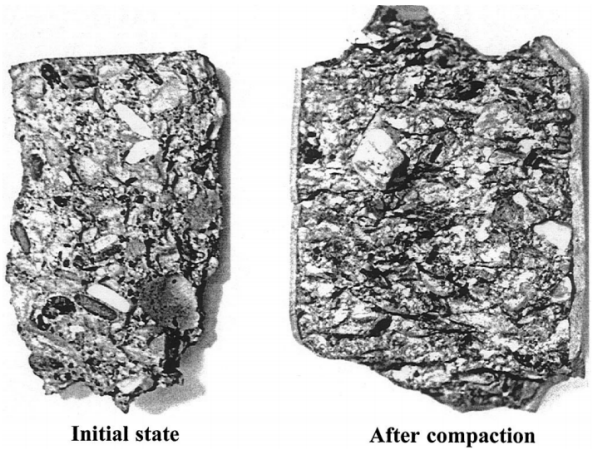

Figure 2.9: Confined concrete before and after compaction [11]

pores under compression (i.e. decrease in porosity). This explanation, however, somehow contradicts the argument of Hansen [97, 98]. He indicated that the pore space cannot be changed by the external load as the solid skeleton of concrete and hardened cement paste is very stiff. Besides, if this theory would be true, pore space would become larger and concrete would lose strength under tensile load [12]. Another argument against the compaction or consolidation theory pertains to the strength under cyclic loading. Under the action of repeated load the consolidation process should be more rapid, which will give a larger strength increase compared to that under sustained load [96]. However, the experimental data on compressive strength and modulus of elasticity under cyclic load did not show an obvious increase compared with that under sustained load. In conclusion, more tests are needed to study what really happens to the void ratio, capillary porosity,

gel porosity and gel structure under sustained load [99].

(3) Redistribution of internal stress concentrations around crack tips by creep [12]

This assumption is proposed by Wittmann and Zaitsev [12]. Since the compaction theory seems not valid for the tensile loading, they did a series of experiments on the hardened cement paste with water-cement ratio of 0.45 under very high tensile stress levels (around 80%-100% of ultimate stress). A higher strength was observed in the samples loaded for 30 or 60 minutes, compared to the load-free samples (Fig. 2.10). In order to study the cause of the strengthening effect, two artificial cracks were created in the specimens for both compressive and tensile test. Small strain gauges were fixed near the crack tips and normal strain gauges were glued in the region of homogeneous undisturbed stress distribution (Fig. 2.11). High stress concentrations were expected around the crack tips when the specimens were loaded. If the load was kept constant for some time, creep near the crack tips reduced the stresses. These cracks became more stable. An unstable crack propagation can only be obtained at a higher external stress. According to this theory, the gain in strength under both sustained compressive and tensile loading was explained.

(4) Reduction of stress concentrations and self-healing of micro-cracks [37, 88]

Many authors assigned the increase in strength under sustained load to the self-healing of micro-cracks during the creep process [37, 88, 96]. It is assumed that micro-cracking and self-healing could be two opposing mechanisms influencing the long-term performance of cementitious materials [100]. As mentioned in Section 2.1, micro-cracking has been detected by acoustic emission techniques during the creep process. The heterogeneity of concrete material provides a favourable condition for the formation of micro-cracks. These cracks can jeopardize strength, stiffness, durability and safety of concrete structures. However, the existence of micro-cracks offers a great potential for self-healing, since micro-cracks can expose the unhydrated cement to and facilitate the water transport in the crack. The self-healing potential of concrete material will be presented below.

2.4. SELF-HEALING POTENTIAL OF CONCRETE MATERIAL

SELF-HEALING of cracks is considered to have a significant potential to extend the service life of concrete structures and reduce economic, social and environmental costs [101]. Unlike many other materials, concrete has a relatively large potential for self-healing because of its heterogeneous nature and presence of unhydrated cement. Theoretically complete reaction of cement requires a water-cement ratio of 0.4. However, in practice about only 70% of cement will completely react in a mixture with water-cement ratio of 0.4. The remaining 30% is left unused in cement paste. The coarser the cement, or the lower the water-cement ratio, the higher the amount of unused cement. The heterogeneous nature of concrete facilitates the occurrence of cracks. Because of cracks, unhydrated cement may be exposed to water and hydration starts again. Hydration products can then start to fill up the crack. This is one of the known self-healing

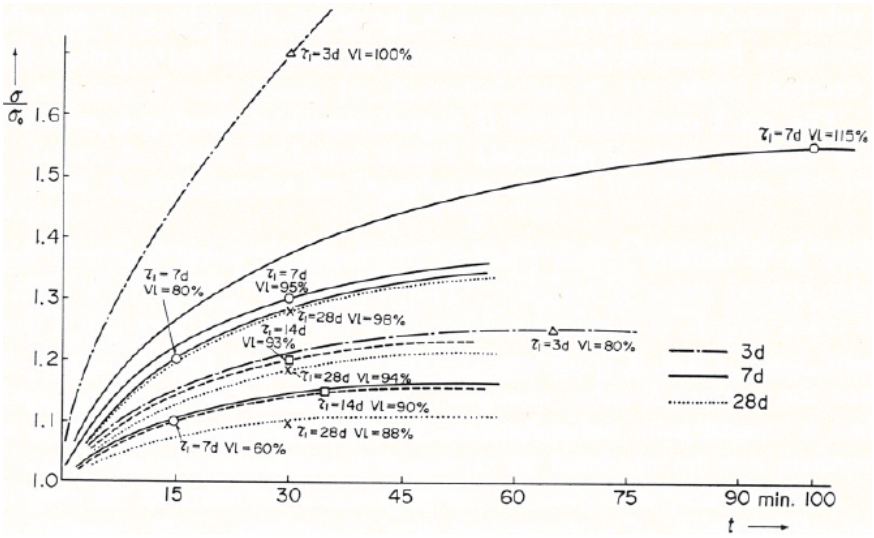

Figure 2.10: Influence of loading duration and tensile stress level on the tensile strength of hardened cement paste. The age at loading is 3 days to 28 days. The increase in strength is described in percentage of the average ultimate tensile stress of the load-free samples (σ is the tensile strength of loaded sample; σ_0 is the tensile strength of load-free sample; τ_1 is age at loading and Vl is stress level) [12]

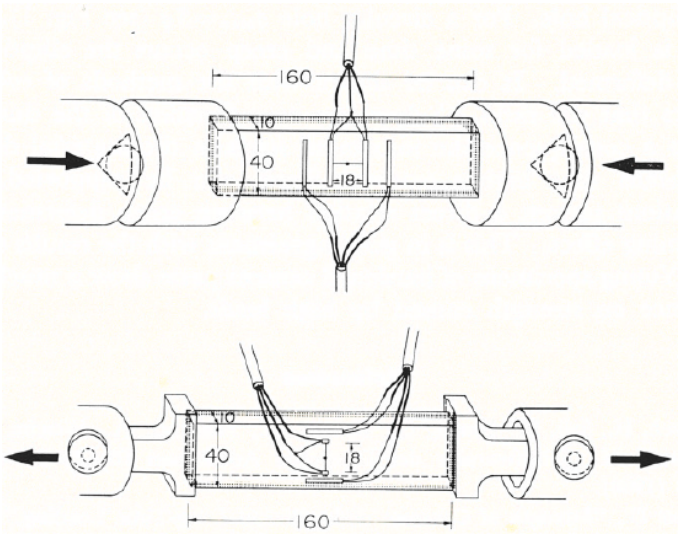

Figure 2.11: Artificial cracks in compression and tension and the position of strain gauges in the specimens [12]

mechanisms: further hydration of the unhydrated cement clinker, i.e. autogenous self-healing.

Autogenous self-healing of cracks has already been investigated in the water retaining structures, culverts and pipes by the French Academy of Science in 1836 [102]. At the end of 19th century Hyde and Smith continued to study this phenomenon [103, 104] and a more systematic research on this topic can be found in the work of Glanville [105]. Four possible mechanisms have been investigated in detail, as shown in Fig. 2.12 and explained in (a)-(d). Hearn [103] concluded that dissolution and deposition of soluble hydrates, e.g. $Ca(OH)_2$, are the main mechanisms for self-healing in the mature concrete. Further hydration is considered as the second important mechanism. By detecting the growth of hydration products in bridge decks, Sorker and Denson [106], Brandeis [107] and Turner [108] assumed that autogenous self-healing was a result of continuing hydration. Self-healing is considered to be the main cause to the reduction of permeability [109, 110] and chloride ingress [111–113] according to intensive experimental observations.

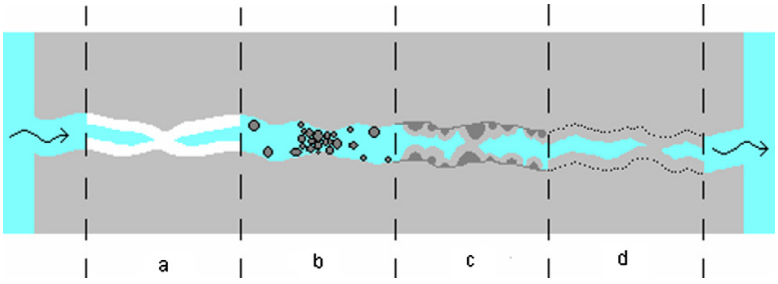

Figure 2.12: Self-healing mechanisms in cementitious materials [13]: (a) Formation of calcium hydroxide or calcium carbonate; (b) Crack blocked by impurities in water or loose concrete particles coming from crack spalling; (c) Further hydration of the unhydrated cement; (d) Swelling of C-S-H due to water absorption.

Compared with the study on the effect of self-healing on permeability, quite a number of studies have also been carried out on the effect of self-healing on the mechanical properties of cement paste/concrete. Jacobsen and Sellevold [114] studied self-healing of high strength concrete after a rapid freeze/thaw test. They found that self-healing caused the compressive strength to recover by 4-5% after an initial loss of 22-29% by the deterioration due to freeze/thaw. Self-healing could, to a certain extent, prevent concrete from deterioration caused by freeze/thaw. Pimienta and Chanvillard [115] observed that the mechanical properties of cracked samples (damaged under three point bending) were not much affected by the severe conditions (hot water, sodium chloride solution and wet-dry cycles). An increase in the overall rigidity of the samples was observed. Ter Heide [116] also observed a gain in strength of early age cracked concrete (crack width is 20 to 50μm) after autogenous self-healing. Granger et al [117] measured strength and stiffness of healed concrete specimens. They found a full recovery of stiffness after 20 weeks of healing and a slow improvement of strength (crack width is 10μm). Self-healing of the pre-existing cracks was mainly attributed to the hydration of anhydrous clinker on the cracked surface. The stiffness of newly formed crystals was close

to that of primary C-S-H. Some studies have focused on the improvement of the autogenous self-healing of cementitious material by using mineral additions [118–120], crystalline admixtures [121–123], superabsorbent polymers (SAPs [124–126]) and non-SAP polymer additions (e.g. polymer-modified concrete or polymer Portland cement concrete [127–129])[3]. The results of these studies showed that the samples with the aforementioned additions generally exhibited an improved self-healing capacity and an extra strength compared to those without the additions. As shown above, autogenous self-healing can be considered effective for the recovery of mechanical properties.

Self-healing is highly dependent on the water-cement ratio, crack width, type of cement, age of concrete and ambient conditions. The self-healing mechanism and the required preconditions are still not fully understood [134]. The potential of self-healing is considered higher if the water-cement ratio is lower and the cement coarser. Munday et al [135] conducted a series of tests on the self-healing of concrete with four different types of cement cured to various ages (1, 7, 14, 28 days) and under different temperatures. They investigated self-healing at different conditions: dry, humid, submerged. By comparing the strengths before and after healing, they found that recovery of strength always took place. He found that the percentage by which the strength was recovered decreases with the increase of age of the concrete at test. Specimens healed under high humidity gained more strength than those immersed in the water. Also the type of cement had an impact on the results. Water flow and self-healing in cracks in concrete specimens were studied by Clear [136]. The crack widths varied from 0.1, 0.2 to 0.3 mm. He found that the smaller the initial width of a crack, the faster the healing of the crack. Fan and Li [137] adopted x-ray computed microtomography (μCT) to derive three dimensional morphological data on micro-cracks in engineered cementitious materials before and after healing. They found that the extent and rate of self-healing depend not only on the initial crack width, but also on the crack depth. Cracks below the surface from 0 to around 50-150 μm can be healed quickly by crystalline precipitates. Reinhardt and Jooss [109] performed permeability and self-healing tests on concrete specimens with crack widths between 0.05 and 0.20 mm and under different temperatures between 20 and 80°C. They concluded that a faster self-healing process was favoured by a higher temperature and a smaller crack width. On the assumption of stable crack edges, crack width smaller than 0.1 mm can be considered to be completely closed by the self-healing process.

Recently, much attention has been paid to numerical simulations on autogenous self-healing of cementitious materials. Some researchers focused on the self-healing potential of concrete with different water-cement ratios, cement type and fineness. In the work of Huang [14] on the simulation of self-healing of micro-cracks based on thermodynamics, a crack was created in the porous cement paste, along the border of some unhydrated cement grains. When water was supplied, the reactive particles started to form inner product (C-S-H), outer product (C-S-H) and portlandite (C-H). The outer product

[3]This paragraph mainly focuses on the effect of autogenous self-healing on the improvement of mechanical properties of cementitious materials. Autogenous self-healing capacity in cementitious materials relies upon the "conventional" constituents of the cementitious matrix and can also be stimulated through the above mentioned tailored additions [101, 130]. Recent studies on autonomous self-healing in cementitious materials, i.e. via, application of micro-, macro-, or vascular encapsulated polymers, minerals, or bacteria, has been thoroughly reviewed by De Belie et al [131], Sidiq et al [132] and Ferrara et al [133].

and C-H were assumed to precipitate at the surface of the crack, i.e. filling the crack. This is shown in Fig. 2.13. He et al [138, 139] studied numerically the underlying self-healing capacity of concrete with various water-cement ratios and cement fineness. The influence of the density and spacing distribution of the unhydrated cement nuclei (UCN) on the self-healing capacity was simulated by concurrent algorithm-based computer simulation system SPACE. They found that the water-cement ratio, compared with cement fineness, is dominant for self-healing capacity. The higher the water-cement ratio, the lower the self-healing capacity, since the amount of UCN is less. For concrete with same water-cement ratios (the volume fraction of UCN is similar), the one made with finer cement was excepted to have a better self-healing capacity due to the high surface area density of UCN. However, this expectation is in contradiction to the conclusions from Huang [14] and Rahmani [140], who observed in experiments that concrete with coarser cement has a better self-healing capacity. Lv and Chen [141, 142] modelled self-healing in the cracks based on further hydration of the unhydrated cement. They found that volume fraction, particle size distribution of unhydrated cement and crack modes, (i.e. splitting crack mode and the dome-like crack mode) all play a role in the self-healing efficiency of the cracks in hardened cement paste. It is noted that in this study the self-healing efficiency was studied qualitatively. Experiments should be used to validate the model.

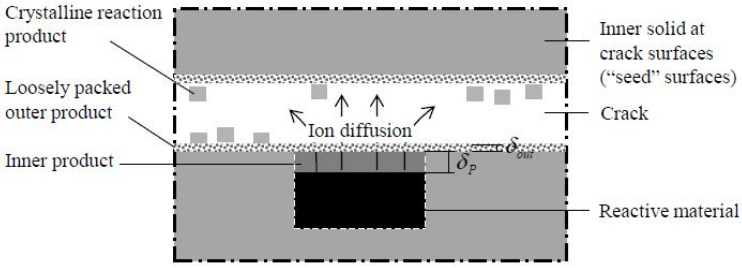

Figure 2.13: Schematic diagram of the self-healing of a micro-crack [14]

Some studies have been conducted on the development of numerical models concerning the recovery of mechanical properties due to self-healing. Both the continuum damage model (e.g. smeared crack model) and the discrete damage model are usually employed to consider the self-healing capacity [143–154]. The general approach is that the damage parameter/degree is modified once the self-healing process is initiated. For example, three stages of the self-healing process, i.e. fracture, transport of healing agents and recovery of mechanical properties, were modelled by Schimmel and Remmers [146], Remmers and de Borst [155] and Joseph [154]. Once the amount of water/healing agent has reached the threshold level in a crack, the self-healing process was initiated and the strength and stiffness were assumed to be partially or fully recovered (i.e. damage parameter is reduced). In the micro-damage healing model proposed by Abu Al-Rub et al [147], two processes, i.e. the wetting (i.e. the closure of the free surfaces of a crack) and diffusion (i.e. the flow of healing agent), were considered and incorporated in the intrinsic healing function to describe the influence of the self-healing at the micro-scale on the mechanical properties at macro-scale. They concluded that this model can effec-

tively predict the service life of asphalt under repeated loading. Based on a thermodynamic framework developed by Abu Al-Rub and Darabi [156, 157] and Darabi et al [144], Alsheghri and Abu Al-Rub [148, 149] developed a cohesive zone elastic-damage-healing model. The damage and healing conjugate thermodynamics forces are decomposed into energetic (based on Helmholtz free energy) and dissipative components (based on the rate of energy dissipation). The simulated stress intensity factor (used to represent self-healing efficiency) were generally in good agreement with the experiment data of polymethyl methacrylate. A hygro-chemo-mechanical model for autogenous self-healing has been proposed by Hilloulin et al [158]. In his model, the self-healing potential of cracked concrete was evaluated. Then the ingress of water was simulated and a hydration model was employed to model the further hydration of the unhydrated cement. To a certain extent, the crack filled up with hydration products and the local damage value was reduced. Subsequently, the recovery of mechanical properties was calculated. Mergheim and Steinmann [150] proposed a phenomenological model for self-healing polymers. Two important features of this model are that a realistic exponential curing function is adopted to describe the curing process of healing agent and catalyst, and that the healing agent is cured under a stress-free condition. This approach is considered to better represent the coupled physicochemical mechanisms of real healing processes observed in experiments, compared to the approach that the evolution of healing is treated much like the evolution of damage but with the opposite sign [159].

2.5. CONCLUSIONS

THIS chapter presents the outcome of a literature survey regarding the behaviour of concrete under sustained load. It comprises a brief introduction of creep mechanisms, followed by a review of the current state-of-the-art research on the prediction of long-term creep. The strength development of concrete under sustained load was discussed. In the end, the autogenous self-healing phenomenon in cementitious materials was elaborated. It seems that many problems, contradictions and indistinctnesses related to the behaviour of concrete under sustained load stem directly from the lack of a deep understanding of the behaviour of concrete under sustained load. For example, the origin (or "real mechanism") of creep is still unclear. The reason behind the increase in strength of the concrete under sustained load still requires more investigation. Despite that self-healing mechanisms and their effect on the recovery of mechanical properties of concrete are not fully understood, self-healing does provide a good perspective for the durability and serviceability of concrete materials and structures.

Prediction of long-term creep has always been a challenge in both academia and practice. Apart from the "real mechanism", many other "apparent mechanisms" also play a role, such as, hydration, drying, temperature and micro-cracking. Without a proper evaluation of the effects of these apparent mechanisms, the prediction could not be expected accurate. In this thesis, the effect of micro-cracking on the long-term creep of concrete will be dealt with. However, the fact that micro-cracking leads to the reduction in strength is inconsistent with the strengthening of concrete under sustained load (at low stress levels). Self-healing is considered to be a potential mechanism to remedy this discrepancy. Therefore, the effect of self-healing is modelled to investigate the evolution of long-term creep and strength of concrete under sustained load (Chapter 3). The role

of water-cement ratio (Chapter 4) and aggregate stiffness (Chapter 5) in the interaction between creep, micro-cracking and self-healing will be studied.

3

BEHAVIOUR OF CONCRETE UNDER SUSTAINED LOAD: EFFECT OF MICRO-CRACKING AND SELF-HEALING

There is a crack, a crack in everything.
That's how the light gets in.

Leonard Cohen

In this chapter, the effect of micro-cracking and self-healing on the long-term creep and strength development of concrete under sustained load is studied. Firstly, an in-house lattice model for fracture analysis is modified to take long-term creep into consideration. The activation energy concept is used to model creep. Secondly, a mechanism that explains the extra increase in strength of concrete under sustained load is proposed. It includes two aspects: self-healing of the cracks and densification of the paste adjacent to the cracks. This mechanism is, then, incorporated in the modified lattice model. The effect of micro-cracking and self-healing on the long-term creep deformation of concrete under sustained load (water-cement ratio is 0.50; stress level is 30% of 14-day compressive strength) is simulated. The strength after loading is calculated and compared with the strength of load-free concrete. For a first validation step, the simulated results (both deformation and strength) are compared with experimental data of Brooks' 30-year creep test.

Parts of this chapter have been published in Proceedings of the Symposium on Concrete Modelling: CONMOD2018 (Rilem proceedings; no. PRO 127) [160].

3.1. INTRODUCTION

THE responses of concrete structures subjected to any form of loading, e.g. self-weight, traffic, temperature and moisture, can be subdivided into instantaneous and time-dependent ones. The stress-induced time-dependent deformations are generally called creep. In Chapter 2 it has been mentioned that the origin (or "real mechanism") of creep is still under discussion. For a reliable creep prediction the "real mechanism" is important. However, the prediction of creep will not be accurate without knowing the effect of other influencing factors, e.g. ongoing hydration, drying, temperature and micro-cracking, as mentioned in Chapter 2. These factors can modify the state of stress in concrete and, consequently, change the creep deformation.

Concrete deforms under sustained load with elapse of time. At the same time its microstructure is continuously changing. For example, concrete continues to hydrate and, meanwhile, micro-cracks occur due to the heterogeneity of the material. Micro-cracking of concrete during creep tests has been detected by acoustic emission measurements [9, 10]. Micro-cracking will lead to a reduction in strength. With ongoing micro-cracking the failure of concrete will occur after a certain time. However, in many creep experiments failure is not found. On the contrary, even an *extra* increase in strength of concrete under sustained load, especially at low and medium stress levels, compared to that of load-free concrete is observed [19, 24, 37, 96]. So, during the creep process there must be other phenomena "resolving" this contradiction. Self-healing is considered to be a promising candidate to explain this phenomenon. Self-healing of cracks could possibly compensate for the loss in strength. However, only self-healing of cracks will never give an *extra* increase in strength. It has been experimentally affirmed that more chemically and physically bond water and calcium hydroxide are found in crept concrete than in the load-free concrete [24, 88]. This suggests that the *extra* increase in strength might come from an extra hydration of the cement in concrete under sustained load.

In this chapter, the effects of continuous hydration, micro-cracking and self-healing on the long-term creep and strength of concrete under sustained load are studied theoretically and numerically. A self-healing mechanism is proposed to explain the extra increase in strength of concrete under sustained load. The mechanism consists of two components, i.e. "self-healing of cracks" and "densification of the paste adjacent to cracks". This self-healing mechanism, together with creep and continuous hydration, are incorporated in an existing lattice fracture model [17, 35]. The model that takes creep, continuous hydration, micro-cracking and self-healing into account, is called the modified lattice model. With this model the interaction between creep, continuous hydration, micro-cracking and self-healing is simulated at meso-scale. At this scale concrete is considered as a three-phase material (mortar, interface zone and aggregate). The model is preliminarily evaluated and the simulation results are compared to the experimental data from Brooks' 30-year creep test [19]. In the next section Brooks' tests are briefly presented.

3.2. BROOK'S TEST ON 30-YEAR CREEP OF CONCRETE

IN the period from 1975 to 2005, Brooks et al [19, 22, 25, 161] carried out a series of experiments on creep of concretes made with five different water-cement ratios and

four types of aggregate: two normal-weight aggregate (North Notts gravel and Stourton) and two lightweight aggregate (Aglite and Lytag). The aggregate-cement ratio by volume was kept constant, while the water-cement ratio varied. The concrete specimens were stored in either water or air during the creep test. In this chapter only the creep of concrete specimens with North Notts (normal-weight aggregate) and water-cement ratio of 0.50 is studied and used to evaluate the numerical model introduced in Section 3.7. The creep deformations were determined on cylinder specimens (76mm × 260mm) stored in water at 23±1 °C. The load was applied at the age of 14 days and the initial stress-strength ratio is 0.3. The mix design, strength and elastic modulus of load-free and loaded specimens are given in Table 3.1. The sum of elastic and creep strain is shown in Table 3.2.

Table 3.1: Mix design and mechanical properties of specimens with a water-cement ratio of 0.50 [19, 25]

w/c	Mix proportion by weight (C:S:A)[2]	Cement paste content r_p by volume (%)	14-day		30-year			
					Load-free		Loaded	
			f_c [1] (MPa)	E [1] (GPa)	f_c (MPa)	E (GPa)	f_c (MPa)	E (GPa)
0.50	1:1.71:3.04	31.1	36.80	29.76	50.60	40.70[3]	61.60	54.40

[1] E=elastic modulus; f_c=compressive strength;
[2] C:S:A=Cement:Sand:Aggregate;
[3] Assumed value; 30-year elastic modulus of the unloaded specimen is not given; it is assumed to increase by same percentage as the 30-year strength, compared with 14-day values.

Table 3.2: Sum of elastic and creep strain of specimens with a water-cement ratio of 0.50 [19]

Time (day)	0	1	3	7	14	28	100	365	1095	3650	10950
Strain ($\times 10^{-4}$)	3.71	4.40	4.86	5.26	5.57	5.91	6.62	7.42	8.32	9.47	11.12

From the data in Table 3.1 it can be inferred that after 30 years both the compressive strength and elastic modulus of load-free specimens increase by 37% compared with 14-day compressive strength and elastic modulus. This increase is due to the continuous hydration of concrete. Furthermore, the 30-year compressive strength of loaded specimen is 22% higher than that of load-free specimen. Similar observations on the extra increase in strength of concrete under sustained load were also found by Hughes and Ash [37], Washa and Fluck [34], Cook and Chindaprasirt [96], Bisschop [88] and Coutinho [24].

3.3. STRENGTHENING BY SELF-HEALING CONCEPT: BASIC IDEA

AMONG the four theories that are supposed to explain the extra increase in strength of concrete under sustained load mentioned in Chapter 2, the compaction theory and self-healing of cracks are supported by most researchers [37, 88]. The compaction theory, which is briefly discussed in Appendix A, was found to play only a minor role in the extra strength increase. It will not be considered further in this thesis. The hypothesis worked out further in this thesis regards the concept of micro-cracking and self-healing

to explain the extra increase in strength. Based on this hypothesis the basic idea of this research is introduced in this chapter.

As have been discussed in Section 3.1, micro-cracking will lead to a reduction in strength. Continuous micro-cracking may even lead to failure of concrete. However, according to some experiments [19, 24, 37, 96], no failure is found, but even an extra increase in strength of concrete under sustained load has been observed, especially at low and medium stress levels. Self-healing is assumed to be the phenomenon that could explain the extra increase in strength of concrete under sustained load. In the next subsection the basic idea used to explain the extra strength increase is introduced.

3.3.1. BASIC IDEA

Besides the gradual increase in deformation under sustained load, three other processes are supposed to take place in concrete under sustained load, viz.:

1. Continuous hydration
2. Micro-cracking
3. Self-healing

These three processes have an impact on the strength of concrete and, as a consequence, also on the stress-strength ratio and the creep deformation (see Fig. 3.1).

- Ad. 1: When concrete is loaded at a constant stress (constant stress creep test), and if the strength of concrete is constant over time (i.e. continuous hydration does not occur), the stress-strength ratio is constant as well (black dashed line in Fig. 3.1b). If continuous hydration takes places, the strength of concrete continues to increase (black solid line in Fig. 3.1a). As a consequence, the stress-strength ratio decreases and the creep deformation is smaller compared to that when the continuous hydration does not occur.
- Ad. 2: Due to the heterogeneity of concrete, micro-cracking may occur during the creep process. Micro-cracking reduces the strength of concrete (blue line in Fig. 3.1a). In a constant stress creep test, the stress-strength ratio will now gradually become higher and the creep deformation larger (blue line in Fig. 3.1b and 3.1c), compared to that when only continuous hydration takes place (black solid line in Fig. 3.1b and 3.1c).
- Ad. 3: The occurrence of micro-cracks may trigger self-healing to take place. Self-healing compensates for the loss in strength due to micro-cracks and an extra increase in strength might be possible and will be explained below (red line in Fig. 3.1a). Thus, the stress-strength ratio and the creep strain become smaller (red lines in Fig. 3.1b and 3.1c) than that when only continuous hydration is considered.

3.3.2. MAIN CONTENT OF THE FOLLOWING SECTIONS

This basic idea as explained above is investigated theoretically and numerically in the following sections using the lattice model [17]. The main content of these sections is as follows:

- In Section 3.4 a self-healing mechanism, i.e. self-healing of cracks and the densification of the paste adjacent to the cracks, is proposed to explain the extra increase

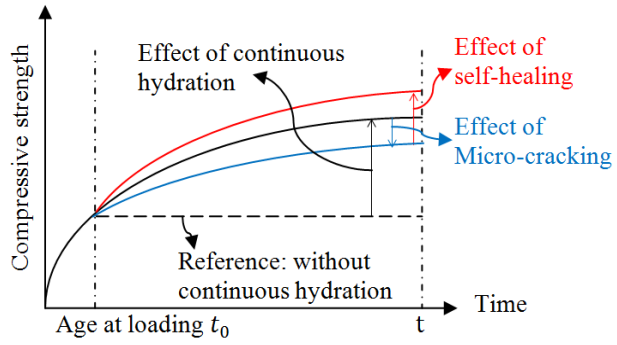

(a) Compressive strength

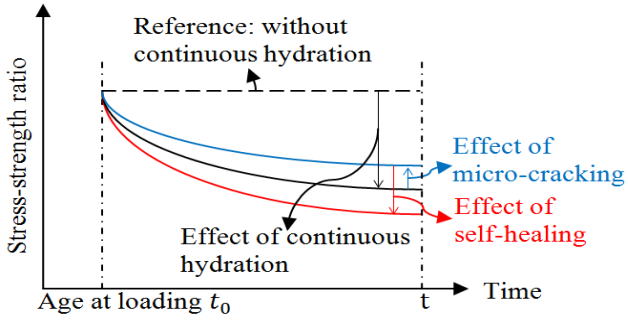

(b) Stress-strength ratio

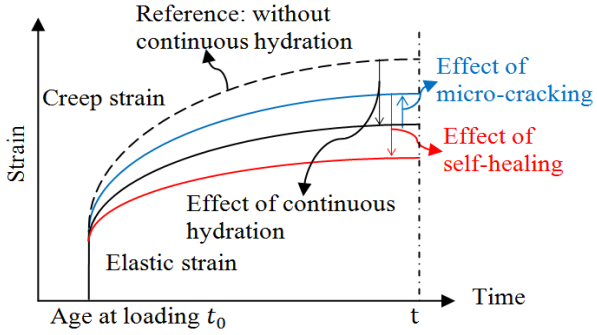

(c) Creep deformation

Figure 3.1: Effect of continuous hydration, micro-cracking and self-healing on the evolution of compressive strength, strength-stress ratio and creep strain of concrete loaded at t_0 at a constant stress: schematic diagram

in strength of loaded concrete. The extra increase in strength comes from the additional hydration of the paste adjacent to the cracks. A simple mathematical approach is introduced in Section 3.5 to calculate the additional degree of hydration and extra strength increase.

- In Section 3.6 the activation energy concept, which is assumed to be the "real mechanism" for creep, is briefly described. Besides, how different factors, e.g, micro-cracking and self-healing, influence the "real creep" is described.
- Creep, continuous hydration and self-healing are incorporated in a lattice fracture model [17, 35] in Section 3.7. In Section 3.8 the model is evaluated and the simulation results are compared with the experimental data from Brooks' test.

3.4. SELF-HEALING AND EXTRA INCREASE IN STRENGTH OF CONCRETE UNDER SUSTAINED LOAD

3.4.1. EXPERIMENTAL OBSERVATION OF THE SELF-HEALING PHENOMENON

The extra increase in strength of concrete under sustained load is supposed to be related to self-healing of micro-cracks, as suggested by some researchers [37, 88]. Unlike other materials, concrete has a large potential of self-healing because of the presence of unhydrated cement. Huang [14] performed a series of experiments on self-healing of cracks. He found that when water was supplied to the cracks, the exposed unhydrated cement particles on the crack surface started to form hydration products which gradually filled up the cracks. A BSE image, indicating the self-healing of a crack, is shown in Fig. 3.2.

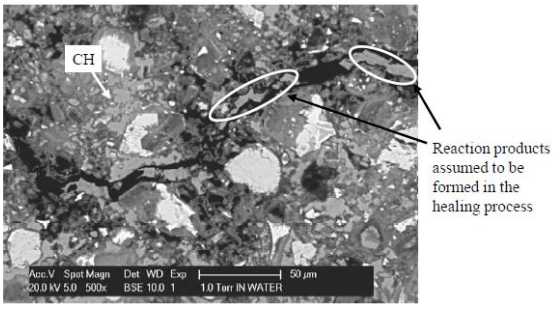

Figure 3.2: BSE image of a crack in Portland cement paste after curing in water for 200 hours [14]

Due to self-healing of cracks, the strength can be recovered up to the original value. However, self-healing of cracks will not lead to an *additional* strength. An experiment of self-healing of a cracked specimen performed by Huang [15] might provide a possible answer to the question what the cause of the extra increase in strength under sustained load could be. Through a nuclear magnetic resonance (NMR) test, Huang found that the zone adjacent to the crack became denser as a result of the reaction between unhydrated cement in this zone and the water migrating from the crack to the bulk paste. Fig. 3.3 illustrates this schematically. The mechanism leading to enhanced hydration is sketched in Fig. 3.4. Fig. 3.4a shows an uncracked porous cement paste. It is assumed that the

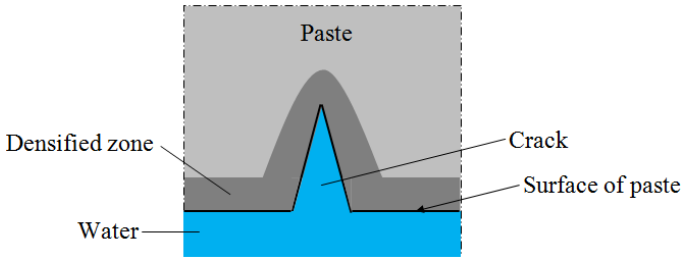

Figure 3.3: Schematic diagram illustrating the densification of the zone adjacent to crack surface due to absorption of water by bulk cement paste [15]

cement paste is immersed in water[1]. This guarantees that water is always available for cement hydration to take place. Upon the occurrence of a crack in the cement paste (Fig. 3.4b), water goes into the crack due to capillary suction. It gradually migrates into the paste through pores (Fig. 3.4c). This reduces the ion concentrations in the paste adjacent to the crack. A concentration gradient is created: low ion concentration in the crack and the paste adjacent to the crack and high ion concentration in the paste far from the crack or adjacent to the unhydrated cement grains. This promotes the dissolution of the unhydrated cement grains (Fig. 3.4d), i.e. the dissolution rate increases. More ions will diffuse into the crack and to the pore solution in the paste adjacent to the crack (Fig. 3.4d). Reaction products start to precipitate if the pore solution is saturated (Fig. 3.4d). Consequence of this mechanism is that the hydration degree in the paste adjacent to the crack will be higher than that in the sample without cracks, i.e. the paste becomes denser and stronger.

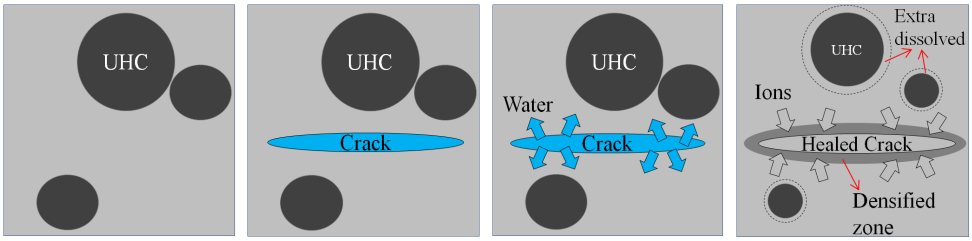

(a) Uncracked porous cement paste

(b) Paste with a crack filled with water

(c) Water migrates from crack to paste

(d) Paste with healed crack

Figure 3.4: Schematic diagram illustrating the self-healing mechanism for the extra strength increase in concrete under sustained load: (a) Uncracked porous cement paste; (b) Cracked cement paste (water does into the crack due to capillary suction); (c) Migration of water from the crack into the paste; (d) Dissolution of unhydrated cement grains (uhc), diffusion of the ions to the crack and the pore solution in the paste adjacent to the crack, precipitation of ions in the crack and the paste adjacent to the crack.

[1] Is the situation in Brooks' test

3.4.2. NUMERICAL SIMULATION OF THE SELF-HEALING PHENOMENON

The self-healing phenomenon, i.e. self-healing of the micro-cracks and densification of the paste adjacent to a crack, is simulated with a model for autogenous self-healing developed by Chen and Ye [16]. This model takes cement dissolution, ion transport and nucleation of hydration products into account. Firstly, a 14-day virtual cement paste sample (water-cement ratio=0.50; size is $100\mu m \times 100\mu m$) is generated by using HYMOSTRUC 3D [2] [162]. An artificial crack is created in the sample. Then the dissolution rate of individual cement particles in the area adjacent to the crack is simulated with the self-healing model. In order to study the effect of the crack widths on the densification of the paste adjacent to the crack, three different crack widths (0-30μm) are considered and the dissolution rates are simulated. All the samples are shown in Fig. 3.5.

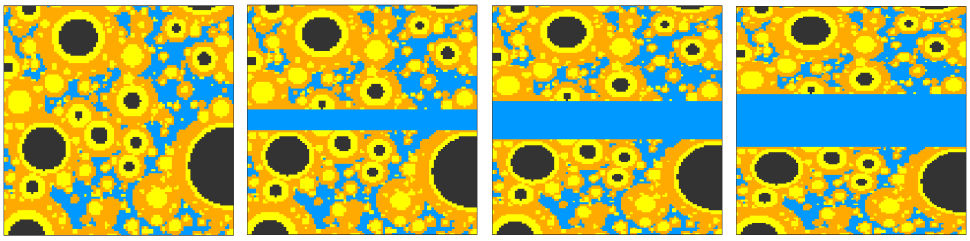

(a) $\omega = 0\mu m$ (b) $\omega = 10\mu m$ (c) $\omega = 20\mu m$ (d) $\omega = 30\mu m$

Figure 3.5: Cement paste samples with different crack widths (water-cement ratio=0.50; age=14 days; black=uhc, yellow=inner products, orange=outer products, blue=water; ω=crack width)

The dissolution rates of the cement paste samples with different crack widths are simulated with the autogenous self-healing model and shown in Fig. 3.6 [3]. After about 120 hours the samples with cracks (red, green and purple lines in Fig. 3.6) present larger dissolution rates than the samples without cracks (blue line in Fig. 3.6). This indicates that additional hydration occurs in the paste adjacent to cracks. As a result, the paste becomes denser.

Fig. 3.6 shows that with the increase of the crack width the dissolution rate of unhydrated cement particles in the paste adjacent to cracks is hardly affected by the crack width. That implies that the crack width has little effect on densification of the paste adjacent to cracks.

[2] HYMOSTRUC 3D is a computer-based model for simulating the hydration and the microstructure development of Portland cement pastes.

[3] In the autogenous self-healing model the dissolution rate of small cement particles is higher than that of large cement particles (effect of difference in specific surface areas). After around 120 hours most of the small cement particles are dissolved, which leads to a sudden drop of the dissolution rate of the uncracked smaple (blue curve). At around 280 hours the dissolution rate of the cracked samples (red, green and purple lines) slightly increases. This is because the precipitation of the ions becomes faster than the dissolution of the cement particles, which accelerates the dissolution rate of the cement particles.

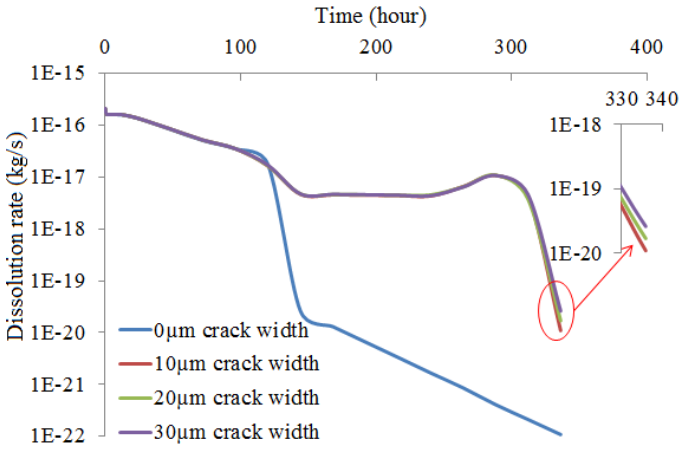

Figure 3.6: Simulated dissolution rate of the unhydrated cement in the samples with different crack widths (water-cement ratio=0.50)[Simulations performed by Jiayi Chen [16]]

3.5. HYDRATION AND STRENGTH INCREASE TRIGGERED BY CRACKS

3.5.1. CONTINUOUS/NORMAL HYDRATION AND STRENGTH INCREASE

In a load-free paste specimen (reference specimen), hydration continues over time (continuous/normal hydration). In this study, Eq. 3.1 [163] is adopted to describe the hydration kinetics of cement in plain cement paste:

$$\alpha(t) = \alpha_u \cdot e^{-(\frac{b}{t})^{\beta}} \tag{3.1}$$

where α is the degree of hydration; b and β are empirical constants, related to the chemical composition and particle size distribution of the cement and independent of the water-cement ratio [163]; t is the age of the paste; α_u is ultimate degree of hydration, which is strongly dependent on the water-cement ratio. It can be approximated with Eq. 3.2 [164]:

$$\alpha_u = \frac{1.031 \cdot w/c}{0.194 + w/c} \tag{3.2}$$

The degree of hydration of the cement determines many properties of concrete/paste, such as porosity and strength. A linear relationship between the strength and degree of hydration has been reported by many researchers [162, 165–167]:

$$f_c[\alpha(t)] = f_{c,max} \frac{\alpha(t) - \alpha_0}{1 - \alpha_0} \tag{3.3}$$

where $f_{c,max}$ is the fictitious maximum strength in case of complete hydration and α_0 is the critical degree of hydration below which the strength is zero. These two are constants, which vary with the water-cement ratio [164]. This linear relationship is shown schematically in Fig. 3.7.

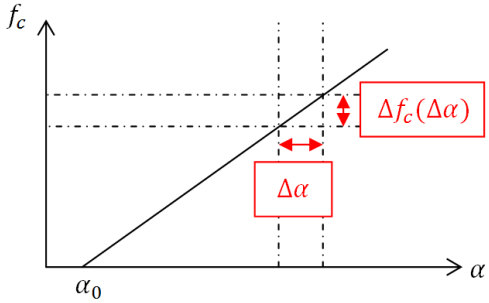

Figure 3.7: Relationship between degree of hydration and strength for a mixture with an arbitrary w/c

3.5.2. ADDITIONAL HYDRATION TRIGGERED BY MICRO-CRACKS AND EXTRA STRENGTH INCREASE

RELATIONSHIP BETWEEN THE ADDITIONAL OVERALL DEGREE OF HYDRATION AND THE NUMBER OF MICRO-CRACKS

In Section 3.4 a self-healing mechanism has been proposed to explain the extra increase in strength of concrete under sustained load. This extra increase in strength is assumed to originate from additional hydration in the paste adjacent to the cracks.

It is assumed that during time step Δt_i the number of micro-cracks appearing in the paste specimen is n_i (see Fig. 3.8a). For *each* micro-crack (or the jth crack[4], additional hydration occurs in the paste adjacent to this crack and the additional degree of hydration within time interval Δt_i is $\Delta\alpha_{add,j}$ (see Fig. 3.8b). The additional overall degree of hydration of the paste adjacent to n_i micro-cracks formed within Δt_i is $\Delta\alpha_{add,i}$ (see Fig. 3.9b). It follows:

$$\Delta\alpha_{add,i} = \Delta\alpha_{add}(\Delta t_i) = n_i(\Delta t_i) \cdot \frac{V_{ac,p,j}}{V_p} \cdot \Delta\alpha_{add,j} \tag{3.4}$$

in which V_p, $V_{ac,p,j}$ and $\Delta\alpha_{add,j}$ will be explained in detail after Eq. 3.6. If the total number of micro-cracks occurring in the paste specimen during the loading period $(t_r - t_0)$ is $N = \sum_{i=0}^{r} n_i$ (see Fig. 3.9a), the total additional overall degree of hydration caused by these N micro-cracks is $\Delta\alpha_{add,tot} = \sum_{i=0}^{r} \Delta\alpha_{add,i}$ (see Fig. 3.9b). It can be calculated with:

$$\Delta\alpha_{add,tot} = \sum_{i=0}^{r} \Delta\alpha_{add,i} = \frac{V_{ac,p,j}}{V_p} \cdot \Delta\alpha_{add,j} \cdot \sum_{i=0}^{r} n_i = \frac{V_{ac,p,j}}{V_p} \cdot \Delta\alpha_{add,j} \cdot N \tag{3.5}$$

Effect of overlap of paste adjacent to the cracks

It can be seen from Eq. 3.5 that the larger the number of micro-cracks the larger the total additional degree of hydration can be, provided that the adjacent-to-crack paste

[4] In the following text and chapters the jth crack refers to *any arbitrary* crack. Accordingly, $\Delta\alpha_{add,j}$ refers to the additional degree of hydration of the paste adjacent to *any* crack and $V_{RP,add,j}$ is the reaction product produced during the additional hydration of the paste adjacent to *any* crack, which is available for filling up the crack and densification of the paste adjacent to the crack.

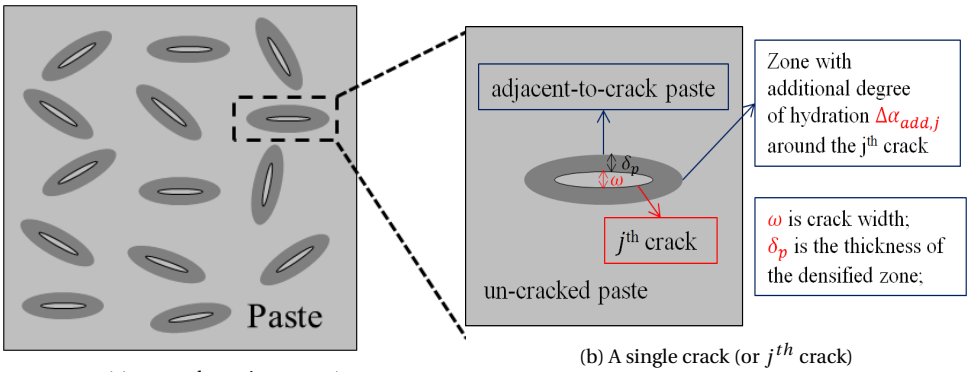

(a) n_i cracks at time step $\triangle t_i$

(b) A single crack (or j^{th} crack)

Figure 3.8: Cracked paste specimen and densification of the paste adjacent to the cracks at the end of time step $\triangle t_i$

zones do not overlap. Hence, the total additional degree of hydration is proportional to the number of micro-cracks, i.e. damage degree[5]. Fig. 3.10 presents two identical paste specimens (each consisting of four identical unit areas) with different damage degrees. The paste specimen with a large damage degree (Fig. 3.10b) will have a higher total additional degree of hydration than the paste specimen with a low damage degree (Fig. 3.10a). If the pastes adjacent to the micro-cracks overlap, the crack density[6] (i.e. the number of micro-cracks per unit area) increases in the paste specimen (see Fig. 3.11b). For two identical paste specimen with same damage degree (i.e. same number of micro-cracks), the paste specimen with a high crack density (Fig. 3.11b) has a smaller total additional degree of hydration than the paste specimen with a low crack density (Fig. 3.11a). Once overlap occurs, the total additional degree of hydration is not proportional to the number of micro-cracks and Eq. 3.5 *overestimates* the total additional degree of hydration. If the percentage overlap area of the paste adjacent to N cracks is assumed to be r_{ol}, Eq. 3.5 can be transformed into:

$$\triangle\alpha_{add,tot} = \frac{V_{ac,p,j} \cdot N \cdot (1 - r_{ol})}{V_p} \cdot \triangle\alpha_{add,j} \tag{3.6}$$

The parameters in Eq. 3.5 and 3.6 are explained as follows:

- V_p is the volume of the paste specimen (unit: mm^3 [in 3D] or mm^2 [in 2D]). Although the paste deforms under sustained load and the volume decreases, the volume change within the loading period $(t - t_0)$ is very small compared to the initial volume. Therefore, V_p is considered constant.
- $V_{ac,p,j}$ is the volume of the densified zone (unit: mm^3 [in 3D] or mm^2 [in 2D]), which is a function of the thickness of the densified zone adjacent to each crack

[5]Studied in detail in Chapter 4. Damage degree can be defined the number of micro-cracks per specimen with a certain size (in this research the size of specimen is $100 \times 100 mm^2$). In the lattice model introduced in Section 3.7 damage degree can be defined as the ratio of the broken beams (i.e. micro-cracks) to the total number of beams.

[6]Studied in detail in Chapter 4.

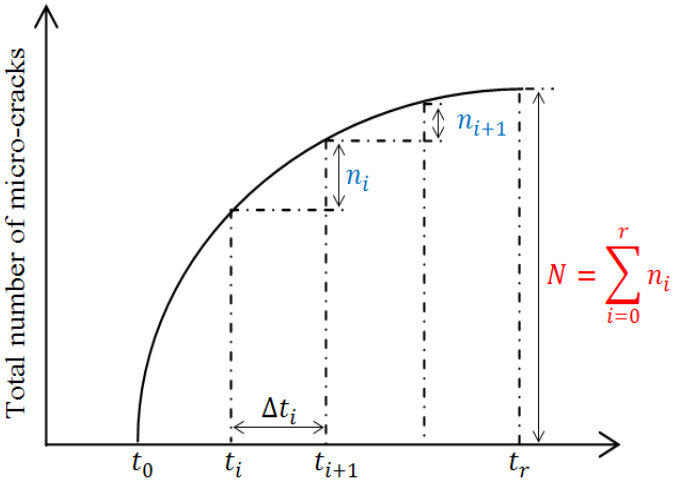

(a) Total number of micro-cracks over time [a]

[a] According to the experiments from Rossi [9], the creep strain is proportional to the total number of acoustic events. It is known that creep rate decreases with time. This linear relationship implies that the rate of micro-cracking (i.e. the number of micro-cracks per time step) decreases with time.

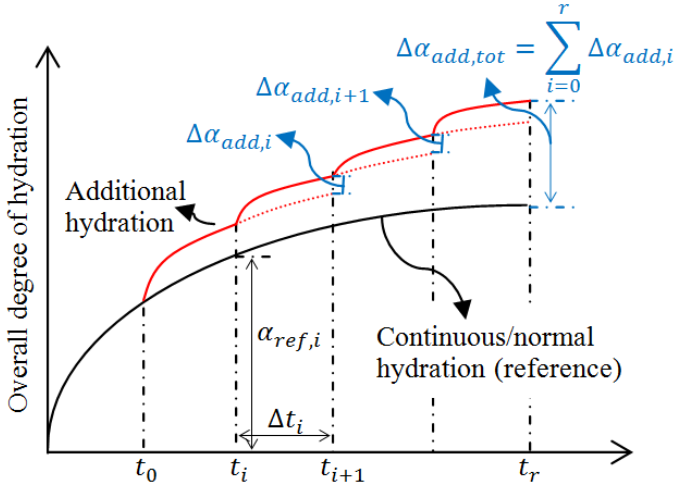

(b) Overall degree of hydration over time

Figure 3.9: Influence of micro-cracks on the overall degree of hydration (conceptual)

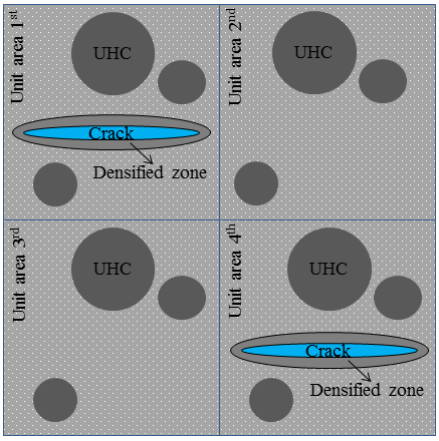

(a) Paste specimen with small damage degree

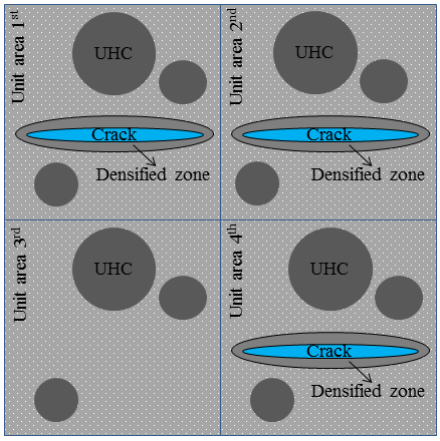

(b) Paste specimen with large damage degree

Figure 3.10: Damage degree in two identical paste specimen: small and large damage degree

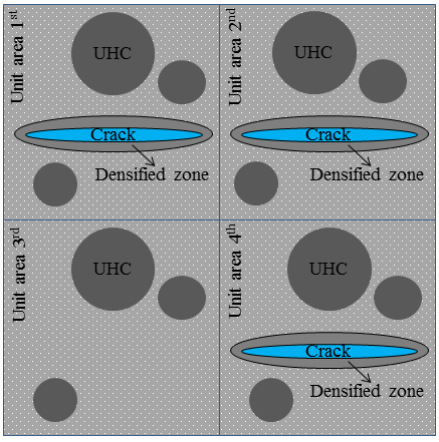

(a) Paste specimen with low crack density

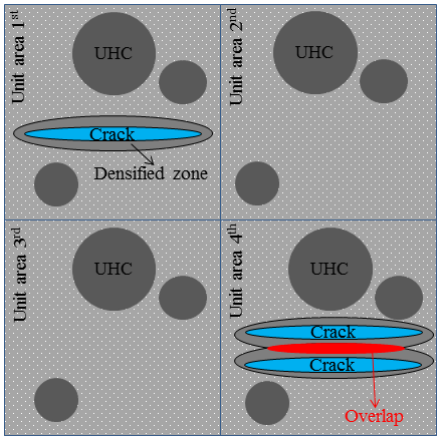

(b) Paste specimen with high crack density

Figure 3.11: Crack density in two identical paste specimen: low and high crack density

(δ_p) and the length of the crack (see Fig. 3.8b). δ_p is supposed to be related to the diffusion coefficient. Ions diffuse into the capillary pores of the paste adjacent to the crack and start to precipitate once the ion concentration in those pores is high enough. Consequently, the thickness of the densified zone (δ_p) gradually increases and, at the same time, the capillary porosity decreases. With decreasing capillary porosity the ion diffusivity decreases [168]. Finally the capillary porosity of the densified zone is so low that the diffusion of ions ceases. Then δ_p is not increasing anymore, i.e. reaches its maximum. In this research, it is assumed that δ_p reaches its maximum within time step Δt_i and it remains constant afterwards. In this study δ_p and $V_{ac,p,j}$ are considered as unknowns and will be determined in

Section 3.8.3.

- $\triangle\alpha_{add,j}$ is the additional degree of hydration of the paste adjacent to any crack within time interval $\triangle t_i$. In reality the amount of unhydrated cement decreases over time. Therefore, $\triangle\alpha_{add,j}$ at time step $\triangle t_i$ will be larger than that at the next time step $\triangle t_{i+1}$. In this research, however, $\triangle\alpha_{add,j}$ is assumed to be independent of the moment at which it occurs, i.e. $\triangle\alpha_{add,j}(\triangle t_i) = \triangle\alpha_{add,j}(\triangle t_{i+1})$=constant[7]. $\triangle\alpha_{add,j}$ is assumed to be independent of the number of micro-cracks and dependent on paste properties (e.g. water-cement ratio). It could be determined with numerical simulations (e.g. using the model in [16]) or experiments [14]. In this chapter its value for concrete with a water-cement ratio of 0.50 is deduced from the relationship between the strength development and increase of degree of hydration[8]. This value of $\triangle\alpha_{add,j}(w/c = 0.50)$ is then taken as a reference. For concretes with other water-cement ratios, $\triangle\alpha_{add,j}$ is estimated with Eq. 3.7 [9], viz.:

$$\triangle\alpha_{add,j}(wcr) = \frac{V_{uhc,i}(wcr)}{V_{uhc,i}(wcr_0)}\triangle\alpha_{add,j}(wcr_0) \tag{3.7}$$

where wcr is the water-cement ratio of the mixture in view and $wcr_0 = 0.50$ in this research. $V_{uhc,i}$ is the volume of unhydrated cement (uhc) in the paste specimen at time t_i. It follows:

$$V_{uhc,i}(wcr) = (1 - \alpha_{ref,i}) \cdot V_{uhc,0}(wcr) \tag{3.8}$$

where $\alpha_{ref,i}$ is the reference degree of hydration at t_i (see Fig. 3.9b) of uncracked specimen and $V_{uhc,0}$ is the volume of unhydrated cement in the mixture at the initial stage:

$$V_{uhc,0}(wcr) = \frac{V_p}{1 + \frac{w}{c} \cdot \frac{\rho_c}{\rho_w}} \tag{3.9}$$

where ρ_c is specific mass of cement $[kg/m^3]$ and ρ_w is density of water $[kg/m^3]$. Inserting this equation to Eq. 3.8 yields:

$$V_{uhc,i}(wcr) = (1 - \alpha_{ref,i}) \cdot \frac{V_p}{1 + \frac{w}{c} \cdot \frac{\rho_c}{\rho_w}} \tag{3.10}$$

VOLUME OF THE REACTION PRODUCTS PRODUCED DURING ADDITIONAL HYDRATION IN PASTE ADJACENT TO THE jth CRACK AND THE EXTRA STRENGTH INCREASE

During the additional hydration of the cement adjacent to a crack, additional reaction products are produced. If the amount of additional reaction products $V_{RP,add,j}$ is enough

[7] For young hydrating cement this approach will not apply, while for more mature paste it is expected to work.

[8] For concrete with a water-cement ratio of 0.50 $\triangle\alpha_{add,j}$ is back-calculated with Eq. 3.5 and 3.6, where $\triangle\alpha_{add,tot}$ is deduced from the relationship between the 30-year strength and degree of hydration (see Section 3.8.2 and 3.8.3).

[9] Eq. 3.7 is used in Section 4.4.3 and 5.4.3. Note that this equation is valid only when the hydration rate at time t_i is approximately the same for concretes with different water-cement ratios, i.e. when the degree of hydration almost reaches its ultimate value α_u (e.g. curves in Fig. 4.11 are more or less horizontal at around 30 years). In this case, $\triangle\alpha_{add,j}$ is proportional to the amount of unhydrated cement $V_{uhc,i}$. $\triangle\alpha_{add,j}$ is then higher for concrete with a low water-cement ratio than for concrete with a high water-cement ratio.

to fill up the crack and also densify the paste adjacent to the crack, an extra increase in strength can be generated. Otherwise, no extra increase in strength can be achieved. The amount of additional reaction products $V_{RP,add,j}$ produced during the additional hydration is calculated as follows.

According to literature [162], the volume of reaction product is 2.2 times larger than the volume of hydrated cement. 45% of the reaction product is used to fill up the volume of hydrated cement. 55% is available for self-healing of the crack and densification of the paste adjacent to the crack. Thus, the volume of reaction products produced during the additional hydration of the paste adjacent to any crack within time interval $\triangle t_i$, which is available for filling up the crack and densifying the paste adjacent to the crack, follows from:

$$\begin{aligned} V_{RP,add,j}(\triangle t_i) = 1.2 \cdot V_{hyc,add,j}(\triangle t_i) &= 1.2 \cdot \triangle\alpha_{add,j} \cdot \frac{V_{ac,p,j}}{V_p} \cdot V_{uhc}(t_i) \\ &= 1.2 \cdot \triangle\alpha_{add,j} \cdot \frac{V_{ac,p,j}}{V_p} \cdot V_{uhc,i} \end{aligned} \tag{3.11}$$

where $V_{hyc,add,j}$ is the volume of additional hydrated cement in the paste adjacent to any crack. Inserting Eq. 3.10 in Eq. 3.11:

$$\begin{aligned} V_{RP,add,j}(\triangle t_i) &= 1.2 \cdot \triangle\alpha_{add,j} \cdot \frac{V_{ac,p,j}}{V_p} \cdot [1 - \alpha_{ref}(t_i)] \cdot \frac{V_p}{1 + \frac{w}{c} \cdot \frac{\rho_c}{\rho_w}} \\ &= 1.2 \cdot \triangle\alpha_{add,j} \cdot V_{ac,p,j} \cdot (1 - \alpha_{ref,i}) \cdot \frac{1}{1 + \frac{w}{c} \cdot \frac{\rho_c}{\rho_w}} \end{aligned} \tag{3.12}$$

where $\alpha_{ref,i}$ is the reference degree of hydration α_{ref} at time t_i (see Fig. 3.9b). As aforementioned, $\triangle\alpha_{add,j}$ is assumed to be constant through the whole time period. Then, the volume of reaction product produced during the additional hydration of the paste adjacent to any crack within time interval $\triangle t_i$, $V_{RP,add,j}$ in Eq. 3.12, depends on the reference degree of hydration at time t_i ($\alpha_{ref,i}$)[10].

If the volume of the reaction products is larger than the volume of the crack ($V_{c,j}(\omega)$), i.e. $V_{RP,add,j} > V_{c,j}(\omega)$, the reaction products can fill up the crack, while some products are left to densify the paste adjacent to the crack (see Fig. 3.12a). Then it is reasonable to assume that some extra strength can be generated ($\triangle\alpha \rightarrow \triangle f(\triangle\alpha)$). If $V_{RP,add,j} \leq V_{c,j}(\omega)$, it is assumed that the entire amount of reaction products will be used to fill up a part of (or the whole) volume of the crack and no reaction products are left to densify the paste adjacent to the crack (see Fig. 3.12b). Then any extra strength increase cannot be achieved[11]. This will be further discussed in Section 3.7.3 and 3.8.3.

[10] In Section 3.8.3 $V_{RP,add,j}$ is calculated with the maximum value of $\alpha_{ref,i}$ (i.e. α_{ref} at the end of loading period).

[11] This is further discussed in Section 3.7.3. This section section presents the modified lattice model. In the model the strength recovery degree of a crack is described by κ ($0 \leq \kappa \leq 1$, Eq. 3.25 and 3.26). An effective additional hydration of the paste adjacent to a crack, $\triangle\alpha_{add',j}$, is defined to describe the extra strength increase (Eq. 3.27 and 3.28.)

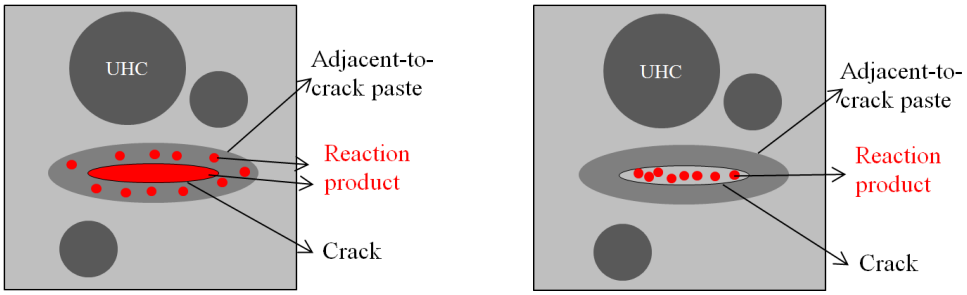

(a) $V_{RP,add,j} > V_{c,j}(\omega)$ (b) $V_{RP,add,j} \leq V_{c,j}(\omega)$

Figure 3.12: (a) The reaction products can fill up the crack and there are some left to densify the paste adjacent to the crack; (b) The reaction products can fill up a part of or whole volume of the crack and no reaction products are left to densify the paste adjacent to the crack

3.6. CREEP HYPOTHESIS

3.6.1. ACTIVATION ENERGY CONCEPT

In Chapter 2, a brief summary of the existing theories of creep was presented. Although many creep theories have been proposed, the real mechanism for creep is still under discussion. When searching the cause of creep one should realize that creep is not a specific feature only of concrete, but a phenomenon that occurs in all other materials as well [21]. Creep should then be possible to be traced back to one physical cause with universal validity that describes time-dependent deformation as a function of the prevailing stress in the material. Any additional factor/mechanism should not be considered as a real source of creep, but as a factor that may cause a change of the state of stresses to a certain extent and may, as such, affect the time-dependent deformations of materials and structures at macroscale [21]. The activation energy concept, which is widely-applied for creep in metals, polymers and ceramics, etc., seems promising as the basic mechanism for creep of concrete.

The activation energy concept was first proposed by Arrhenius in 1889 to describe the influence of temperature on the rate of inversion of sucrose. The concept that certain reactions need an activation energy to proceed has been considered fundamentally valid for describing the temperature dependency of rate process of numerous materials, including cementitious materials [169]. In a creeping material, it is assumed that there are numerous "creep centres" whose initial energy states vary. In the activation energy concept, these energy centres are characterised by their activation energy and activation volume [20, 169]. Initially, these "creep centres" are kept in stable positions. Once an external load or a higher temperature is applied, the "centres" with lower energy states, which need only a small amount of additional energy, will "jump" to another place and be equipped with a higher level of energy. Gradually more and more "centres" become qualified to "jump" and consequently the probability that a "centre" will get sufficient additional energy to move from its equilibrium position will decrease. At macro level, this will be observed as a gradual decrease of the creep rate. The mathematical form of the activation energy concept is presented with Eq. 3.13 [20], viz.:

$$\dot{\epsilon}_{cr} = C \cdot \exp(-\frac{Q}{RT}) \cdot \sinh(d\sigma) \tag{3.13}$$

where C is a constant; Q is the activation energy [J/mol]; σ is stress [MPa]; T is temperature [K]; R is gas constant [8.31 $J \cdot mol^{-1} \cdot K^{-1}$] and d is related to the activation volume[12]. For low stress levels, the integral of Eq. 3.13 can be simplified into Eq. 3.14 [20, 21], viz.:

$$\epsilon_{cr} = a \cdot t^n \cdot \sigma \tag{3.14}$$

where a is an empirical ageing factor, which is highly dependent on the age at loading, the initial water-cement ratio, type of cement and moisture content [20, 172]. t is loading duration. n is a proportionality factor, generally $n = 0.3$ (Section 4.4.1). The derivative of Eq. 3.14 is given as follows:

$$\dot{\epsilon}_{cr} = a \cdot n \cdot t^{-m} \cdot \sigma \tag{3.15}$$

where m is also a proportionality factor, which follows $m = 1 - n = 0.7$. In this research the activation energy concept is considered as the "real mechanism" for creep. The creep deformation calculated with this concept (Eq. 3.14) is called "real creep".

3.6.2. FACTORS THAT INFLUENCE THE "REAL CREEP"

With the activation energy concept creep, as a pure material property, can be considered to have no direct relation with other sources of time-dependent deformation as long as the latter would not influence the state of stress (σ in Eq. 3.15) in a body under consideration. Any change of the actual stress by any other source will affect the real creep process and result in changes of time-dependent deformations. Taking an arbitrary body as an example, the following phenomena will affect the state of stress and lead to time-dependent deformations [21]:

(1) Real creep: it is defined as deformation in excess of the elastic deformation and directly related to the applied stress; it can be calculated with Eq. 3.15.
(2) Shrinkage or swelling: it induces internal stresses. The stresses will lead to or affect "real creep".
(3) Maturing creep: it is related to the continuous hydration of cement; new hydration products can take a share of load while previously formed hydration products are less stressed. This will reduce the "real creep" [44].
(4) Micro-cracking: it influences the stress distribution; the cracked parts cannot carry load and other parts are more stressed. This will increase the "real creep".
(5) Self-healing: it influences stress distribution; after self-healing the healed cracks and the additional hydration products can take a share of the load; this affects the "real creep".
(6) Time-dependent deformations resulting from changes of the hydration products due to: e.g. carbonation.

How continuous hydration, micro-cracking and self-healing affect/modify the real creep process is depicted schematically in Fig. 3.13. Due to continuous hydration new hydration products can gradually take a share of the external load and the original hydration products are less stressed. The observed creep strain will then be lower (black

[12] The activation volume is related to the mechanical work involved in the creep process [170]. The thermodynamic significance of the activation energy and activation volume has been discussed by Gibbs [171].

line in Fig. 3.13) compared to the "real creep". When micro-cracking occurs, the cracked parts cannot carry load any more and other parts are more stressed. The observed deformation (dashed blue line in Fig. 3.13) is larger than the "real creep" as calculated with Eq. 3.15. If self-healing is taken into account (Section 3.4), the hydration products produced during the additional hydration in the paste adjacent to the cracks can take an extra share of the external load other than the hydration products produced during continuous hydration. Thus the observed creep strain (red line in Fig. 3.13) is lower than that with the effect of continuous hydration. The effects of continuous hydration, micro-cracking and self-healing on the long-term creep of concrete will be modelled using a lattice model presented in the next section.

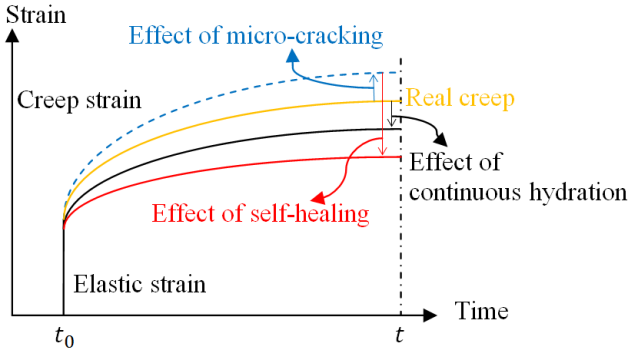

Figure 3.13: Effect of continuous hydration, micro-cracking and self-healing on the creep deformation of concrete loaded at a constant stress (real creep can be calculated with Eq. 3.15)

3.7. MODIFIED LATTICE MODEL: DESCRIPTION OF THE MODEL

LATTICE models are widely used for modelling the fracture process of heterogeneous materials. The material is schematised as a lattice network of Timoshenko beam elements, which can transmit axial forces, shear forces, bending moments and torsional moments, as shown in Fig. 3.14.

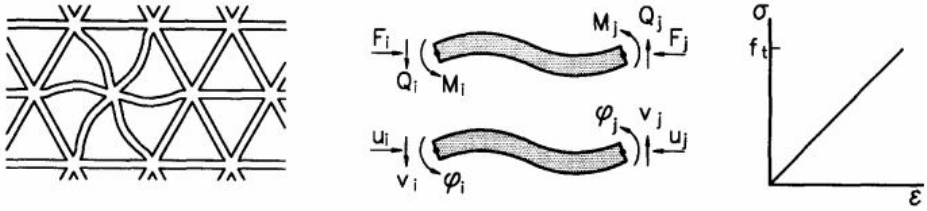

Figure 3.14: (left) Regular triangular lattice of beams, (middle) external forces and deformations on a single beam element, and (right) stress-strain relation for an element [17]

In this study, the lattice model developed by Schlangen [17] and Qian [35], which is mainly used for fracture simulations, is modified in order to take creep (Section 3.7.1), continuous hydration (Section 3.7.2) and self-healing (Section 3.7.3) of individual beams into consideration.

In order to reduce computation time, the numerical simulations are performed on 2D specimens. In the 2D lattice approach, the meso-structure of concrete is considered as a composite consisting of three phases: mortar, interface (bond) and aggregate. Aggregate particles are modelled as disks surrounded by an interface and embedded in the bulk mortar matrix. The procedures for discretization of the meso-structure, including pixel generation, node placement, lattice generation and overlay procedure, are shown in Fig. 3.15.

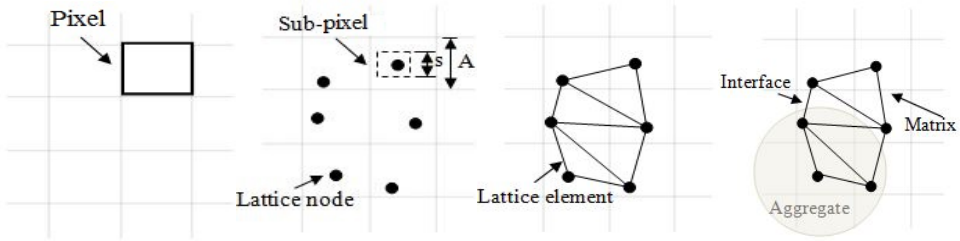

(a) Pixel generation (b) Node placement (c) Lattice generation (d) Overlay procedure

Figure 3.15: Schematics of the generation of meso-structure of concrete

In the lattice model, the mechanical properties of the beams are represented by four parameters: the compressive strength f_c, the tensile strength f_t, the elastic modulus E and the shear modulus G. The tensile strength f_t is usually taken as $0.1 f_c$ [17]. The shear modulus can be calculated with Eq. 3.16, viz.:

$$G = \frac{E}{2(1+\upsilon)} \tag{3.16}$$

where υ is the poisson's ratio.

Creep of individual beam

It is assumed that only the mortar and bond beams are creeping, while the aggregate beams are assumed to behave linear elastically. The creep is modelled using the activation energy concept (Eq. 3.13 and Eq. 3.15). Creep strains $\epsilon_{cr,i+1}$ at time t_{i+1} are obtained by solving Eq. 3.15 based on Euler's method [173], viz.:

$$\epsilon_{cr,i+1} = a \cdot n \cdot (t_i + \triangle t_i)^{-m} \cdot \sigma_i \cdot \triangle t_i + \epsilon_{cr,i} \tag{3.17}$$

where σ is the stress in a lattice beam.

Strength of individual beam resulting from continuous hydration

If continuous hydration of cement is considered, the strength and elastic modulus of the mortar and bond beams increase with time. Based on Eq. 3.3, the compressive strength f_c at time t_{i+1} of the mortar and bond beams can be calculated with Eq. 3.18:

$$f_{c,i+1} = f_c[\alpha(t_{i+1})] = f_{c,max}\frac{\alpha(t_i + \triangle t_i) - \alpha_0}{1 - \alpha_0} \tag{3.18}$$

where α is (reference) degree of hydration of the mortar and bond beam, which is calculated with Eq. 3.1 for $t = t_{i+1} = t_i + \triangle t_i$. The elastic modulus E of the mortar and bond

beams can be calculated as [174, 175]:

$$E_{i+1} = E[\alpha(t_{i+1})] = c_1 \cdot \{f_c[\alpha(t_{i+1})]\}^{c_2} \tag{3.19}$$

where c_1 and c_2 are material parameters which depend on w/c and cement type.

In the following subsections creep, continuous hydration and self-healing are incorporated in the lattice model, as described in subsection 3.7.1, 3.7.2 and 3.7.3. Subsection 3.7.4 summarizes the modelling procedure for the effect of continuous hydration, micro-cracking and self-healing on creep. The model, extended with options for dealing with creep, continuous hydration and self-healing, is called the *modified lattice model*.

3.7.1. INCORPORATION OF CREEP IN THE LATTICE MODEL

In this section creep (Eq. 3.17) is incorporated in the lattice model. At the beginning of the first time step ($i = 0$; $t_0 = 0$; $\epsilon_{cr,0} = 0$), only an external load is present at the top of a concrete specimen and stresses are distributed among the beams. The stresses of the beams are calculated with Eq. 3.20 [13]:

$$\sigma_i = E_i \epsilon_i \quad (i = 0) \tag{3.20}$$

In the following time steps ($i > 0$), the stresses of the beams are calculated with Eq. 3.21:

$$\sigma_{i+1} = E_{i+1}(\epsilon_{i+1} - \epsilon_{cr,i+1}) \quad (i > 0) \tag{3.21}$$

Then the creep strains of the mortar and bond beams $\epsilon_{cr,i+1}$ are calculated with Eq. 3.17 and the creep strains of beams are converted into axial forces $f_{cr,i+1}$ according to:

$$f_{cr,i+1} = \epsilon_{cr,i+1} \cdot E_{i+1} \cdot A \tag{3.22}$$

where A is the area of cross section of the beams. The axial forces $f_{cr,i+1}$ are applied to the mortar and bond beams, as shown in Fig. 3.16, together with the constant external force applied to the whole concrete specimen. Due to the heterogeneity of the material,

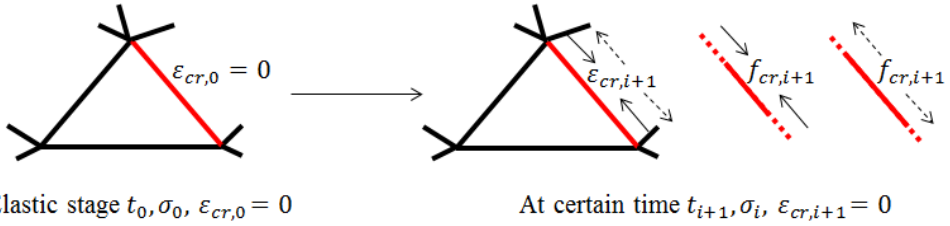

Figure 3.16: Creep deformation and local axial force of an individual mortar or bond beam (Arrow on the right side means that creep can be tensile or compressive creep, depending on the sign of stress in the beam)

local stress concentrations will occur. Once the stress in a beam exceeds the strength of that beam, the beam is considered to be broken and will be removed from the lattice network and its axial force will be released. Other beams, initially connected to the broken

[13] This equation will also be used to calculate the stresses of the beams during the stress redistribution step (see flow chart of Fig. 3.18)

beams, are then less restrained. The stresses will be redistributed among the remaining unbroken beams. In the model, the stress redistribution is realized by executing one more calculation step without changing the time step, while keeping the external load at the top of the specimen (the axial forces $f_{cr,i+1} = 0$ in Fig. 3.16). The stress redistribution will result in an increase of the stress in the remaining beams. Then the creep strain calculated from these stresses in the next time step will increase. This will further influence the development of micro-cracking. Finally, an overall deformation, taking the interaction between creep and micro-cracking into account, is obtained.

If continuous hydration is taken into account during the interaction between creep and micro-cracking, the strength and elastic modulus of the beams are updated at each time step using Eq. 3.18 and 3.19. Otherwise $E_i = E_0$ and $f_{c,i} = f_{c,0}$. The modelling procedure for the effect of micro-cracking on creep with and without consideration of continuous hydration is shown in the flow chart of Fig. 3.18 in Section 3.7.4.

3.7.2. INCORPORATION OF CONTINUOUS HYDRATION IN THE LATTICE MODEL: EFFECT OF CONTINUOUS HYDRATION ON CREEP

As described in Section 3.3, continuous hydration of cement will result it an increase of the strength of the mortar and bond beams, and hence an increase of the strength of the concrete specimen. The stress-strength ratio decreases when concrete is loaded at a constant stress. Consequently, the creep strain is lower than in case continuous hydration does not occur. The modelling procedure for the effect of continuous hydration on creep of concrete is shown in the flow chart of Fig. 3.18.

3.7.3. INCORPORATION OF SELF-HEALING IN THE LATTICE MODEL: EFFECT OF SELF-HEALING ON CREEP

In Section 3.4 self-healing of cracks and densification of the paste adjacent to the cracks has been proposed to explain the *extra* increase in strength of concrete under sustained load. If the stress in a beam exceeds the strength of the beam in the lattice model, this beam is taken out from the lattice network. This broken beam represents a crack in the paste (the jth crack in Fig. 3.17a and the red beam in Fig. 3.17b). In the lattice network the beams, which are connected to the broken beam, are considered to represent the paste adjacent to the crack (dark grey beams in Fig. 3.17b). Therefore, in the lattice network there are three types of beams:

- Broken beam (red beam in Fig. 3.17b) represents a crack;
- Beams which are connected to the broken beam (dark grey beams in Fig. 3.17b) represents the paste adjacent to the crack;
- Other beams (light grey beams in Fig. 3.17b) represent the un-cracked paste.

The strength of the un-cracked paste continues to increase due to continuous hydration of the bulk paste. Once a crack occurs in the paste, additional hydration will occur in the paste adjacent to the crack according to the self-healing mechanism (Section 3.4). The reaction products will fill up (a part of) the crack and might also densify the paste adjacent to the crack. Then the strength of the paste could be recovered and the adjacent-to-crack paste could gain an extra strength. The evolution of the strength and elastic modulus of the three types of beams is then as follows:

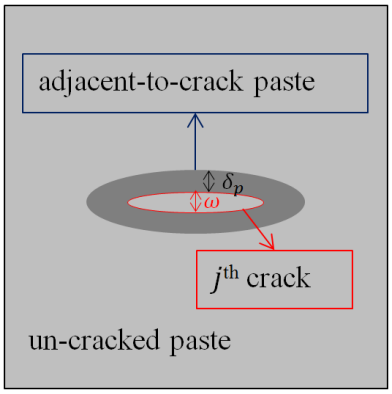

(a) Cement paste with a single crack

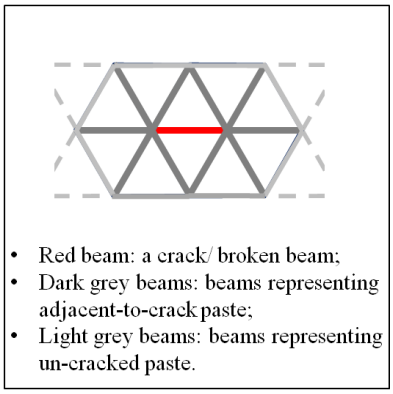

(b) Three types of beams in a lattice network

Figure 3.17: (a) Cement paste with a single crack (j^{th} crack); (b) Three types of beams in the matrix of a lattice network [Note: The lattice network in this figure represents a *paste* sample and it is assumed regular. Later, in the simulations the irregular lattice network will be generated to represent the concrete specimen consisting of mortar, bond and aggregate beams (see Fig. 3.20). The beams, which are connected to the broken beam, can include aggregate beams (see Fig. 3.36). The densification due to self-healing only applies to non-aggregate beams, which are connected to the broken beam.]

- The strength and elastic modulus of beams representing the un-cracked paste, resulting from the continuous hydration, follow Eq. 3.18 and 3.19.
- The strength $f_{c,hc}$ and elastic modulus E_{hc} of the broken beam, representing a crack, after self-healing follow from:

$$f_{c,hc,i+1} = \kappa \cdot f_c[\alpha(t_i)] = \kappa \cdot f_{c,max} \frac{\alpha(t_i) - \alpha_0}{1 - \alpha_0} \tag{3.23}$$

$$E_{hc,i+1} = \kappa \cdot E[\alpha(t_i)] = \kappa \cdot c_1 \cdot \{f_c[\alpha(t_i)]\}^{c_2} \tag{3.24}$$

where κ is a recovery degree of the strength and elastic modulus of the broken beam after self-healing. κ ranges from 0 to 1. If the reaction products produced during the additional hydration in the paste adjacent to any crack, $V_{RP,add,j}$ (Eq. 3.12), can fill up the whole crack $V_{c,j}(\omega)$, the strength is assumed to be fully recovered: $\kappa = 1$. If the reaction products with volume $V_{RP,add,j}$ can only fill up a part of the volume of the crack $V_{c,j}(\omega)$, then the strength is partly recovered: $0 < \kappa < 1$. Hence,

$$\kappa = 1 \quad \text{for} \quad V_{RP,add,j} > V_{c,j}(\omega) \tag{3.25}$$

$$\kappa = \frac{V_{RP,add,j}}{V_{c,j}(\omega)} \quad \text{for} \quad V_{RP,add,j} \leq V_{c,j}(\omega) \tag{3.26}$$

- The aforementioned two situations have been shown schematically in Fig. 3.12a and 3.12b. For these two situations, the *effective* additional degree of hydration of the paste adjacent to any crack, $\Delta\alpha_{add',j}$, follows:

$$\Delta\alpha_{add',j} = \frac{V_{RP,add,j} - V_{c,j}(\omega)}{V_{RP,add,j}} \cdot \Delta\alpha_{add,j} \quad \text{for} \quad V_{RP,add,j} > V_{c,j}(\omega) \tag{3.27}$$

$$\triangle\alpha_{add',j} = 0 \qquad \text{for} \quad V_{RP,add,j} \leq V_{c,j}(\omega) \tag{3.28}$$

The strength $f_{c,ac}$ and elastic modulus E_{ac} of beams which are connected to the broken beam (representing the adjacent-to-crack paste) after self-healing follow from:

$$f_{c,ac,i+1} = f_c[\alpha(t_i + \triangle t_i)] + f_c[\triangle\alpha_{add',j}(\triangle t_i)] \tag{3.29}$$

$$E_{ac,i+1} = E[\alpha(t_i + \triangle t_i)] + E[\triangle\alpha_{add',j}(\triangle t_i)] \tag{3.30}$$

The modelling procedure for the effect of self-healing on creep of concrete is shown in the flow chart of Fig. 3.18.

3.7.4. SUMMARY OF THE MODIFIED LATTICE MODEL

In Sections 3.7.1 to 3.7.3, the original lattice model has been modified to take creep, continuous hydration and self-healing into account. The flow chart in Fig. 3.18 presents the structure of the simulation programme. The programme stops when t_{i+1} exceeds the predefined time t_{pre} or the strain of the specimen $\epsilon_{cr,i+1}$ is larger than the critical strain ϵ_{cri} [14].

The important input parameters in the modified lattice model are:

- The empirical ageing factor a in Eq. 3.17 for calculating the creep strains;
- The evolution of strength and elastic modulus of the mortar and bond beams resulting from the continuous hydration, $f_c[\alpha(t)]$ and $E[\alpha(t)]$ (Eq. 3.18 and 3.19);
- The additional degree of hydration of the paste adjacent to any crack, $\triangle\alpha_{add,j}$ (needed in Eq. 3.27 to 3.30).

In the next section the aforementioned input parameters will be determined and the modified lattice model will be evaluated preliminarily.

3.8. PRELIMINARY EVALUATION OF MODIFIED LATTICE MODEL

3.8.1. CONCRETE SPECIMEN USED FOR EVALUATION OF MODIFIED LATTICE MODEL

NUMERICAL CONCRETE SPECIMEN AND MATERIAL PROPERTIES

The material characteristics of the concrete specimen used for a preliminary evaluation of the modified lattice model are listed in Table 3.3 (taken from Brooks' test [Section 3.2]). The concrete specimen is loaded at 14 days at a constant stress (stress level of 30% of 14-day compressive strength) and the loading duration is 30 years. During the whole loading period the specimen is stored in water at a temperature of $23 \pm 1\,^{\circ}C$.

The meso-structure of the numerical concrete specimen includes three phases: mortar, bond and aggregate. The dimension of the specimen is $100 \times 100 mm^2$, meshed at the resolution of 0.5mm/pixel. The aggregate is positioned randomly in the specimen and its particle size distribution complies with the Fuller's curve (see Fig. 3.19). The maximum aggregate diameter is 16mm. Aggregate particles with diameters smaller than 2mm are

[14] In the modified lattice model concrete fails and the simulation is terminated if the overall strain of concrete reaches a threshold value (or critical value) $\epsilon > \epsilon_{cri}$. The critical strain ϵ_{cri} is set at an axial strain of 1% [176, 177].

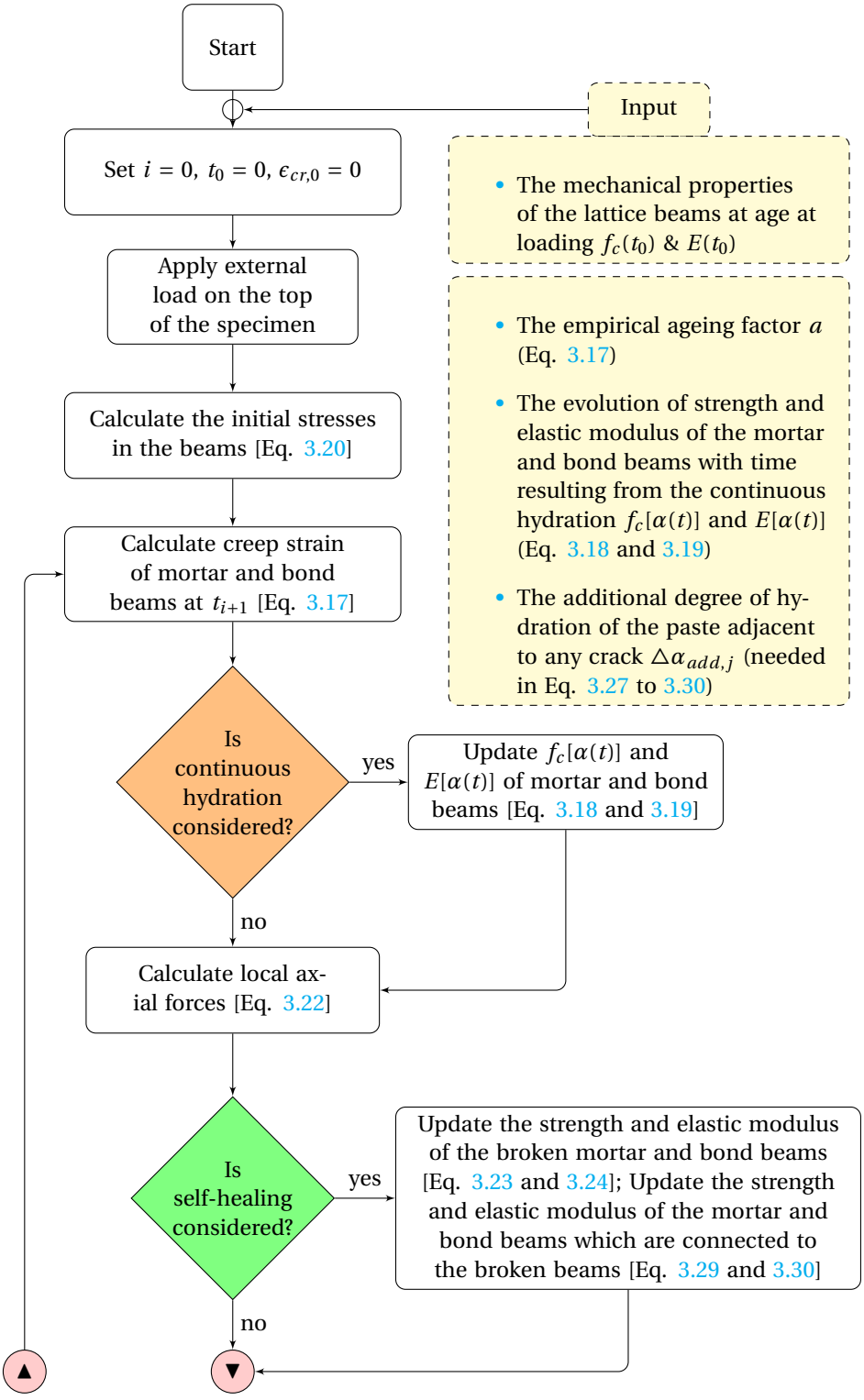
Start
Input
Set $i = 0$, $t_0 = 0$, $\epsilon_{cr,0} = 0$
• The mechanical properties of the lattice beams at age at loading $f_c(t_0)$ & $E(t_0)$
Apply external load on the top of the specimen
Calculate the initial stresses in the beams [Eq. 3.20]
• The empirical ageing factor a (Eq. 3.17)
• The evolution of strength and elastic modulus of the mortar and bond beams with time resulting from the continuous hydration $f_c[\alpha(t)]$ and $E[\alpha(t)]$ (Eq. 3.18 and 3.19)
• The additional degree of hydration of the paste adjacent to any crack $\Delta\alpha_{add,j}$ (needed in Eq. 3.27 to 3.30)
Calculate creep strain of mortar and bond beams at t_{i+1} [Eq. 3.17]
Is continuous hydration considered?
yes
Update $f_c[\alpha(t)]$ and $E[\alpha(t)]$ of mortar and bond beams [Eq. 3.18 and 3.19]
no
Calculate local axial forces [Eq. 3.22]
Is self-healing considered?
yes
Update the strength and elastic modulus of the broken mortar and bond beams [Eq. 3.23 and 3.24]; Update the strength and elastic modulus of the mortar and bond beams which are connected to the broken beams [Eq. 3.29 and 3.30]
no

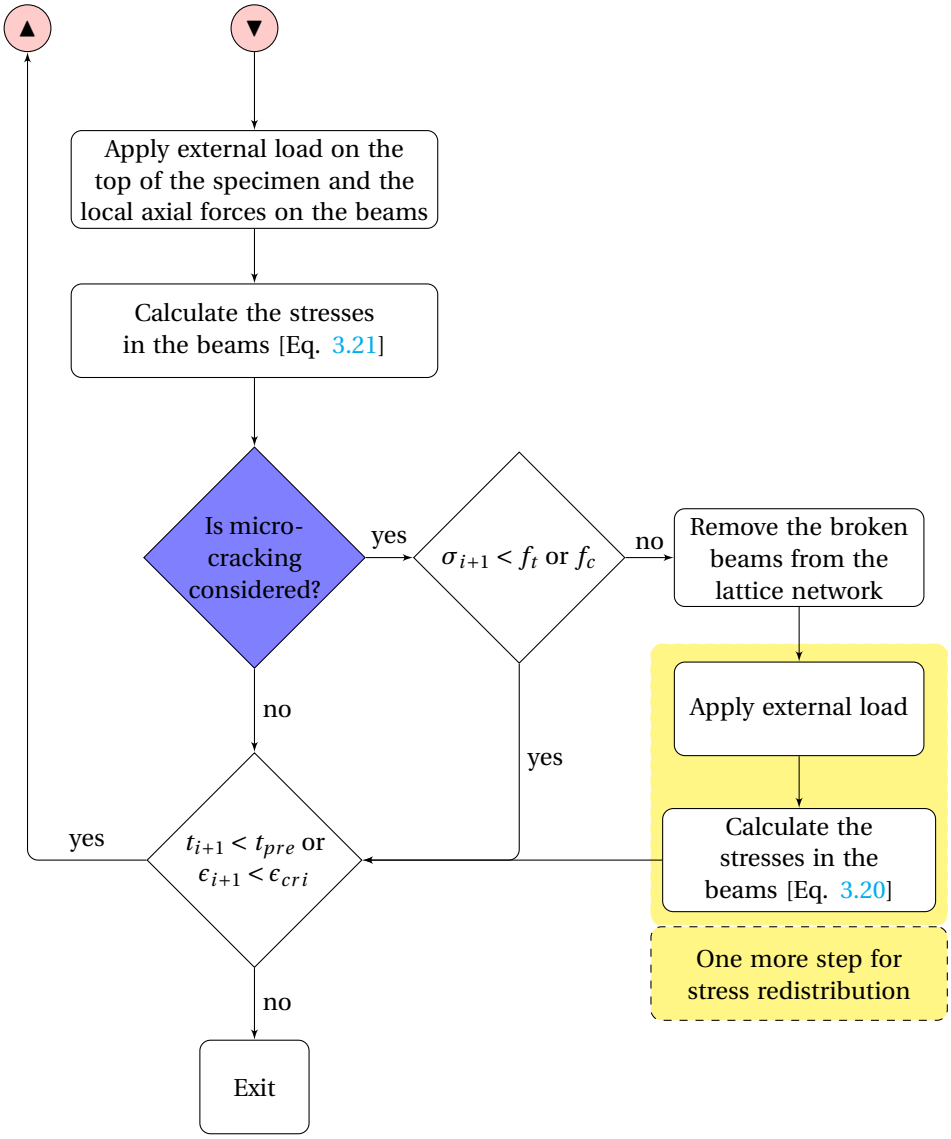

Figure 3.18: Flow chart: modelling procedure

Table 3.3: Material characteristics of the concrete specimen (taken from Brooks' test [Section 3.2])

w/c	Mix proportion by weight (C:S:A)[1]	Cement paste content by volume (%)	14-day		30-year	
			f_c [2] (MPa)	E [2] (GPa)	f_c (MPa)	E (GPa)
0.50	1:1.71:3.04	31.1	36.8	29.8	50.6	40.7

[1] C:S:A=Cement:Sand:Aggregate
[2] f_c=compressive strength of concrete; E=elastic modulus of concrete

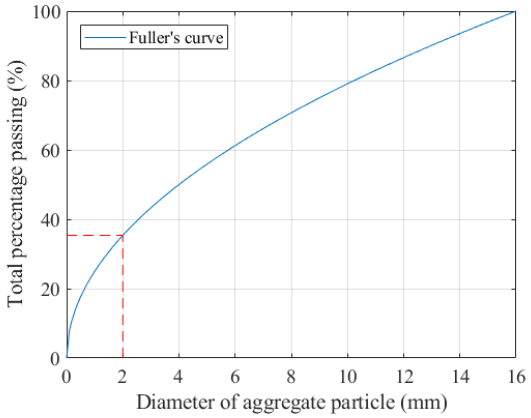

Figure 3.19: Fuller's curve for aggregate particle size distribution

excluded from the generated aggregate structures, since the aggregate particles should be two or three times larger than the mesh size (0.5mm) [17]. The distance between the centre of two particles is larger than the minimum distance $1.1 \times (d_1 + d_2)/2$ [15] suggested by Hsu [178]. The aggregate volume of particles with diameters larger than 2mm is 40% of the total 2D volume of the specimen. The final meso-structure of concrete specimen used for the evaluation is shown in Fig. 3.20.

The boundary conditions of the numerical specimen for the compressive strength and creep simulations are: nodes at the bottom are not allowed to translate in Y direction, but are allowed to translate in X direction and to rotate in XY direction; nodes at the top are allowed to translate in X and Y direction and to rotate in XY direction.

It is noted that the generated aggregate volume in the numerical concrete specimen is 40%, which is smaller than the experimental data (100% − 31.1% = 68.9%; see Table 3.3). This is because, as aforementioned, the aggregate particles with diameters smaller than 2mm are not placed in the numerical specimen. Aggregate particles with diameters smaller than 2mm are considered as fine aggregates and embedded in the cement paste, together forming the mortar phase (blue beams in Fig. 3.20). Then the volumes of the coarse aggregate and mortar (fine aggregate and cement paste) in the numerical concrete specimen (Fig. 3.20) are around 40% and 60% (25%+31%)[16], respectively.

[15] d_1 and d_2 are diameters of two aggregate particles
[16] As can be seen in Fig. 3.19, the total percentage of aggregate particles with diameters smaller than 2mm (fine aggregates) is around 35% of the total volume of the aggregate particles. Then the volume of fine aggregates

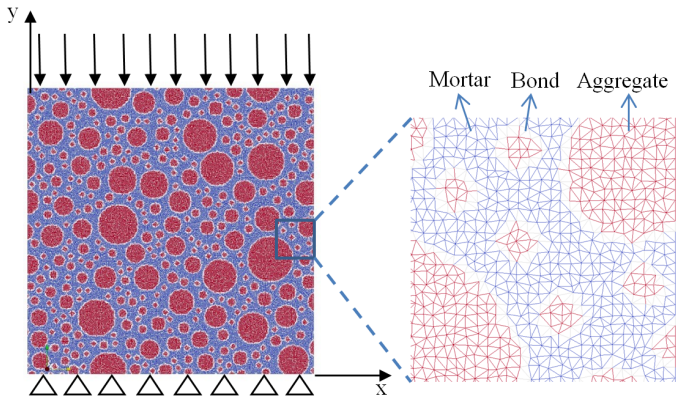

Figure 3.20: The meso-structure of the numerical concrete specimen with a water-cement ratio of 0.50

14-DAY MECHANICAL PROPERTIES OF LATTICE BEAMS: $f_c(t_0)$ & $E(t_0)$

The concrete specimen is loaded at 14 days. The input values for the 14-day mechanical properties of the mortar, bond and aggregate beams are listed in Table 3.4. It should be noted that the input values for the 14-day mechanical properties of the beams are estimated values in order to fit with the 14-day compressive strength and elastic modulus of the concrete specimen listed in Table 3.3. The estimations are based on theoretical equations or experimental data, as explained below.

Table 3.4: 14-day mechanical properties of the mortar, bond and aggregate beams (input for the creep simulations)

w/c	Elastic modulus (GPa) M|B|A[1]	Compressive strength (MPa) M|B|A	Tensile strength (MPa) M|B|A	Poisson's ratio[2]
0.5	25.0|25.0|50.0	90.0|30.0|240	9.0|3.0|24.0	0.24

[1] M=mortar, B=bond, A=aggregate
[2] Shear modulus = elastic modulus / [2*(1 + Poisson's ratio)]

- Since the interface is the weakest component in the normal-weight aggregate concrete, the strength of bond beams is the smallest among the three types of beams. Zhang et al [179] predicted the tensile strength of the ITZ at the micrometre length scale using a lattice fracture model [17, 35]. For a water-cement ratio of 0.30, the 28-day tensile strength of ITZ was around 3.5MPa on average. The 14-day tensile strength of ITZ (bond beam) in our numerical concrete specimen with a water-cement ratio of 0.50 is estimated at 3MPa (compressive strength is 10 times the tensile strength, i.e. 30MPa, as shown in Table 3.4), which is considered reasonable.

- In line with suggestions by Schlangen [17], Vervuurt [180] and Lilliu and van Mier

is around 35% × 68.9% = 25% of the total volume of the concrete specimen. Therefore, in the numerical concrete specimen (Fig. 3.20) the volumes of mortar (fine aggregate and cement paste) is 60% (25%+31%).

[181] the elastic modulus of the bond beams is considered equal to that of the mortar beams.

- As can be seen in Table 3.4, the 14-day compressive strength of the mortar beam is estimated as 90MPa and the tensile strength is $\frac{90}{10}$ = 9MPa. In the modified lattice model the size of the beam is $0.5 \times 0.5 mm^2$ (length=0.5mm and diameter of cross section[17]=0.5mm)[18]. In other words, the tensile strength of the mortar specimen with a water-cement ratio of 0.50 with a size of $0.5 \times 0.5 mm^2$ is 9MPa. Zhang et al [185] tested the 28-day splitting tensile strength of the cement paste with a water-cement ratio of 0.40 and a size of $0.5 \times 0.5 \times 0.5 mm^3$ is around 11MPa. The 28-day tensile strength of this cement paste is around 11MPa [19]. For a cement paste with a higher water-cement ratio, the tensile strength is supposed to be lower than 11MPa. Also, for the strength of mortar specimen with the same size and water-cement ratio as the paste, it might be slightly lower than that of the paste [187], since the strength is mostly determined by the interface between paste and sand. Therefore, 9MPa is considered a reasonable tensile strength of the mortar with a water-cement ratio of 0.50 with a size of $0.5 \times 0.5 mm^2$.

- The elastic modulus of normal weight aggregate (e.g. granite and quartzite) ranges from 45GPa to 130GPa and the compressive strength from 110MPa to 280MPa [188]. In our research the elastic modulus of aggregate is set as 50GPa and the compressive strength 240MPa [20]. The elastic modulus of the mortar is estimated with the parallel-series model (Eq. 3.31) [192], viz.:

$$\frac{1}{E} = \frac{1-\chi}{E_M} + \frac{\chi}{\lambda E_A + (1-\lambda) E_M} \tag{3.31}$$

where E is elastic modulus of concrete, while E_M and E_A are elastic modulus of mortar and aggregate. χ and λ are volumetric parameters (see Fig. 3.21) and $\chi\lambda$ = A_g = volume of aggregate particles per unit volume of concrete. It is assumed that χ equals λ. Their values can be calculated with Eq. 3.32.

$$\frac{\chi\lambda}{1-\chi\lambda} = \frac{V_A}{V_M} \tag{3.32}$$

where V_A and V_M are volumes of aggregate and mortar. Then the elastic modulus of mortar can be calculated with Eq. 3.31 [21] and the value is around 25GPa.

[17] The diameter of the cross section of the beam has been calibrated by matching the elastic modulus of the beam with the global elastic modulus of the homogeneous numerical specimen (same mesh as in Fig. 3.20 without three phases) [182].

[18] It is a thick beam and its deformation due to shear cannot be ignored. Timoshenko beam theory, used in the lattice model, takes into account shear deformation and rotational bending effects, which is suitable for describing the behaviour of thick beams [183, 184].

[19] The tensile strength is around 95% the splitting tensile strength [186].

[20] It is noted that the elastic modulus of the aggregate (50GPa) is close to the lower bound of the range (45GPa-130GPa), while the compressive strength (240MPa) is close to the upper bound of the range (110MPa-280MPa). The compressive strength of the aggregate has very little effect on the strength of concrete except when aggregate has lower strength than the matrix [189–191]. It is considered to be reasonable as long as the compressive strength of the aggregates is in the range between 110MPa and 280MPa.

[21] where E = 29.8GPa, E_A = 50GPa and $\chi = \lambda = 0.63$, which is calculated with Eq. 3.32 for $V_A/V_M = 0.4/0.6 = 0.67$.

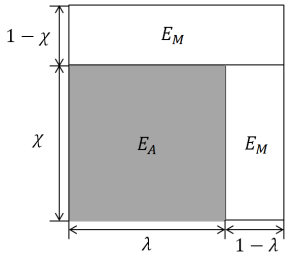

Figure 3.21: Series-parallel coupling model for the interaction of aggregate and mortar in concrete [18]

With the 14-day mechanical properties of the lattice beams, the 14-day compressive strength and elastic modulus of the concrete specimen are simulated with the lattice fracture model [17, 35, 193]. The simulated results are 36.3MPa and 32.8GPa, respectively, which fit well with the experimentally obtained values listed in Table 3.3. The simulated 14-day stress-strain relationship is shown in Fig. 3.22.

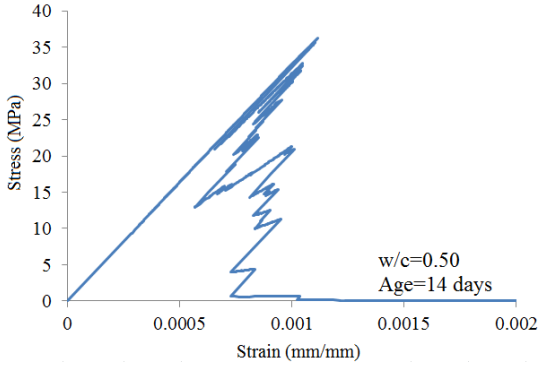

Figure 3.22: Simulated stress-strain curve of the concrete specimen (w/c=0.50; age=14 days)

30-YEAR MECHANICAL PROPERTIES OF LATTICE BEAMS AFTER CONTINUOUS HYDRATION

From the data presented in Table 3.3 it can be inferred that the measured strength of concrete specimen increases by 37.5% from 14 days to 30 years. It is assumed that the strength of the mortar and bond beams of the lattice model also increases by 37.5% from 14 day to 30 years. The 30-year mechanical properties of the mortar and bond beams are listed in Table 3.5. With these 30-year mechanical properties of the beams, the 30-year compressive strength and elastic modulus of the concrete specimen are calculated at 52.4MPa and 40.1GPa, respectively, which fit well with the measured 30-year strength and elastic modulus (Table 3.3). The simulated 30-year stress-strain relationship is shown in Fig. 3.23.

3.8.2. VALUES OF MODEL PARAMETERS

IN this section, the values of the input parameters used in the modified lattice model for creep predictions (Section 3.7.4) are determined.

Table 3.5: 30-year mechanical properties of the mortar, bond and aggregate beams (used for the calculations of the parameters in Eq. 3.18 in Section 3.8.2)

w/c	Elastic modulus (GPa) M|B|A[1]	Compressive strength (MPa) M|B|A	Tensile strength (MPa) M|B|A	Poisson's ratio[2]
0.5	34.1|34.1|50.0	123.8|41.3|240	12.38|4.13|24.0	0.24

[1] M=mortar, B=bond, A=aggregate
[2] Shear modulus = elastic modulus / [2*(1 + Poisson's ratio)]

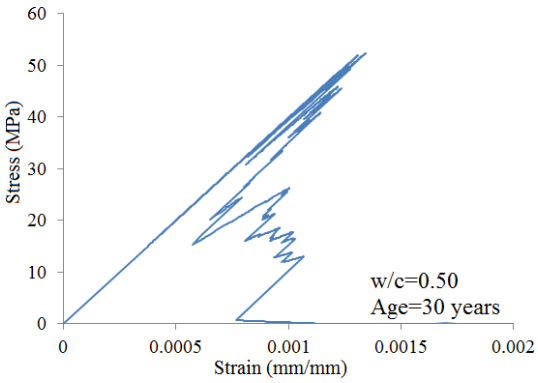

Figure 3.23: Simulated stress-strain curve of the concrete specimen (w/c=0.50; age=30 years)

EMPIRICAL AGEING FACTOR a

The empirical ageing factor a in Eq. 3.17 depends on the age at loading, the initial water-cement ratio, type of cement and moisture content [20, 172]. The values of a are obtained from an analysis of the experimental data of Wittmann [20]. The detailed calculation procedure for a is given in Section 4.4.1. There the value of a for the concrete specimen with a water-cement ratio of 0.50 loaded at 14 days is determined at 3×10^{-6}.

EVOLUTION OF STRENGTH $f_c[\alpha(t)]$ AND ELASTIC MODULUS $E[\alpha(t)]$ OF MORTAR AND BOND BEAMS RESULTING FROM CONTINUOUS HYDRATION

The strength of the mortar and bond beams, as a function of the degree of hydration, can be calculated with Eq. 3.18:

$$f_{c,i+1} = f_c[\alpha(t_{i+1})] = f_{c,max}\frac{\alpha(t_i + \Delta t_i) - \alpha_0}{1 - \alpha_0}$$

where α is calculated with Eq. 3.1:

$$\alpha(t) = \alpha_u \cdot e^{-(\frac{b}{t})^{\beta}}$$

where $t = t_{i+1} = t_i + \Delta t_i$; α_u can be calculated with Eq. 3.2 for w/c=0.5, $\alpha_u = 0.74$.

In these equations the parameters b, β, $f_{c,max}$ and α_0 are unknown. In order to obtain these four parameters, at least four strength values are needed. However, only the

14-day and 30-year strength are known[22] (see Table 3.4 and 3.5). In the following calculations the values of b and β are taken from the literature. According to Riding et al [163], b and β are related to the chemical composition of the cement and independent of the water-cement ratio. For different concrete mixtures with a wide range of compositions, they found ranges for b and β from 0.4 to 4 and 0.4 to 1.5, respectively. The influence of b and β on the hydration curves of a mixture with water-cement ratio of 0.50 is shown in Fig. 3.24. According to the simulations of hydration of Portland cement conducted

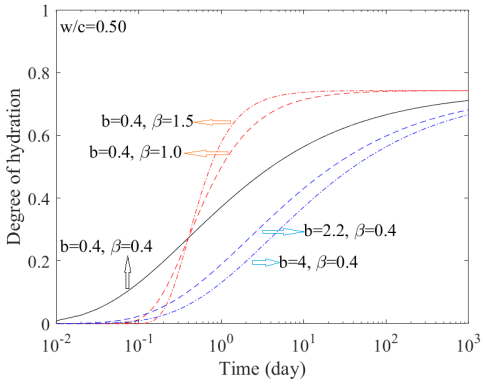

Figure 3.24: Influence of b and β on the degree of hydration of a mixture with water-cement ratio of 0.50

by Liao et al [194], a good fit with the experimental data of the degree of hydration of Portland cement was found for $b = 0.6$ and $\beta = 0.6$. These two values are adopted in this research.

By substituting b, β, 14-day and 30-year strength of the mortar and bond beams (Table 3.4 and 3.5) into Eq. 3.18, the values for $f_{c,max}$ and α_0 are obtained (see Table 3.6). The elastic modulus of the mortar and bond beams is calculated with Eq. 3.19:

$$E_{i+1} = E[\alpha(t_{i+1})] = c_1 \cdot \{f_c[\alpha(t_{i+1})]\}^{c_2}$$

The parameters c_1 and c_2 in this equation are obtained through back calculation from the 14-day and 30-year elastic modulus of the mortar and bond beams (Table 3.4 and 3.5) and shown in Table 3.6. The strength curve of the mortar beam is calculated with Eq. 3.18 and presented at both linear and logarithmic scale, as shown in Fig. 3.25.

Table 3.6: The values of the parameters for calculating the strength and elastic modulus of the mortar and bond beams in Eq. 3.18 and 3.19

w/c	b	β	$f_{c,max}$ (MPa) (mortar|bond)	α_0	c_1 (mortar|bond)	c_2
0.5	0.6	0.6	209|70	0.36	310|905	0.98

[22] It is emphasised that only 14-day and 30-year strength and elastic modulus are known in Brooks' test. No data about degree of hydration is available.

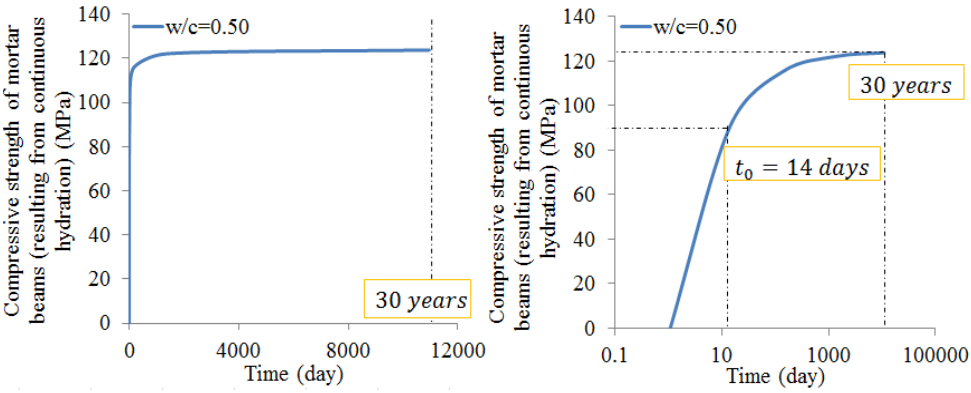

(a) Normal scale

(b) Semi-log scale

Figure 3.25: Calculated compressive strength of mortar beams versus time (Eq. 3.18)

A remark on α_0

It is noted that the critical degree of hydration α_0 is larger than expected (around 0.25 for w/c=0.50 [44]). This is because the back calculation with Eq. 3.3 from the 14-day and 30-year strength overestimates α_0. If α_0 would be close to the expected value, e.g. about 0.25, $f_{c,max}$ can be back calculated with Eq. 3.3 for $\alpha_0 = 0.25$, $f_c(14d) = 36.8$MPa (Table 3.1) and $\alpha(14d) = 0.64$ (calculated with Eq. 3.1) and the value is $f_{c,max} = 71$MPa. With $\alpha_0 = 0.25$ and $f_{c,max} = 71$MPa, the relationship between the strength and degree of hydration is plotted with the red dashed line in Fig. 3.26. It can be seen that, with the expected value of α_0, Eq. 3.3 underestimates the long-term strength. $\alpha_0 = 0.36$ (back-calculated) is considered more convenient here, since it describes the evolution of strength from 14 days to 30 years a bit better.

Furthermore, it has to be noted that the above analysis is based on the assumption that the relationship between strength and elastic modulus is linear (Eq. 3.3). If strength increases exponentially with increasing the degree of hydration (black dashed line in Fig. 3.26) [175], the calculated α_0 (through back calculation from strength) would be close to the expected value, e.g. 0.25.

ADDITIONAL DEGREE OF HYDRATION $\Delta\alpha_{add,j}$ OF PASTE ADJACENT TO ANY CRACK

The overall degree of hydration at time t, $\alpha(t)$, resulting from the continuous hydration (reference degree of hydration) is calculated with Eq. 3.1 with $b = 0.6$ and $\beta = 0.6$. For the numerical concrete specimen with a water-cement ratio of 0.50 (Fig. 3.20), the overall degree of hydration $\alpha(t)$ is shown in Fig. 3.27. It can be seen from Fig. 3.27 that after 30 years the ultimate degree of hydration ($\alpha_u = 0.74$) has been reached. The total additional overall degree of hydration $\Delta\alpha_{add,tot}$ cannot be larger than $1 - 0.74 = 0.26$, i.e. $0 \leq \Delta\alpha_{add,tot} < \Delta\alpha_{add,tot,max} = 0.26$.

In Brooks' test the extra increase in strength of loaded concrete with a water-cement ratio of 0.50 in the period of 14 days to 30 years is around 22% (Section 3.2). In order to generate this extra increase in strength, the total additional degree of hydration, $\Delta\alpha_{add,tot}$, should be around 0.082 [23]. The value of the additional degree of hydration of

[23] Calculated with Eq. 3.3. In this equation, $f_{c,max} = 85.6$MPa and $\alpha_0 = 0.36$ (Table 3.1). Inserting 30-year

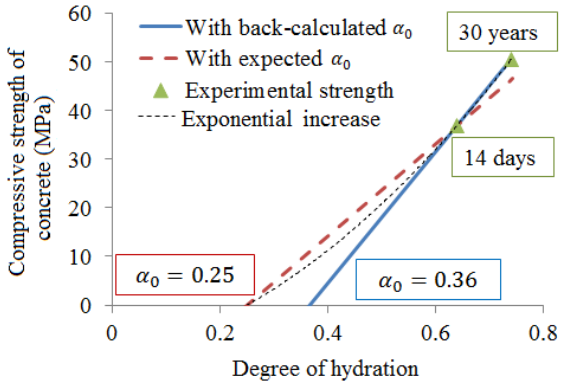

Figure 3.26: Compressive strength versus degree of hydration of concrete with a water-cement ratio of 0.50: with back-calculated α_0 and expected α_0

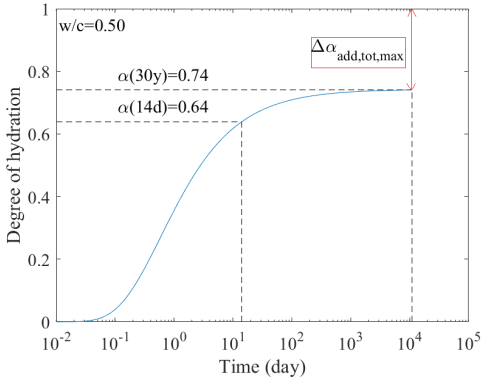

Figure 3.27: Calculated overall degree of hydration $\alpha(t)$ for the concrete specimen with a water-cement ratio of 0.50 ($b = 0.6$ and $\beta = 0.6$ in Eq. 3.1)

the paste adjacent to any crack, $\Delta\alpha_{add,j}$, for concrete with a water-cement ratio of 0.50 will be calculated with Eq. 3.6 with the number of micro-cracks (N) that occur during the creep process (Section 3.8.3).

3.8.3. SIMULATION RESULTS AND DISCUSSIONS

EFFECT OF CONTINUOUS HYDRATION ON THE LONG-TERM CREEP

The effect of continuous hydration on the long-term creep of the concrete specimen with a water-cement ratio of 0.50 is simulated for two situations:

(1) Continuous hydration is considered. The strength and elastic modulus of the mortar and bond beams are calculated with Eq. 3.18 and 3.19, respectively, with the values of the parameters, $f_{c,max}$, α_0, c_1 and c_2, as given in Table 3.6.

strength of loaded concrete (61.6MPa, Table 3.1) into this equation, 30-year degree of hydration $\alpha(30y)$ of loaded concrete is calculated at 0.822. The total additional degree of hydration is 0.822-0.74=0.082.

(2) Continuous hydration is *not* considered. The strength and elastic modulus of the mortar and bond beams are constant and equal to the 14-day values (Table 3.4). Consequently, the strength of the concrete specimen is a constant and the stress-strength ratio is also constant.

The creep strain of the mortar and bond beams is calculated with Eq. 3.17 for $a = 3 \times 10^{-6}$ (Section 3.8.2), $n = 0.3$ and $m = 0.7$ (Section 3.6.1).

The compressive strength of the concrete specimen with the effect of continuous hydration is simulated with the lattice fracture model and shown in Fig. 3.28a. The stress-strength ratio with and without the effect of continuous hydration is shown in Fig. 3.28b. The simulated creep strains of the concrete specimen are plotted in Fig. 3.29 and compared to the creep strains without the effect of continuous hydration (the "real creep"). This figure shows that the simulated creep strain after 30 years is 11% smaller than that without the effect of continuous hydration. Although the creep strains are smaller when continuous hydration is taken into account, a discrepancy still exists between these creep strains (solid line in Fig. 3.29) and the experimental data from Brooks' test. In this stage of the study no attempts will be made to adjust the creep parameters in order to improve the fit. The focus is on the effect of micro-cracking and self-healing on the long-term creep.

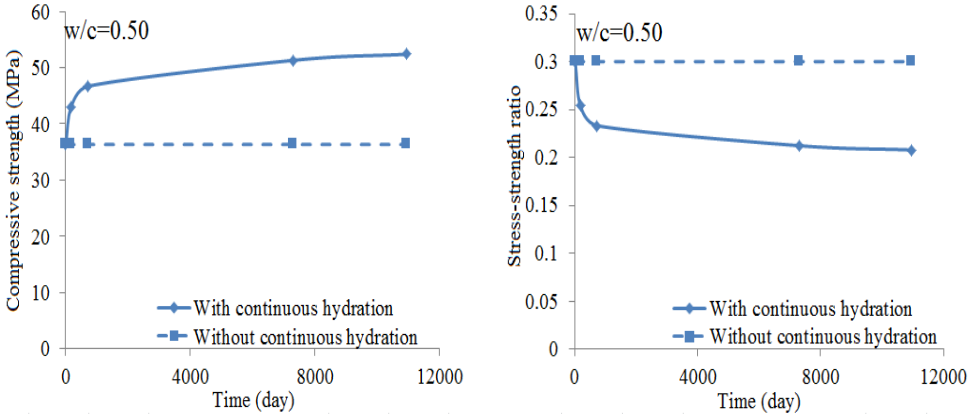

(a) Strength (b) Stress-strength ratio

Figure 3.28: Simulated evolution of compressive strength and stress-strength ratio of the concrete specimen with a water-cement ratio of 0.50 loaded at 14 days at a stress level of 30% of compressive strength: with and without effect of continuous hydration

EFFECT OF MICRO-CRACKING ON THE LONG-TERM CREEP AND STRENGTH

The effect of micro-cracking on the long-term creep and strength of concrete specimen with a water-cement ratio of 0.50 is simulated for two situations: with and without considering micro-cracking. In both situations continuous hydration is considered. The strength and elastic modulus of the mortar and bond beams are calculated with Eq. 3.18 and 3.19 with values of the parameters, $f_{c,max}$, α_0, c_1 and c_2, as given in Table 3.6. The creep strain of the mortar and bond beams is calculated with Eq. 3.17 for $a = 3 \times 10^{-6}$, $n = 0.3$ and $m = 0.7$.

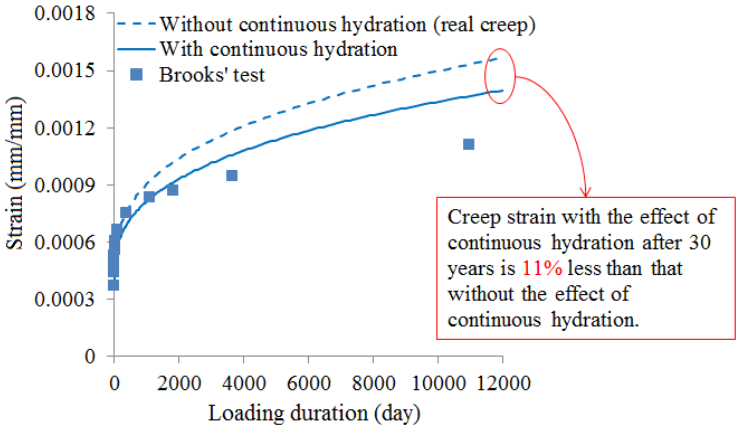

Figure 3.29: Simulated creep strains of concrete with a water-cement ratio of 0.50 loaded at 14 days at a stress level of 30% compressive strength: with and without the effect of continuous hydration

The simulated strains with and without the effect of micro-cracking are shown in Fig. 3.30. The number of micro-cracks that occur during the creep process is shown in Fig. 3.31a. The number gradually increases over time and after 30 years the total number of micro-cracks in the numerical concrete specimen is more than 8000. In the simulation micro-cracking causes 7% additional deformation after 30 years (see Fig. 3.31b). Fig. 3.31c shows the relationship between the extra deformation caused by micro-cracking and the total number of micro-cracks. It can be seen that the extra deformation increases exponentially with increasing number of micro-cracks. When micro-cracking is taken into account, the discrepancy between the simulated creep strains (dashed line in Fig. 3.30) and the experimental data further increases compared to that in case only continuous hydration is considered (solid line in Fig. 3.30).

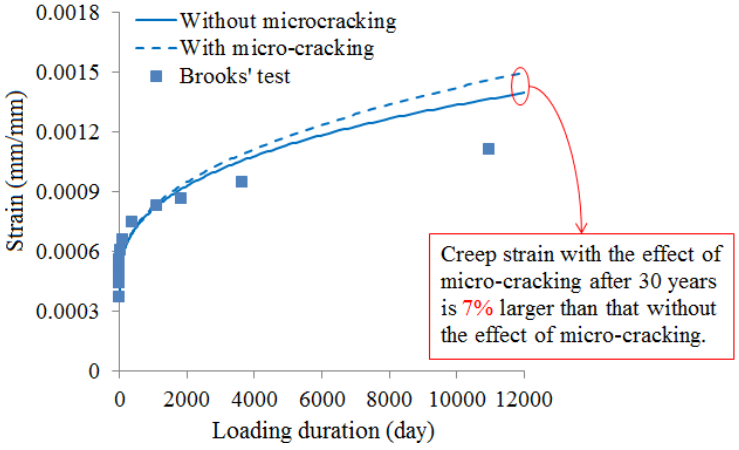

Figure 3.30: Simulated creep strains of concrete with a water-cement ratio of 0.50 loaded at 14 days at a stress level of 30% compressive strength: with and without the effect of micro-cracking

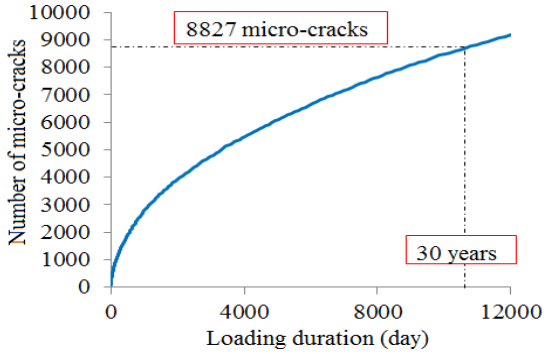

(a) Number of micro-cracks

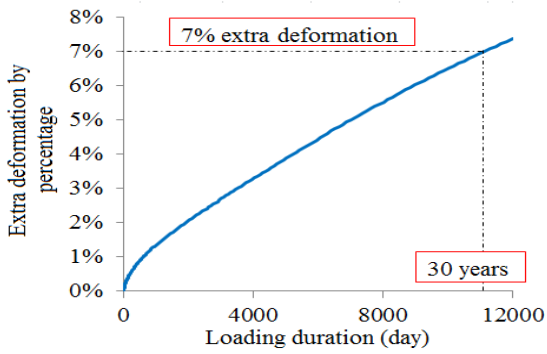

(b) Extra deformation by percentage

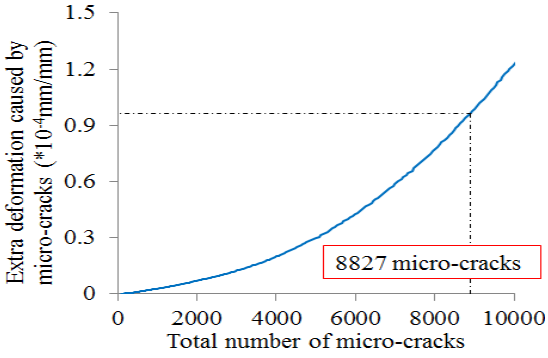

(c) Extra deformation versus number of micro-cracks

Figure 3.31: (a) Total number of cracks during the creep process; (b) Percentage of additional deformation caused by micro-cracking [extra deformation by percentage = (deformation with micro-cracking - deformation without micro-cracking) / deformation without micro-cracking]; (c) The extra deformation caused by micro-cracking versus total number of micro-cracks

Crack width during the creep process

The crack width ω in the lattice model is defined as the difference between the length of a lattice beam at the moment of cracking t_i and the original length of the beam at time t_0. The maximum crack width of the micro-cracks is shown in Fig. 3.32. This figure shows that the maximum crack width of the micro-cracks during the creep process increases with time. After 30 years the calculated maximum crack width ω_{max} is close to $3\mu m$. This is as large as medium-sized capillary pores (ranging from $50nm$ to $10\mu m$ [195]).

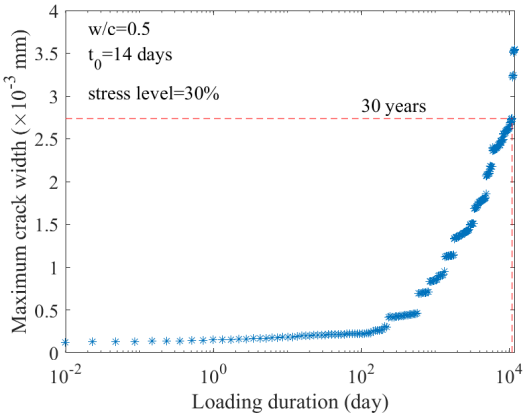

Figure 3.32: Maximum crack width of the micro-cracks occurring during the creep process of the concrete specimen with a water-cement ratio of 0.50

Strength after micro-cracking

Continuous micro-cracking also leads to a reduction of the strength of concrete. The compressive strength of the concrete specimen with[24] and without micro-cracking is simulated with the lattice fracture model and shown in Fig. 3.33. The 30-year stress-strain curves with and without the effect of micro-cracking are shown in Fig. 3.34. After 30 years, the compressive strength after cracking is 49.5MPa, which is 6% lower than that in case no micro-cracking occurs.

EFFECT OF SELF-HEALING ON THE LONG-TERM CREEP AND STRENGTH

Estimation of $\triangle\alpha_{add,j}$ for concrete with a water-cement ratio of 0.50

As discussed in Section 3.8.2, the total additional degree of hydration, $\triangle\alpha_{add,tot}$, should be around 0.082 in order to ensure that the extra strength increase of the loaded concrete reaches 22%. This total additional degree of hydration is made up of the additional degree of hydration $\triangle\alpha_{add,j}$ of the cement adjacent to N micro-cracks.

The additional degree of hydration of the paste adjacent to any crack, $\triangle\alpha_{add,j}$, can be back-calculated with Eq. 3.5 (in case no overlap occurs in the pastes adjacent to the

[24] The compressive strength with the effect of micro-cracking is the remaining load bearing capacity of the specimen.

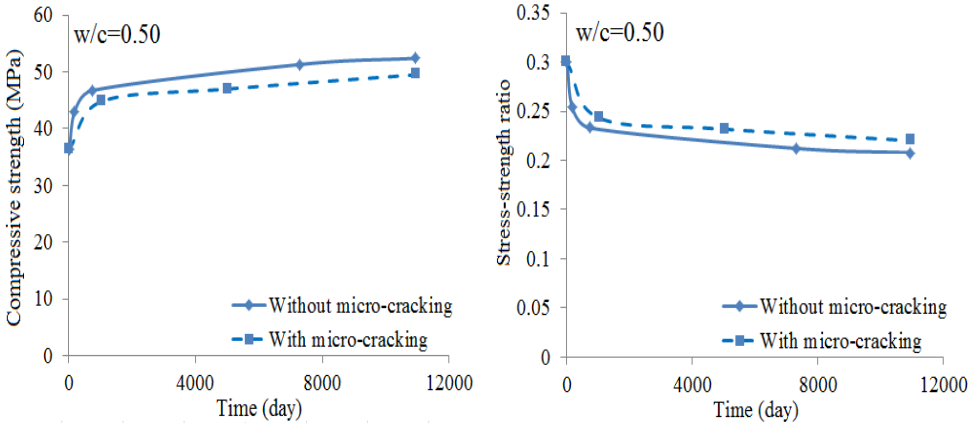

(a) Strength (b) Stress-strength ratio

Figure 3.33: Simulated evolution of compressive strength and stress-strength ratio of the concrete specimen with a water-cement ratio of 0.50 loaded at 14 days at a stress level of 30% of compressive strength: with and without the effect of micro-cracking

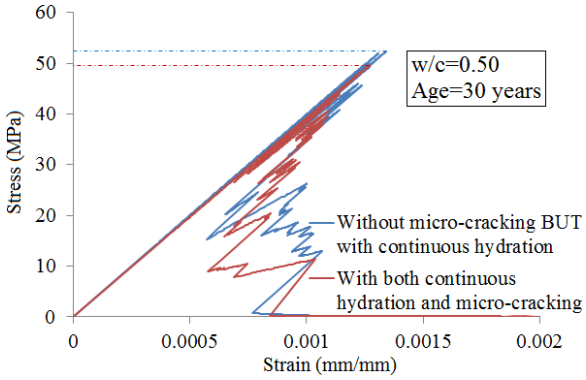

Figure 3.34: Simulated 30-year stress-strain curve with and without the effect of micro-cracking

cracks) or Eq. 3.6 (if overlap takes place). In the lattice network the volume (or area) of a crack is represented by the dashed red area in Fig. 3.35b and can be calculated as:

$$V_{c,j} = \omega \cdot l_2 \tag{3.33}$$

The volume (or area in 2D dimension) of the concrete adjacent to any crack, $V_{ac,c,j}$, is represented by the dashed dark blue area in Fig. 3.35b. The thickness of the layer of concrete adjacent to the crack, δ_c, is assumed to be equal to the length l_1 of a beam of the lattice model. The dark blue dashed area adjacent to the crack can contain aggregate phase (see Fig. 3.36). The relationship between the volume of paste adjacent to the crack, $V_{ac,p,j}$, and the volume of concrete adjacent to the crack, $V_{ac,c,j}$, can be described

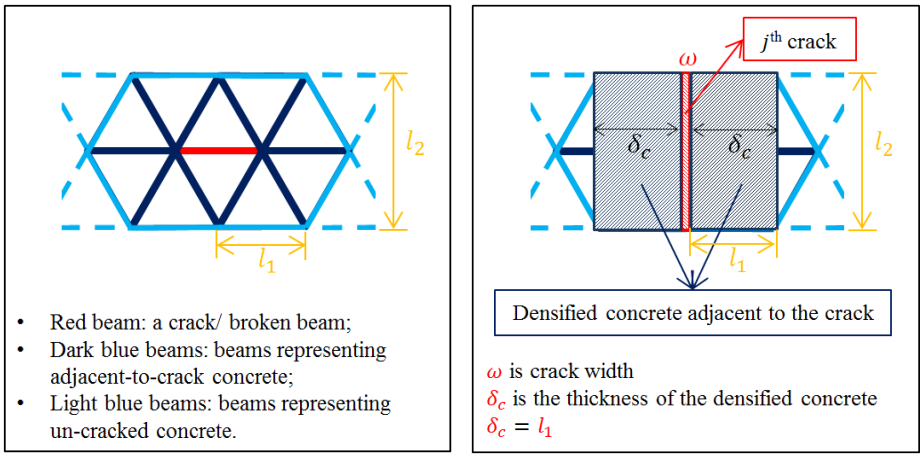

(a) Three types of beams in the lattice network

(b) The areas representing the crack and adjacent-to-crack concrete in the lattice network

Figure 3.35: (a) Three types of beams in the lattice network; (b) The areas representing the crack and the concrete adjacent to the crack in the lattice network [Note: The lattice network representing the concrete specimen is irregular (see Fig. 3.20); here for calculating the area of concrete adjacent to the crack it is simplified as regular network.]

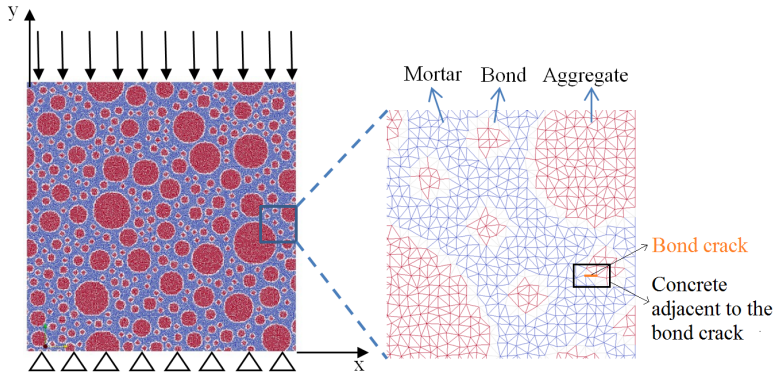

Figure 3.36: The area of concrete adjacent to a bond crack in the lattice network, as shown inside the black frame, contains aggregate phase

with the expression:

$$V_{ac,p,j} = V_{ac,c,j} \cdot r_p = 2\delta_c l_2 \frac{V_p}{V} = 2 l_1 l_2 \frac{V_p}{V} \tag{3.34}$$

where l_1 is the length of a lattice beam; V is volume of concrete and V_p is the volume of paste; r_p is volume fraction of the paste in concrete ($r_p = V_p/V$). The length of the beams (irregular lattice network in Fig. 3.20) ranges from 0.5mm to 1.9mm. For modelling the effect of additional hydration it is assumed that the length of the beams equals 0.5mm, i.e. $l_1 = 0.5mm$. The triangles in regular lattice network are assumed as equi-

lateral triangles. For l_2 it then follows $l_2 = 0.86mm$. The volume (area) of the paste adjacent to the crack, $V_{ac,p,j}$, is calculated with Eq. 3.34 for $l_1 = 0.5mm$, $l_2 = 0.86mm$ and $V_p/V = r_p = 0.31$ (third column in Table 3.1):

$$V_{ac,p,j} = 2 l_1 l_2 \frac{V_p}{V} = 2 \times 0.5 \times 0.86 \times 0.31 = 0.27 mm^2 \tag{3.35}$$

After inserting $V_{ac,p,j} = 0.27mm^2$, $\triangle\alpha_{add,tot} = 0.082$, $V_p = 0.31 \times 100 \times 100 mm^2$ and $N = 8827$ (total number of micro-cracks after 30 years) in Eq. 3.5, the additional degree of hydration of the paste adjacent to any crack, $\triangle\alpha_{add,j}$, is calculated: $\triangle\alpha_{add,j} = 0.11$.

It should be noted that the overlap of the paste adjacent to the cracks is not considered in Eq. 3.5. Given that concrete is very heterogeneous and many cracks are concentrated in the interface zone, it is unlikely that there is no overlap of the paste adjacent to the cracks (see Fig. 3.37). The number of *effective* beams, $n_{ac,eff}$, which are connected

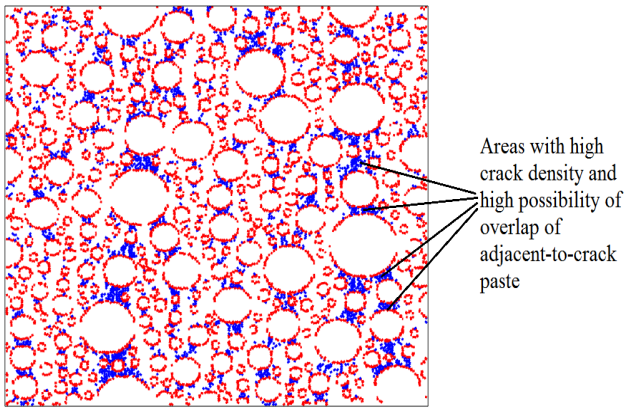

Figure 3.37: Micro-cracks in concrete with a water-cement ratio of 0.50 loaded at a stress of 30% of compressive strength after 30 years (Blue: mortar beams; Red: bond beams)

to the broken beams, is determined in the simulations of the effect of micro-cracking on the long-term creep with the modified lattice model. *Effective* means that, if overlap occurs, the beams in the overlap area (i.e. overlap beams, as shown with the orange beams in Fig. 3.38b and 3.38c), n_{ol}, will be counted only once. If no overlap occurs, the total number of the beams, $n_{ac,tot}$, which are connected to the N broken beams, follows from:

$$n_{ac,tot} = 10N \tag{3.36}$$

where N is the number of broken beams and 10 is the number of beams which are connected to a broken beam (dark blue beams in Fig. 3.35a or 3.38a). With $n_{ac,eff}$ and $n_{ac,tot}$, the percentage overlap areas/volumes/beams of the paste adjacent to the cracks (r_{ol}) can be calculated with Eq. 3.37, viz.:

$$r_{ol} = \frac{n_{ac,tot} \cdot r_p - n_{ac,eff} \cdot r_p}{n_{ac,tot} \cdot r_p} = \frac{n_{ac,tot} - n_{ac,eff}}{n_{ac,tot}} \tag{3.37}$$

In this particular case of a mixture with a water-cement ratio of 0.50 the total number of micro-cracks (broken beams) after 30 years is 8827 (Fig. 3.37). The number of beams

connected to the broken beam follows then $n_{ac,tot} = 10 \times 8827 = 88270$. The number of identified *effective* beams $n_{ac,eff}$, which are connected to 8827 broken beams, was calculated at 46173. By inserting these values for $n_{ac,tot}$ and $n_{ac,eff}$ into Eq. 3.37, the percentage overlap area of the paste adjacent to the cracks (r_{ol}) is calculated at 50%. For $r_{ol} = 50\%$ Eq. 3.6 gives $\triangle\alpha_{add,j} = 0.21$.

Calculation of κ and $\triangle\alpha_{add',j}$

The hypothesis in the foregoing is that the entire extra strength increase (22%) originates from the additional hydration of the paste adjacent to the cracks ($\triangle\alpha_{add,tot} = 0.082$ and $\triangle\alpha_{add,j} = 0.21$). This has still to be verified[25]. In order to illustrate the significance of the "strengthening by self-healing" mechanism for the extra strength increase, a range for $\triangle\alpha_{add,j}$, i.e. $0 \leq \triangle\alpha_{add,j} \leq 0.21$, is considered in the following calculations, which means that the entire, or only a part of the extra strength increase of 22% comes from the additional hydration of the paste adjacent to the cracks. For example, if $\triangle\alpha_{add,j} = 0$, no additional hydration occurs and no extra strength increase will be obtained due to the additional hydration (there must be other sources for this extra increase). If the value of $\triangle\alpha_{add,j}$ is between 0 and 0.21, the total additional degree of hydration is smaller than 0.082 and only a part of extra strength increase comes from the additional hydration. If $\triangle\alpha_{add,j} = 0.21$, the total additional degree of hydration reaches 0.082 and the extra strength increase reaches 22%.

For $0 \leq \triangle\alpha_{add,j} \leq 0.21$, the recovery degree κ (used in Eq. 3.23 and 3.24) and the *effective* additional degree of hydration of the paste adjacent to any crack $\triangle\alpha_{add',j}$, (used in Eq. 3.29 and 3.30) is calculated in the following text.

In Section 3.5.2 it has been explained how the volume (or area in 2D dimension) of reaction products ($V_{RP,add,j}$) produced during the additional hydration of the paste adjacent to any crack, which is available for filling up the crack and densifying the paste adjacent to the crack, is calculated (Eq. 3.12). In that equation $\alpha_{ref,i}$ is the reference degree of hydration at time t_i, which increases with time. Mathematically, when the value of $\alpha_{ref,i}$ has reached its maximum value, i.e. $\alpha_{ref,max}$, the minimum value of $V_{RP,add,j}$, i.e. $V_{RP,add,j,min}$, is obtained, as shown in Eq. 3.38, viz.:

$$V_{RP,add,j,min} = 1.2 \cdot \triangle\alpha_{add,j} \cdot V_{ac,p,j} \cdot (1 - \alpha_{ref,max}) \cdot \frac{1}{1 + \frac{w}{c} \cdot \frac{\rho_c}{\rho_w}} \tag{3.38}$$

If the minimum volume of the reaction product $V_{RP,add,j,min}$ can fill up the largest crack $V_{c,j} = 0.0026mm^2$ [26] and some products are left to densify the paste adjacent to the crack, then other cracks, smaller than the largest one, can be filled up and the paste adjacent to these cracks can be densified. For the concrete specimen used in the simulations (Fig. 3.20), the maximum value of $\alpha_{ref,i}$ is $\alpha(t = 30\text{years}) = \alpha_u = 0.74$. Inserting $0 \leq \triangle\alpha_{add,j} \leq 0.21$, $\alpha_{ref,max} = 0.74$, $\rho_c = 3000kg/m^3$, $\rho_w = 1000kg/m^3$ and $V_{ac,p,j} = 0.27mm^2$ in Eq. 3.38, the minimum value of $V_{RP,add,j}$ is obtained: $0 \leq V_{RP,add,j,min} \leq$

[25] Maybe *all* or *only part of* the extra strength increase originates from the additional hydration of the paste adjacent to the crack. Other possible strengthening mechanisms are discussed in Section 6.4 in Chapter 6.

[26] The calculated maximum crack width after 30 years for the concrete specimen in view was found to be close to $3\mu m$ (Fig. 3.32). The volume (area) of the crack $V_{c,j}$ is calculated with Eq. 3.33 for $\omega = 3\mu m$ and $l_2 = 0.86mm$.

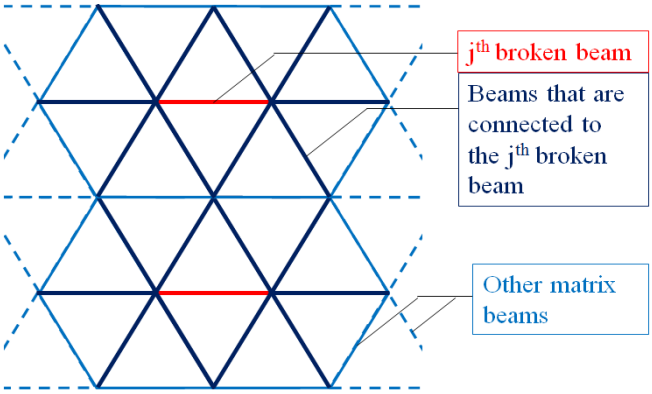

(a) Broken beams are not connected or do not share connections

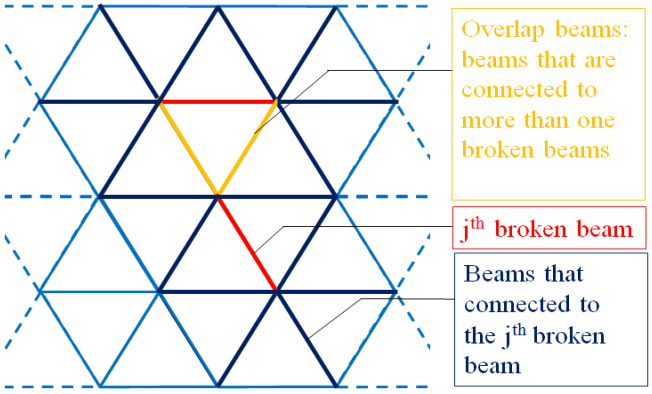

(b) Broken beams are not connected but share connections

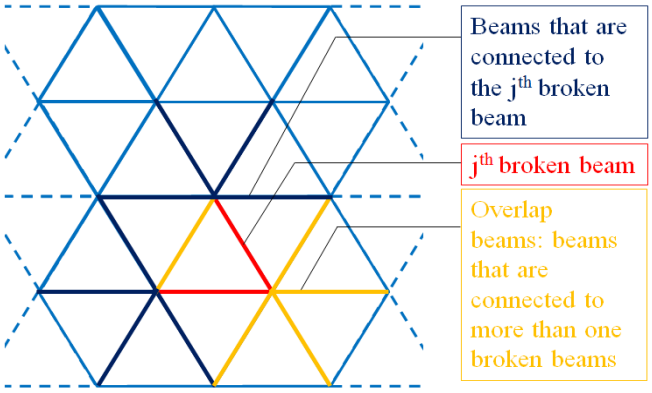

(c) Broken beams are connected

Figure 3.38: Three different kinds of beams in the mesh (red beams: broken beams or cracks; dark blue beams: beams which are connected to *one* broken beam; orange beams: overlap beams)

$0.010mm^2$. In the following four cases (see Fig. 3.39) are analysed for four different values of $\triangle\alpha_{add,j}$:

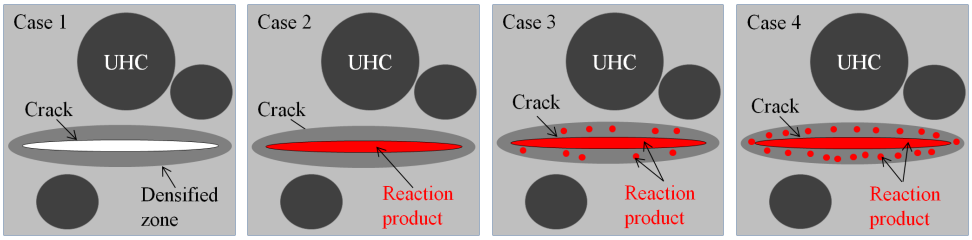

(a) $\triangle\alpha_{add,j} = 0$, $\kappa = 0$, $\triangle\alpha_{add',j} = 0$

(b) $\triangle\alpha_{add,j} = 0.078$, $\kappa = 1$, $\triangle\alpha_{add',j} = 0$

(c) $\triangle\alpha_{add,j} = 0.11$, $\kappa = 1$, $\triangle\alpha_{add',j} = 0.04$

(d) $\triangle\alpha_{add,j} = 0.21$, $\kappa = 1$, $\triangle\alpha_{add',j} = 0.16$

Figure 3.39: Four cases analysed in the simulations of the effect of self-healing on the long-term creep of concrete with a water-cement ratio of 0.50

- Case 1: *no additional hydration occurs in the paste adjacent to cracks and no reaction products are produced ($\triangle\alpha_{add,j} = 0$; see Fig. 3.39a)*

  In this case $\triangle\alpha_{add,j} = 0$. The crack cannot be filled up with reaction product and the paste adjacent to the crack cannot be densified. Consequently, the recovery degree κ is 0 and the *effective* additional degree of hydration of the paste adjacent to any crack $\triangle\alpha_{add',j}$ is 0.

- Case 2: *the reaction products are just enough to fill up the crack and no product is left to densify the paste adjacent to the crack (the value of $\triangle\alpha_{add,j}$ is between 0 and 0.21: $\triangle\alpha_{add,j} = 0.078$ [27]; see Fig. 3.39b)*

  In this case the entire volume of the reaction products is used to fill up the crack and no products are left to make the paste adjacent to the crack denser. This means: $V_{RP,add,j,min} = V_{c,j} = 0.0026mm^2$. κ and $\triangle\alpha_{add',j}$ are calculated with Eq. 3.25 to 3.28 and they hold $\kappa = 1$ and $\triangle\alpha_{add',j} = 0$.

- Case 3: *the reaction products are enough to fill up the crack and some products are left to densify the paste adjacent to the crack (the value of $\triangle\alpha_{add,j}$ is between 0 and 0.21: $\triangle\alpha_{add,j} = 0.11$; see Fig. 3.39c)*

  In this case $\triangle\alpha_{add,j} = 0.11$. $V_{RP,add,j,min}$ is calculated with Eq. 3.38 and the value is $0.004mm^2$. For $V_{RP,add,j,min} = 0.004mm^2$ and $V_{c,j} = 0.0026mm^2$, κ and $\triangle\alpha_{add',j}$ are calculated with Eq. 3.25 to 3.28 and they hold $\kappa = 1$ and $\triangle\alpha_{add',j} = 0.04$.

- Case 4: *the reaction products are enough to fill up the crack and some products (more than Case 3) are left to densify the paste adjacent to the crack ($\triangle\alpha_{add,j}$ reaches its maximum: $\triangle\alpha_{add,j} = 0.21$; see Fig. 3.39d)*

  In this case $\triangle\alpha_{add,j} = 0.21$. $V_{RP,add,j,min}$ is calculated with Eq. 3.38 and its value is $0.010mm^2$. With this value and $V_{c,j} = 0.0026mm^2$, κ and $\triangle\alpha_{add',j}$ are calculated with Eq. 3.25 to 3.28, respectively, and they hold $\kappa = 1$ and $\triangle\alpha_{add',j} = 0.16$.

[27] $\triangle\alpha_{add,j}$ is back-calculated with Eq. 3.38 for $V_{RP,add,j,min} = V_{c,j} = 0.0026mm^2$, $\alpha_{ref,max} = 0.74$, $\rho_c = 3000kg/m^3$, $\rho_w = 1000kg/m^3$ and $V_{ac,p,j} = 0.27mm^2$ and it holds $\triangle\alpha_{add,j} = 0.078$.

The variations of κ and $\triangle\alpha_{add',j}$ in the above four cases are summarized in Table 3.7. They are used in the simulations for the effect of self-healing on the long-term creep and strength of concrete with a water-cement ratio of 0.50, loaded at 14 days at a stress level of 30% of the compressive strength.

Table 3.7: Four cases that will be studied in the simulations for the effect of self-healing on creep and strength (different variations of κ and $\triangle\alpha_{add',j}$)

Parameters	Equation	Unit	Cases			
			Case 1 [1]	Case 2 [2]	Case 3	Case 4
$\triangle\alpha_{add,tot}$	Eq. 3.6	[-]	0	0.030	0.042	0.082
$\triangle\alpha_{add,j}$	Eq. 3.6	[-]	0	0.078	0.11	0.21
$V_{RP,add,j,min}$	Eq. 3.38	$[mm^2]$	0	0.0026	0.004	0.01
κ	Eq. 3.25 to 3.26	[-]	0	1	1	1
$\triangle\alpha_{add',j}$	Eq. 3.27 to 3.28	[-]	0	0	0.04	0.16

[1] Case 1: no self-healing occurs.
[2] Case 2: the crack can be self-healed and the strength can be recovered, while the paste adjacent to the crack cannot be densified since the entire volume of the reaction products are used to fill up the crack.

Simulation of the effect of self-healing on the long-term creep and strength (w/c=0.50)

For Case 2 to 4[28] the effect of self-healing on the long-term creep of the concrete specimen with a water-cement ratio of 0.50 is simulated, following the scheme in Fig. 3.18. The input parameters for calculating the strength and elastic modulus of the mortar and bond beams resulting from the continuous hydration and for calculating the creep strains are the same as those in the simulations for the effect of micro-cracking on the long-term creep. Besides, two parameters, κ and $\triangle\alpha_{add',j}$ for calculating the strength and elastic modulus of the broken beams after self-healing (Eq. 3.23 and 3.24), and the beams which are connected to the broken beams after densification (Eq. 3.29 and 3.30), are given in Table 3.7.

The simulated creep strains with the effect of the self-healing (solid lines) are shown in Fig. 3.40. They are compared to the strains with (dotted dashed line) and without (dashed line) the effect of micro-cracking. The compressive strength of the concrete specimen after self-healing[29] is simulated with lattice fracture model and shown in Fig. 3.41a. The evolution of the stress-strength ratio is shown in Fig. 3.41b. The 14-day and 30-year experimental compressive strength and stress-strength ratio of loaded concrete are also shown in this Fig. for comparison.The simulated 30-year stress-strain curves of the loaded concrete specimen after self-healing is shown in Fig. 3.42.

As can be seen from Fig. 3.40, if the effect of self-healing is considered, the creep strains (solid lines in Fig. 3.40) are lower than that with the effect of micro-cracking (without the effect of self-healing; dotted dashed line in Fig. 3.40). The simulated 30-year compressive strength after self-healing (solid lines in Fig. 3.41a) is larger than that with the effect of micro-cracking (dotted dashed line in Fig. 3.41a). When the entire volume

[28] For Case 1 no self-healing occurs. The creep strains have been simulated and shown in Fig. 3.30.
[29] In the modified lattice model the broken beams (i.e. cracks) and the beams connected to the broken beams (i.e. concrete adjacent to the cracks) are marked at each time step. The corresponding strengths of these beams at t_i are put into the lattice fracture model to calculate the compressive strength (at t_i).

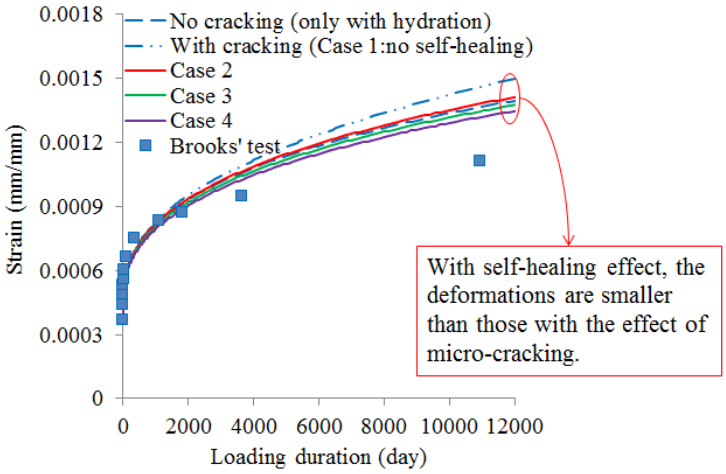

Figure 3.40: Simulated creep strains of the concrete specimen with a water-cement ratio of 0.50 loaded at 14 days at a stress level of 30% of compressive strength: with and without the effect of self-healing

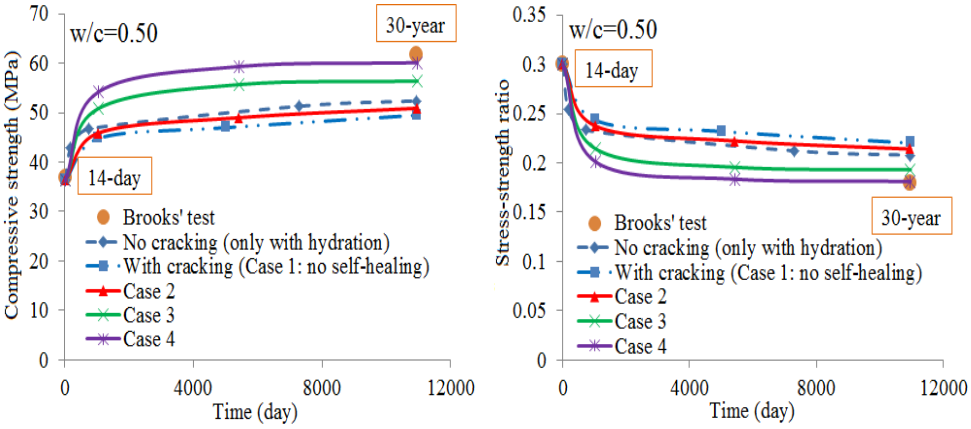

(a) Strength

(b) Stress-strength ratio

Figure 3.41: Simulated and experimental compressive strength and stress-strength ratio of the concrete specimen with a water-cement ratio of 0.50 loaded at 14 days at a stress level of 30% of compressive strength: with and without the effect of self-healing

of the reaction product produced during the additional hydration of the paste adjacent to the cracks is used to fill up the cracks and no product is left to densify the paste adjacent to the cracks (Case 2), the simulated creep curve (red solid line in Fig. 3.40) gets close to (but still above) that with only the effect of continuous hydration (dashed blue line in Fig. 3.40). The strength of concrete (red solid line in Fig. 3.41a) is also getting close to that with only the effect of continuous hydration (blue dashed line in Fig. 3.41a), i.e. the strength is recovered. When the volume of the reaction product produced during the additional hydration of the paste adjacent to the cracks can fill up the cracks and

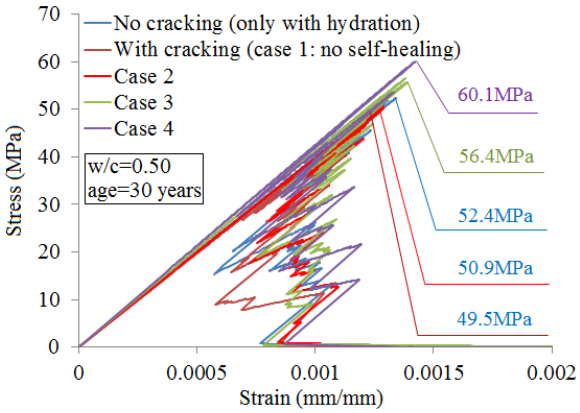

Figure 3.42: Simulated 30-year stress-strain curve of the loaded concrete specimen with a water-cement ratio of 0.50

some are left to densify the paste adjacent to the cracks (Case 3 and 4), the simulated creep strains (green and purple solid lines in Fig. 3.40) are lower than those with only the effect of continuous hydration. The simulated strength (green and purple solid lines in Fig. 3.41a) is larger than that with only the effect of continuous hydration, i.e., an extra strength increase is achieved.

By comparing the curves in Fig. 3.41b and 3.40, it can be seen that, when the stress-strength ratio is lower[30], the simulated creep strains are also lower. This may imply that the creep deformation is positively correlated to the stress-strength ratio.

With increasing additional degree of hydration of the paste adjacent to the cracks ($\Delta\alpha_{add,j}$), the simulated creep strains and compressive strength get closer to the experimental data. A discrepancy between the experimental creep strains and 30-year strength and the simulated creep strains and 30-year strength with the effect of self-healing is still found. Since only one specimen (one set of experimental data) is simulated in this chapter, it is too early to speculate about the reason for the discrepancy between the simulation results and the experimental data. This will be further discussed in Chapter 6.

3.9. CONCLUSIONS

IN this chapter the effect of micro-cracking and self-healing on the long-term creep and strength of concrete under sustained load was studied. A self-healing mechanism that explains the extra increase in strength of concrete under sustained load, i.e. self-healing of micro-cracks and densification of the paste adjacent to the micro-cracks, was proposed. This mechanism, together with creep and continuous hydration, are incorporated in a lattice model. The modified lattice model is able to simulate the effects of continuous hydration, micro-cracking and self-healing on the long-term creep and strength development of concrete under sustained load. Based on the simulation results and discussions, the following conclusions can be drawn:

[30] In our simulations stress is constant.

- Concrete continues to hydrate and its strength gradually increases. If this is taken into consideration in the analysis of the creep process, the creep deformation is 11% smaller than that without the effect of continuous hydration due to the decrease of the strength-stress ratio (constant stress test, Fig. 3.29).

- During the creep process micro-cracks will occur due to the stress concentrations resulting from the heterogeneity of concrete. The number of micro-cracks increases with time under load and the calculated crack width also increases. When concrete is loaded at a low stress level (30% of compressive strength), the crack width is small (only a few micro-meters, Fig. 3.32). Micro-cracking causes 7% additional overall deformation after 30 years (Fig. 3.30 and 3.31b) and reduces the 30-year strength by 6%.

- If the effect of self-healing is considered, the creep strains are lower than in case self-healing does not occur (Fig. 3.40). The strength is also larger compared to that without the effect of self-healing (Fig. 3.41a). With increasing the additional degree of hydration of the paste adjacent to the crack, extra strength increase becomes larger and the simulated creep strains and compressive strength get closer to the experimental data.

- A discrepancy between the experimental creep strains and 30-year strength and the simulated creep and strength with the effect of self-healing was found. Since only one specimen (one set of experimental data) is simulated in this chapter, it is too early to speculate about the reason for the discrepancy between the simulation results and the experimental data. This will be further discussed in Chapter 6.

4

INTERACTION BETWEEN CREEP, MICRO-CRACKING AND SELF-HEALING IN CONCRETE UNDER SUSTAINED LOAD: ROLE OF WATER-CEMENT RATIO

Not everything that can be counted counts,
and not everything that counts can be counted.

Albert Einstein

The water-cement ratio is one of the most important characteristics of concrete. It influences not only creep, but also micro-cracking and self-healing. In this chapter, the role of the water-cement ratio in the interaction between creep, micro-cracking and self-healing of concrete under sustained load is studied using the modified lattice model. The effects of micro-cracking and self-healing on the long-term creep and strength of concretes with five water-cement ratios (0.50-0.80) are simulated. The concretes are loaded at 14 days at a stress level of 30% of the 14-day compressive strength. The simulations results are compared with the experimental data from Brooks' 30-year creep test.

4.1. INTRODUCTION

IN Chapter 3, a self-healing mechanism was proposed to explain the additional strength increase in concrete under sustained load. The additional increase in strength is supposed to be related to the self-healing of cracks and the densification of the paste adjacent to cracks. With the modified lattice model the effects of micro-cracking and self-healing on the long-term creep and strength of concrete have been simulated for a mixture with a water-cement ratio of 0.50 as a first evaluation of the model.

The water-cement ratio is an important characteristic of concrete. It has an influence not only on creep, but also on micro-cracking. Generally speaking, concrete with a high water-cement ratio exhibits a lower strength and larger creep strains compared to concrete with a low water-cement ratio. Concrete with a high water-cement ratio is weaker and thus more susceptible to cracking. Therefore, *the total number of micro-cracks (i.e. damage degree, see Section 3.5.2)* in concrete under sustained load is expected to be higher for concrete with a high water-cement ratio than for concrete with a low water-cement ratio. Besides, the *crack density (i.e. the number of cracks per unit area, see Section 3.5.2)* might be different in concretes with different water-cement ratios. Lindquist et al [196] observed a lower crack density in bridge decks with higher water-cement ratios.

The water-cement ratio has also an effect on the self-healing efficiency of concrete. Concrete with a high water-cement ratio has a lower amount of unhydrated cement compared to concrete with a low water-cement ratio. Hence, in case water is sufficiently available, the self-healing efficiency of concrete with a low water-cement ratio is supposed to be higher than of concrete with a high water-cement ratio. However, the self-healing efficiency not only depends on the amount of unhydrated cement, but also on the crack width, crack density and damage degree [197]. Zhong and Yao [197] measured the damage degree of concrete before and after self-healing using ultrasonic pulse velocity (UPV) and the compressive strength before and after self-healing. They concluded that, if the damage degree is less than a certain threshold value, the self-healing ratio (i.e. the ratio of compressive strength after self-healing to the strength before self-healing) increases with increasing damage degree. If the damage degree exceeds the threshold value, the self-healing ratio decreases with increasing damage degree. The crack density also has an effect on the self-healing of concrete. If the cracks are relatively dispersed in concrete, the self-healing efficiency might be better compared to concrete with local concentration of cracks, i.e. relatively high crack density (see Section 3.5.2).

In this chapter, the role of the water-cement ratio on the interaction between creep, micro-cracking and self-healing of concrete under sustained load will be investigated using the modified lattice model (flow chart in Fig. 3.18). The effects of damage degree and crack density on the self-healing of concrete will be discussed. The simulation results are compared to the experimental data from Brooks' test [19].

4.2. LONG-TERM CREEP DATA FROM BROOKS' TEST

IN Section 3.2, the details of Brooks' test have been described. In Chapter 4, the creep deformations of concrete specimens with North Notts (normal-weight aggregate) and water-cement ratio of 0.50-0.80 are studied. The creep deformations were determined

on specimens (76 × 260 mm cylinders) stored in water at 23 ± 1 °C. The load was applied at the age of 14 days and the initial stress-strength ratio is 0.3. The mix design, compressive strength and elastic modulus of load-free and loaded specimens are given in Table 4.1. The measured creep strains are shown in Fig. 4.1. Fig. 4.1 shows that creep strain increases with increasing water-cement ratio, with the exception of the mixture with a water-cement ratio of 0.67.

Table 4.1: Mix design, compressive strength and elastic modulus of concrete specimens with water-cement ratios of 0.50-0.80 in Brooks' test [19, 25]

w/c	Mix proportion by weight (C:S:A)[2]	Cement paste content r_p by volume (%)	14-day mechanical properties		30-year mechanical properties			
					Load-free		Loaded	
			f_c[1] (MPa)	E[1] (GPa)	f_c (MPa)	E (GPa)	f_c (MPa)	E (GPa)
0.50	1:1.71:3.04	31.1	36.8	29.8	50.6	40.7*[3]	61.6	54.4
0.54		32.6	32.8	28.1	46.6	39.6*	50.8	52.1
0.58		33.7	30.9	25.6	36.7	30.3*	45.4	40.8
0.67		36.6	19.6	20.9	26.9	28.5*	36.2	29.1
0.80		40.5	14.7	16.2	20.2	22.1*	21.5	20.9

[1] E=elastic modulus; f_c=compressive strength;
[2] C:S:A=Cement:Sand:Aggregate;
[3] *=assumed value; 30-year elastic modulus of the load-free specimen is not given; it is assumed to increase by same percentage as 30-year strength, compared to 14-day values.

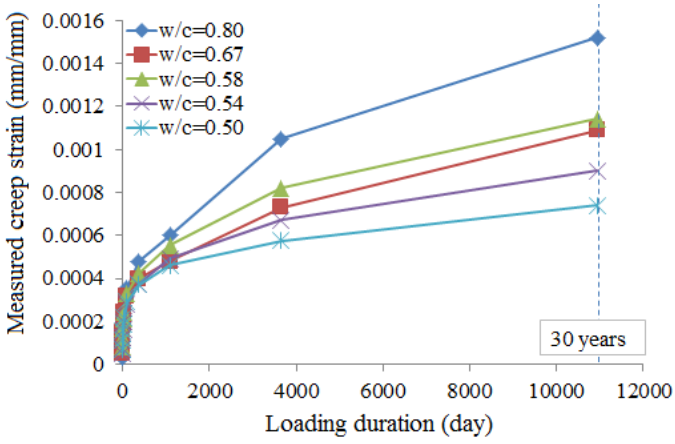

Figure 4.1: Measured creep strains of wet-stored concrete in Brooks' test (constant stress creep test; age at loading is 14 days; loading level is 30% of 14-day compressive strength) [19]

The 14-day and 30-year compressive strength of load-free and loaded concretes with water-cement ratios of 0.50-0.80 are depicted in Fig. 4.2. The compressive strength of loaded specimens after 30 years is compared to that of load-free specimens. The comparison is shown in Fig. 4.3. After 30 years the compressive strength of loaded specimens is 6% to 35% larger than that of load-free specimens (green line in Fig. 4.3). Similar ob-

servations on the extra increase in strength of concrete under sustained load were also found by Hughes and Ash [37], Washa and Fluck [34], Cook and Chindaprasirt [96], Bisschop [88] and Coutinho [24].

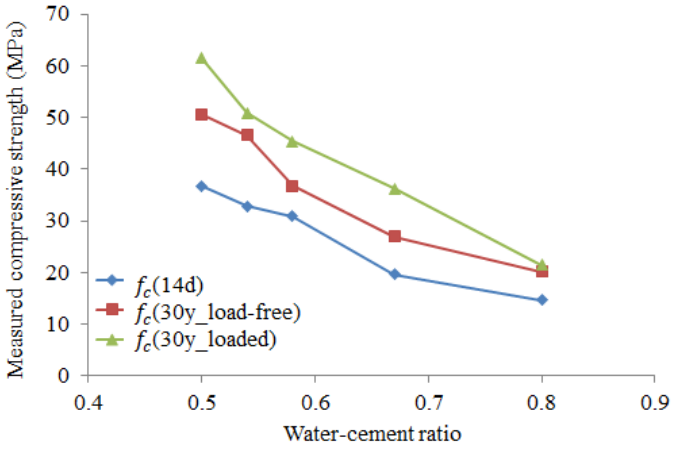

Figure 4.2: Measured 14-day and 30-year compressive strength of load-free and loaded concretes with water-cement ratios of 0.50-0.80 (f_c *(14d)* is compressive strength at age of loading (14 days); f_c *(30y_loaded)* is compressive strength of loaded specimens after 30 years, while f_c *(30y_load-free)* is compressive strength of load-free specimens.) [19]

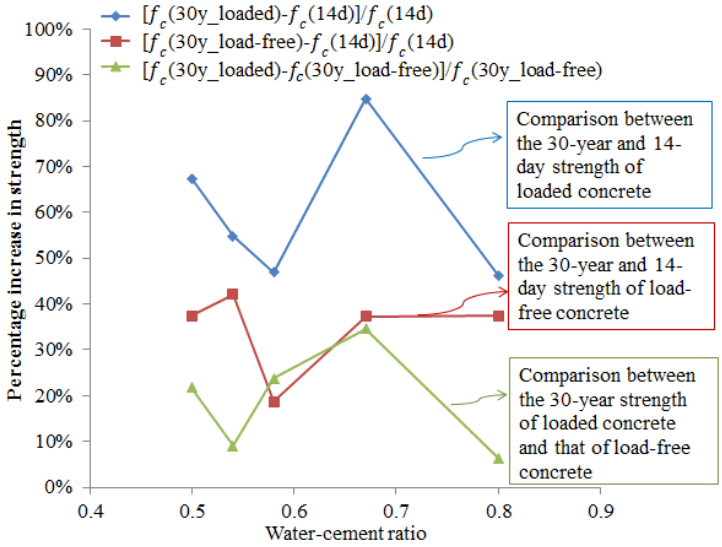

Figure 4.3: Percentage increase in strength of wet-stored concrete specimens with different water-cement ratios (f_c *(14d)* is compressive strength at age of loading (14 days); f_c *(30y_loaded)* is compressive strength of loaded specimens after 30 years, while f_c *(30y_load-free)* is compressive strength of load-free specimens.) [19]

Fig. 4.1 shows that creep strain generally increases with increasing water-cement ratios. However, there is one exception: the concrete specimen with a water-cement ratio of 0.67 exhibited lower creep than the specimen with a water-cement ratio of 0.58. It is also noted that the percentage increase in strength from 14 days to 30 years of loaded concrete with a water-cement ratio of 0.67 is larger than that of concretes with water-cement ratios of 0.50-0.58 and 0.80 (see blue curve in Fig. 4.3). The decrease of the stress-strength ratio during the creep process is greater than that of other concretes. This could explain why the creep deformation of concrete with a water-cement ratio of 0.67 is lower than that of concrete with a water-cement ratio of 0.58.

4.3. THE NUMERICAL SPECIMENS WITH W/C=0.50-0.80

4.3.1. NUMERICAL SPECIMENS

The dimension of the numerical specimens with water-cement ratios of 0.50-0.80 is 100× $100mm^2$, meshed at the resolution 0.5mm/pixel. The aggregate is positioned randomly in the specimen and its distribution complies with the Fuller's curve. The maximum aggregate diameter is 16mm. Aggregate particles with diameters smaller than 2mm are excluded from the generated aggregate structures, since it is suggested that the smallest diameter of the aggregate particles should be two or three times larger than the mesh size. The distance between the centre of two particles is larger than the minimum distance $1.1 \times (d_1 + d_2)/2$ [1] suggested by Hsu [178]. The generated aggregate volumes [2] are 40%, 39.7%, 39.5%, 39% and 36%, respectively, of the total 2D volume of the specimens with water-cement ratios of 0.50-0.80. The meso-structure of these concrete specimens is shown in Fig. 4.4.

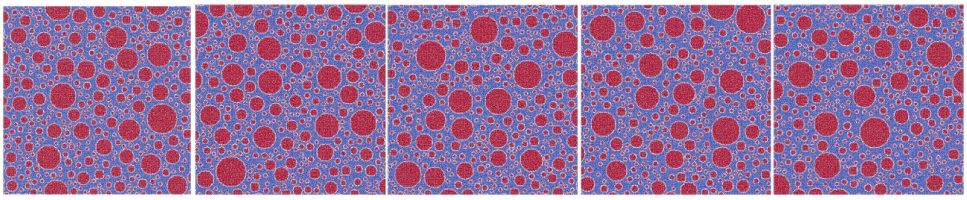

(a) w/c=0.50 (b) w/c=0.54 (c) w/c=0.58 (d) w/c=0.67 (e) w/c=0.80

Figure 4.4: Meso-structure of concrete specimens with water-cement ratios of 0.50-0.80 (dimension of specimens: $100 \times 100mm^2$; percentages volume of aggregate are (a) 40%, (b) 39.7%, (c) 39.5%, (d) 39% and (e) 36%)

4.3.2. 14-DAY MECHANICAL PROPERTIES OF LATTICE BEAMS: $f_c(t_0)$ AND $E(t_0)$

The values for the 14-day mechanical properties of the mortar, bond and aggregate beams for the specimens with water-cement ratios of 0.50-0.80 are listed in Table 4.2. These

[1] d_1 and d_2 are diameters of two aggregate particles.

[2] The aggregate volumes of the numerical specimens are smaller than those in Brooks' test. This is because the aggregates with diameters smaller than 2mm are not placed in the specimen and they are considered as find aggregates which are embedded in the paste. This has been explained in detailed in Chapter 3.

values are roughly estimated[3] on the basis of the values of the lattice beams for the specimen with a water-cement ratio of 0.50 which has been discussed in Section 3.8.1.

Table 4.2: Estimated 14-day mechanical properties of the mortar, bond and aggregate beams for the concrete specimens with water-cement ratios of 0.50-0.80 in order to fit the experimental strength and elastic modulus (input for the creep simulations)

w/c	Elastic modulus (GPa) M|B|A[1]	Compressive strength (MPa) M|B|A	Tensile strength (MPa) M|B|A	Poisson's ratio[2]
0.80	11.0|11.0|50.0	39.1|13.0|240	3.91|1.30|24.0	
0.67	14.0|14.0|50.0	58.6|19.5|240	5.86|1.95|24.0	
0.58	18.0|18.0|50.0	79.8|26.5|240	7.98|2.65|24.0	0.24
0.54	22.3|22.3|50.0	82.8|27.6|240	8.28|2.76|24.0	
0.50	25.0|25.0|50.0	90.0|30.0|240	9.0|3.0|24.0	

[1] M=mortar, B=bond, A=aggregate;
[2] Shear modulus = elastic modulus / [2*(1 + Poisson's ratio)].

With the 14-day mechanical properties of the lattice beams, the 14-day compressive strength and elastic modulus of the concrete specimens with water-cement ratios of 0.50-0.80 are simulated with the lattice fracture model [17, 35, 193]. The results are shown in Table 4.3. A comparison between the experimental and simulated values is depicted in Fig. 4.5. This figure shows that with the 14-day mechanical properties of the three phases of the lattice model given in Table 4.2, the simulated 14-day compressive strength and elastic modulus fit well with the experimental values (Table 4.1). This means that the input values for the 14-day mechanical properties of the lattice beams are reasonable and the numerical specimens are reliable as the starting point for the numerical simulations of creep. The simulated 14-day stress-strain relationships are shown in Fig. 4.6.

Table 4.3: Simulated 14-day compressive strength and elastic modulus of concrete specimens with water-cement ratios of 0.50-0.80

w/c	14-day compressive strength (MPa)		14-day elastic modulus (GPa)	
	Experiment	Simulation	Experiment	Simulation
0.80	14.7	14.8	16.2	17.2
0.67	19.6	19.6	20.9	21.6
0.58	30.9	30.1	25.6	26.0
0.54	32.8	33.7	28.1	30.4
0.50	36.8	36.3	29.8	32.8

[3] The elastic modulus and compressive strength of aggregate beams are 50GPa and 240MPa, respectively. The elastic modulus of mortar beams is estimated with Eq. 3.31. The compressive strength of mortar beams is roughly estimated based on the fact that the strength decreases with increasing water-cement ratios.

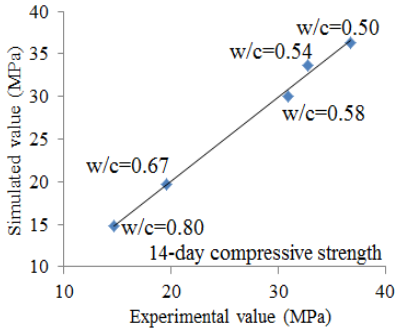

(a) Experimental and simulated 14-day compressive strength

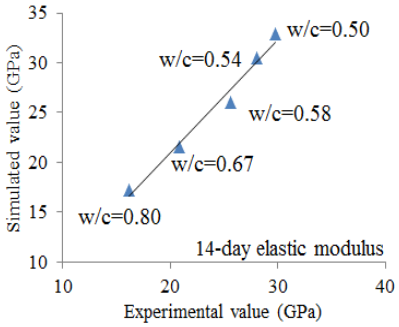

(b) Experimental and simulated 14-day elastic modulus

Figure 4.5: Comparison between experimental and simulated 14-day compressive strength and elastic modulus of concretes with water-cement ratios of 0.50-0.80

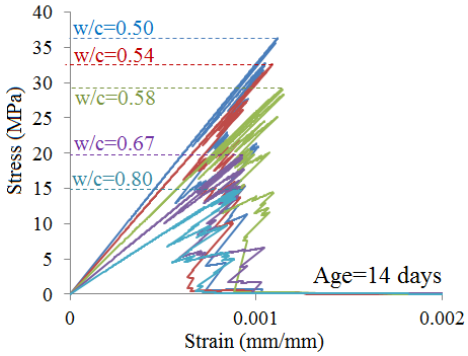

Figure 4.6: Simulated stress-strain relationship of concretes with water-cement ratios of 0.50-0.80 (age=14 days)

4.3.3. 30-YEAR MECHANICAL PROPERTIES OF LATTICE BEAMS AFTER CONTINUOUS HYDRATION

Due to continuous hydration the strength of the mortar and bond beams increases. According to Table 4.1, the compressive strengths of the load-free concrete specimens with water-cement ratios of 0.50-0.80 increase by 37.5%, 42.0%, 18.8%, 37.2% and 37.4%, respectively, from 14 days to 30 years. It is assumed that due to continuous hydration the strengths of the mortar and bond beams also increase by the same percentages from 14 day to 30 years as the concrete specimens. The 30-year mechanical properties of the mortar, bond and aggregate beams for the concrete specimens with water-cement ratios of 0.50-0.80 are listed in Table 4.4.

With the 30-year mechanical properties of the lattice beams given in Table 4.4, the 30-year compressive strength and elastic modulus of the load-free concrete specimens with water-cement ratios of 0.50-0.80 are simulated using the lattice fracture model. The simulated 30-year compressive strength and elastic modulus are shown in Table 4.5. Fig.

4.7 shows a comparison between the experimental and simulated values. The simulated 30-year stress-strain relationships of the load-free specimens with water-cement ratios of 0.50-0.80 are shown in Fig. 4.8.

Table 4.4: 30-year mechanical properties of the mortar, bond and aggregate beams for the load-free concrete specimens with water-cement ratios of 0.50-0.80 (used for the calculations of the parameters in Eq. 3.18)

w/c	Elastic modulus (GPa) M|B|A[1]	Compressive strength (MPa) M|B|A	Tensile strength (MPa) M|B|A	Poisson's ratio[2]
0.80	15.0|15.0|50.0	53.7|17.9|240	5.37|1.79|24.0	
0.67	19.1|19.1|50.0	80.4|26.8|240	8.04|2.68|24.0	
0.58	21.3|21.3|50.0	94.8|31.6|240	9.48|3.16|24.0	0.24
0.54	31.4|31.4|50.0	117.7|39.2|240	11.77|3.92|24.0	
0.50	34.1|34.1|50.0	123.8|41.3|240	12.38|4.13|24.0	

[1] M=mortar, B=bond, A=aggregate;
[2] Shear modulus = elastic modulus / [2*(1 + Poisson's ratio)].

Table 4.5: Simulated 30-year compressive strength and elastic modulus of the load-free concrete specimens with water-cement ratios of 0.50-0.80

w/c	30-year compressive strength (MPa)		30-year elastic modulus (GPa)	
	Experiment	Simulation	Experiment	Simulation
0.80	20.2	21.1	22.1	21.9
0.67	26.9	28.3	28.5	27.0
0.58	36.7	36.5	30.3	29.2
0.54	46.6	50.1	39.6	38.0
0.50	50.6	52.4	40.7	40.1

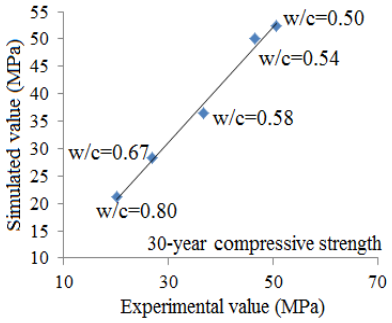

(a) Experimental and simulated 30-year compressive strength

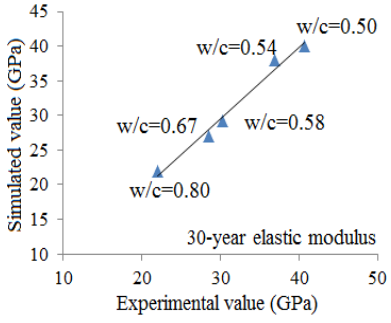

(b) Experimental and simulated 30-year elastic modulus

Figure 4.7: Comparison between experimental and simulated 30-year compressive strength and elastic modulus of load-free concretes with water-cement ratios of 0.50-0.80

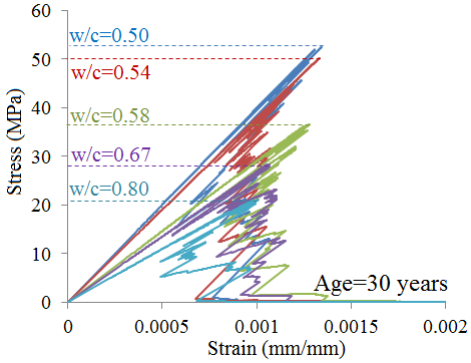

Figure 4.8: Simulated stress-strain relationships of load-free concretes with water-cement ratios of 0.50-0.80 (age=30 years)

4.4. VALUES OF MODEL PARAMETERS

FOR simulating the effect of continuous hydration, micro-cracking and self-healing on the long-term creep of concretes with different water-cement ratios, the following parameters used in the modified lattice model have to be determined:

- The empirical ageing factor a in the Eq. 3.17;
- The evolution of strength and elastic modulus of the mortar and bond beams with time resulting from continuous hydration, $f_c[\alpha(t)]$ and $E[\alpha(t)]$ (Eq. 3.18 and 3.19);
- The additional degree of hydration of the paste adjacent to any crack, $\triangle\alpha_{add,j}$ (needed in Eq. 3.27 to 3.30).

4.4.1. EMPIRICAL AGEING FACTOR a FOR DIFFERENT WATER-CEMENT RATIOS

The empirical ageing factor a is highly dependent on the age at loading, the initial water-cement ratio, type of cement and moisture content [20, 172]. This means that a changes for different water-cement ratios. In the following a is determined following the procedure proposed by van Breugel [21].

The activation energy concept for creep can be described with Eq. 3.14. This equation can be further simplified into Eq. 4.1 [20], viz.:

$$\epsilon_{cr} = a_0 \cdot t^n \tag{4.1}$$

with $a_0 = a \cdot \sigma$ [21]; n is proportionality factor.

Since a is related to the age at loading and type of cement (here, the moisture content is not taken into account since it is considered constant in this research), it can be described as a function of these two variables (Eq. 4.2).

$$a = q \cdot t_0^{-z} \tag{4.2}$$

where z is a coefficient related to the type of cement, varying from 0.3 (slow cement) to 0.4 (rapid cement) [21] and q is discussed later. Then a_0 can be written as Eq. 4.3.

$$a_0 = a \cdot \sigma = q \cdot t_0^{-z} \cdot \sigma = q \cdot t_0^{-z} \cdot P \cdot f_c(t_0) \tag{4.3}$$

where P is stress-strength ratio $P = \sigma / f_c(t_0)$; $f_c(t_0)$ is the compressive strength of concrete at age of loading.

The log-log plot of a_0 against t_0 yields a straight line [21]. This leads to the assumption that either $f_c(t_0)$ can be described by a power function with a constant value of power, or q is not a constant but a function of $f_c(t_0)$. Here, q is considered as a function of $f_c(t_0)$, as shown in Eq. 4.4.

$$q = \zeta / f_c(t_0) \tag{4.4}$$

where ζ is assumed to be a constant, independent of age at loading. Substituting Eq. 4.4 in Eq. 4.3, the function of a_0 is obtained:

$$a_0 = \zeta \cdot P \cdot t_0^{-z} \tag{4.5}$$

Wittmann [20] investigated the parameters a_0 and n for different water-cement ratios, based on the experimental data of creep tests (Fig. 4.9). In his creep tests the paste

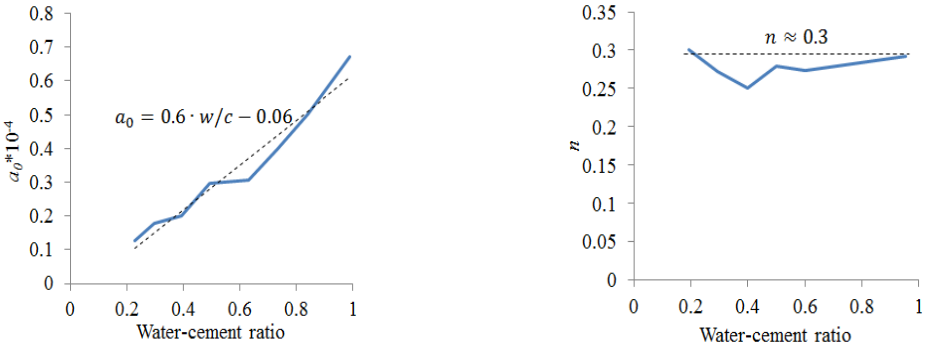

(a) $a_0(w/c)$ (b) n

Figure 4.9: Parameter a_0, n as a function of water-cement ratio (age at loading = 35 days; stress-strength ratio = 0.3; stress is constant) [20, 21]

specimens were loaded at 35 days at a stress level of 30% of the 35-day compressive strength ($P = 0.3$, $t_0 = 35$days). As can be seen in Fig. 4.9, the value of n remains more or less constant for different water-cement ratios[4], while a_0 increases with increasing water-cement ratio. Based on Eq. 4.1, with a fixed value of n, creep strains should be proportional to water-cement ratio at each time point, since a_0 is a function of the water-cement ratio. This is consistent with the work of Haranki [198].

Based on the curve in Fig. 4.9a, the values of a_0 for cement pastes with different water-cement ratios loaded at 35 days ($t_0 = 35$days) could be determined with the function:

$$a_0(w/c, t_0 = 35\text{days}) = 0.6 \cdot w/c - 0.06 \tag{4.6}$$

The procedure for calculating a for concretes with water-cement ratios of 0.50-0.80 loaded at 14 days ($t_0 = 14$days) is now as follows:

- Calculate $a_0(w/c, t_0 = 35\text{days})$ using Eq. 4.6.

[4] n is a constant: $n = 0.3$. Thus, in Eq. 3.15 and 3.17, $m = 0.7$.

- Calculate ζ using Eq. 4.5. Here t_0 = 35days, z = 0.375 (estimation; rapid cement was used in the creep test) and P = 0.3.
- Calculate q using Eq. 4.4. Here, $f_c(t_0 = 14\text{days})$ can be found in Table 4.1.
- Calculate $a(w/c, t_0 = 14\text{days})$ using Eq. 4.2. Here t_0 = 14days, z = 0.375 (estimation; rapid cement was used in the creep test) and P = 0.3.

The calculated values of a are shown in Table 4.6.

Table 4.6: Values of the empirical ageing factor a (Eq. 3.17) for concretes with water-cement ratios of 0.50-0.80 loaded at 14 days

w/c	0.50	0.54	0.58	0.67	0.80
a ($\times 10^{-5}$)	0.30[1]	0.38	0.44	0.82	1.34

[1] The value of a for concrete with a water-cement ratio of 0.50 has been used in Chapter 3.

4.4.2. EVOLUTION OF STRENGTH $f_c[\alpha(t)]$ AND ELASTIC MODULUS $E[\alpha(t)]$ OF MORTAR AND BOND BEAMS RESULTING FROM CONTINUOUS HYDRATION

Due to continuous hydration, the strength of the mortar and bond beams increases with time. Consequently the strength of the concrete specimen increases. The evolution of strength and elastic modulus of the mortar and bond beams can be calculated with Eq. 3.18 and 3.19. The procedure for determining the parameters (b, β, $f_{c,max}$, α_0, c_1 and c_2) in these equations has been described in Section 3.8.2. Table 4.7 gives the values of these parameters[5].

As can be seen in Table 4.7, the critical degree of hydration α_0 increases with increasing water-cement ratio, while $f_{c,max}$ decreases with increasing water-cement ratio. This is consistent with the findings of Lokhorst [44]. Fig. 4.10 shows the calculated evolution of the compressive strength of mortar beams of the concrete specimens calculated with Eq. 3.18.

Table 4.7: The values of the parameters for calculating the strength and elastic modulus of the mortar/bond beams in Eq. 3.18 and 3.19 for the concrete specimens with water-cement ratios of 0.50-0.80

w/c	b	β	$f_{c,max}$ (MPa) (mortar|bond)	α_0 *	c_1 (mortar|bond)	c_2
0.50	0.6	0.6	209|70	0.37	310|905	0.98
0.54	0.6	0.6	199|66	0.40	300|875	0.98
0.58	0.6	0.6	127|42	0.10	253|738	0.97
0.67	0.6	0.6	121|40	0.39	264|772	0.98
0.80	0.6	0.6	76|25	0.41	308|901	0.98

* α_0 is in general larger than expected. The reason has been explained in Section 3.8.2.

[5] Note that only two data points (14-day and 30-year strength and elastic modulus) are available in Brooks' test (Table 4.1) for calculating these parameters.

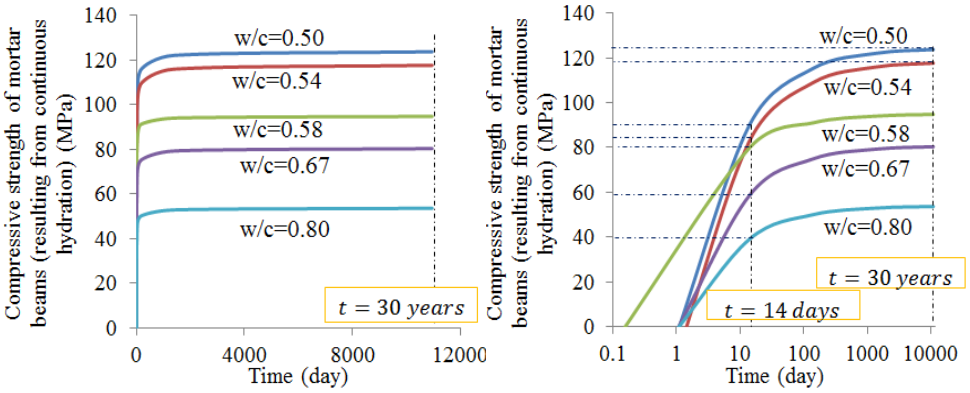

(a) Normal scale

(b) Semi-log scale

Figure 4.10: Calculated compressive strength of mortar beams versus time for the concrete specimens with water-cement ratios of 0.50-0.80 (Eq. 3.18)

4.4.3. ADDITIONAL DEGREE OF HYDRATION $\Delta\alpha_{add,j}$ OF PASTE ADJACENT TO ANY CRACK

MAXIMUM TOTAL ADDITIONAL OVERALL DEGREE OF HYDRATION $\Delta\alpha_{add,tot,max}$

The degree of hydration $\alpha(t)$ resulting from the continuous hydration (reference degree of hydration) is calculated with Eq. 3.1 for mixtures with water-cement ratios of 0.50-0.80 and shown in Fig. 4.11. After 30 years the degree of hydration, $\alpha(30y)$, has almost

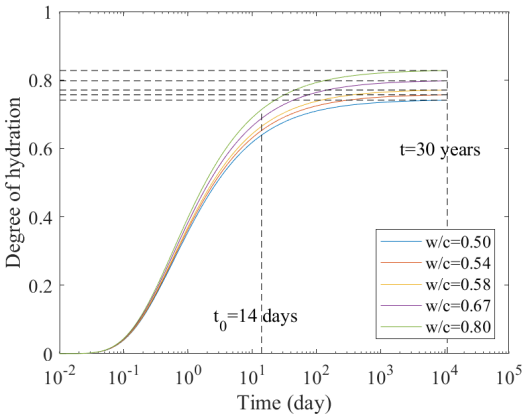

Figure 4.11: Calculated degree of hydration $\alpha(t)$ for the concrete specimens with water-cement ratios of 0.50-0.80 ($b = 0.6$ and $\beta = 0.6$ in Eq. 3.1)

reached its asymptote (i.e. the ultimate degree of hydration α_u). The total additional degree of hydration $\Delta\alpha_{add,tot}$ cannot be larger than $\Delta\alpha_{add,tot,max} = 1 - \alpha_u$. The ultimate degree of hydration α_u and the maximum additional degree of hydration $\Delta\alpha_{add,tot,max}$ for the concrete specimens with water-cement ratios of 0.50-0.80 are shown in Table 4.8 and plotted in Fig. 4.12.

Table 4.8: The (reference) degree of hydration after 30 years, α_u, and the maximum total additional degree of hydration $\Delta\alpha_{add,tot,max}$ for mixtures with different water-cement ratios

w/c	0.50	0.54	0.58	0.67	0.80
α_u	0.74	0.76	0.77	0.80	0.83
$\Delta\alpha_{add,tot,max}$	0.26	0.24	0.23	0.20	0.17

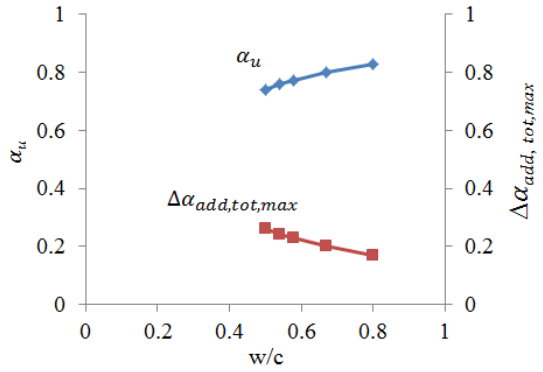

Figure 4.12: Ultimate degree of hydration α_u and maximum additional overall degree of hydration $\Delta\alpha_{add,tot,max}$ for mixtures with water-cement ratios of 0.50-0.80

ADDITIONAL DEGREE OF HYDRATION $\Delta\alpha_{add,j}$ OF PASTE ADJACENT TO ANY CRACK

The additional degree of hydration of the paste adjacent to any crack, $\Delta\alpha_{add,j}$, is estimated with Eq. 3.7, where $wcr_0 = 0.50$. $V_{uhc,i}$ is the volume of unhydrated cement in the paste at time t_i and can be calculated with Eq. 3.10. In this equation $\rho_c = 3000kg/m^3$ and $\rho_w = 1000kg/m^3$. For time t_i=30years[6], $V_{uhc,30y}$ is calculated for the values of V_p and $\alpha_{ref,30y}$ shown in Table 4.9. The calculated values of $V_{uhc,30y}$ are listed in Table 4.9. With the calculated values of $V_{uhc,30y}$ and for $\Delta\alpha_{add,j}(wcr = 0.50)$=0.21 (Section 3.8.3), the additional degree of hydration of the paste adjacent to any crack, $\Delta\alpha_{add,j}$, for concretes with water-cement ratios of 0.50-0.80 are calculated with Eq. 3.7 and listed in Table 4.9. Fig. 4.13 shows that $\Delta\alpha_{add,j}$ decreases with increasing the water-cement ratios.

4.5. SIMULATION RESULTS AND DISCUSSIONS

4.5.1. EFFECT OF CONTINUOUS HYDRATION ON THE LONG-TERM CREEP OF CONCRETES: W/C=0.50-0.80

The input parameters for simulation of the effect of continuous hydration on the long-term creep of concrete are as follows:

- If continuous hydration is considered, the evolution of strength and elastic modulus of the mortar and bond beams ($f_c[\alpha(t)]$ and $E[\alpha(t)]$) are calculated with Eq.

[6]The rate of hydration for concretes with water-cement ratios of 0.50-0.80 after 14 days does not differ too much. For concrete with w/c=0.50, the rate of hydration from 14 days to 30 years is 0.0041 to 1.1×10^{-7} per day (calculated with derivative of Eq. 3.1). For concrete with w/c=0.80, the rate of hydration from 14 days to 30 years is 0.0046 to 1.2×10^{-7} per day. The rate of degree of hydration after 30 years is approximately zero for concretes with different water-cement ratios.

Table 4.9: Values of the additional degree of hydration of the paste adjacent to any crack $\Delta\alpha_{add,j}$ for concretes with water-cement ratios of 0.50-0.80, calculated with Eq. 3.7

Parameters	Equation	Unit	w/c				
			0.50	0.54	0.58	0.67	0.80
V_p	$V_p = r_p V$ [1]	$[mm^2]$	3100	3260	3370	3660	4050
$\alpha_{ref,30y}$ [2]	Eq. 3.1	[-]	0.74	0.76	0.77	0.80	0.83
$V_{uhc,30y}$	Eq. 3.10	$[mm^2]$	322	299	283	243	203
$\Delta\alpha_{add,j}$	Eq. 3.7	[-]	0.210	0.195	0.185	0.160	0.132

[1] $V_p = r_p V$ where r_p is the volume fraction of the paste, which is given in the third column Table 4.1 and $V = 100 \times 100 mm^2$.

[2] $\alpha_{ref,30y}$ is the reference degree of hydration after 30 years, which can be calculated with Eq. 3.1. It equals the ultimate degree of hydration α_u (Table 4.8).

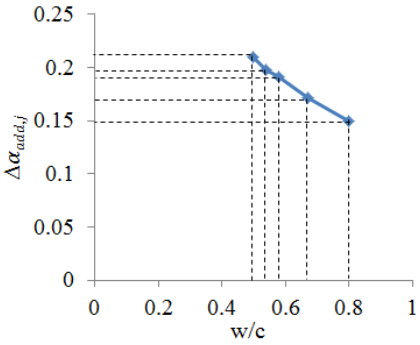

Figure 4.13: Calculated additional degree of hydration of the paste adjacent to any crack, $\Delta\alpha_{add,j}$, for mixtures with water-cement ratios of 0.50-0.80

3.18 and 3.19. The values of the parameters, $f_{c,max}$, α_0, c_1 and c_2, are given in Table 4.7. If continuous hydration is *not* considered, the strength and elastic modulus of the mortar and bond beams are constant and equal to the 14-day values (Table 4.2).

- The creep strain of the mortar and bond beams of the lattice model is calculated with Eq. 3.17. The values of a are shown in Table 4.6, n and m are 0.3 and 0.7, respectively (Section 4.4.1).

The compressive strength of the concrete specimens with and without the effect of continuous hydration is simulated with the lattice fracture model and shown in Fig. 4.14. The stress-strength ratio with and without the effect of continuous hydration is also calculated and shown in Fig. 4.14.

The simulated creep strains of concretes with water-cement ratio of 0.50-0.80 *without* and *with* considering the effect of continuous hydration are shown in Fig. 4.15a and Fig. 4.15b, respectively. When continuous hydration is considered, 30-year creep strains are 7%-15% lower than that without the effect of continuous hydration. As a typical example of the effect of continuous hydration on the long-term creep, the simulated creep strains of concrete with a water-cement ratio of 0.54 are shown in Fig. 4.16. A discrep-

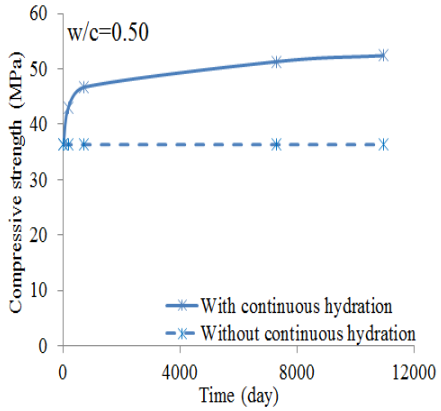

(a) Strength

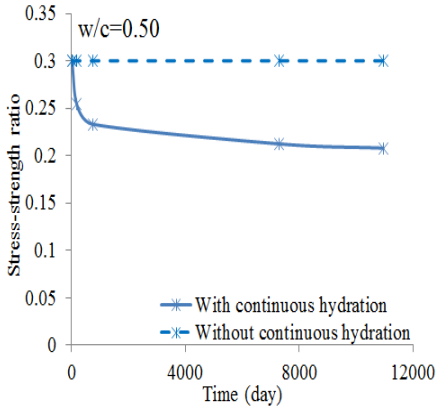

(b) Stress-strength ratio

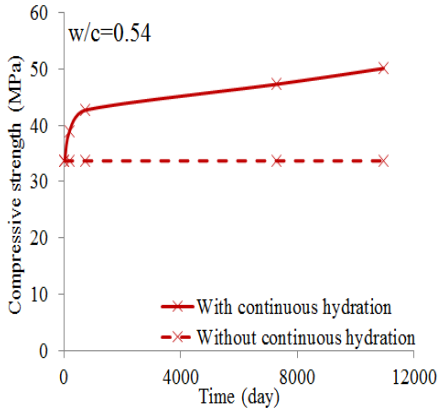

(c) Strength

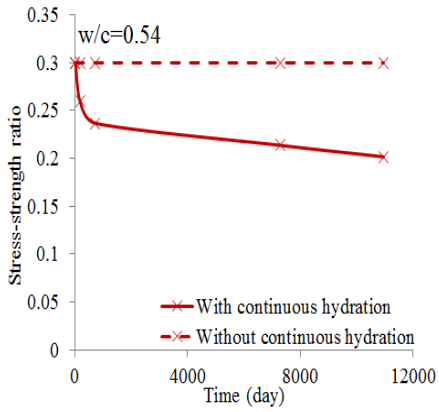

(d) Stress-strength ratio

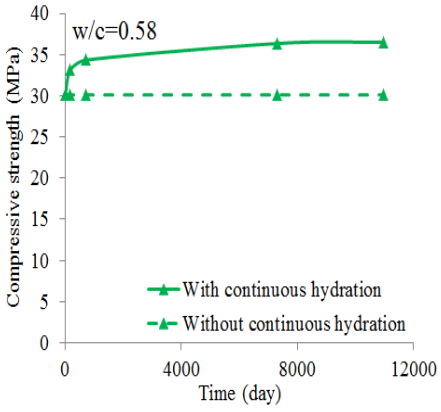

(e) Strength

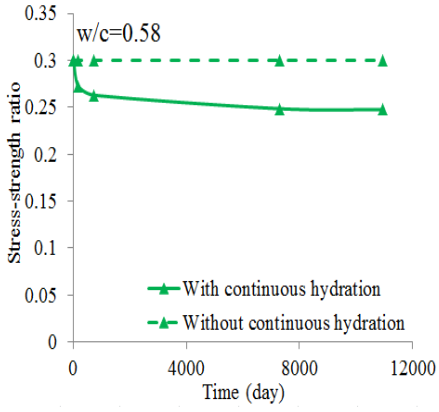

(f) Stress-strength ratio

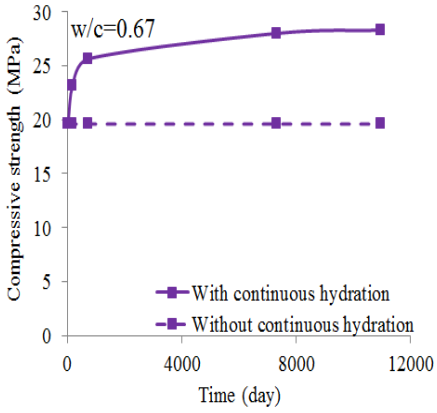

(g) Strength

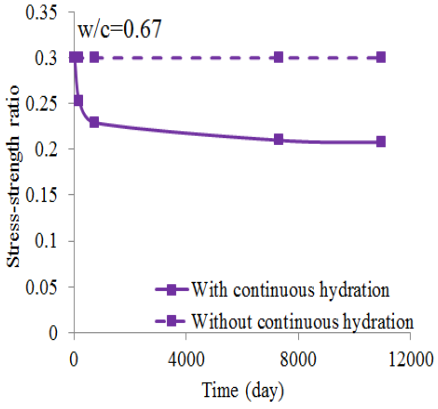

(h) Stress-strength ratio

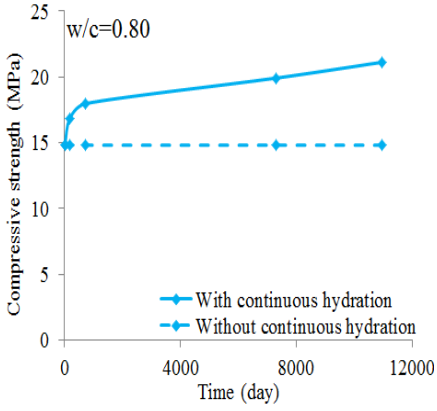

(i) Strength

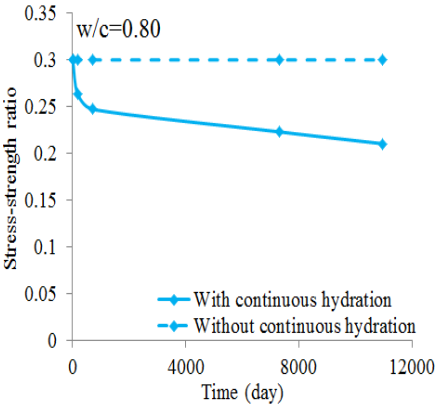

(j) Stress-strength ratio

Figure 4.14: Simulated compressive strength and stress-strength ratio of the concrete specimens with water-cement ratios of 0.50-0.80 loaded at 14 days at a stress level of 30% of compressive strength: with and without effect of continuous hydration

ancy is found between the experimental data and simulated strains. Since the goal of this study is to investigate the effect of continuous hydration, micro-cracking and self-healing on the long-term creep, no attempts will be made to adjust the creep parameters in this stage of the study in order to improve the fit.

4.5.2. EFFECT OF MICRO-CRACKING ON THE LONG-TERM CREEP AND COMPRESSIVE STRENGTH OF CONCRETE: W/C=0.50-0.80

The effect of micro-cracking on the long-term creep and compressive strength is simulated for concretes with water-cement ratios of 0.50-0.80. The input parameters for calculating the strength (Eq. 3.18), elastic modulus (Eq. 3.19), and creep (Eq. 3.17) of the mortar and bond beams are the same as those in Section 4.5.1.

The simulated creep strains *without* and *with* the effect of micro-cracking are shown

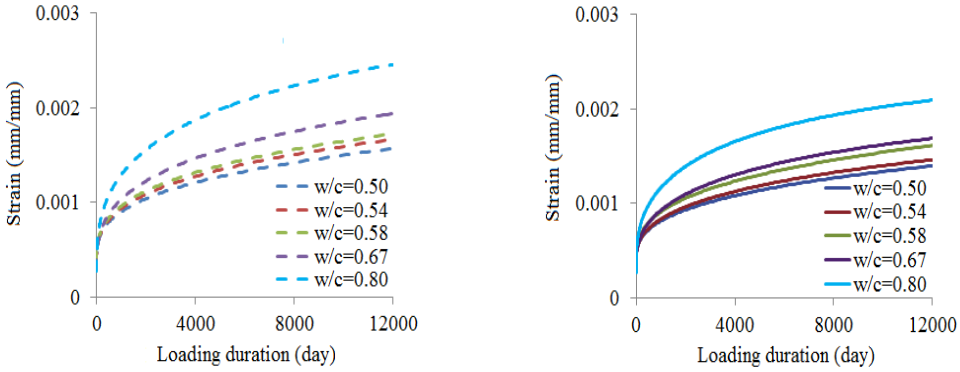

(a) continuous hydration is not considered

(b) continuous hydration is considered

Figure 4.15: Simulated creep strains of concrete specimens with water-cement ratios of 0.50-0.80: with and without the effect of continuous hydration (age at loading=14 days; stress level=30% of 14-day compressive strength)

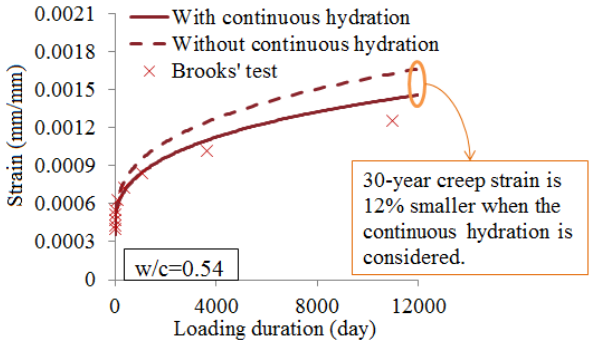

Figure 4.16: Simulated creep strains with and without the effect of continuous hydration for concrete with a water-cement ratio of 0.54 (age at loading=14 days; stress level=30% of 14-day compressive strength)

in Fig. 4.17a and Fig. 4.17b, respectively. When the effect of micro-cracking is considered, the creep strains are larger than those without the effect of micro-cracking. As a typical example of the effect of micro-cracking on the long-term creep, the simulated creep strains of concrete with a water-cement ratio of 0.54 is shown in Fig. 4.18. When micro-cracking occurs, the simulated strains deviate more from the experimental data than that in case only continuous hydration is considered.

With increasing water-cement ratio, the number of micro-cracks generated during the creep process increases (see Fig. 4.19a) and the additional overall deformations caused by micro-cracking become larger (see Fig. 4.19b). After 30 years the extra creep deformation due to micro-cracking for concretes with water-cement ratios of 0.50-0.58 reaches 8% to 15%. For concretes with water-cement ratios of 0.67-0.80, these percentages are almost two times higher, i.e. 20% to 30% after 30 years. Fig. 4.19c shows the relationship between the extra deformation caused by micro-cracking and the total number

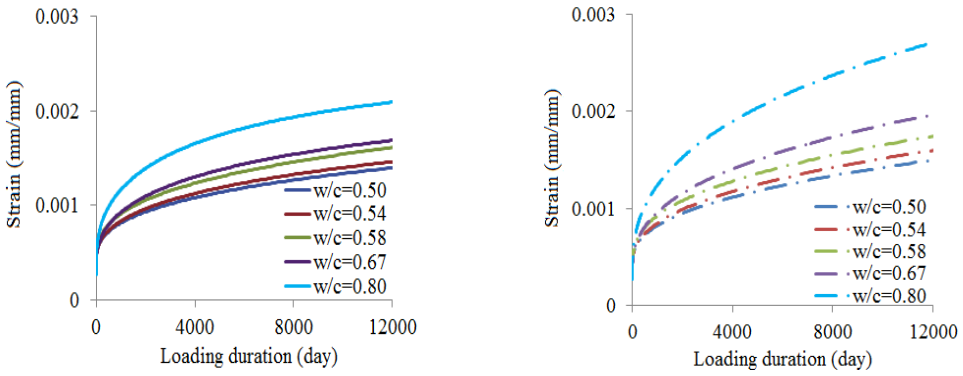

(a) Micro-cracking is not considered

(b) Micro-cracking is considered

Figure 4.17: Simulated creep strains of concretes with water-cement ratios of 0.50-0.80: with and without the effect of micro-cracking (age at loading=14 days; stress level=30% of 14-day compressive strength)

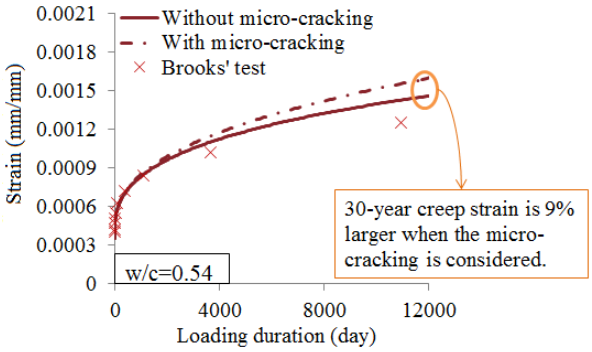

Figure 4.18: Simulated creep strains with and without the effect of micro-cracking for concrete with a water-cement ratio of 0.54 (age at loading=14 days; stress level=30% of 14-day compressive strength)

of micro-cracks. It can be seen that the extra deformation increases exponentially with increasing number of micro-cracks.

CRACK WIDTH DURING THE CREEP PROCESS

The calculation of the crack width with the lattice model has been explained in Chapter 3. For mixtures with water-cement ratios of 0.50-0.80 the calculated maximum crack width of the micro-cracks occurring during the creep process is shown in Fig. 4.20. This figure shows that the maximum crack width of the micro-cracks during the creep process increases with time. The maximum crack widths after 30 years for concretes with water-cement ratios of 0.50-0.80 are $3\mu m$, $4\mu m$, $3.7\mu m$, $4.7\mu m$ and $7.4\mu m$, respectively. The maximum crack width generated during the creep process is larger for concrete with a high water-cement ratio than for concrete with a low water-cement ratio.

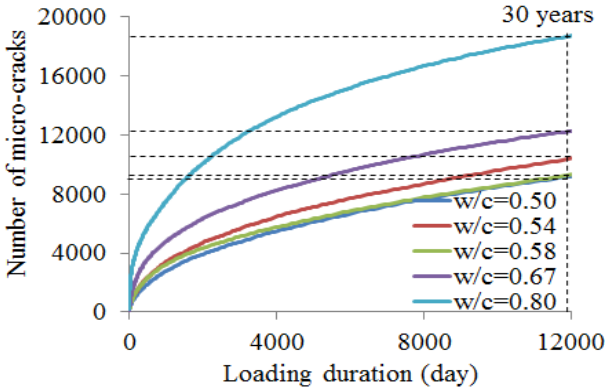

(a) Number of micro-cracks

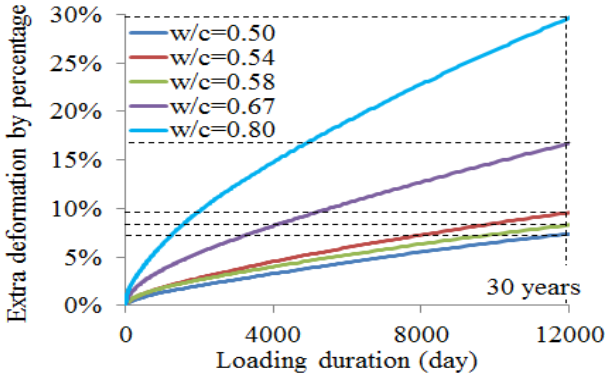

(b) Extra deformation by percentage

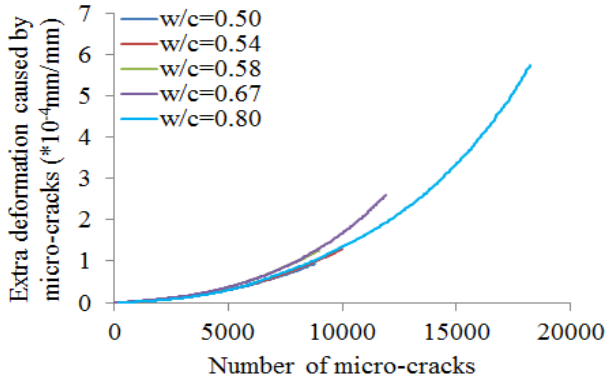

(c) Extra deformation versus number of micro-cracks

Figure 4.19: (a) Number of cracks during the creep process; (b) Percentage of additional deformation caused by micro-cracking [extra deformation by percentage = (deformation with micro-cracking - deformation without micro-cracking) / deformation without micro-cracking]; (c) The extra deformation caused by micro-cracking versus total number of micro-cracks

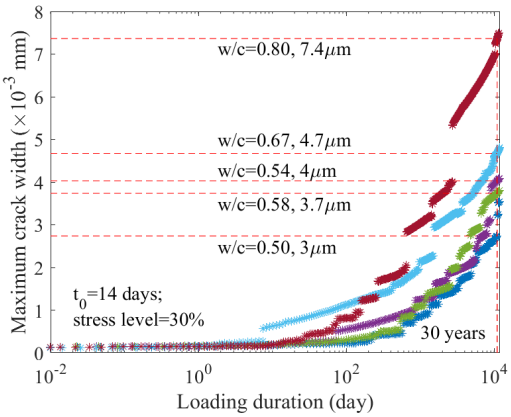

Figure 4.20: Maximum crack width of the micro-cracks occurring during the creep process of the concrete specimens with water-cement ratios of 0.50-0.80

COMPRESSIVE STRENGTH AFTER MICRO-CRACKING

The simulated compressive strength of concretes with water-cement ratios of 0.50-0.80 after micro-cracking is shown in Fig. 4.21. The stress-strength ratio is also calculated and shown in Fig. 4.21. It can be seen from the graphs in this figure that the compressive strength is smaller than that in case micro-cracking does not occur. While micro-cracking takes place, the strength still increases over time for concrete with a water-cement ratio of 0.50 (blue dotted dashed line in Fig. 4.21a). However, for concretes with higher water-cement ratios (0.54, 0.58 and 0.80), the compressive strength first increases and then decreases with time (red, green and blue dotted dashed lines in Fig. 4.21c, 4.21e and 4.21i). This is because the reduction of the strength due to micro-cracking exceeds the increase of the strength due to continuous hydration.

Due to micro-cracking during the creep process, the 30-year compressive strength of concretes with water-cement ratios of 0.50-0.80 is 5%-17% smaller than that when the micro-cracking is not taken into account (see Table 4.10).

Table 4.10: Comparison between simulated 30-year compressive strength with and without the effect of micro-cracking for concretes with water-cement ratios of 0.50-0.80

w/c	Simulated 30-year strength (MPa)		Reduction in strength caused by micro-cracking (%)
	Without micro-cracking (only with hydration)	With micro-cracking	
0.50	52.4	49.5	5.5
0.54	50.1	41.8	16.7
0.58	36.5	33.5	8.2
0.67	28.3	27.8	1.8
0.80	21.1	17.6	16.6

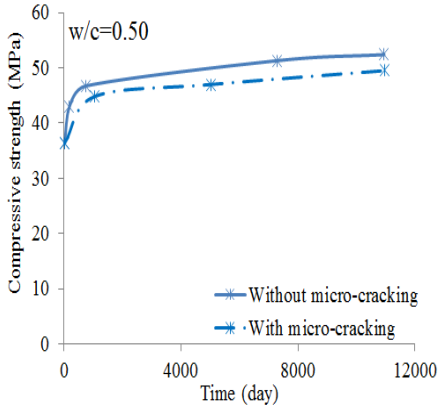

(a) Strength

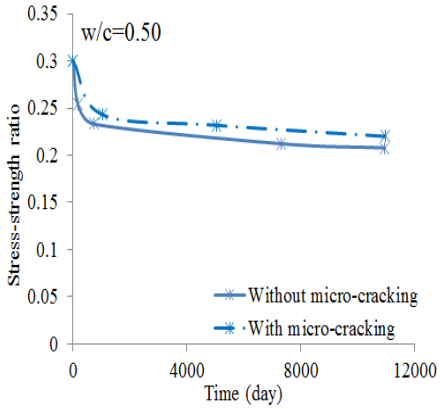

(b) Stress-strength ratio

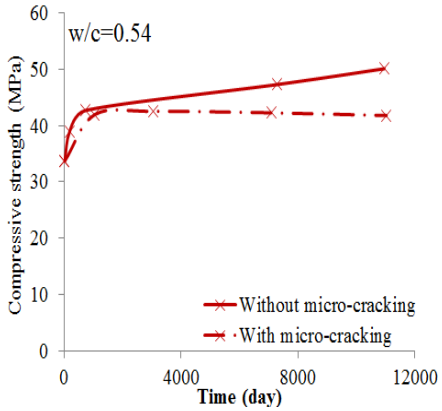

(c) Strength

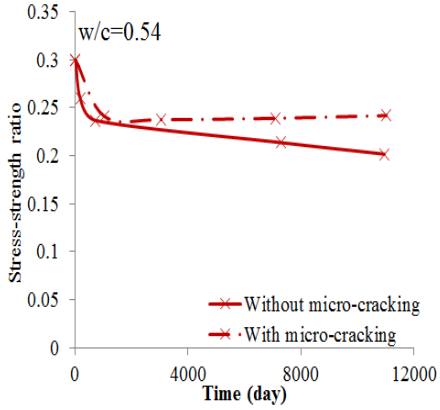

(d) Stress-strength ratio

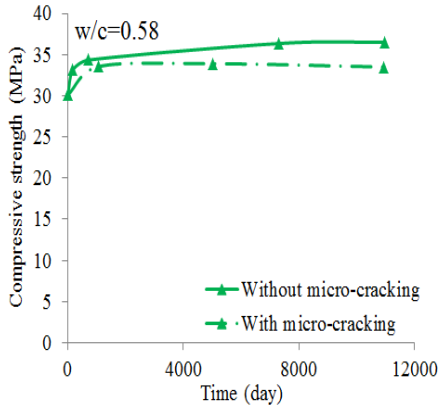

(e) Strength

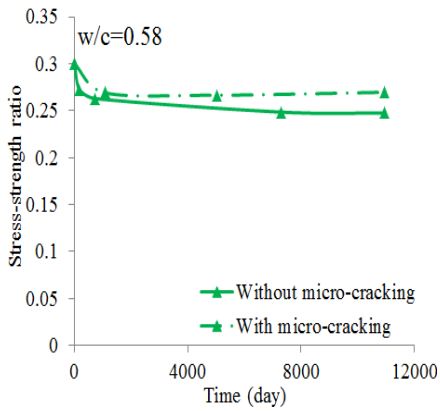

(f) Stress-strength ratio

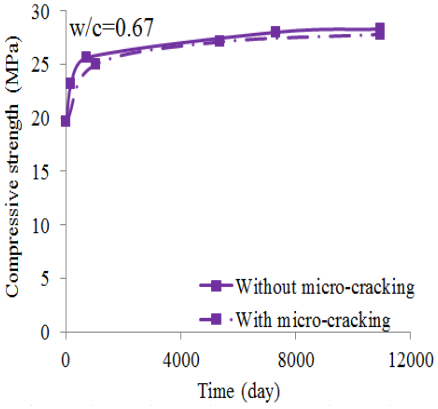

(g) Strength

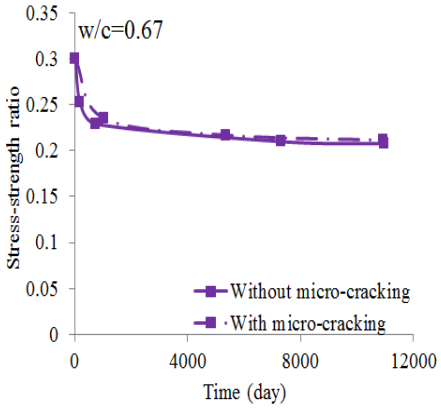

(h) Stress-strength ratio

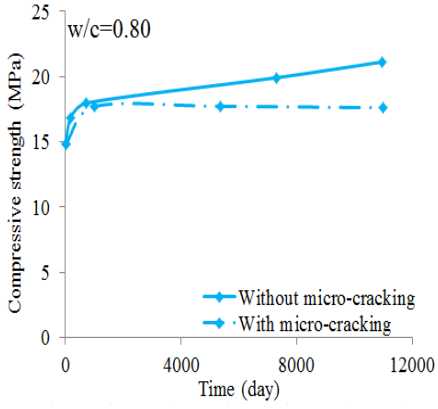

(i) Strength

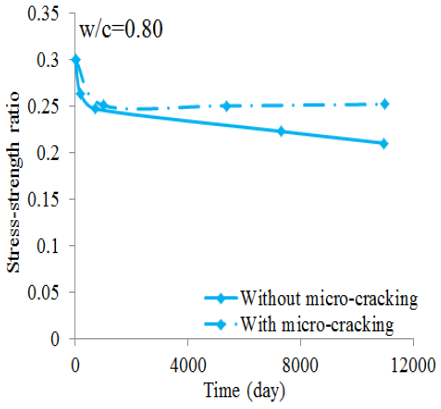

(j) Stress-strength ratio

Figure 4.21: Simulated evolution of compressive strength and stress-strength ratio of the concrete specimens with water-cement ratios of 0.50-0.80 loaded at 14 days at a stress level of 30% of compressive strength: with and without the effect of micro-cracking

SOME REMARKS

- It is noted that the number of micro-cracks in concrete with a water-cement ratio of 0.58 is slightly higher than that in concrete with a water-cement ratio of 0.50 and lower than that in concrete with a water-cement ratio of 0.54 (Fig. 4.19a). Similar trend was also found for the maximum crack width (Fig. 4.20). The stress-strength ratio during the creep process of concrete with a water-cement ratio of 0.58 is higher than 0.25 (Fig. 4.21f), while for other concretes the stress-strength ratio is below 0.25 (Fig. 4.21). The higher stress-strength ratio may lead to higher stress relaxation in the lattice beams, which postpones the micro-cracking [199].
- Based on the simulation results in this section it can be concluded that, for the same stress-strength ratios at the moment of application of the load, concrete with a high water-cement ratio is more susceptible to micro-cracking during the creep

process due to its lower strength compared to concrete with a low water-cement ratio. In the long term, the number of micro-cracks is larger and the contribution of the micro-cracks to the additional overall deformation and the reduction of the strength is larger for concrete with a high water-cement ratio than for concrete with a low water-cement ratio.

4.5.3. EFFECT OF SELF-HEALING ON THE LONG-TERM CREEP AND COMPRESSIVE STRENGTH OF CONCRETE: W/C=0.50-0.80

Generally speaking, the amount of unhydrated cement in concrete with a low water-cement ratio is larger than that in concrete with a high water-cement ratio at the same age. Hence, if the unhydrated particles are exposed to water in the cracks, the self-healing efficiency is expected to be higher for concrete with a low water-cement ratio than for concrete with a high water-cement ratio. However, the amount of unhydrated cement is not the only parameter influencing the self-healing. Damage degree [197] and crack density [196] are also supposed to be two important factors influencing the self-healing efficiency (Section 4.1). As mention in Section 3.5.2, with increasing damage degree (i.e. with increasing number of broken beams) the total additional degree of hydration increases, while a higher crack density (i.e. a larger percentage overlap areas r_{ol} of the paste adjacent to the cracks) will give a lower total additional degree of hydration. In the following subsections, the effect of self-healing on the long-term creep and strength of concretes with water-cement ratios of 0.50-0.80 is analysed. The influence of crack density and damage degree on the self-healing process are then discussed.

CALCULATION OF κ (EQ. 3.23 AND 3.24) AND $\triangle\alpha_{add',j}$ (EQ. 3.29 AND 3.30)

The minimum volume of the reaction products produced during additional hydration of the paste adjacent to any crack, $V_{RP,add,j,min}$), which is available for filling up the crack and densification of the paste adjacent to the crack, was discussed in Section 3.8.3 and is calculated with Eq. 3.38, viz.:

$$V_{RP,add,j,min} = 1.2 \cdot \triangle\alpha_{add,j} \cdot V_{ac,p,j} \cdot (1 - \alpha_{ref,max}) \cdot \frac{1}{1 + \frac{w}{c} \cdot \frac{\rho_c}{\rho_w}}$$

The values of the parameters $\triangle\alpha_{add,j}$, $V_{ac,p,j}$ and $\alpha_{ref,max}$ in this equation depend on the water-cement ratio and are listed in Table 4.11. With the parameters in this table $V_{RP,add,j,min}$ is calculated with Eq. 3.38 [7] and shown in Table 4.12. The values of strength recovery degree κ and the effective additional degree of hydration of the paste adjacent to any crack $\triangle\alpha_{add',j}$ are determined with Eq. 3.25 to 3.28 and listed in Table 4.12 as well.

As can be seen from Table 4.12, for concrete with a water-cement ratio of 0.80 the volume of reaction product $V_{RP,add,j,min}$ is smaller than the volume of the largest crack $V_{c,j}$. The reaction product is not enough to fill up the largest crack and no reaction product is left to densify the paste adjacent to this largest crack[8]. Cracks smaller than the largest

[7] In Eq. 3.38 $\rho_c = 3000 kg/m^3$ and $\rho_w = 1000 kg/m^3$

[8] Based on the assumption that the reaction product is first used to fill up the crack and then, if some product is left, it will be used to densify the paste adjacent to the crack.

crack can be filled up with reaction product and some product might be left to densify the paste adjacent to these cracks. For concrete with a water-cement ratio of 0.80, a critical crack width (ω_{cri}) is defined. A crack with the critical width can be just filled up the amount of reaction product $V_{RP,add,j,min}$ and no product is left to densify the paste adjacent to this crack. The critical crack width can then be calculated with Eq. 4.7, viz.:

$$\omega_{cri} = V_{RP,add,j,min}/l_2 \tag{4.7}$$

where l_2 is the length of a crack (see Fig. 3.35b). Cracks with a width below the critical crack width can be filled up with the reaction products and some product is left to densify the paste adjacent to the crack, i.e. $\kappa = 1$ and $0 \leq \triangle\alpha_{add',j} < \triangle\alpha_{add,j}$ (see Fig. 4.22a). If the crack width is larger than the critical crack width, the crack will partly be filled up with reaction product and the rest product is used to densify the paste adjacent to the crack[9], i.e. $\kappa = x \cdot V_{RP,add,j,min}$ [10] and $\triangle\alpha_{add',j} = (1-x)\cdot\triangle\alpha_{add,j}$ (see Fig. 4.22b) where x is volume fraction of reaction product precipitating in a crack larger than the critical crack. In order to determine x experiments or numerical simulations (e.g. thermodynamic analysis) are needed to study the precipitation of the reaction product in the crack and the area around a crack. Here, the value of x is assumed at 0, which implies that the strength will not be recovered if the crack is not fully filled up with reaction product. The values of κ and $\triangle\alpha_{add',j}$ for concrete with a water-cement ratio of 0.80 are listed in Table 4.13. These values will be used in the following simulations instead of the values in the seventh column in Table 4.12.

Table 4.11: Parameters for calculating κ and $\triangle\alpha_{add',j}$

Parameters	Section	Unit	w/c				
			0.50	0.54	0.58	0.67	0.80
$\triangle\alpha_{add,j}$	4.4.3	[-]	0.210	0.195	0.185	0.160	0.132
$V_{ac,p,j}$ [1]	3.8.3	$[mm^2]$	0.27	0.28	0.29	0.31	0.35
$\alpha_{ref,max}$ [2]	4.4.3	[-]	0.74	0.76	0.77	0.80	0.83
ω_{max} [3]	4.5.2	$[\mu m]$	3	4	3.7	4.7	7.4

[1] $V_{ac,p,j}$ is the volume of the paste adjacent to any crack, which follows Eq. 3.34 where the percentage volume of the paste ($V_p/V = r_p$) is given in Table 4.1. δ_c in Eq. 3.34 is assumed to be the same for concretes with different water-cement ratios.

[2] $\alpha_{ref,max}$ is the reference degree of hydration after 30 years: $\alpha_{ref,max} = \alpha(30y) = \alpha_u$ which are given in Table 4.8.

[3] ω_{max} is the maximum crack width after 30 years, which is shown in Fig. 4.20, needed for calculation of $V_{c,j}$ shown in Table 4.12.

[9] A modification for the assumption[8]: if the crack width is smaller than the critical width, the reaction product is first used to fill up the crack and then, if some product is left, it will be used to densify the paste adjacent to the crack. If the crack width is larger than the critical width, the reaction product will partly fill up the crack and the rest product is used to densify the paste adjacent to the crack.

[10] The crack width in concrete with a high water-cement ratio is generally (especially at later age) larger than that in concrete with a low water-cement ratio (Fig. 4.20). The reaction product tends to precipitate in smaller cracks, instead of larger cracks. Therefore, it is more difficult for a larger crack to be filled up with reaction product and gain strength.

Table 4.12: Values of κ and $\Delta\alpha_{add',j}$ for concretes with water-cement ratios of 0.50-0.80

Parameters	Unit	w/c				
		0.50	0.54	0.58	0.67	0.80
$V_{RP,add,j,min}$	$[mm^2]$	0.0100	0.0061	0.0055	0.0042	0.0030
$V_{c,j}$ [1]	$[mm^2]$	0.0026	0.0034	0.0032	0.0040	0.0060
κ	[-]	1	1	1	1	0.5 [2]
$\Delta\alpha_{add',j}$	[-]	0.160	0.085	0.078	0.008	0 [2]

[1] The volumes $V_{c,j}$ of the cracks with the maximum crack width are calculated with Eq. 3.33 for $\omega = \omega_{max}$. The maximum crack width ω_{max} is given in Table 4.11.

[2] For concrete with a water-cement ratio of 0.80 the volume of reaction product $V_{RP,add,j,min}$ is smaller than the volume of the largest crack $V_{c,j}$. The reaction product is not enough to fill up the largest crack and no reaction product is left to densify the paste adjacent to this largest crack. It is further discussed in the following text.

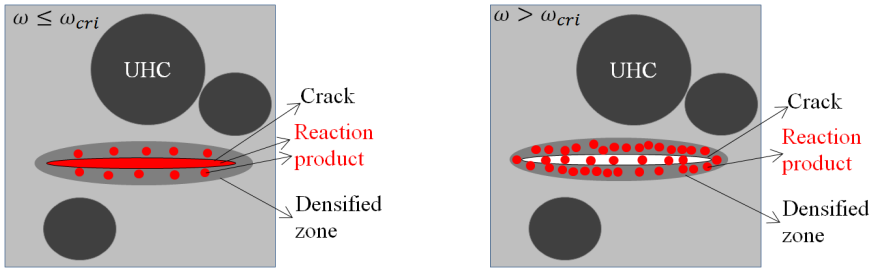

(a) $\omega \leq \omega_{cri}$: crack filled up

(b) $\omega > \omega_{cri}$: crack not filled up

Figure 4.22: (a) When $\omega \leq \omega_{cri}$, the crack is filled up with reaction product and some product is left to densify the paste adjacent to the crack; (b) when $\omega > \omega_{cri}$, the crack will *not* be filled up with reaction product and *all* the reaction product produced during the additional hydration is used to densify the paste adjacent to the crack

Table 4.13: Values of κ and $\Delta\alpha_{add',j}$ for concrete with a water-cement ratio of 0.80

w/c	Parameters						
	ω_{cri} (μm)	$V_{c,j}$ [1] (mm^2)	$V_{RP,add,j,min}$ (mm^2)	$\omega \leq \omega_{cri}$		$\omega > \omega_{cri}$	
				κ	$\Delta\alpha_{add',j}$	κ	$\Delta\alpha_{add',j}$
0.80	3.4	0.0030	0.0030	1	0	0	0.132

[1] The volumes $V_{c,j}$ of the cracks with the critical crack width are calculated with Eq. 3.33 for $\omega = \omega_{cri}$.

SIMULATION RESULTS

The input parameters for calculating the strength and elastic modulus after continuous hydration and creep of the mortar and bond beams of the mixtures are the same as those in Section 4.5.1. The strength and elastic modulus of the broken beams after self-healing are calculated with Eq. 3.23 and 3.24, while the strength and elastic modulus of the beams which are connected to the broken beams are calculated with Eq. 3.29 and 3.30. Two parameters, κ and $\Delta\alpha_{add',j}$, in those equations are given in Table 4.12 and 4.13.

The simulated creep strains are shown in Fig. 4.23. They are compared to the experimental data from Brook's test (Section 4.2). The simulated compressive strength and stress-strength ratio of the concrete specimens is shown in Fig. 4.24.

Fig. 4.23 shows that due to self-healing the simulated creep strains after 30 years (solid lines) of concretes with water-cement ratios of 0.50-0.80 are lower than those when self-healing is not considered (double dotted dashed lines). The total number of micro-cracks formed during the creep process is larger for concrete with a high water-cement ratio than for concrete with a low water-cement ratio (without the effect of self-healing, see Fig. 4.19a) and thus the additional overall strain caused by micro-cracking is larger for the former than for the latter (see Fig. 4.19b). Self-healing prevents the occurrence of the additional overall creep deformation caused by micro-cracking. Therefore, the creep curve is close to or coincides with the curve without the effect of micro-cracking (with only continuous hydration; dashed lines in Fig. 4.23). Due to the densification of the paste adjacent to cracks, the concrete specimen gains an extra increase in strength (see Fig. 4.24). The creep curves with the effect of self-healing are thus below the curves without the effect of micro-cracking (with only continuous hydration; dashed lines in Fig. 4.23).

When self-healing takes place, concretes gain an extra increase in strength (see Fig. 4.24). For concretes with water-cement ratios of 0.50-0.54 the strength increases with time, which is shown with the blue and red solid lines in Fig. 4.24a and 4.24c. However, for concretes with higher water-cement ratios (0.58-0.80), the strength first increases and then decreases over time (green, purple and blue solid lines in Fig. 4.24e, 4.24g and 4.24i). This indicates that, after a certain period under load, self-healing cannot contribute to an extra increase in strength of concrete. This is because the total number of micro-cracks increases over time and the crack density becomes larger. The overlap areas become larger and thus the total additional overall hydration will remain lower.

The 30-year experimental and simulated compressive strength of load-free and loaded concrete specimens with water-cement ratios of 0.50-0.80 are shown in Table 4.14. This table shows that concrete specimens with water-cement ratios of 0.50, 0.54, 0.58, 0.67 and 0.80 gain 14.69%, 11.69%, 16.00%, 4.13% and -0.43% extra increase in strength, respectively. Despite these percentages, in general, are lower than the experimental values in Brooks' test (fourth column in Table 4.14), the trend is similar to the experimental values: the extra strength increase is smaller for concrete with a high water-cement ratio than for concrete with a low water-cement ratio (see dashed lines in Fig. 4.25).

DISCUSSION ON THE DAMAGE DEGREE AND CRACK DENSITY FOR CONCRETES WITH DIFFERENT WATER-CEMENT RATIOS

As aforementioned, the extra increase in strength is generally larger for concrete with a low water-cement ratio than for concrete with a high water-cement ratio (see dashed lines in Fig. 4.25). The damage degree (or total number of cracks) at the end of creep period in loaded concrete with a high water-cement ratio is larger than that in concrete with a low water-cement ratio (Fig. 4.19a) [11]. The crack density will also be larger than

[11] Qian [35] performed numerical uniaxial tensile test on cement paste with different water-cement ratios. The crack pattern at final failure stage is more dispersed for paste with a high water-cement ratio than for paste with a low water-cement ratio. Opposite results are obtained in our study: the crack density is higher

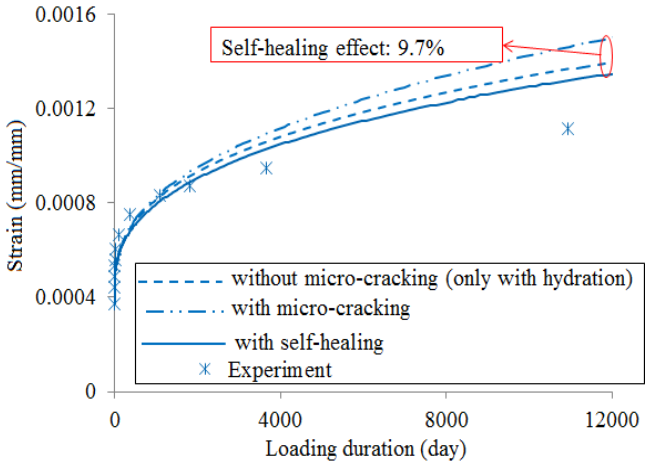

(a) w/c=0.50

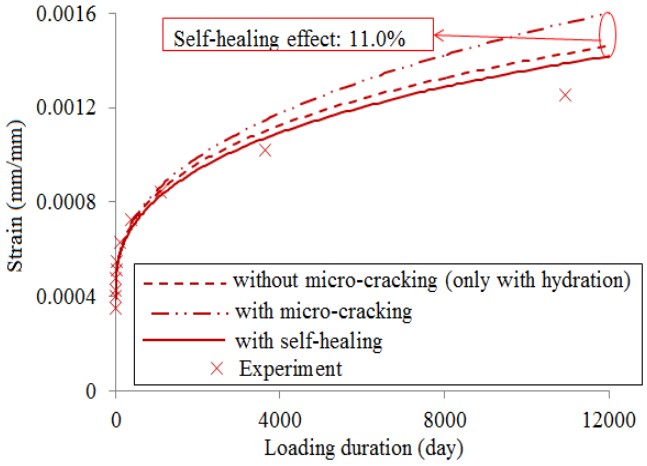

(b) w/c=0.54

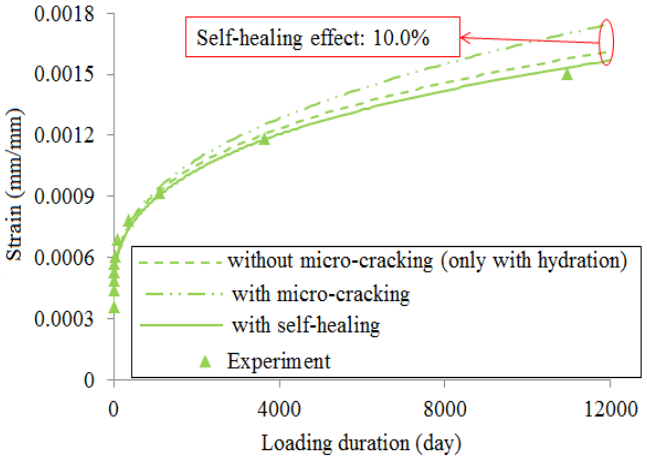

(c) w/c=0.58

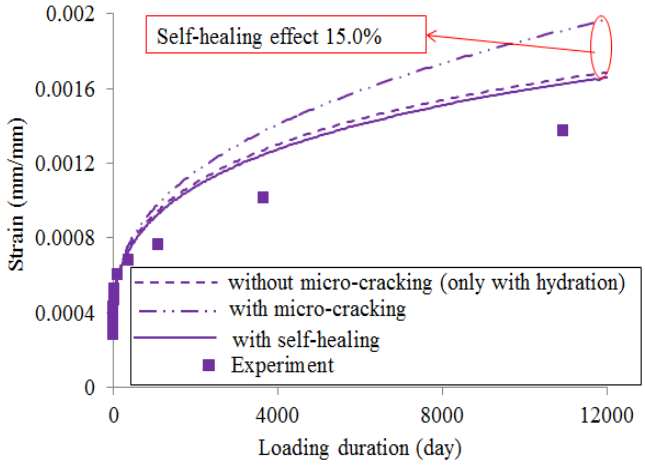

(d) w/c=0.67

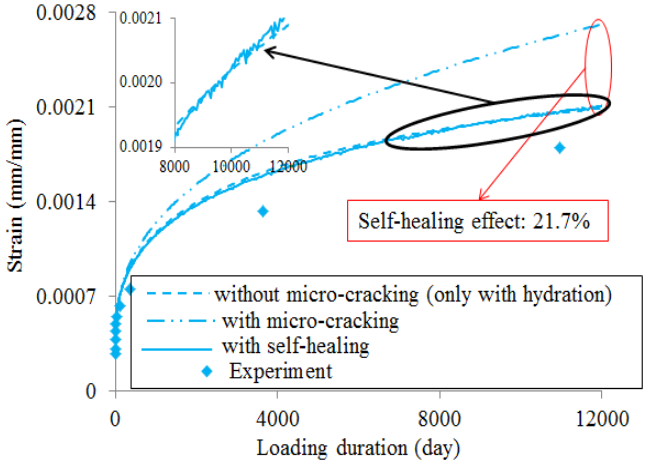

(e) w/c=0.80

Figure 4.23: Simulated creep strains of concrete specimens with water-cement ratios of 0.50-0.80: effect of self-healing (age at loading=14 days; stress level=30% of 14-day compressive strength)

that in concrete with a low water-cement ratio. Thus more overlap volume/area appears in the pastes adjacent to the cracks. The percentage overlap area of the pastes adjacent

for concrete with a high water-cement ratio than for concrete with a low water-cement ratio. Our model involves time which leads to a quite difference in the crack pattern. When the number of micro-cracks is not high (shortly after application of loading), the crack density might be slightly lower for concrete with a high water-cement ratio than for concrete with a low water-cement ratio (e.g. r_{ol} of concretes with water-cement ratios of 0.67 and 0.80 is slightly lower than that of other concretes when N is lower than 3000 to 5000). Over time, concrete with a high water-cement ratio has a much larger number of micro-cracks than concrete with a low water-cement ratio (Fig. 4.19a). The crack density is then larger for the former concrete than for the latter concrete.

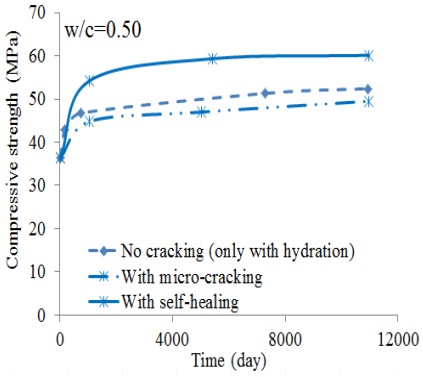

(a) Strength

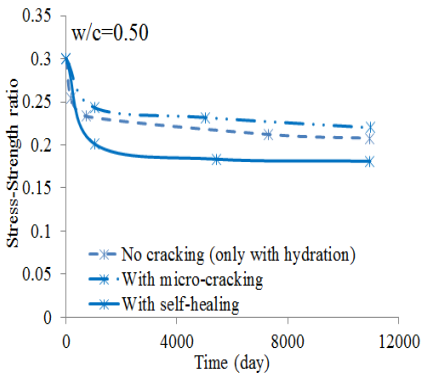

(b) Stress-strength ratio

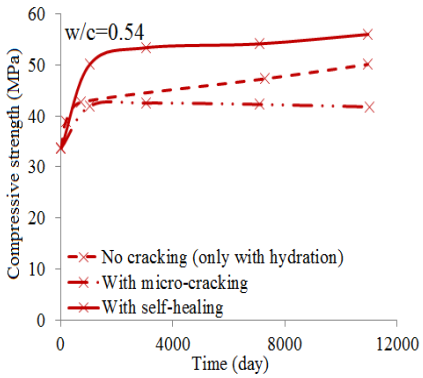

(c) Strength

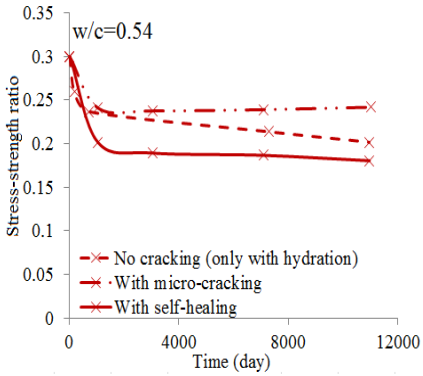

(d) Stress-strength ratio

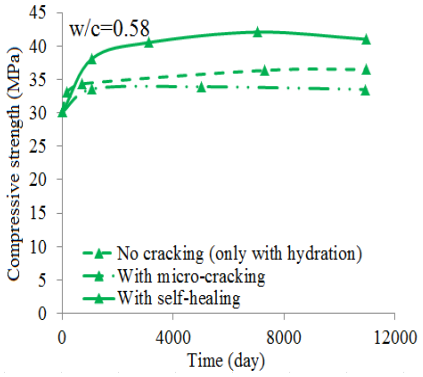

(e) Strength

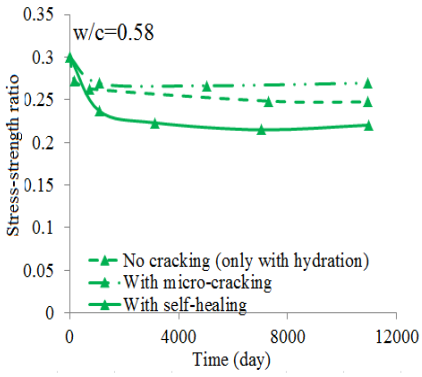

(f) Stress-strength ratio

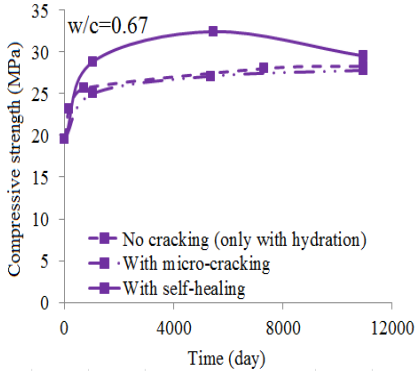

(g) Strength

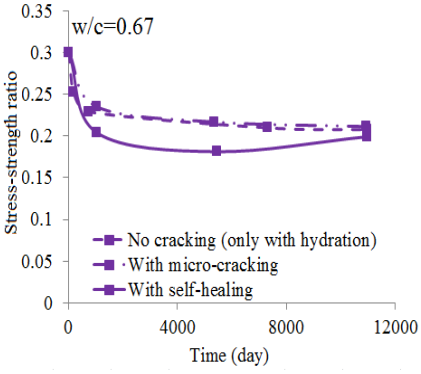

(h) Stress-strength ratio

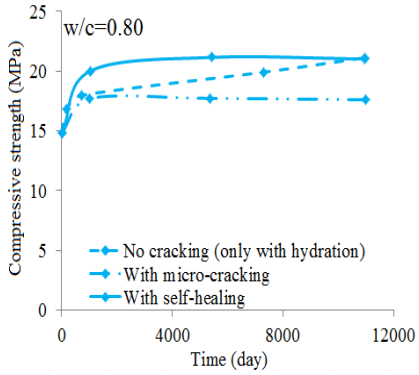

(i) Strength

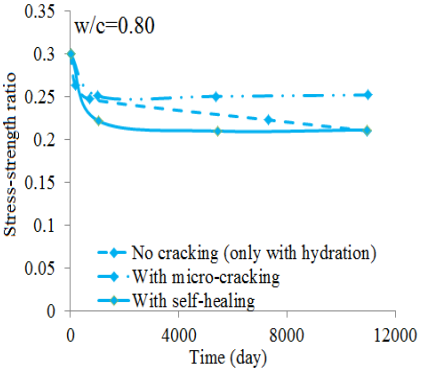

(j) Stress-strength ratio

Figure 4.24: Simulated compressive strength and stress-strength ratio of the concrete specimen with water-cement ratios of 0.50-0.80 loaded at 14 days at a stress level of 30% of compressive strength: with and without the effect of self-healing

to the cracks at time t_i, $r_{ol}(t_i)$, can calculated with Eq. 4.8 [12], viz.:

$$r_{ol}(t_i) = \frac{n_{ac,tot}(t_i) - n_{ac,eff}(t_i)}{n_{ac,tot}(t_i)} \tag{4.8}$$

where the parameters are determined as follows:

- $n_{ac,tot}(t_i)$ is total number of the beams which are connected to the broken beams at time t_i. $n_{ac,tot}$ can be calculated with Eq. 3.36, viz.:

  $$n_{ac,tot} = 10N$$

  where N is the number of broken beams, which has been plotted in Fig. 4.19a. Fig. 4.26a depicts the relationship between the number of the beams which are connected to the broken beams ($n_{ac,tot}$) and the number of broken beams (N).

[12] Same as Eq. 3.37.

Table 4.14: Experimental and simulated compressive strength of load-free and loaded concrete specimens with water-cement ratios of 0.50-0.80 after 30 years

w/c	30-year strength in Brooks' test			30-year strength in simulation			
	Load-free concrete (MPa)	Loaded concrete (MPa)	Extra increase in strength (%)	With continuous hydration[1] (MPa)	With micro-cracking[2] (MPa)	With self-healing[3] (MPa)	Extra increase in strength (%)
0.50	50.6	61.6	21.74	52.4	49.5	60.1	14.69
0.54	46.6	50.8	9.01	50.1	41.8	56.0	11.69
0.58	36.7	45.4	23.77	36.5	33.5	41.0	16.00
0.67	26.9	36.2	34.57	28.3	27.8	29.5	4.13
0.80	20.2	21.5	6.44	21.1	17.6	21.0	-0.43

[1] With continuous hydration represents the simulations without the effect of micro-cracking but with continuous hydration; the values in this column should be compared with those in the second column;

[2] With micro-cracking represents the simulations with the effect of micro-cracking and continuous hydration;

[3] With self-healing represents the simulations with the effect of self-healing; the values in this column should be compared with those in the third column.

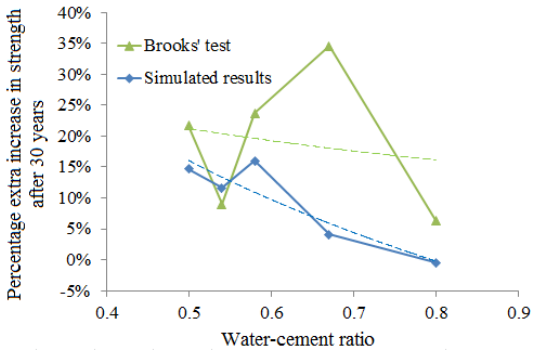

Figure 4.25: Experimental and simulated percentage extra increase in strength after 30 years for concretes with water-cement ratios of 0.50-0.80 (percentage extra increase in strength after 30 years = [30-year compressive strength of loaded concrete - 30-year compressive strength of load-free concrete] / 30-year compressive strength of load-free concrete)

- $n_{ac,eff}(t_i)$ is the number of *effective* beams which are connected to the broken beams at time t_i, which is determined during the creep simulations with the modified lattice model. Fig. 4.26b [13] shows $n_{ac,eff}$ versus N.

With Eq. 4.8 the percentage overlap area of the pastes adjacent to the cracks, r_{ol}, is calculated and presented in Fig. 4.26c (horizontal axis is the number of broken beams N) and 4.26d (horizontal axis is the loading duration in days).

[13] In this figure the number of *effective* beams which are connected to the broken beams ($n_{ac,eff}$) increases with increasing number of micro-cracks (N). The rate of this increase gradually decreases. When the number of micro-cracks is high enough, $n_{ac,eff}$ could start to decrease with increasing N. This can be seen from the trend of two lines in this figure representing concretes with water-cement ratios of 0.67 and 0.80.

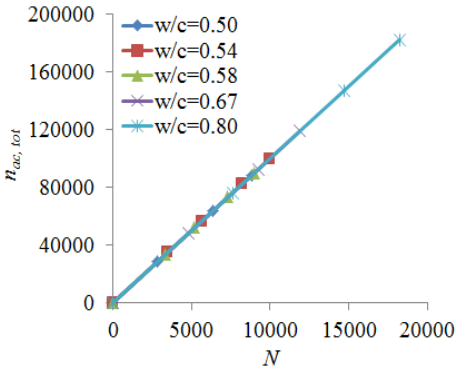

(a) $n_{ac,tot}$ versus N

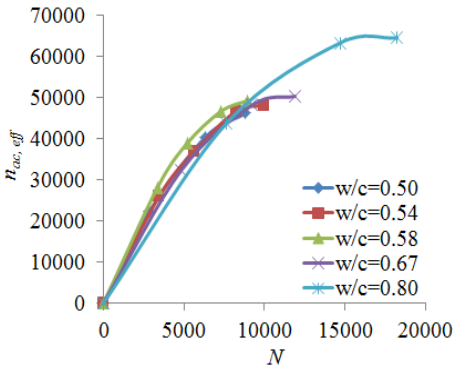

(b) $V_{ac,eff}$ versus N

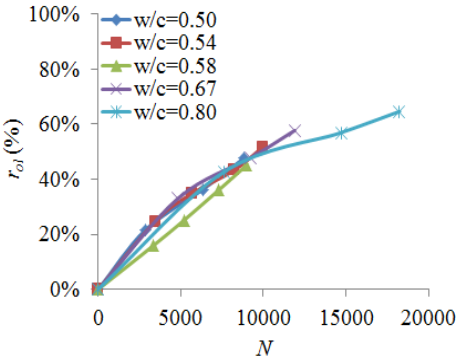

(c) r_{ol} versus N

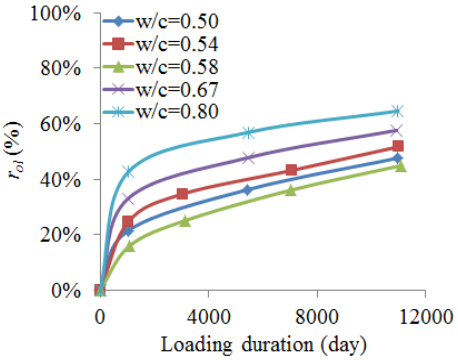

(d) r_{ol} versus loading duration

Figure 4.26: Total number of the beams which are connected to the broken beams ($n_{ac,tot}$), the number of *effective* beams which are connected to the broken beams ($n_{ac,eff}$) and percentage overlap area of the paste adjacent to the cracks (r_{ol})

Indeed, as shown in Fig. 4.26d, the overlap volume of the pastes adjacent to the cracks for concrete with a high water-cement ratio is larger than for concrete with a low water-cement ratio (with the exception of the mixture with a water-cement ratio of 0.58). Therefore, the volume of the pastes where additional hydration occurs, and thus the total additional degree of hydration (i.e. the extra increase in strength), is smaller in concrete with a high water-cement ratio than that in concrete with a low water-cement ratio.

It should be noted that there appears to be an optimum for the additional increase in strength after 30 years (see Fig. 4.25). In the simulations this optimum appears in concrete with a water-cement ratio of 0.58, while in the experiments the optimum appears in concrete with a water-cement ratio of 0.67. As shown in Fig. 4.19a, the total number of micro-cracks (i.e. damage degree) after 30 years in concrete with a water-cement ratio of 0.58 is slightly higher than that in concrete with a water-cement ratio of 0.50, but lower than that in concrete with other water-cement ratios. If the volumes of the densified paste do not overlap, the total volume of paste adjacent to the cracks (represented by $n_{ac,tot}$ shown in Fig. 4.26a) increases with increasing damage degree (i.e. number of

micro-cracks N), and thus the total additional degree of hydration increases. However, with increasing damage degree, also the crack density increases. Overlap of the volumes of densified paste will then occur and increase (see Fig. 4.26c). When the crack density is high enough, the effective volume of the paste adjacent to the cracks (represented by $n_{ac,eff}$ as shown in Fig. 4.26b) will become smaller and the total additional degree of hydration becomes smaller as well. In the concrete specimen with a water-cement ratio of 0.58, the damage degree (i.e. number of micro-cracks, see Fig. 4.19a) is lower than other concretes and the percentage overlap area of the paste adjacent to the cracks is lower (green line in Fig. 4.26c). The effective volume of the paste adjacent to the cracks is then larger (green line in Fig. 4.26b). The total additional overall degree of hydration and associated extra strength increase is higher than in other concretes.

Regarding the reason for the difference in the optimum in the simulations and experiments, it is still not clear. Possible reasons might be:

- Since only the 14-day and 30-year strength are known in Brooks' test, the parameters for the hydration curve (b and β in Eq. 3.2) and evolution of strength ($f_{c,max}$ and α_0 in Eq. 3.18) had to be determined merely based on these two strength data. This might lead to a difference between the shape of the hydration curve considered in the simulations and the real ones in the experiments. This will further influence the number of micro-cracks (or damage degree) and crack density during the creep process and the total additional degree of hydration. Thus, inappropriate input for the hydration curve of the mixture with a water-cement ratio of 0.67 might be a reason for a small extra strength increase in the simulations.

- The additional degree of hydration of the paste adjacent to any crack, $\triangle\alpha_{add,j}$, is assumed constant through the whole loading period. This might lead to underestimation of the self-healing efficiency, since $\triangle\alpha_{add,j}$ is supposed to be larger at early age than at later age. There is a possibility that $\triangle\alpha_{add,j}$ for the mixture with a water-cement ratio of 0.67 at early age is larger than that of other mixtures, which leads to a higher self-healing efficiency and a larger extra strength increase.

4.6. CONCLUSIONS

IN this chapter, the effects of micro-cracking and self-healing on the long-term creep of concrete mixtures with different water-cement ratios (0.50-0.80) was investigated using the modified lattice model. The mixtures are loaded at 14 days at a stress level of 30% of the compressive strength (constant stress). Based on the simulation results and discussions, the following conclusions can be drawn:

- Concrete with a high water-cement ratio has a lower strength and seems more prone to ongoing cracking over time while under load. In the long run, the total number of micro-cracks (i.e. damage degree[14]) in concrete with a high water-cement ratio is larger than that in concrete with a low water-cement ratio. The additional creep deformation caused by micro-cracking is thus larger for concrete with a high water-cement ratio than for concrete with a low water-cement ratio.

[14] Definition is explained in Section 3.5.2.

The simulation results (Fig. 4.19b) show that after 30 years micro-cracking causes 8% to 15% additional creep deformation of concrete with a water-cement ratio of 0.50-0.58. For concrete with a high water-cement ratio of 0.67-0.80, the effect of micro-cracking is almost doubled: 20% to 30% after 30 years. The extra deformation caused by micro-cracking is proportional to the number of micro-cracks (Fig. 4.19c).

- When the effect of self-healing is considered, the numerically simulated creep strain is lower than that without the effect of self-healing. The effect of self-healing prevents the occurrence of the additional creep deformation and the reduction in strength caused by micro-cracking. According to the simulation results, the concrete specimens with different water-cement ratios gain an additional increase in strength, except the concrete with a water-cement ratio of 0.80. In general, the simulated additional increase in strength due to the self-healing of micro-cracks is smaller for concrete with a high water-cement ratio than for concrete with a low water-cement ratio.

- The damage degree (or the number of micro-cracks) and crack density (i.e. number of micro-cracks per unit area) vary in concretes with different water-cement ratios and influences the total additional degree of hydration. If the volumes of densified paste adjacent to cracks do not overlap, the total additional degree of hydration increases with increasing damage degree (positive effect of damage degree). If the volumes of densified paste overlap, i.e. crack density increases, the total additional degree of hydration will be lower (negative effect of crack density). In general, the number of micro-cracks generated during the creep process is larger for concrete with a high water-cement ratio than for concrete with a low water-cement ratio. The crack density is higher for concrete with a high water-cement ratio than for concrete with a low water-cement ratio. The increase of the crack density, implying more "overlap-paste", reduces the positive effect of the damage degree on the total additional overall degree of hydration. Therefore, under sustained load concrete with a high water-cement ratio gains less additional strength than concrete with a low water-cement ratio. It can be concluded that concrete with a low water-cement ratio has a better performance (higher potential to increase its strength while under load) under long-term sustained loading than concrete with a high water-cement ratio.

5

BEHAVIOUR OF LIGHTWEIGHT AGGREGATE CONCRETE UNDER SUSTAINED LOAD: EFFECT OF MICRO-CRACKING AND SELF-HEALING

Always and never are two words you should always remember never to use.

Wendell Johnson

Different from normal-weight aggregate concrete, the weakest component of lightweight aggregate concrete is not the interfacial transition zone but the aggregates. The aggregates crack under sustained load and they might not be self-healed. In this chapter, the effect of continuous hydration, micro-cracking and self-healing on the long-term creep of lightweight aggregate concretes with water-cement ratios of 0.55-0.86 is simulated using the modified lattice model. The effect of micro-cracking and self-healing on the strength of lightweight aggregate concretes under sustained load is studied as well.

5.1. INTRODUCTION

IN Chapter 3 and 4, the effect of micro-cracking and self-healing on the long-term creep of normal-weight aggregate concrete (NWAC) has been studied. Aggregate is considered to be the strong phase in concrete and was considered not to creep. In concrete, creep mainly originates from the cement paste. Its magnitude is influenced by a wide range of variables [200], including intrinsic properties of the concrete mixture (e.g., water-cement ratio, cement type, aggregate content and stiffness) and extrinsic environmental factors (e.g., applied stress, duration of loading, ambient humidity and temperature). Generally speaking, aggregate particles provide physical restraint against the deformation of cement paste and thus reduce the magnitude of the creep deformation of concrete. The degree of restraint depends on the volume fraction and stiffness of aggregate.

The development of lightweight aggregate concrete (LWAC) has been paid great attention [201–208]. Compared to NWAC, LWAC reduces the structural dead load. This makes it possible to increase the length of spans or decrease the cross section of structural elements, and reduce the amount of required steel and even the foundation dimensions [201]. However, the higher porosity and lower stiffness of lightweight aggregate make LWAC more deformable. The lower the stiffness of the aggregates, the less restraint the aggregates provide. In this case, the creep deformation of concrete made of lightweight aggregate will be larger than that of concrete made of normal-weight aggregate loaded at the same stress levels.

Different from NWAC, the weakest component of LWAC is not necessarily the interfacial transition zone (ITZ), but often the aggregate. When load is applied, cracks will penetrate into aggregate particles instead of circumventing them. Moreover, these micro-cracks in the aggregates can not easily be self-healed, since aggregate does not hydrate (provided that no cement particles will be transported through pores into the aggregates). This will lower the self-healing efficiency and affect the creep deformation and strength of LWAC. In this chapter, the effect of micro-cracking and self-healing on the long-term creep and strength development of LWAC is investigated using the modified lattice model (flow chart in Fig. 3.18). The structure of this chapter is the same as Chapter 4.

5.2. BROOKS' TEST ON CREEP OF CONCRETE WITH LIGHTWEIGHT AGGREGATE

5.2.1. GENERAL INTRODUCTION

It is commonly assumed that the creep of LWAC is larger than that of NWAC. Troxell et al [209] observed that creep of concrete made with sandstone aggregates was almost 2.5 times higher than that of concrete made with limestone aggregate, with other factors being equal. Similar results were also found by Jensen and Richart [210] and Kordina [211]. Generally, sandstone is more porous and its elastic modulus is lower than that of limestone. Similarly, the elastic modulus of the lightweight aggregate is lower than that of the normal-weight aggregate. Therefore, the restraining effect on the deformation of the paste is smaller and thus concrete with lightweight aggregates is expected to have a higher creep. However, other behaviour has been observed as well. Accord-

ing to Schieler's results [212], the creep curve of concrete made with gravel falls in the middle of the range of creep values of the LWACs made with American lightweight aggregates. Best and Polivka [213] also concluded, based on their experiments that, with other things being equal, LWACs made with expanded-shale aggregates from the west coast of United States may not creep more, or perhaps less, than NWACs of comparable strength. The different observations might result from the experimental conditions and the mineralogical character of the aggregates used in the tests.

In Brooks' 30-year creep tests, different trends regarding the creep strain of LWACs were found [19, 22]. Concretes made from Aglite (expanded clay) generally exhibit a larger creep compared to concretes made from normal weight aggregates, while concretes made from Lytag (sintered fly ash) have a lower creep. With respect to these two types of concrete (NWAC and LWAC) there is no agreement on which type creeps more. The point of this chapter is *not* to compare the creep strains of LWAC and NWAC, but to investigate the micro-cracking and self-healing phenomenon during the creep process of LWAC and their effects on the strength of LWAC under sustained load.

5.2.2. EXPERIMENTAL DATA OF LWAC

In Section 3.2, the details of Brooks' tests have been described. In this chapter the data of lightweight aggregate concrete (Lytag: sintered fly ash aggregate) are studied. The specimens were stored in water at $23 \pm 1\,^{\circ}C$. Concrete specimens were loaded at 14 days at a stress level of 30% of compressive strength. The mix design, compressive strength and elastic modulus of loaded and load-free concretes with water-cement ratios of 0.55-0.86 are given in Table 5.1. The measured creep strains are shown in Fig. 5.1 [1].

Table 5.1: Mix design, compressive strength and elastic modulus of concretes with lightweight aggregate (Lytag) [19, 25]

w/c	Mix proportion by weight (C:S:A)[2]	Cement paste content r_p by volume (%)	14-day mechanical properties		30-year mechanical properties			
					Load-free		Loaded	
			f_c [1] (MPa)	E [1] (GPa)	f_c (MPa)	E (GPa)	f_c (MPa)	E (GPa)
0.55	1:1.71:1.52	36.0	31.2	23.0	44.0	32.4*[3]	50.0	34.5
0.63		38.7	30.2	18.9	50.8	31.8*	41.3	33.0
0.75		42.5	25.9	17.7	41.0	28.0*	31.2	34.8
0.86		45.7	17.6	11.7	35.8	23.8*	27.0	12.8

[1] E=elastic modulus; f_c=compressive strength.
[2] C:S:A=Cement:Sand:Aggregate.
[3] *=assumed value; 30-year elastic modulus of the load-free specimen is not given; it is assumed to increase by same percentage as 30-year strength, compared to 14-day values.

The 14-day and 30-year compressive strength of load-free and loaded LWACs with water-cement ratios of 0.55-0.86 are depicted in Fig. 5.2. The compressive strength of loaded LWACs after 30 years is compared to that of load-free LWACs. The comparison

[1] There are two sets of creep data at each water-cement ratio, which comes from two papers of Brooks [19, 22]; it is assumed that these data come from the same batch. The 30-year creep data on the lines with marker "•" are extrapolated values (Fig. 5.1).

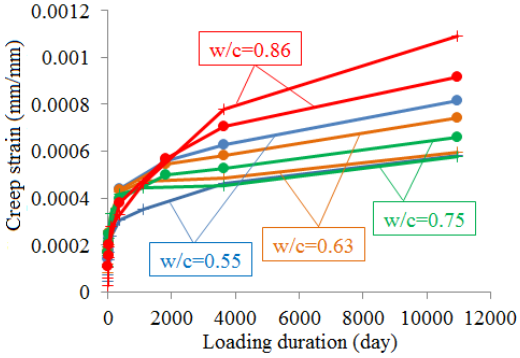

Figure 5.1: Measured creep strains of wet-stored concretes with Lytag aggregates in Brooks' test (constant stress creep test; age at loading is 14 days; loading level is 30% of 14-day compressive strength) [19, 22]

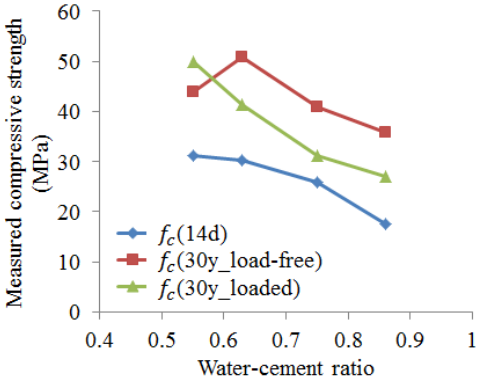

Figure 5.2: Measured 14-day and 30-year compressive strength of load-free and loaded LWACs with water-cement ratios of 0.55-0.86 (f_c *(14d)* is compressive strength at age of loading (14 days); f_c *(30y_loaded)* is compressive strength of loaded specimens after 30 years, while f_c *(30y_load-free)* is compressive strength of load-free specimens.) [19]

is shown in Fig. 5.3. The compressive strengths of load-free LWACs with water-cement ratios of 0.55-0.86 after 30 years are 41.03%-103.41% larger than the 14-day compressive strength (red line in Fig. 5.3). This is attributed to the continuous hydration. If the LWACs are loaded for 30 years, the strength is generally lower than that of the load-free LWACs (green line in Fig. 5.3). Only one exception is found: the LWAC with a water-cement ratio of 0.55 gained an extra increase in strength if under loading. A similar situation is also found in the concretes made with Aglite aggregate in Brooks' test [19]. This is different from concretes made with normal-weight aggregates: loaded NWACs generally gain extra increase in strength at low stress levels compared to load-free NWACs (Chapter 4), as observed in Brooks' test. The difference between NWAC and LWAC will be investigated in this chapter.

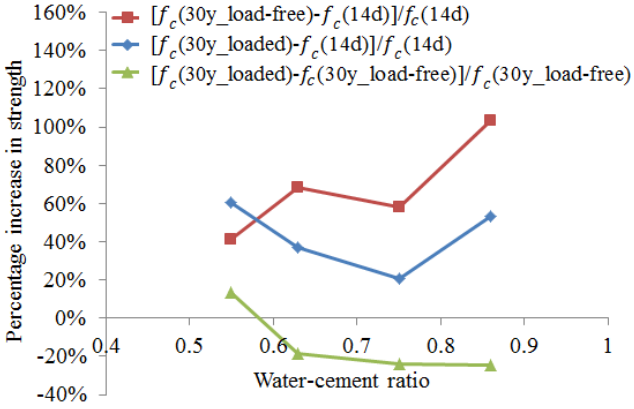

Figure 5.3: Percentage increase in strength of wet-stored concrete specimens with different water-cement ratios ($f_c(14d)$ is compressive strength at age of loading (14 days); $f_c(30y_loaded)$ is compressive strength of loaded specimens after 30 years, while $f_c(30y_load\text{-}free)$ is compressive strength of load-free specimens.) [19]

5

5.3. NUMERICAL SPECIMENS WITH LIGHTWEIGHT AGGREGATE WITH WATER-CEMENT RATIOS OF 0.55-0.86

5.3.1. NUMERICAL SPECIMENS

The dimension of the numerical LWAC specimens with water-cement ratios of 0.55-0.86 is $100\times100mm^2$, meshed at the resolution 0.5mm/pixel. The maximum aggregate diameter is 16mm. The generated aggregate volumes[2] are 40%, 38%, 35% and 32%, respectively, of the total 2D volume of the specimens. The meso-structure of the LWACs are shown in Fig. 5.4.

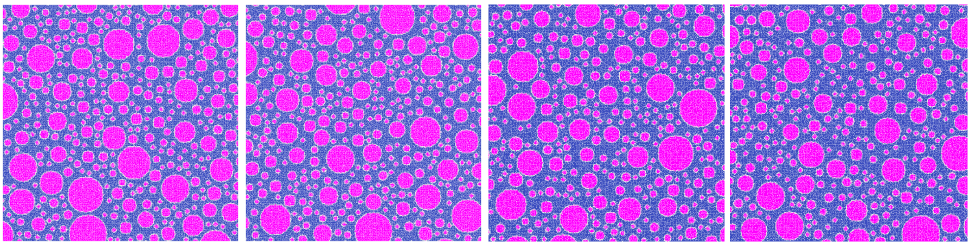

(a) w/c=0.55 (b) w/c=0.63 (c) w/c=0.75 (d) w/c=0.86

Figure 5.4: Meso-structure of LWAC with water-cement ratios of 0.55-0.86 (dimension of specimens: $100\times100mm$; percentages volume of aggregate are (a) 40%, (b) 38%, (c) 35% and (d) 32%)

[2]The aggregate volumes of the numerical specimens are smaller than those in Brooks' test. This is because the aggregates with diameters smaller than 2mm are not placed in the specimen and they are considered as fine aggregates embedded in the paste. This has been explained in detailed in Chapter 3.

5.3.2. 14-DAY MECHANICAL PROPERTIES OF LATTICE BEAMS: $f_c(t_0)$ & $E(t_0)$

The input values for the 14-day mechanical properties of the mortar, bond and aggregate beams for the numerical LWACs are listed in Table 5.2. The elastic modulus of the lightweight aggregate ranges from 10 to 18GPa [214] and the compressive strength (sintered fly ash aggregate) ranges from 25 to 40MPa [188]. In our research the elastic modulus of aggregate is set at 10GPa and the compressive strength 30MPa. The elastic modulus of the mortar[3] is estimated with the parallel-series model described with Eq. 3.31 [192], where λ and χ are volumetric parameters (see Fig. 3.21). λ is assumed to be equal to χ and are calculated with Eq. 3.32, in which r_A is the volume percentage of aggregate and its values for the LWAC specimens are 40%, 38%, 35% and 32% (Section 5.3.1).

Table 5.2: Estimated 14-day mechanical properties of the mortar, bond and aggregate beams of the lattice model for the LWACs with water-cement ratios of 0.55-0.86 in order to fit the experimental strength and elastic modulus (input for the creep simulations)

w/c	Elastic modulus (GPa) M|B|LA[1]	Compressive strength (MPa) M|B|LA	Tensile strength (MPa) M|B|LA	Poisson's ratio[2]
0.86	12.9|12.9|10.0	40.0|13.0|30.0	4.0|1.3|3.0	0.24
0.75	25.0|25.0|10.0	70.0|23.3|30.0	7.0|2.33|3.0	
0.63	29.1|29.1|10.0	94.0|31.0|30.0	9.4|3.1|3.0	
0.55	38.0|38.0|10.0	104.0|34.0|30.0	10.4|3.4|3.0	

[1] M=mortar, B=bond, LA=Lytag aggregate;
[2] Shear modulus = elastic modulus / [2*(1 + Poisson's ratio)].

With the 14-day mechanical properties of the beams of the lattice model given in Table 5.2, the simulated 14-day compressive strength and elastic modulus of the LWAC specimens are shown in Table 5.3. Fig. 5.5 shows that the 14-day compressive strength and elastic modulus simulated with the lattice model fit well with the experimental values (Table 5.1). This means that the input values for the 14-day mechanical properties of the lattice beams are reasonable and the numerical specimens are reliable as the starting point for the numerical simulations of creep.

Table 5.3: Simulated 14-day compressive strength and elastic modulus of LWACs with water-cement ratios of 0.55-0.86

w/c	14-day compressive strength (MPa)		14-day elastic modulus (GPa)	
	Experiment	Simulation	Experiment	Simulation
0.86	17.6	17.2	11.7	12.0
0.75	25.9	25.7	17.7	18.1
0.63	30.2	30.4	18.9	19.4
0.55	31.2	31.0	23.0	22.2

[3] The elastic modulus of bond beams is assumed to be the same as the mortar beams and the reason for this is given in Section 3.8.1.

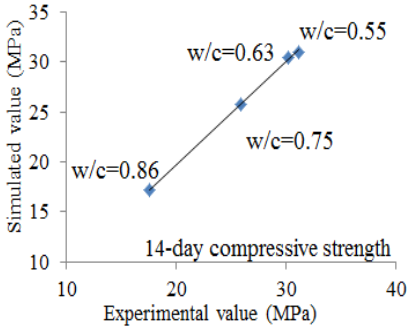

(a) Experimental and simulated 14-day compressive strength

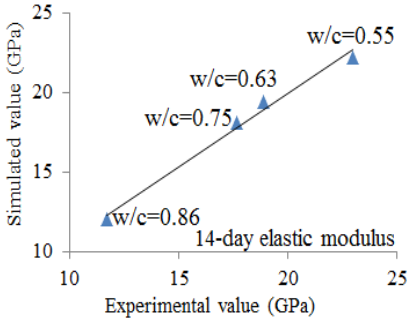

(b) Experimental and simulated 14-day elastic modulus

Figure 5.5: Comparison between experimental and simulated 14-day compressive strength and elastic modulus of LWACs with water-cement ratios of 0.55-0.86

5.3.3. 30-YEAR MECHANICAL PROPERTIES OF LATTICE BEAMS AFTER CONTINUOUS HYDRATION

The 30-year mechanical properties of the mortar, bond and aggregate beams are listed in Table 5.4. With these values, the simulated 30-year compressive strength and elastic modulus of load-free LWACs are shown in Table 5.5. Fig. 5.6 shows the simulated 30-year compressive strength and elastic modulus fit quite well with the experimental values (Table 5.1). This means that the input values for the 30-year mechanical properties of the lattice beams are reasonable and the numerical specimens are reliable as the starting point for the numerical simulations of creep.

Table 5.4: 30-year mechanical properties of the mortar, bond and aggregate beams of the lattice model for load-free LWACs with water-cement ratios of 0.55-0.86

w/c	Elastic modulus (GPa) M|B|LA[1]	Compressive strength (MPa) M|B|LA	Tensile strength (MPa) M|B|LA	Poisson's ratio[2]
0.86	38.0|38.0|10.0	120.0|40.0|30.0	12.0|4.0|3.0	0.24
0.75	50.0|50.0|10.0	240.0|80.0|30.0	24.0|8.0|3.0	
0.63	61.4|61.4|10.0	390.0|130.0|30.0	39.0|13.0|3.0	
0.55	67.3|67.3|10.0	330.0|110.0|30.0	33.0|11.0|3.0	

[1] M=mortar, B=bond, LA=Lytag aggregate;
[2] Shear modulus = elastic modulus / [2*(1 + Poisson's ratio)].

5.4. VALUES OF MODEL PARAMETERS

FOR simulating the effect of continuous hydration, micro-cracking and self-healing on the creep deformation with the modified lattice model, the parameters, i.e. the empirical ageing factor a in creep formula (Eq. 3.17), the strength and elastic modulus of mortar and bond beams with time resulting from the continuous hydration, $f_c[\alpha(t)]$ and $E[\alpha(t)]$ (Eq. 3.18 and 3.19), and the additional degree of hydration of the paste adjacent to any crack, $\triangle\alpha_{add,j}$ (Eq. 3.27 to 3.30), need to be determined.

Table 5.5: Simulated 30-year compressive strength and elastic modulus of load-free LWACs with water-cement ratios of 0.55-0.86

w/c	30-year compressive strength (MPa)		30-year elastic modulus (GPa)	
	Experiment	Simulation	Experiment	Simulation
0.86	35.8	34.8	23.8	24.5
0.75	41.0	41.7	28.0	28.3
0.63	50.8	47.4	31.8	31.2
0.55	44.0	42.8	32.4	31.7

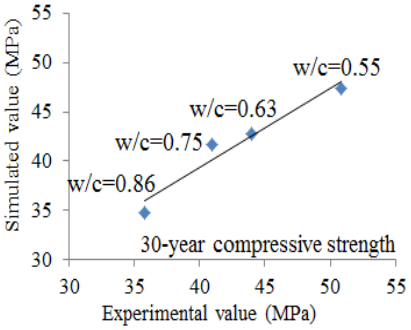

(a) Experimental and simulated 30-year compressive strength

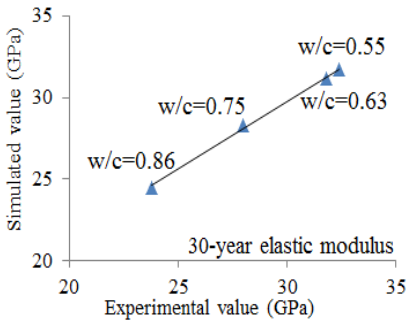

(b) Experimental and simulated 30-year elastic modulus

Figure 5.6: Comparison between experimental and simulated 30-year compressive strength and elastic modulus of load-free LWACs with water-cement ratios of 0.55-0.86

5.4.1. EMPIRICAL AGEING FACTOR *a*

Following the calculation procedure for the empirical ageing factor a in Eq. 3.17 introduced in Section 4.4.1, the values of a for the LWACs are calculated and listed in Table 5.6. It should be noted that in the calculation procedure for a described in Section 4.4.1 the relationship between the ageing factor and water-cement ratio depicted in Fig. 4.9a does not involve possible effect of the absorption characteristics of the lightweight aggregate on the water-cement ratio. This may suggest that the empirical ageing factor a for LWACs with water-cement ratios of 0.55-0.86, calculated based on this procedure, might be overestimated since the effective water-cement ratio[4] is lower than the initial water-cement ratio (assuming that the aggregates added in the mixture was not saturated). This will be further discussed in Section 5.6.4.

[4] In this chapter the effective water-cement ratio is the water-cement ratio at final setting after the absorption of water by the lightweight aggregate. The definition of the effective water-cement ratio is quite complex for LWACs. Due to the absorption of water by the lightweight aggregates (assuming the aggregates added in the mixture were not saturated), the amount of water available for the hydration of cement (at final setting) is less than the amount of water added in the mixture. The ratio of this water amount to the weight of cement can be defined as the effective water-cement ratio. During the hydration process the occurrence of self-desiccation of the paste might cause the water in the lightweight aggregate to flow back to the paste. This also leads to changes in the effective water-cement ratio.

Table 5.6: The values of empirical ageing factor a for LWACs with water-cement ratios of 0.55-0.86 (calculation procedure in Section 4.4.1)

w/c	0.55	0.63	0.75	0.86
a ($\times 10^{-5}$)	0.39	0.48	0.69	1.19

5.4.2. EVOLUTION OF STRENGTH $f_c[\alpha(t)]$ AND ELASTIC MODULUS $E[\alpha(t)]$ OF MORTAR AND BOND BEAMS RESULTING FROM CONTINUOUS HYDRATION

The evolution of strength of the mortar and bond beams during the creep process can be calculated with Eq. 3.18, where $\alpha(t)$ is calculated with Eq. 3.1. By substituting $b = 0.6$ and $\beta = 0.6$ (Section 3.8.2), 14-day and 30-year strength of the mortar and bond beams (Table 5.2 and 5.4) into Eq. 3.18, the values for $f_{c,max}$ and α_0 for the LWAC mixtures are obtained and listed in Table 5.7. The elastic modulus of the mortar and bond beams is calculated with Eq. 3.19. Inserting the 14-day and 30-year elastic modulus of the mortar and bond beams (Table 5.2 and 5.4) into this equation, the values of c_1 and c_2 are obtained and listed in Table 5.7. Fig. 5.7 shows the compressive strength of mortar beams for LWACs calculated with Eq. 3.18.

Table 5.7: Parameter values for calculating the strength and elastic modulus of the mortar and bond beams in Eq. 3.18 and 3.19 for LWACs with water-cement ratios of 0.55-0.86

w/c	b	β	$f_{c,max}$ (MPa) (mortar|bond)	α_0 *	c_1 (mortar|bond)	c_2
0.55	0.6	0.6	848|284	0.61	3814|6827	0.49
0.63	0.6	0.6	974|325	0.64	2682|4865	0.52
0.75	0.6	0.6	700|233	0.67	2734|4762	0.50
0.86	0.6	0.6	585|195	0.69	533|1286	0.80

* α_0 is in general larger than expected. The reason has been explained in Section 3.8.2.

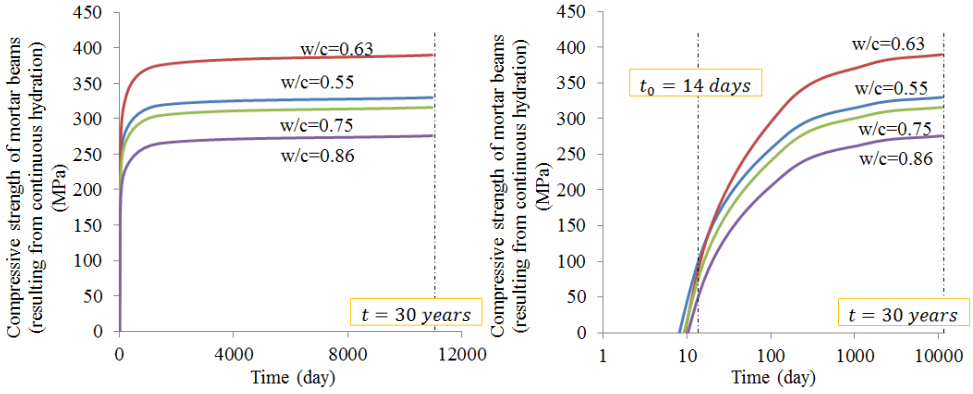

(a) Normal scale (b) Semi-log scale

Figure 5.7: Calculated compressive strength of mortar beams versus time for the LWAC specimens with water-cement ratios of 0.55-0.86 (Eq. 3.18)

5.4.3. ADDITIONAL DEGREE OF HYDRATION $\triangle\alpha_{add,j}$ OF PASTE ADJACENT TO ANY CRACK

MAXIMUM TOTAL ADDITIONAL OVERALL DEGREE OF HYDRATION $\triangle\alpha_{add,tot,max}$

The (reference) degree of hydration $\alpha(t)$ for LWACs with water-cement ratios of 0.55-0.86 calculated with Eq. 3.1 is shown in Fig. 5.8. After 30 years the degree of hydration ($\alpha(30y)$) has almost reached its asymptote: $\alpha(30y) = \alpha_u$. The maximum total additional degree of hydration $\triangle\alpha_{add,tot,max}$ follows $\triangle\alpha_{add,tot,max} = 1 - \alpha_u$ and its value is given in Table 5.8.

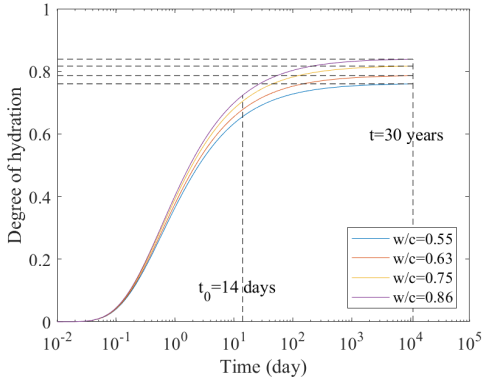

Figure 5.8: Calculated degree of hydration $\alpha(t)$ for LWACs with water-cement ratios of 0.55-0.86 ($b = 0.6$ and $\beta = 0.6$ in Eq. 3.1)

Table 5.8: The (reference) degree of hydration after 30 years α_u and the maximum total additional degree of hydration $\triangle\alpha_{add,tot,max}$ for LWACs with water-cement ratios of 0.55-0.86

w/c	0.55	0.63	0.75	0.86
α_u	0.77	0.79	0.82	0.84
$\triangle\alpha_{add,tot,max}$	0.23	0.21	0.18	0.16

ADDITIONAL DEGREE OF HYDRATION $\triangle\alpha_{add,j}$ OF PASTE ADJACENT TO ANY CRACK

The additional degree of hydration of the paste adjacent to any crack, $\triangle\alpha_{add,j}$, for LWACs with water-cement ratios of 0.55-0.86 is calculated with Eq. 3.7, where $wcr_0 = 0.50$. $V_{uhc,i}$ is the volume of unhydrated cement in the paste at time t_i and is calculated with Eq. 3.10. In this equation $\rho_c = 3000kg/m^3$ and $\rho_w = 1000kg/m^3$. For time t_i=30years, $V_{uhc,30y}$ is calculated for the values of V_p and $\alpha_{ref,30y}$ shown in Table 5.9. The calculated values of $V_{uhc,30y}$ are listed in Table 5.9. With the calculated values of $V_{uhc,30y}$ and for $V_{uhc,30y}(wcr_0 = 0.50) = 322mm^2$ (Table 4.9), $\triangle\alpha_{add,j}(wcr_0 = 0.50)$=0.21 (Section 3.8.3), $\triangle\alpha_{add,j}$ for LWACs with water-cement ratios of 0.55-0.86 are calculated with Eq. 3.7 and listed in Table 5.9.

5.5. CREEP OF LIGHTWEIGHT AGGREGATE

CREEP of concrete mainly originates from cement paste. Aggregate acts elastically and hardly creeps. Actually rocks do creep, but creep is very small [38] and neglectable

Table 5.9: Values of the additional degree of hydration of the paste adjacent to any crack, $\triangle\alpha_{add,j}$, for LWACs with water-cement ratios of 0.55-0.86

Parameters	Equation	Unit	w/c			
			0.55	0.63	0.75	0.86
V_p	$V_p = r_p V$ [1]	$[mm^2]$	3600	3870	4250	4570
$\alpha_{ref,30y}$ [2]	Eq. 3.1	[-]	0.77	0.79	0.82	0.84
$V_{uhc,30y}$	Eq. 3.10	$[mm^2]$	312	281	235	204
$\triangle\alpha_{add,j}$	Eq. 3.7	[-]	0.20	0.19	0.16	0.13

[1] $V_p = r_p V$, where r_p is the volume fraction of the paste, which is given in the third column Table 5.1 and $V = 100 \times 100 mm^2$.

[2] $\alpha_{ref,30y}$ is the reference degree of hydration after 30 years, which can be calculated with Eq. 3.1. It equals the ultimate degree of hydration α_u (Table 5.8).

compared to the creep of cement paste. Neville [38] referred to Morlier's classification of rocks with regards to their creep behaviour [215]. There are three types of rocks:

(1) The first type shows elasto-brittle behaviour. Creep occurs but it never exceeds 10% of the elastic deformation. Hard limestone and quartzite belong to this type.

(2) The second type is visco-elastic rocks, such as shale, porous limestone and granular gypsum. The creep of these rocks is 12% to 40% of the elastic deformation.

(3) The last type exhibits visco-plastic behaviour. The creep deformation is completely irreversible. Chalk falls into this category.

Griggs [216] found that the creep strain of limestone was 140×10^{-6} after 450 days at a stress level of 50% (138MPa). Hardy [23] observed that the primary creep deformation of two sandstones were very small at high stress levels and the rate of creep gradually dropped to 0 after 10 days of loading, as shown in Fig. 5.9. Usually the stress to which the aggregates are subjected in concrete does not reach to the aforementioned (high) level. In this case, the creep of aggregates, including porous ones or lightweight aggregates, is assumed to be small and hardly contribute to the long-term creep of concrete. In the following sections, the creep of lightweight aggregate (Lytag) is considered neglectable.

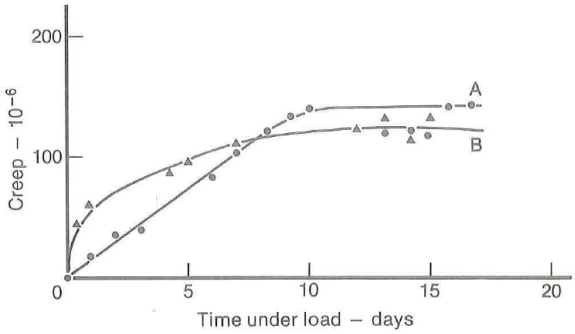

Figure 5.9: Creep of two sandstones: A, Springhill sandstone and applied stress = 55MPa; B, Wabana sandstone and applied stress = 101MPa [23]

5.6. SIMULATION RESULTS AND DISCUSSIONS

IN this section, the effects of continuous hydration, micro-cracking and self-healing on the long-term creep and compressive strength of LWACs with water-cement ratios of 0.55-0.86 are simulated. The LWAC specimens are stored in water and loaded at 14 days with a stress level of 30% of compressive strength.

5.6.1. EFFECT OF CONTINUOUS HYDRATION ON THE LONG-TERM CREEP AND COMPRESSIVE STRENGTH OF LWACS: W/C=0.55-0.86

The input parameters for simulation of the effect of continuous hydration on the long-term creep of LWACs with different water-cement ratios are as follows:

- If continuous hydration is considered, the evolution of strength and elastic modulus of the mortar and bond beams ($f_c[\alpha(t)]$ and $E[\alpha(t)]$) are calculated with Eq. 3.18 and 3.19. The values of the parameters, $f_{c,max}$, α_0, c_1 and c_2, are given in Table 5.7. If continuous hydration is *not* considered, the strength and elastic modulus of the mortar and bond beams are assumed constant and equal to the 14-day values (Table 5.2).
- The creep strain of the mortar and bond beams is calculated with Eq. 3.17. In this equation the values of the empirical ageing factor a are shown in Table 5.6, while n and m are 0.3 and 0.7, respectively (Section 4.4.1).

The simulated compressive strength and calculated stress-strength ratio of LWACs with and without the effect of continuous hydration are shown in Fig. 5.10. The simulated creep strains of LWACs with water-cement ratio of 0.55-0.86 without and with the effect of continuous hydration are shown in Fig. 5.11a and Fig. 5.11b, respectively.

When continuous hydration is considered, 30-year creep strains are 17.9%-39.7% lower than that without the effect of the continuous hydration. As an example of the effect of continuous hydration on the long-term creep, the simulated creep strains of LWAC with a water-cement ratio of 0.55 are shown in Fig. 5.12.

When continuous hydration is taken into account, the simulated creep strains of LWAC with a water-cement ratio of 0.86 (red line in Fig. 5.11b) is smaller than those of LWAC with a water-cement ratio of 0.75 (green line in Fig. 5.11b). This is opposite to the results in case no hydration occurs (Fig. 5.11a). This is because the increase in strength due to hydration of LWAC with a water-cement ratio of 0.86 is larger than that for LWAC with a water-cement ratio of 0.75, and thus the stress-strength ratio of the former LWAC is smaller than that of the latter LWAC (Fig. 5.10e to 5.10h).

5.6.2. EFFECT OF MICRO-CRACKING ON THE LONG-TERM CREEP AND COMPRESSIVE STRENGTH OF LWACS: W/C=0.55-0.86

The effect of micro-cracking on the long-term creep and compressive strength of LWACs is simulated for two situations: micro-cracking is considered or not considered. The input parameters for calculating the strength (Eq. 3.18), elastic modulus (Eq. 3.19), and creep (Eq. 3.17) of the mortar and bond beams are the same as those in Section 5.6.1.

The simulated creep strains without and with the effect of micro-cracking are shown in Fig. 5.13a and 5.13b, respectively. When micro-cracking is considered, the creep

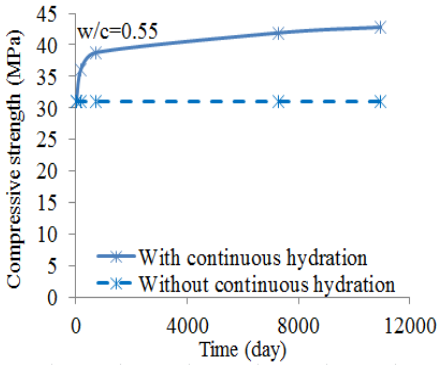

(a) Strength

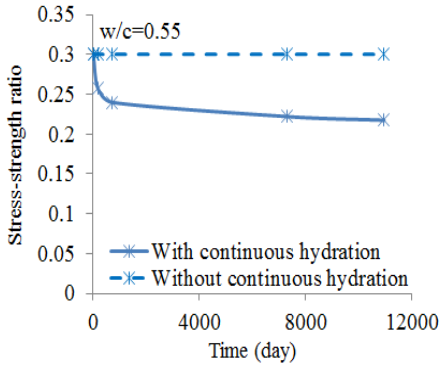

(b) Stress-strength ratio

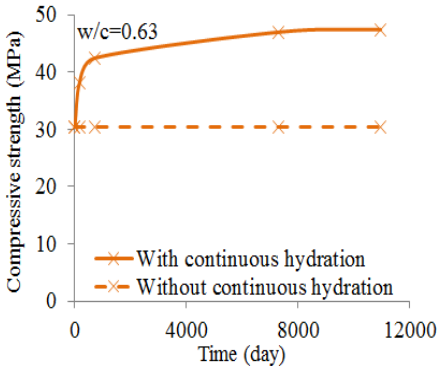

(c) Strength

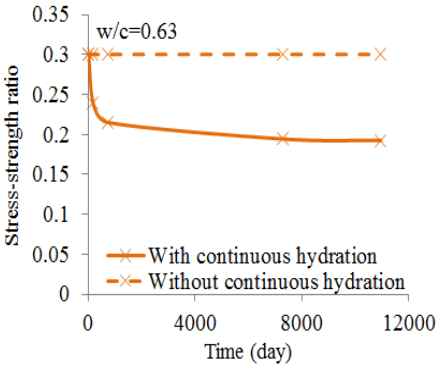

(d) Stress-strength ratio

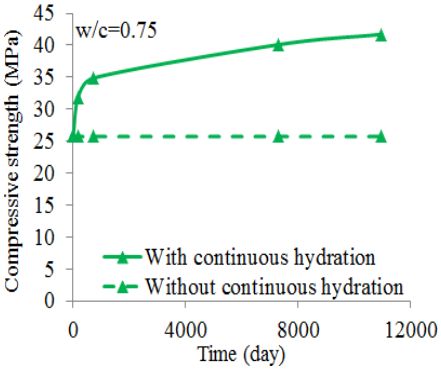

(e) Strength

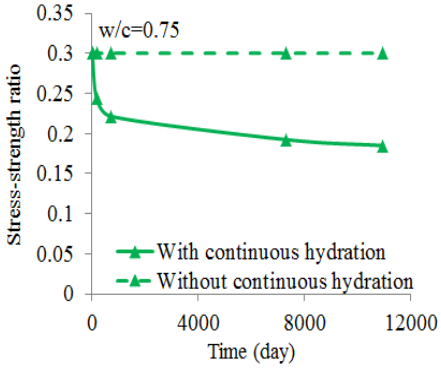

(f) Stress-strength ratio

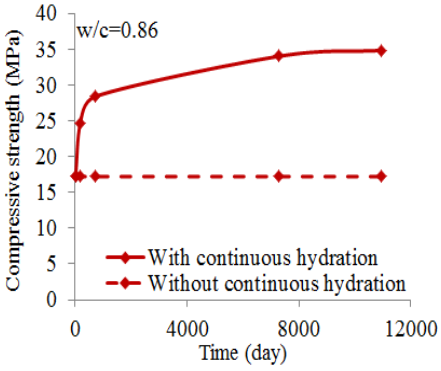

(g) Strength

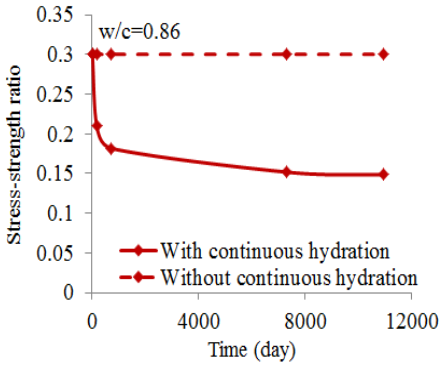

(h) Stress-strength ratio

Figure 5.10: Simulated compressive strength and stress-strength ratio of LWACs with water-cement ratios of 0.55-0.86 loaded at 14 days at a stress level of 30% of compressive strength: with and without effect of continuous hydration

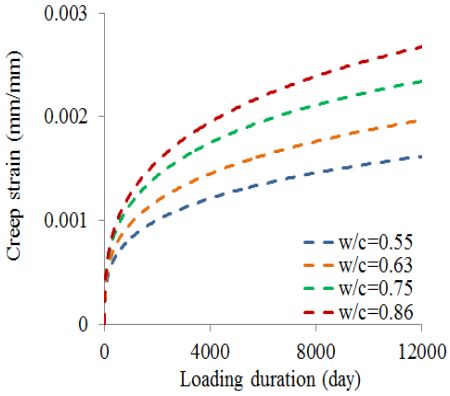

(a) continuous hydration is not considered

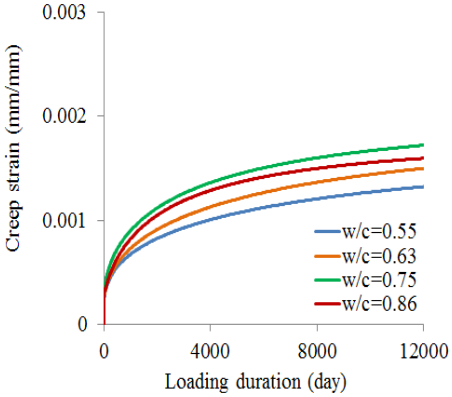

(b) continuous hydration is considered

Figure 5.11: Simulated creep strains of LWACs with water-cement ratios of 0.55-0.86: with and without the effect of continuous hydration (age at loading=14 days; stress level=30% of 14-day compressive strength)

strains are larger than those without micro-cracking (Fig. 5.13). As an example of the effect of micro-cracking on the long-term creep, the simulated creep strains of LWAC with a water-cement ratio of 0.55 is shown in Fig. 5.14. This figure shows that micro-cracking has a minor effect on the creep strain. This is due to the small number of micro-cracks (Fig. 5.15a) and small crack width (Fig. 5.17), resulting from the dense microstructure of the LWAC[5] (compared to the number of micro-cracks and crack width of NWAC, as shown in Fig. 4.19a and 4.20).

With increasing water-cement ratios of the specimens, the number of micro-cracks

[5]The input values for the 14-day and 30-year strength of the mortar and bond beams of the numerical LWAC specimens (Table 5.2 and 5.4) are larger than those of the numerical NWAC specimens (Table 4.2 and 4.4).

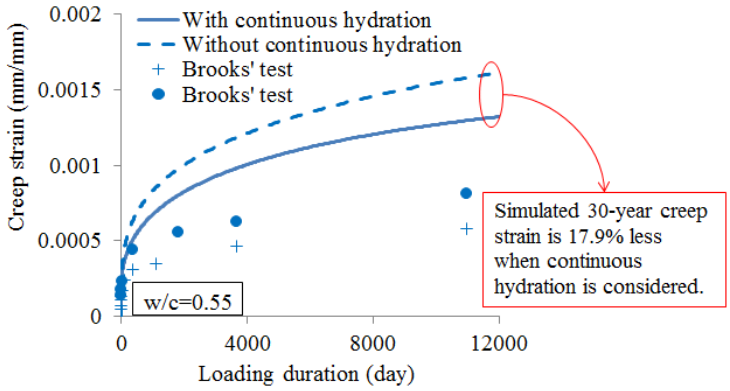

Figure 5.12: Simulated creep strains with and without the effect of continuous hydration for LWAC with a water-cement ratio of 0.55 (age at loading=14 days; stress level=30% of 14-day compressive strength)

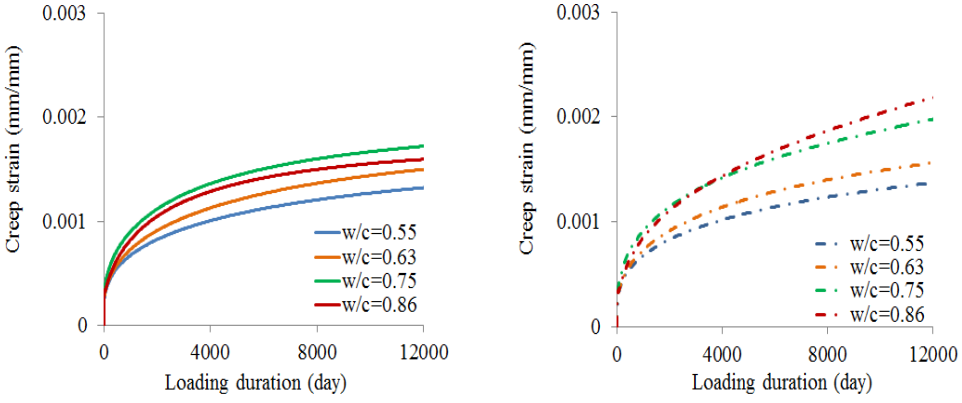

(a) Micro-cracking is not considered

(b) Micro-cracking is considered

Figure 5.13: Simulated creep strains of LWACs with water-cement ratios of 0.55-0.86: with and without the effect of micro-cracking (age at loading=14 days; stress level=30% of 14-day compressive strength)

increases (see Fig. 5.15a) and the additional overall deformations caused by micro-cracking become larger (see Fig. 5.15b). After 30 years the extra creep deformation due to micro-cracking for LWACs with water-cement ratios of 0.55-0.63 reaches 3.8% to 4.3% . For LWACs with water-cement ratios of 0.75-0.86, these percentages are much larger: 13.5% to 34.0% after 30 years. Fig. 5.15c shows the relationship between the extra deformation caused by micro-cracking and the total number of micro-cracks. It can be seen that the extra deformation increases exponentially with increasing number of micro-cracks.

MICRO-CRACKS IN LWACS DURING THE CREEP PROCESS

Different from NWAC, the weakest phase in LWAC is the aggregate instead of the ITZ. Fig. 5.16a shows the simulated micro-cracks in LWAC with a water-cement ratio of 0.55

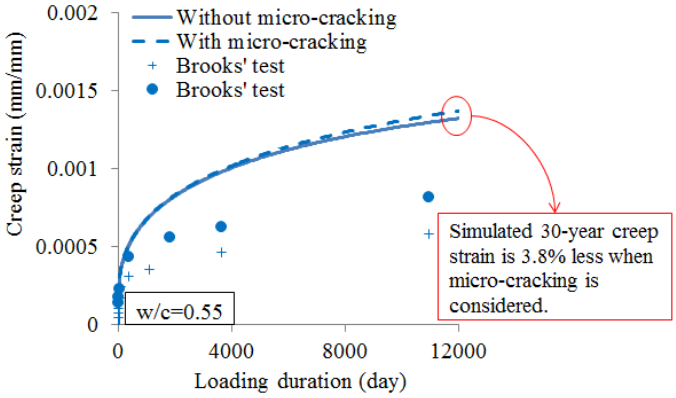

Figure 5.14: Simulated creep strains with and without the effect of micro-cracking for LWAC with a water-cement ratio of 0.55 (age at loading=14 days; stress level=30% of 14-day compressive strength)

5

after 30 years of loading (constant stress: 30% of 14-day compressive strength). It can be seen from this figure that micro-cracks appear in the aggregate phase in LWAC under sustained load, while no cracks are found in the aggregate phase in NWAC.

The crack width as calculated with the lattice model has been defined in Chapter 3. The evolution of the simulated maximum width of the micro-cracks generated during the creep process of LWACs is shown in Fig. 5.17 for different water-cement ratios. The simulated maximum crack widths after 30 years are $3\mu m$, $4\mu m$, $4.8\mu m$ and $5\mu m$, respectively, for different mixtures.

COMPRESSIVE STRENGTH AFTER MICRO-CRACKING

The simulated compressive strength and stress-strength ratio of the LWACs with and without the effect of micro-cracking are shown in Fig. 5.18. It can be seen from this figure that the compressive strength is smaller than that in case micro-cracking does not occur. While micro-cracking occurs, the strength of LWACs still increases over time (dotted dashed lines in Fig. 5.18a, 5.18c, 5.18e and 5.18g). This is because the increase of the strength due to continuous hydration is higher than the reduction of the strength due to micro-cracking[6].

Due to micro-cracking during the creep process the 30-year compressive strength is 1.4%-3.7% lower than that when the micro-cracking is not taken into account (see Table 5.10). Compared to NWAC with a similar strength (Table 4.10), the reduction in strength due to micro-cracking in LWAC is smaller. For example, LWAC with a water-cement ratio of 0.55 is as strong as NWAC with a water-cement ratio of 0.54. After 30 years of loading the calculated strength of NWAC is 16.7% weaker than that of the load-free NWAC (Table 4.10). This percentage is higher than the percentage strength decrease of LWAC with a water-cement ratio of 0.55 (1.4%). The denser micro-structure (larger strength and elastic modulus of the mortar; see Fig. 4.10 and 5.7) of LWAC might be the reason for that. In the next section the effect of self-healing on the long-term creep and strength of LWACs will be studied using the modified lattice model.

[6] At least for the prevailing stress level: 30% of 14-day compressive strength.

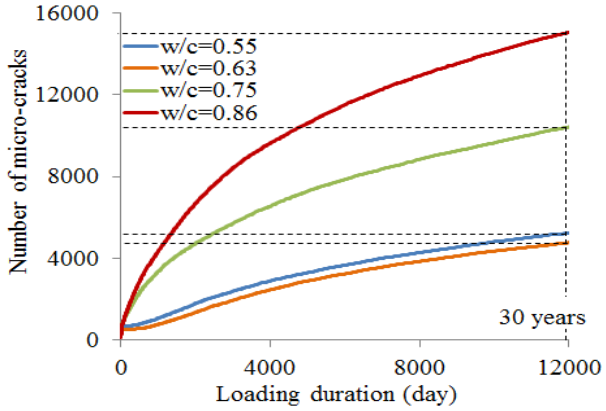

(a) Number of micro-cracks

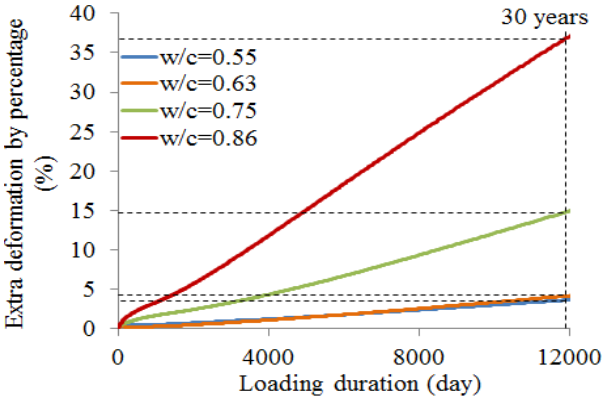

(b) Extra deformation by percentage

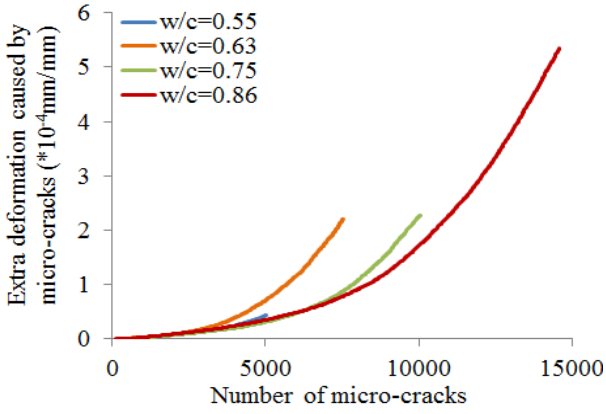

(c) Extra deformation versus number of micro-cracks

Figure 5.15: (a) Total number of cracks during the creep process; (b) Percentage of additional deformation caused by micro-cracking [extra deformation by percentage = (deformation with micro-cracking - deformation without micro-cracking) / deformation without micro-cracking]; (c) The extra deformation caused by micro-cracking versus total number of micro-cracks

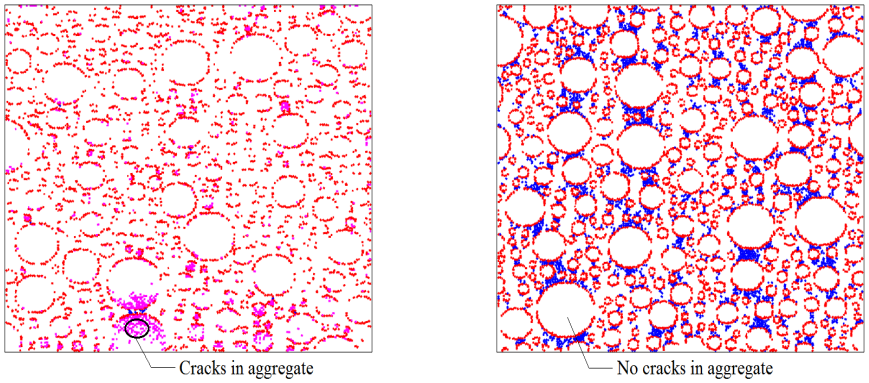

(a) LWAC, w/c=0.55 (b) NWAC, w/c=0.54

Figure 5.16: Simulated micro-cracks in LWAC and NWAC under a stress of 30% of compressive strength after 30 years (Blue: mortar cracks; Red: bond cracks; Magenta: aggregate cracks)

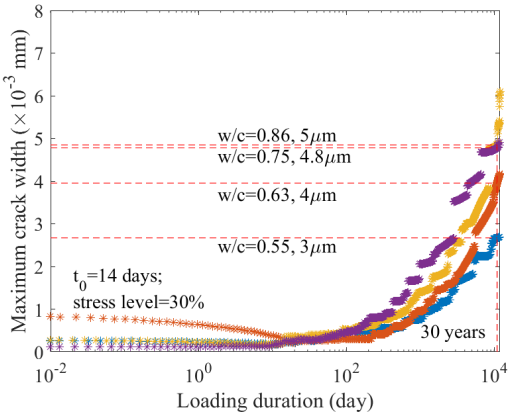

Figure 5.17: Simulated maximum crack width of the micro-cracks occurring during the creep process of LWACs with water-cement ratios of 0.55-0.86

5.6.3. EFFECT OF SELF-HEALING ON THE LONG-TERM CREEP AND COMPRESSIVE STRENGTH OF LWACS: W/C=0.55-0.86

CALCULATION OF κ (EQ. 3.23 AND 3.24) AND $\Delta\alpha_{add',j}$ (EQ. 3.29 AND 3.30)

The minimum volume of the reaction products produced during the additional hydration of the paste adjacent to any crack, $V_{RP,add,j,min}$, which is available for filling up the crack and densification of the paste adjacent to the crack, is calculated with Eq. 3.38 [7] for the values of $\Delta\alpha_{add,j}$, $V_{ac,p,j}$, $\alpha_{ref,max}$ shown in Table 5.11. The values of $V_{RP,add,j,min}$ are shown in Table 5.12. κ and $\Delta\alpha_{add',j}$ are determined with Eq. 3.25 to 3.28 and listed in Table 5.12.

[7] In this equation $\rho_c = 3000kg/m^3$ and $\rho_w = 1000kg/m^3$

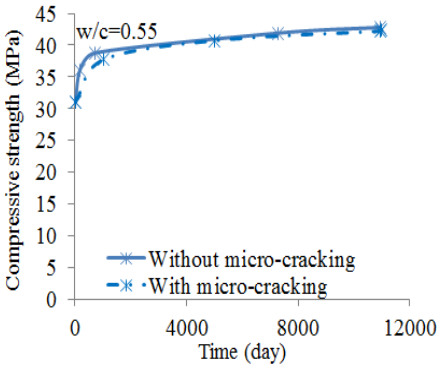

(a) Strength

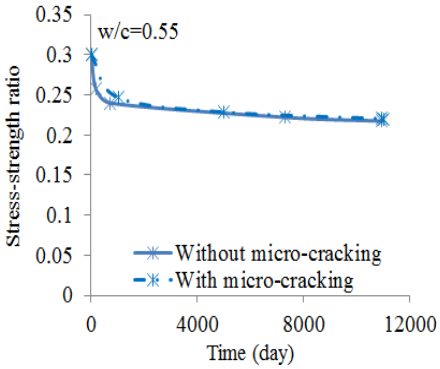

(b) Stress-strength ratio

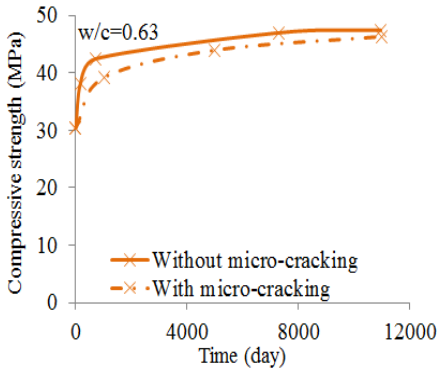

(c) Strength

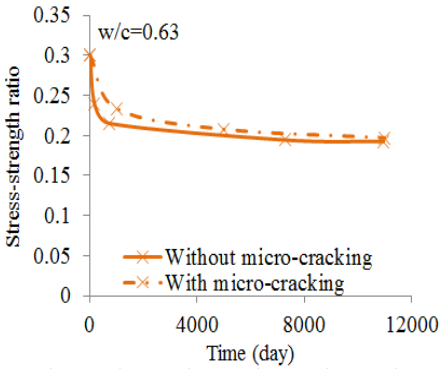

(d) Stress-strength ratio

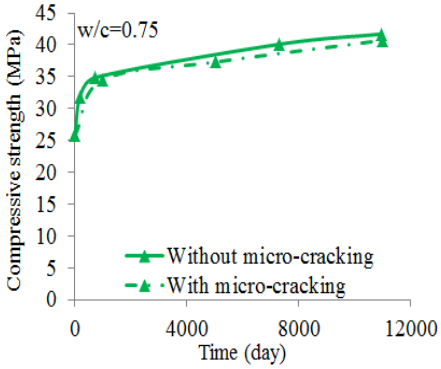

(e) Strength

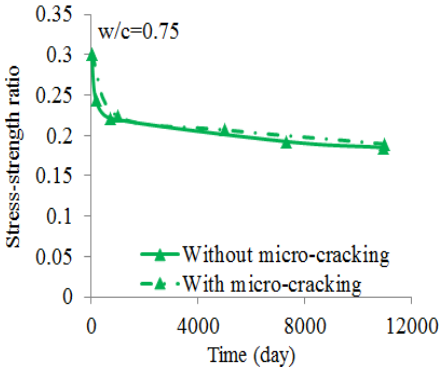

(f) Stress-strength ratio

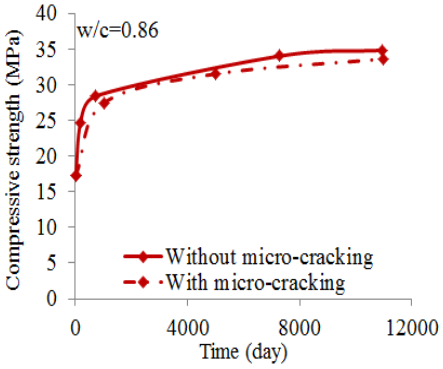

(g) Strength

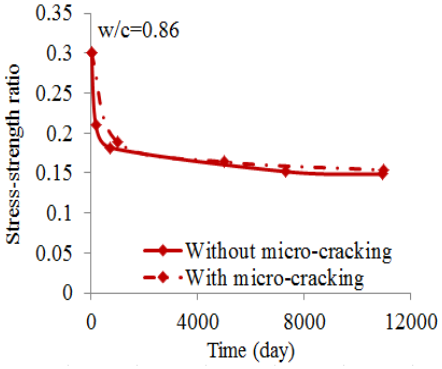

(h) Stress-strength ratio

Figure 5.18: Simulated compressive strength and stress-strength ratio of LWACs with water-cement ratios of 0.55-0.86 loaded at 14 days at a stress level of 30% of compressive strength: with and without the effect of micro-cracking

5

Table 5.10: Comparison between simulated 30-year compressive strength with and without the effect of micro-cracking for LWACs with water-cement ratios of 0.55-0.86

w/c	Simulated 30-year strength (MPa)		Reduction in strength caused by micro-cracking (%)
	Without micro-cracking (only with hydration)	With micro-cracking	
0.55	42.8	42.3	1.4
0.63	47.4	46.3	2.3
0.75	41.7	40.7	2.4
0.86	34.8	33.5	3.7

As can be seen from Table 5.12, for LWAC with a water-cement ratio of 0.86 the volume of reaction product $V_{RP,add,j,min}$ is smaller than the volume of the largest crack $V_{c,j}$. The reaction product is not enough to fill up the largest crack and no reaction product is left to densify the paste adjacent to this largest crack. However, the cracks smaller than the largest crack can still be filled up with reaction product and some product may left to densify the paste. Similar to the NWAC with a water-cement ratio of 0.80 (Table 4.13), a critical crack width (ω_{cri}) is also defined for LWAC with a water-cement ratio of 0.86 (see Table 5.13). Below the critical crack width, the crack can be filled up with the reaction product and some product is left to densify the paste adjacent to the crack, i.e. $\kappa = 1$ and $\triangle\alpha_{add',j} < \triangle\alpha_{add,j}$ (see Fig. 4.22a). If the crack width is larger than the critical crack width, the crack will *not* be filled up the reaction product and *all* the reaction product produced during the additional hydration is used to densify the paste adjacent to the crack, i.e. $\kappa = 0$ and $\triangle\alpha_{add',j} = \triangle\alpha_{add,j}$ (see Fig. 4.22b). The values of κ and $\triangle\alpha_{add',j}$ for LWAC with a water-cement ratio of 0.86 is listed in Table 5.13. These values will be used in the following simulations instead of the values in the sixth column in Table 5.12.

Table 5.11: Some parameters for calculating κ and $\triangle\alpha_{add',j}$

Parameters	Section	Unit	w/c			
			0.55	0.63	0.75	0.86
$\triangle\alpha_{add,j}$	5.4.3	[-]	0.20	0.19	0.16	0.13
$V_{ac,p,j}$ [1]	3.8.3	$[mm^2]$	0.31	0.33	0.37	0.39
$\alpha_{ref,max}$ [2]	5.4.3	[-]	0.77	0.79	0.82	0.84
ω_{max} [3]	5.6.2	$[\mu m]$	3	4	4.8	5

[1] $V_{ac,p,j}$ is calculated with Eq. 3.34.

[2] $\alpha_{ref,max}$ is the reference degree of hydration after 30 years: $\alpha_{ref,max} = \alpha(30y) = \alpha_u$ The values are given in Table 5.8.

[3] ω_{max} is the maximum crack width after 30 years, which is shown in Fig. 5.17.

Table 5.12: Values of κ and $\triangle\alpha_{add',j}$

Parameters	Unit	w/c			
		0.55	0.63	0.75	0.86
$V_{RP,add,j,min}$	$[mm^2]$	0.0067	0.0055	0.0042	0.0030
$V_{c,j}$ [1]	$[mm^2]$	0.0026	0.0034	0.0041	0.0043
κ	[-]	1	1	1	0.7 [2]
$\triangle\alpha_{add',j}$	[-]	0.123	0.071	0.004	0 [2]

[1] The volumes $V_{c,j}$ of the cracks with the maximum crack width are calculated with Eq. 3.33 for $\omega = \omega_{max}$. The maximum crack width (ω_{max}) is given in Table 5.11.

[2] For LWAC with a water-cement ratio of 0.86 the volume of reaction product $V_{RP,add,j,min}$ is smaller than the volume of the crack $V_{c,j}$ (with the maximum width). The reaction product is not enough to fill up the crack with maximum width (largest crack) and no reaction product is left to densify the paste adjacent to this largest crack. It is further discussed in the following text.

Table 5.13: Values of κ and $\triangle\alpha_{add',j}$ for LWAC with a water-cement ratio of 0.86

w/c	Parameters						
	ω_{cri}	$V_{c,j}$ [1]	$V_{RP,add,j,min}$	$\omega \le \omega_{cri}$		$\omega > \omega_{cri}$	
	(μm)	(mm^2)	(mm^2)	κ	$\triangle\alpha_{add',j}$	κ	$\triangle\alpha_{add',j}$
0.86	3.4	0.0030	0.0030	1	0	0	0.13

[1] The volumes $V_{c,j}$ of the cracks with the critical crack width are calculated with Eq. 3.33 for $\omega = \omega_{cri}$.

SIMULATION RESULTS

When micro-cracks occur in the paste, they can be self-healed with reaction products produced during the additional hydration of the paste adjacent to the cracks. The paste adjacent to these micro-cracks will also become denser if some reactions products are left to fill up the pores. The situation, however, is different if the micro-cracks are located in the aggregate phase.

Lightweight aggregates have a porous structure [217]. Swamy and Lambert [217] did a thorough study on the microstructure of the Lytag aggregate (sintered pulverized fuel ash). They observed that large and small voids are evenly mixed and distributed

throughout the entire Lytag pellet. Most large voids are interconnected, while few are discrete and completely sealed. This characteristic creates a possibility for self-healing to occur in the aggregate cracks.

- If the aggregate cracks are located at the boundary between the aggregate and paste, additional hydration may occur in the paste adjacent to these aggregate micro-cracks. These micro-cracks can possibly be filled up with the reaction products produced during crack-induced additional hydration. Besides, due to the porous structure of the lightweight aggregate, the reaction products might penetrate into the aggregate phase adjacent to these aggregate cracks and densify the aggregate.
- If the aggregate cracks are located inside the aggregate (no connection with the paste), no additional hydration will occur in the aggregate phase adjacent to the cracks because aggregate particles do not contain cement. In principle these aggregate cracks will not be closed and the aggregate phase will not be densified. However, due to the porous structure of lightweight aggregate, the reaction products could diffuse into the voids of the aggregate[8] and the aggregate cracks[9]. In this case the closure of the aggregate cracks and densification of the aggregate adjacent to these cracks could still occur.

The *densification* of aggregate particles *adjacent* to cracks seems not realistic and will *not* be considered in this chapter. The possibility of the self-healing (closure) of the aggregate cracks is considered in the simulations for 3 cases:

- Case 1: Not any of aggregate cracks is self-healed (Fig. 5.19a).
- Case 2: The aggregate cracks which are close to the ITZ will be self-healed (Fig. 5.19b).
- Case 3: All aggregate cracks are assumed to be self-healed (Fig. 5.19c).

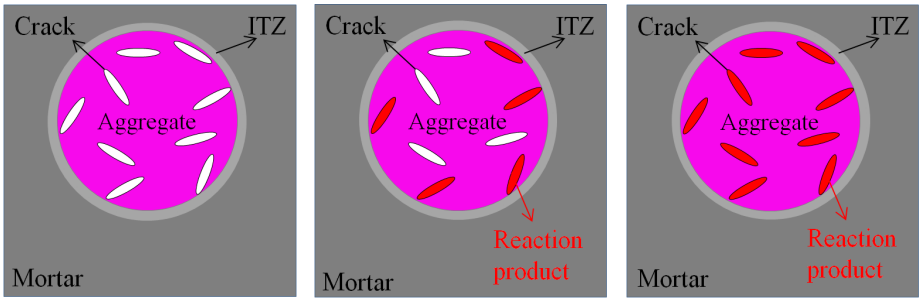

(a) Case 1: No self-healing in aggregate cracks

(b) Case 2: Self-healing in aggregate cracks close to the ITZ

(c) Case 3: Self-healing in all aggregate cracks

Figure 5.19: Three cases for the possibility of the self-healing (closure) of the aggregate cracks

Simulation of the effect of self-healing on the long-term creep of LWACs follows the scheme shown in Fig. 3.18. Calculating the strength recovery and elastic modulus of

[8] Due to concentration gradient.
[9] Due to water diffusion resulting from capillary suction.

the broken mortar and bond beams after self-healing (Eq. 3.23 and 3.24) and that of the mortar and bond beams connected to broken beams after densification (Eq. 3.29 and 3.30) are performed for values of κ and $\triangle\alpha_{add',j}$ given in Table 5.12 and 5.13. If self-healing (closure) of the aggregate cracks is considered, the strength and elastic modulus of the broken aggregate beams are recovered up to the original values of the aggregate beam (given in Table 5.2).

Case 1: Cracks in the aggregate phase are not self-healed

For Case 1 it is assumed in the simulations that not any of the broken aggregate beams is self-healed. The simulated creep strains of LWACs are shown in Fig. 5.20. It

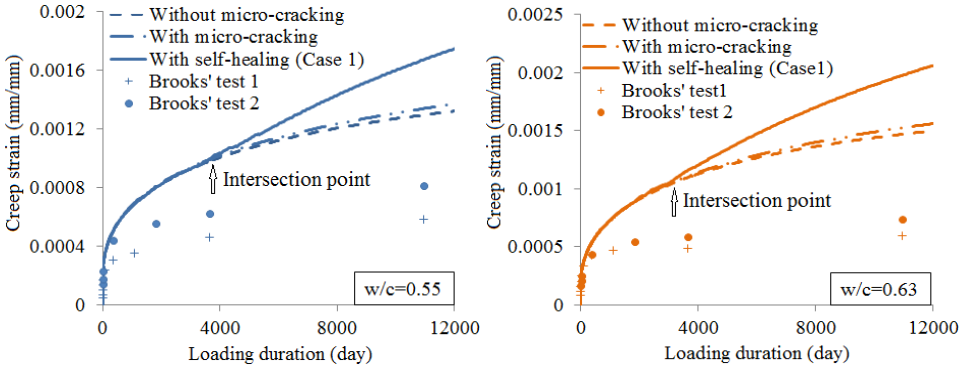

(a) w/c=0.55, Case 1

(b) w/c=0.63, Case 1

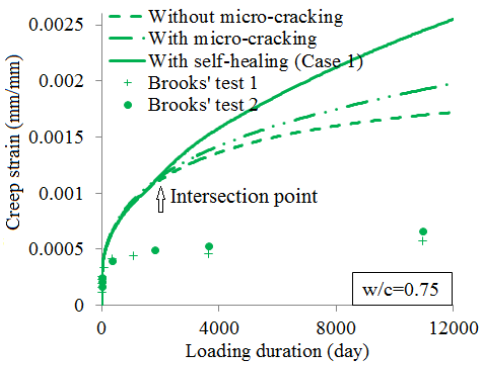

(c) w/c=0.75, Case 1

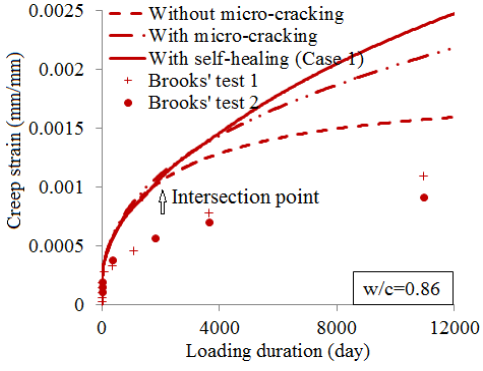

(d) w/c=0.86, Case 1

Figure 5.20: Simulated creep strains of LWACs with water-cement ratios of 0.55-0.86: all the cracks in the aggregate phase are not self-healed (Case 1)

can be seen from this figure that the creep strains of the LWACs in which the effect of self-healing is considered (solid lines) are first slightly smaller and then larger than those with and without the effect of micro-cracking (double-dashed and dashed lines). According to the simulations the creep strain is not reduced when self-healing occurs in the paste (not in the aggregate). The time point at which the solid lines are above the dashed and double dashed lines is called the "intersection point". For LWACs with dif-

ferent water-cement ratios the "intersection points" are located at around 4000 days, 3000 days, 2000 days and 1500 days, respectively.

Before the intersection point, most of micro-cracks occur in the bond area[10] and the number of aggregate cracks is small. The creep strains become smaller due to the self-healing of the bond cracks (broken bond beams) and densification of the paste adjacent to these cracks, compared to those in case no self-healing occurs. With elapse of time, the number of aggregate cracks increases, while no self-healing occurs in these cracks. This results in an additional creep deformation. At the same time, the elastic modulus and strength of the mortar and bond beams increase due to self-healing of the non-aggregate cracks and densification of the paste adjacent to these cracks. The difference between the elastic modulus and strength of the non-aggregate phase and those of the aggregate phase increases over time. This increases the internal stress concentrations, which makes the specimens more prone to micro-cracking. Gradually, the creep strain becomes larger[11].

Case 2: Cracks in aggregate particles close to the ITZ will be self-healed

In the simulations it is assumed that broken aggregate beams which are connected to bond beams are self-healed, while other aggregate cracks are not. The simulated creep strains of LWACs are shown in Fig. 5.21. Similar to Case 1 (Fig. 5.20), the creep strains calculated while considering the effect of self-healing (solid lines in Fig. 5.21) are first smaller, but then larger compared to those without the effect of self-healing (double-dashed and dashed lines in Fig. 5.21). The intersection point occurs later than in Case 1. Self-healing of the aggregate cracks located close to the bond area, obviously shifts this intersection point to a later age. However, over time the creep strain still becomes larger than that without the effect of self-healing. This is because the difference between the elastic modulus and strength of the non-aggregate phase and those of the aggregate phase becomes more significant over time. This increases the internal stress concentrations, which results in more micro-cracks.

Case 3: All aggregate cracks are assumed to be self-healed

In the simulations it is now assumed that all broken aggregate beams are healed. The simulated creep strains of LWACs are shown in Fig. 5.22. When all the micro-cracks, including the aggregate cracks, are self-healed, the creep strains (solid lines in Fig. 5.22) are smaller than those without the effect of micro-cracking (dashed lines in Fig. 5.22) for the entire loading period (30 years). The occurrence of self-healing in the non-aggregate area still increases the difference between the elastic modulus and strength of the non-aggregate phase and those of the aggregate phase. This still increases the magnitude of internal stress concentrations. Continuous self-healing of the aggregate cracks can somehow mitigate the stress concentrations and the proneness to cracking. It should be noted that Case 3, whereby all the aggregate cracks are healed, is hypothetical. Case 1 (no self-healing of aggregate cracks) and Case 2 (self-healing of the aggregate cracks, which are close to the ITZ) are supposed to be close to reality.

Strength after self-healing

The simulated compressive strength and stress-strength ratio of the LWACs are shown

[10] Due to the difference between the elastic modulus of mortar and that of aggregate.
[11] This paragraph shows how the model works with the given input.

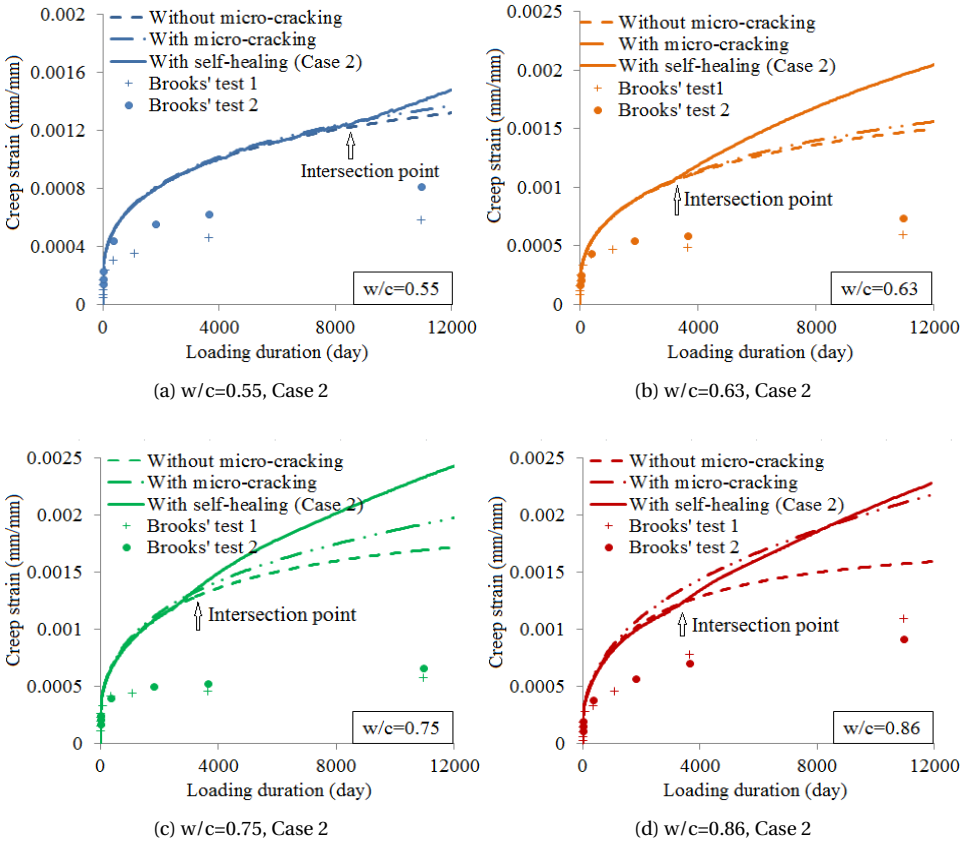

(a) w/c=0.55, Case 2

(b) w/c=0.63, Case 2

(c) w/c=0.75, Case 2

(d) w/c=0.86, Case 2

Figure 5.21: Simulated creep strains of LWACs with water-cement ratios of 0.55-0.86: the aggregate cracks which are close to the ITZ will be self-healed (Case 2)

in Fig. 5.23. When no self-healing occurs in the aggregate cracks (Case 1) or the aggregate cracks which are close to ITZ are healed (Case 2), the compressive strength of the loaded LWACs (light green and blue solid lines in Fig. 5.23) is first larger and then smaller compared to that of the load-free LWACs (dashed lines in Fig. 5.23). This means that no extra strength increase is obtained in the long term. When all the micro-cracks, including the aggregate cracks, are healed (Case 3), the LWACs gain an extra increase in strength (red solid lines in Fig. 5.23).

The 30-year experimental and simulated compressive strength of loaded and load-free LWACs is shown in Table 5.14. With the strength values in this table, the percentage extra increase in strength of the loaded LWACs after 30 years is calculated and plotted in Fig. 5.24. This calculated percentage extra increase is compared to the measured percentage extra increase. It can be seen from Fig. 5.24 that the percentage extra increase in strength of the loaded LWACs decreases with increasing water-cement ratios. Similar findings have been mentioned in Chapter 4, where the results obtained for NWACs were discussed. When no self-healing occurs in the aggregate cracks (Case 1), the strength of the loaded LWACs after 30 years is smaller than that of the load-free LWACs. When the

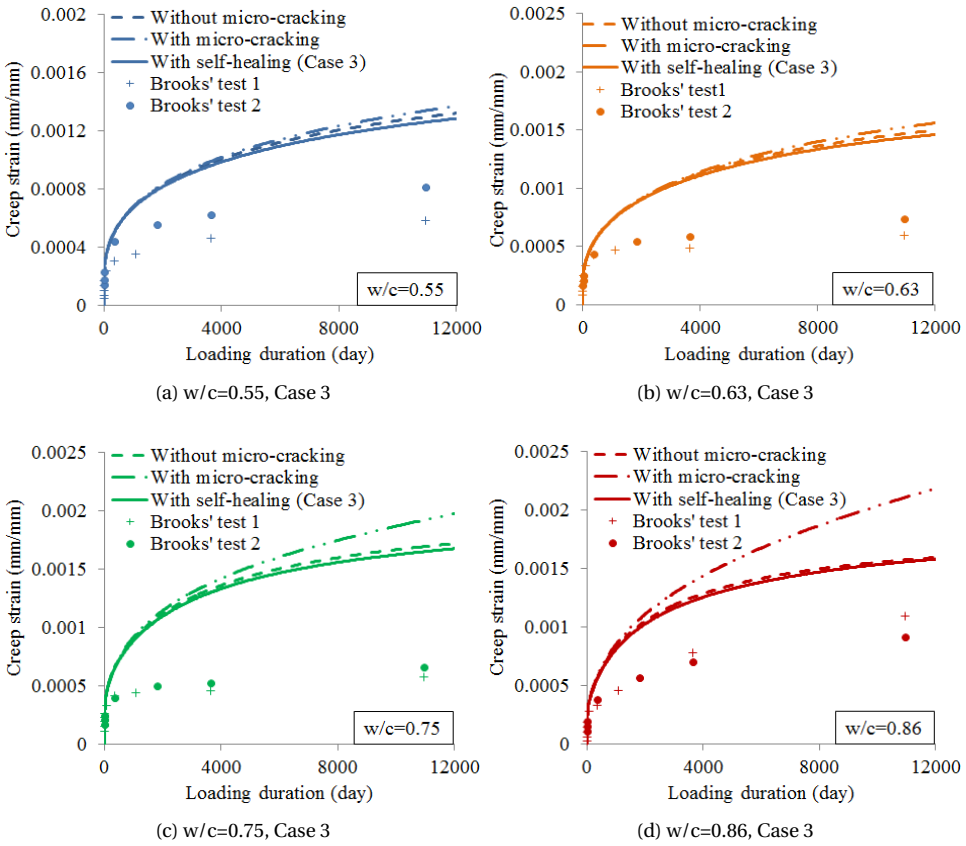

Figure 5.22: Simulated creep strains of LWACs with water-cement ratios of 0.55-0.86: all the aggregate cracks are assumed to be self-healed (Case 3)

aggregate cracks close to the ITZ phase are healed (Case 2), the loaded LWACs with water-cement ratios of 0.55 and 0.63 gain an extra increase in strength, while no extra increase is obtained for LWACs with water-cement ratios of 0.75 and 0.86. When all the aggregate cracks are healed (Case 3), all the LWACs would gain an extra increase in strength. In Brooks' test the percentages extra increase for the loaded LWACs are 13.6%, -18.7%, -23.9% and -24.6% respectively. Comparing the simulated percentages in Case 1, 2 and 3 to the measured percentages, Case 3 (all aggregate cracks are healed) seems not realistic for LWACs, since all LWACs would gain an extra increases in strength in this case. The percentages in Case 1 (no self-healing occurs in the aggregate cracks) and Case 2 (the aggregate cracks close to the ITZ phase are healed) are closer to the measured ones and thus these two cases probably represent more plausible mechanisms for strength development of the loaded LWACs and may give a better fit with the experimental strength.

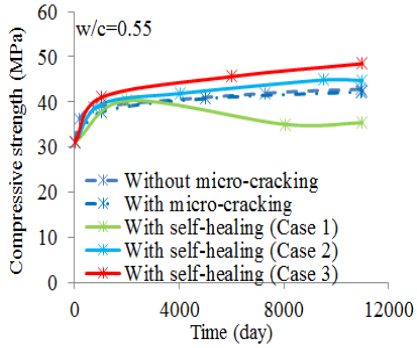

(a) Strength

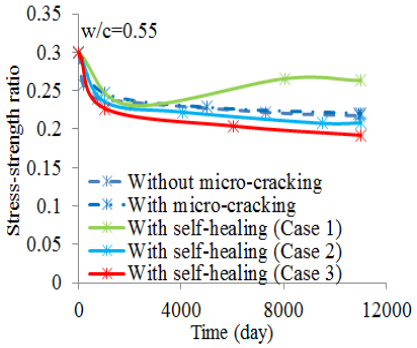

(b) Stress-strength ratio

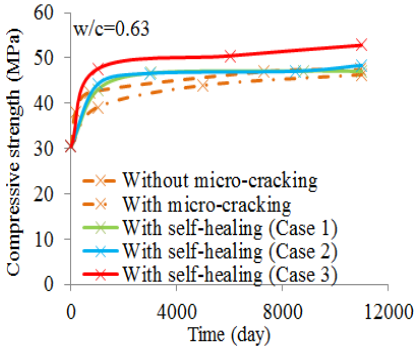

(c) Strength

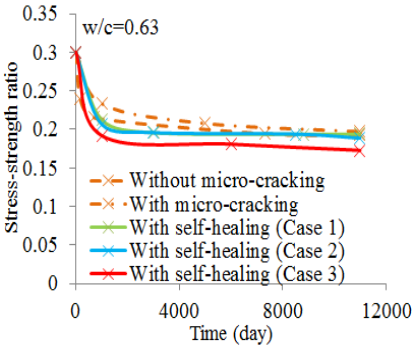

(d) Stress-strength ratio

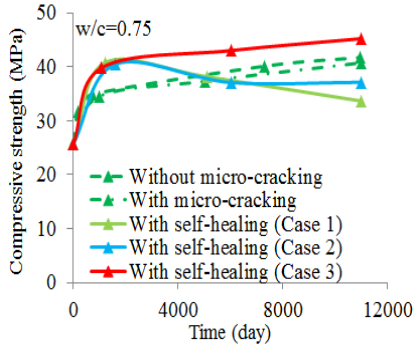

(e) Strength

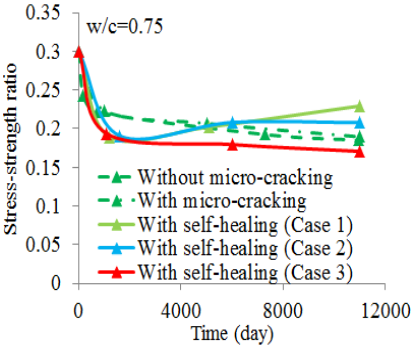

(f) Stress-strength ratio

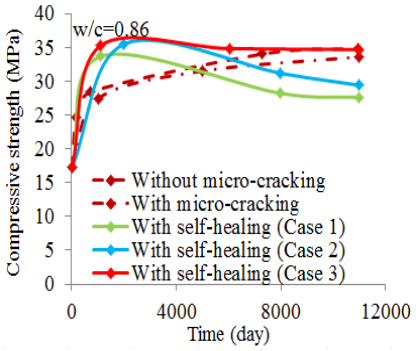

(g) Strength

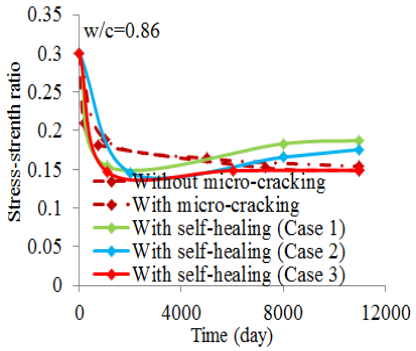

(h) Stress-strength ratio

Figure 5.23: Simulated compressive strength and stress-strength ratio of LWACs with water-cement ratios of 0.55-0.86 loaded at 14 days at a stress level of 30% of compressive strength: with and without the effect of self-healing

5

Table 5.14: Measured and simulated compressive strength of load-free and loaded LWACs with water-cement ratios of 0.55-0.86 after 30 years

w/c	Simulated strength (MPa)					Measured strength (MPa)	
	No cracks[1]	With cracks[2]	No healing in aggregate cracks (Case 1)[3]	Healing in some aggregate cracks (Case 2)[3]	Healing in all aggregate cracks (Case 3)[3]	Loaded specimen	Load-free specimen
0.55	42.8	42.3	35.3	44.7	48.5	50.0	44.0
0.63	47.4	46.3	47.0	48.3	52.8	41.3	50.8
0.75	41.7	40.7	33.6	37.1	45.2	31.2	41.0
0.86	34.8	33.5	27.5	29.4	34.7	27.0	35.8

[1] No cracks: simulations without the effect of micro-cracking but with continuous hydration; the values in this column should be compared with those in the eighth column;
[2] With cracks: simulations with the effect of micro-cracking and continuous hydration;
[3] Case 1, 2 and 3: simulations with the effect of self-healing; the values in this column should be compared with those in the seventh column.

5.6.4. FINAL REMARKS REGARDING THE SIMULATION RESULTS

CREEP RATE

The measured and simulated creep rates are plotted in Fig. 5.25. As can be seen in this figure, the rate of deformation gradually decreases if all aggregate cracks are self-healed (Case 3, red lines without markers). However, when none or part of aggregate cracks are self-healed (Case 1 and 2, light green and blue lines without markers), the simulated creep rate first decreases, while after a certain time it increases a bit. That is to say, a turning point appears in the curves of the rate of simulated creep of LWACs with water-cement ratios of 0.55-0.86 for Case 1 and 2. This turning point also appears on the curves of the measured creep rate of LWACs with water-cement ratios of 0.63 and 0.75 (orange and green lines with markers in Fig. 5.25b and 5.25c). This further proves the aforementioned analysis to be reasonable: Case 1 (no self-healing occurs in the aggregate cracks)

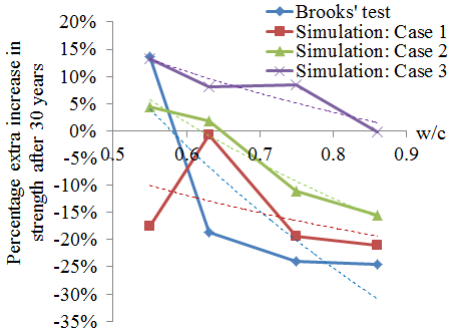

Figure 5.24: Measured and simulated percentage extra increase in strength after 30 years for LWACs with water-cement ratios of 0.55-0.86 (percentage extra increase in strength after 30 years = [30-year compressive strength of loaded concrete - 30-year compressive strength of load-free concrete] / 30-year compressive strength of load-free concrete)

and Case 2 (the aggregate cracks close to the ITZ phase are healed) are probably more plausible mechanisms for the loaded LWACs, compared to Case 3.

5

ABSORPTION OF WATER BY LIGHTWEIGHT AGGREGATE AND THE EMPIRICAL AGEING FACTOR

It can be seen from the simulation results shown in Fig. 5.20 to 5.22 that there is a discrepancy between the simulated creep strains and the experimental data. The possible reason is that the empirical ageing factor a for LWACs is overestimated. Due to the absorption of water by lightweight aggregates, the effective water-cement ratio of LWAC might have been smaller than the initial water-cement ratio used in the mix design (0.55-0.86). In that case the empirical ageing factor a calculated based on the data in Fig. 4.9a will have been smaller than that in case the initial water-cement ratio is used.

The initial degree of saturation of the lightweight aggregate is not given in Brooks' test [19, 22, 25, 161]. However, Brooks mentioned in his paper [19] that during the experiments the lightweight aggregates appears to be prone to induce swelling of concrete in the long term. Besides, the LWACs with water-cement ratios of 0.55-0.86 have similar 14-day strengths as (even larger strength than) the NWACs with water-cement ratios of 0.50-0.80 (see Table 4.1 and 5.1). This means the microstructure of the paste in LWACs must have been denser than that in NWACs[12]. From these observations it is inferred that the lightweight aggregate was not completely pre-saturated and might have absorbed some water.

In the following a calculation is performed in order to estimate the effect of the absorption of water by lightweight aggregates on the water-cement ratio and on the empirical ageing factor a in the creep formula (Eq. 3.17). Due to the absorption of water by lightweight aggregates, the amount of water available for the hydration of cement is less than the total amount of water added in the mixture. The ratio of the available amount of water to the weight of cement is defined as effective water-cement ratio. European standard EN 206 [218] provided a method to calculate the effective water-cement ratio

[12] This can also be seen from the strengths of the mortar beams of the lattice model of LWACs (Table 4.2) and NWACs (Table 5.2).

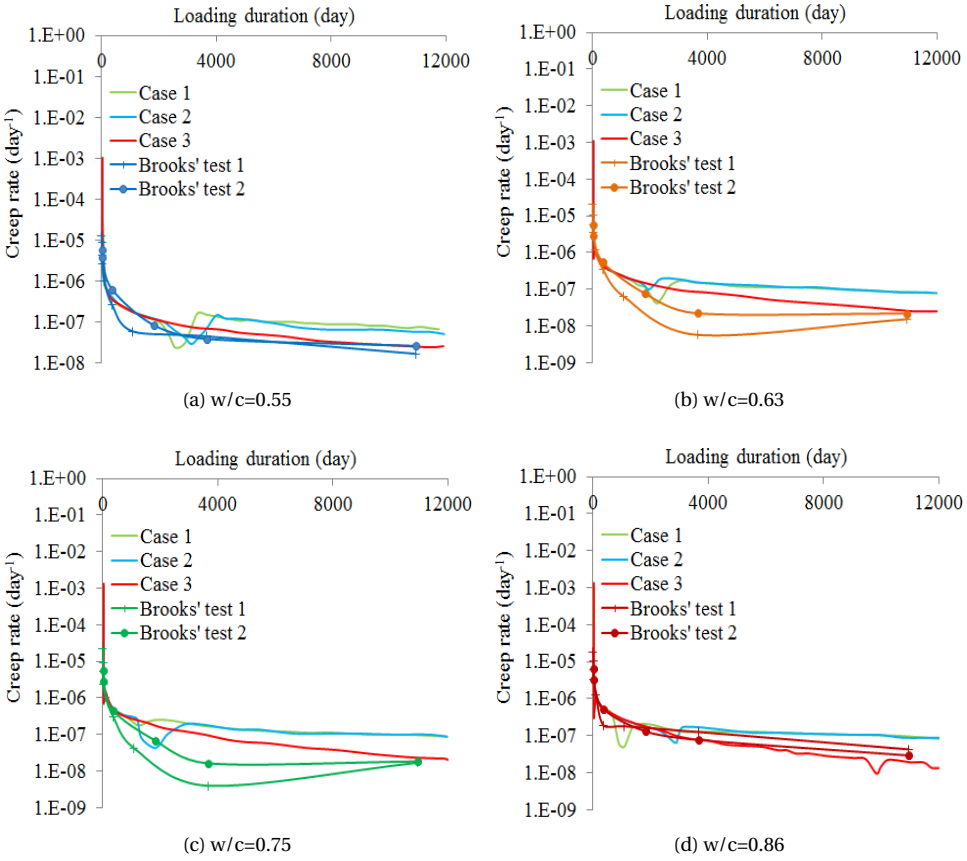

Figure 5.25: The rate of experimental and simulated creep strains of LWACs with water-cement ratios of 0.55-0.86

wcr_{eff}, as shown in Eq. 5.1.

$$wcr_{eff} = \frac{w_{eff}}{c} = \frac{w - w_{ab,1h} \cdot m_{lwa}}{c} \tag{5.1}$$

where w is the total amount of water added in the mixture; $w_{ab,1h}$ is water absorption of lightweight aggregates after 1 hour, specified according to EN 1097-6 [219]; m_{lwa} is the content of lightweight aggregates. According to several sets of experimental data [217, 220–222], the 1 hour water absorption of Lytag aggregates (or sintered fly ash aggregates) is around 10%-17% ($w_{ab,1h} = 0.10 - 0.17$). In Brook's test, the ratio of Lytag aggregates to the cement by weight is 1.52 ($m_{lwa}/c = 1.52$; Table 5.1). Inserting $w_{ab,1h} = 0.10 - 0.17$ and $m_{lwa}/c = 1.52$ in Eq. 5.1, the effective water-cement ratios wcr_{eff} for LWACs are calculated and shown in the third column in Table 5.15. Domagala [220] suggested that the values calculated with Eq. 5.1 underestimate the values of the effective water-cement ratios as compared to the values determined in his tests. The concrete mixtures with sintered fly ash aggregate in his tests showed that the reduction of water-cement ratio is up to 0.19 due to the absorption of water by sintered fly ash aggregates. Based on this,

Table 5.15: Effect of absorption of lightweight aggregates on the value of empirical ageing factor a

w/c	a ($\times 10^{-5}$) (Table 5.6)	wcr_{eff} (Eq. 5.1)	Corrected wcr_{eff}	a_{eff} ($\times 10^{-5}$)	$\frac{a-a_{eff}}{a} \times 100\%$
0.55	0.39	0.29-0.40	0.36-0.40	0.23-0.27	33%-42%
0.63	0.48	0.37-0.48	0.44-0.48	0.31-0.35	28%-36%
0.75	0.69	0.49-0.60	0.56-0.60	0.41-0.44	36%-41%
0.86	1.19	0.60-0.71	0.67-0.71	0.52-0.56	53%-56%

the lower bound of wcr_{eff} in the third column in Table 5.15 is corrected and replaced by $w/c - 0.19$ (w/c from first column in Table 5.15). The corrected effective water-cement ratios are shown in the fourth column in Table 5.15. Using the corrected effective water-cement ratios and the method for calculating a (Section 4.4.1), the "effective" values for empirical ageing factor, a_{eff}, are calculated and given in the fifth column in Table 5.15.

As can be seen in Table 5.15, the effective empirical ageing factor a_{eff} is on average 40% smaller than when absorption of water by the lightweight aggregates is not considered. Based on the linear relationship between a and *real* creep strain described with Eq. 3.14, i.e.

$$\epsilon_{cr} = a \cdot t^n \cdot \sigma$$

the *real* creep strain will also be around 40% smaller. The simulated creep strains with the effect of continuous hydration, micro-cracking and self-healing will then get close to the experimental data.

The creep strains simulated with the lower bound values of a_{eff} (fifth column in Table 5.15) are shown in Fig. 5.26. The simulated 30-year compressive strength of loaded LWACs is given in Table 5.16 and the percentages extra increase in strength after 30 years are shown in Fig. 5.27b. With the effective empirical ageing factor a_{eff}, the simulated creep strains are getting close to the experimental data. When no self-healing occurs in the aggregate cracks (Case 1, light green solid lines in Fig. 5.26) or aggregate cracks close to ITZ are self-healed (Case 2, light blue solid lines Fig. 5.26), the creep strains are still larger than those without the effect of the self-healing (dashed and dotted dashed lines in Fig. 5.26) after a certain time. These intersection points occur later than those in Fig. 5.20 and 5.21.

The creep strains of the beams, calculated[13] with a_{eff} (fifth column in Table 5.15), are smaller compared to the creep strains calculated with a (second column in Table 5.15). As a consequence the number of micro-cracks generated during the creep process is lower (see Fig. 5.28b). The number of broken beams, which are self-healed afterwards, and the number of mortar and bond beams connected to the broken beams, which are densified, are smaller. The contribution of self-healing to the extra strength increase is less significant. The effect of self-healing on the difference between the strength and elastic modulus of non-aggregate phase and those of the aggregate phase (thus on the stress concentrations) is also lower. Therefore, the simulated percentages extra increase in strength for Case 1 and 2 (red and green lines in Fig. 5.27b) are larger than those in Fig. 5.27a. When all the aggregate cracks are self-healed (Case 3), the simulated percentages

[13] Calculated with Eq. 3.17

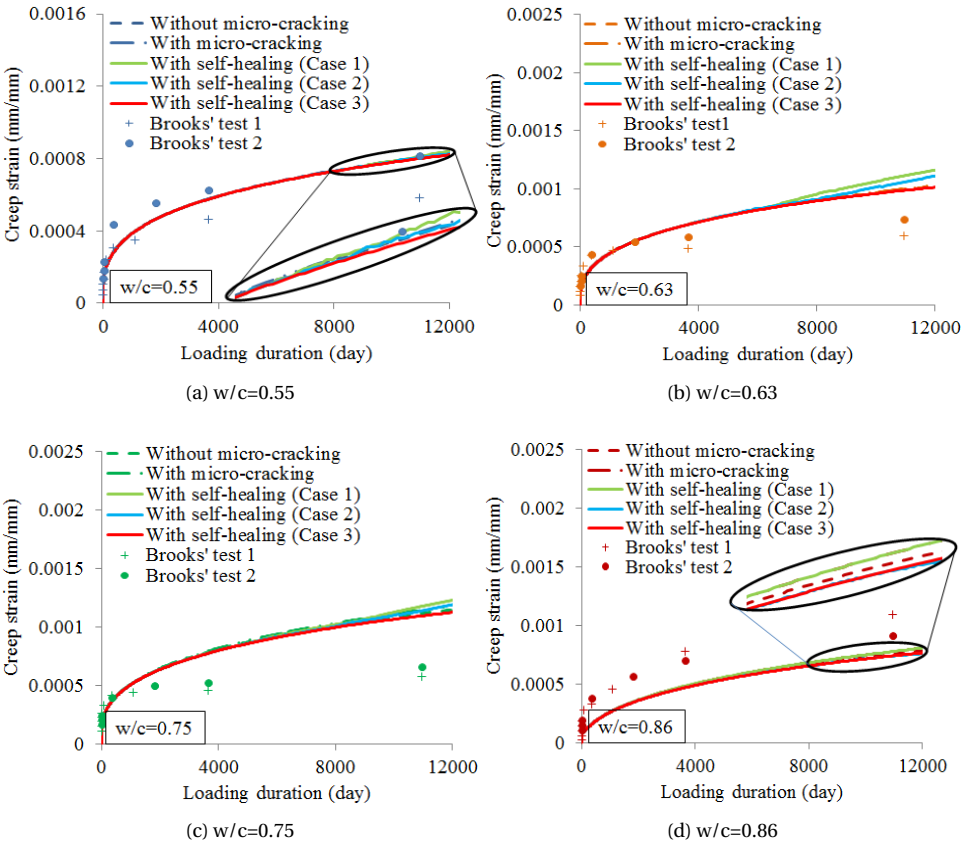

(a) w/c=0.55 (b) w/c=0.63

(c) w/c=0.75 (d) w/c=0.86

Figure 5.26: Simulated creep strains of LWACs with water-cement ratios of 0.55-0.86: with the effective empirical ageing factor a_{eff}

extra strength increase (purple line) are smaller than those in Fig. 5.27a. This is because in the simulations with a_{eff} the number of micro-cracks is smaller and thus the contribution of self-healing to the extra strength increase is less, compared to the simulations with the values of a (second column in Table 5.15).

The effective empirical ageing factor a_{eff} gives a better fit for the creep strains (see Fig. 5.26), but it increases the discrepancy between the simulated and measured percentages extra strength increase of the loaded LWACs (Fig. 5.27b), compared to the simulated results with the original empirical ageing factor a (Fig. 5.20 to 5.22 and Fig. 5.27a). Either with a or a_{eff}, the creep strains calculated with the effect of self-healing (Case 1 and 2) exceed the creep strains calculated without the effect of self-healing at a certain time point. In the simulations self-healing seems not to lower the creep strains of LWACs. This is because, as aforementioned, self-healing of cracks and densification of the paste adjacent to the cracks increase the difference between the elastic modulus and strength of the non-aggregate phase and those of the aggregate phase. This increases the heterogeneity of the material and internal stress concentrations, which induces more micro-cracks in the paste and lightweight aggregate particles.

Table 5.16: Measured and simulated compressive strength of load-free and loaded LWACs with water-cement ratios of 0.55-0.86 after 30 years: with the effective empirical ageing factor a_{eff}

w/c	Simulated strength (MPa)					Measured strength (MPa)	
	No cracks[1]	With cracks[2]	No healing in aggregate cracks (Case 1)[3]	Healing in some aggregate cracks (Case 2)[3]	Healing in all aggregate cracks (Case 3)[3]	Loaded specimen	Load-free specimen
0.55	42.8	42.6	42.8	43.8	47.8	50.0	44.0
0.63	47.4	47.0	46.7	47.6	48.5	41.3	50.8
0.75	41.7	41.2	38.5	40.1	42.2	31.2	41.0
0.86	34.8	34.4	33.4	36.3	36.5	27.0	35.8

[1] No cracks: simulations without the effect of micro-cracking, but with continuous hydration; the values in this column should be compared with those in the eighth column;
[2] With cracks: simulations with the effect of micro-cracking and continuous hydration;
[3] Case 1, 2 and 3: simulations with the effect of self-healing; the values in this column should be compared with those in the seventh column.

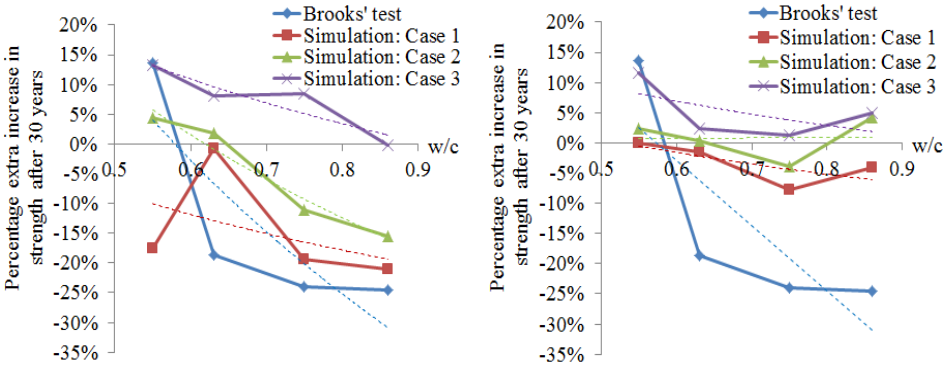

(a) Before correction: with a

(b) After correction: with a_{eff}

Figure 5.27: Measured and simulated percentage extra increase in strength after 30 years for loaded LWACs with water-cement ratios of 0.55-0.86: before and after correction

5.7. CONCLUSIONS

In this chapter, the interaction between creep, micro-cracking and self-healing of concretes with lightweight aggregate with water-cement ratios of 0.55-0.86 has been investigated with the modified lattice model. The LWACs are loaded at 14 days at a stress level of 30% of the compressive strength (constant stress). Based on the results and discussions, the following conclusions can be drawn:

- When continuous hydration after loading is considered, the creep strain of LWAC is smaller than that in case hydration does not occur. Micro-cracks occur in LWAC under sustained load and, because the strength and elastic modulus of the aggregates are lower than those of the paste, most of the micro-cracks appears in the ITZ and aggregate phase. The number of micro-cracks of LWAC with a high

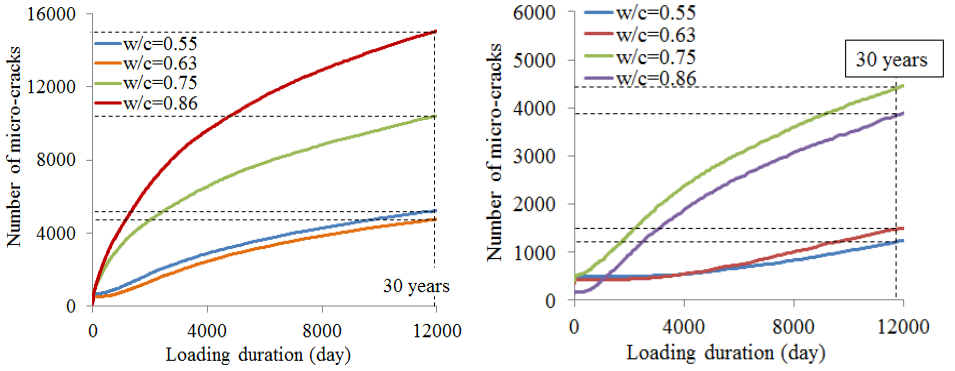

(a) Before correction: with a

(b) After correction: with a_{eff}

Figure 5.28: Simulated number of micro-cracks in LWACs during the creep process: before and after correction

water-cement ratio is larger than that of LWAC with a low water-cement ratio. Micro-cracking contributes to an additional overall deformation and a reduction in strength of LWAC under sustained load. This contribution is more significant for LWAC with high water-cement ratio than for LWAC with low water-cement ratio. This is similar to the findings for NWAC.

- Micro-cracks appear in the lightweight aggregate of LWAC under sustained load. If all aggregate cracks would be healed during the creep process, the creep strain would be less compared to that without the effect of self-healing and the extra strength is achieved. However, this is not very realistic. If the aggregate cracks close to the ITZ phase are healed or no aggregate cracks are healed, the long-term creep strain does not become less than that without the effect of self-healing. Instead, self-healing increases the difference between the strength and elastic modulus (degree of heterogeneity) of the paste and aggregate phases. This increases the heterogeneity of the material and internal stress concentrations. More micro-cracks occur, which further increases the deformation and reduces the strength.

- When the absorption of water by the lightweight aggregate is taken into account, the empirical ageing factor is smaller than that in case absorption is not considered. The simulated creep strains of LWACs are then smaller and fit better with the experimental data, while the discrepancy between the simulated and measured extra strength increase becomes larger. The effects of micro-cracking and self-healing on the long-term creep and strength of loaded LWACs are less significant than in case absorption of water by lightweight aggregate is not considered.

6

RETROSPECTION, CONCLUSIONS AND FURTHER RESEARCH

The only way science moves forward is
to follow the evidence wherever it leads,
even if it makes us sound crazy sometimes.

"The Decision Reverberation"
The big bang theory
Season 12, Episode 20

This chapter summarises the work presented in this thesis. Then the conclusions and contributions of this research are presented. In the end, suggestions for further research are given.

6.1. RETROSPECTION

SUSTAINED load not only deforms concrete, but also continuously changes the microstructure of concrete and its strength and elasticity [99]. Micro-cracking of concrete has been detected experimentally by acoustic emission techniques during creep test of concrete at different stress levels [9, 29]. It could contribute to both an extra deformation and a reduction in the strength and elasticity. This is somehow contradictory to some experimental observations that there is an extra increase in strength (and elastic modulus) of concrete under sustained load, especially at low and medium stress levels, compared with load-free concrete [19, 24, 34, 37, 96]. Self-healing is considered a promising candidate to "resolve" this contradiction. The main aim of this research is to study the interaction between creep, micro-cracking and self-healing of concrete under sustained load. Two subjects were dealt with in parallel: the effects of micro-cracking and self-healing on the long-term creep deformation as well as on the strength of concrete. The research is performed theoretically and numerically. The concrete analysed in this thesis is stored in water at room temperature ($23 \pm 1\,^{\circ}C$). The numerical simulations[1] are performed at meso-scale where concrete is treated as a three-phase material (mortar, bond and aggregate). The numerical creep tests are conducted in a 2D approach in order to reduce the computation time.

Chapter 3 established the basis for this research. Firstly, an in-house lattice model is modified to take long-term creep into consideration. The activation energy concept is employed to model creep. Secondly, a mechanism for the extra increase of the strength of concrete under sustained load is proposed. It includes two aspects: self-healing of cracks and densification of the paste adjacent to cracks. The latter is further studied through a model for autogenous self-healing [16]. This mechanism is, then, incorporated in the modified lattice model and the effect of micro-cracking and self-healing on the long-term creep deformation of concrete under sustained load (water-cement ratio=0.50; stress level=30% of 14-day compressive strength) is simulated. The strength after loading is calculated and compared with the strength of the load-free concrete. The simulated results (both deformation and strength) are compared with experimental data from Brooks' 30-year creep test [19].

In Chapter 4, the role of the water-cement ratio in the interaction between creep, micro-cracking and self-healing of concrete under sustained load is studied with the modified lattice model. Concretes with five water-cement ratios (in the range of 0.50 to 0.80) from Brooks' test are simulated. They are loaded at 14 days at a stress level of 30% of the 14-day compressive strength. The effect of continuous hydration, micro-cracking and self-healing on the long-term creep deformation and compressive strength is quantified. The simulated extra strength increase after 30 years is compared to the experimental one.

Chapter 5 deals with lightweight aggregate concrete (LWAC) under sustained load (at low stress levels). Aggregate is considered as the weakest component in LWAC. The interaction between creep, micro-cracking and self-healing of LWACs with water-cement

[1] The main focus of this research is to investigate the trends in terms of the effect of micro-cracking and self-healing on the long-term creep and strength of concrete. In order to get more precise results, further refinement of the mesh size, the dimension of the numerical specimen (e.g. 3D) and the heterogeneity of the microstructure (e.g. anisotropic mortar phase) is required.

ratios of 0.55 to 0.80 is simulated with the modified lattice model. Regarding self-healing in LWACs under sustained load, the mechanism for the extra strength increase of concrete under sustained load proposed in Chapter 3 is still applied here. The paste adjacent to the cracks is densified. For self-healing of the aggregate cracks, three situations are considered: (a) no healing occurs in the aggregate cracks; (b) aggregate cracks which are close to ITZ are self-healed; (c) all the aggregate cracks are self-healed. These three situations are simulated to investigate the effect of self-healing on the long-term creep and compressive strength of LWACs under sustained load.

6.2. CONCLUSIONS

THE general conclusions of the research are as follows:

- The strength of concrete under sustained load (low stress levels) is larger than that of load-free concrete. This phenomenon has been explained by the compaction theory [37, 88]. However, it was found that compaction can only play a minor role in the extra increase in strength of concrete under sustained load. (Appendix A)

- A self-healing mechanism that explains the extra increase in strength of concrete under sustained load, i.e. self-healing of micro-cracks and densification of the paste adjacent to the micro-cracks, was proposed. This mechanism, together with creep and continuous hydration, are incorporated in a lattice model [17, 35]. The modified lattice model was found to be an appropriate tool to investigate the effects of continuous hydration, micro-cracking and self-healing on the long-term creep and strength development of concrete under sustained load and gives quite good results.

In order to evaluate the proposed model for quantitative analysis of the effect of micro-cracking and self-healing on the long-term creep and strength development of concrete under sustained load (low stress levels), experimental data of Brooks' test [19, 22, 25, 161] are used to validate the simulation results. Based on the simulation results, the following conclusions can be drawn:

- Under sustained load, local stress concentrations and micro-cracking occur due to the heterogeneity of concrete. The micro-cracking contributes to an additional creep deformation and reduces the strength of concrete. With the effect of self-healing, the loss in strength of concrete under sustained load due to the micro-cracking is recovered. On top of that, concrete gains an extra strength, compared to the load-free concrete. Creep strain with the effect of self-healing in hardening concrete is less than that with the effect of continuous hydration only.

- In the long run, the number of micro-cracks (or damage degree) in concrete with a high water-cement ratio (up to w/c=0.80) is greater than that in concrete with a low water-cement ratio (as low as w/c=0.50). The additional creep deformation caused by micro-cracking is thus larger for concrete with a high water-cement ratio than for concrete with a low water-cement ratio. The extra deformation caused by micro-cracking increases exponentially with increasing number of micro-cracks for concretes, irrespective of water-cement ratios.

- Under sustained load concrete with a high water-cement ratio gains less additional strength than concrete with a low water-cement ratio. It can be concluded that concrete with a low water-cement ratio has a better performance (higher potential to increase its strength while under load) under long-term sustained loading compared to concrete with a high water-cement ratio.

  Evaluation: The damage degree (i.e. number of micro-cracks per specimen) and crack density (i.e. number of micro-cracks per unit area) vary in concretes with different water-cement ratios and influence the total additional degree of hydration. If the volumes of densified paste adjacent to cracks do not overlap, the total additional degree of hydration increases with the increasing damage degree (positive effect). If the volumes of densified paste overlap, the total additional degree of hydration increases less fast with increasing crack density. The number of micro-cracks due to sustained load is generally larger for concrete with a high water-cement ratio than for concrete with a low water-cement ratio. Thus, the crack density increases with increasing water-cement ratios. The increase of crack density, implying more "overlap-paste", cancels out the positive effect of additional hydration that was triggered by the formed cracks (damage degree). Therefore, concrete with a high water-cement ratio has a lower total additional degree of hydration, i.e. lower extra strength increase, than concrete with a low water-cement ratio.

- Self-healing increases the difference between the strength and elastic modulus of non-aggregate and those of aggregate phases in LWAC. This increases the degree of heterogeneity and internal stress concentrations. More micro-cracks occur, which further increases the deformation and reduces the strength.

  Evaluation: Similar to NWAC, micro-cracking results in an additional creep deformation and reduces the strength of LWAC under sustained load. Different from NWAC, micro-cracks also appear in the aggregate phase in LWAC under sustained load. This influences the effect of self-healing on creep and strength, since aggregate cracks will not easily be healed. If all aggregate cracks would heal during the creep process, the creep strain would be less compared to that without the effect of self-healing and the extra strength is achieved. However, this is not very realistic. In general, the possibility for aggregate cracks to heal is almost zero. If only the aggregate cracks close to the ITZ phase are healed and/or no aggregate cracks are healed, the long-term creep strain does not become less than that without the effect of self-healing, and no extra strength is obtained.

- There is a possibility that the calculated value of empirical ageing factor a in the creep formula (Eq. 3.17) already includes the effect of hydration, micro-cracking or self-healing, since a is calculated based on the relationship between a_0 ($a_0 = a \times \sigma$) and water-cement ratios, which is derived from the experimental creep data of cement paste [20]. The creep data in [20] was obtained on cement paste loaded at 35 days at a stress level of 30%. Paste at 35 days was assumed to be mature and no further hydration would have occurred. Micro-cracking was also assumed not to occur at low stress levels. In our research, however, micro-cracks were found in concrete loaded at a stress level of 30%. Since paste is more homogeneous than concrete, micro-cracks in paste are supposed to be less than in concrete. Still, some micro-cracks were supposed to occur during the creep test performed by Wittmann [20], and would have had some influence on the creep deformation

and thus on the value of a. This could, to a certain extent, explain the discrepancy between the simulated creep curves and the experimental ones. In addition, the calculation method overestimates the value of a for LWAC, if the lightweight aggregates absorb water from the paste. Due to the absorption of water by the lightweight aggregates, the effective water-cement ratio of LWAC will be lower than the water-cement ratio used in the mixture, which will lead to a smaller value of a.

6.3. CONTRIBUTIONS OF THIS RESEARCH

THE contributions of this study to science and engineering are as follows:

- This research provides an alternative way of looking at the behaviour of concrete under sustained load. Concrete under sustained load continues to hydrate. Meanwhile, micro-cracks occur due to the heterogeneity of concrete. Under favourable conditions (e.g. sufficient water supply) self-healing will take place. All these processes interact with and influence each other. This research combines all these processes and investigates the effect of these processes on the behaviour of concrete under sustained load (e.g. long-term creep deformation and strength development).

- An in-house lattice fracture model is modified to take long-term creep into account. The continuous hydration and self-healing are also incorporated in the modified lattice model. The model is able to consider the micro- or meso- structure of concrete and to model the interaction between creep, hydration, micro-cracking and self-healing of concrete under sustained load. It records stress and strain, strength and elastic modulus, and the status (cracked, non-cracked, healed or densified) of each local beam at each time step. Any change in the structural performance (e.g. global deformation) or material properties (e.g. strength) resulting from the changes in the micro- or meso- structure (local beams) can be calculated. This model builds a link between the behaviour of the micro- or meso-structure and behaviour of concrete under sustained load and can quantify the effects of hydration, micro-cracking and self-healing on the long-term creep and strength of concrete.

- Experimental observations [19, 24, 34, 37, 96] have revealed that the compressive strength of loaded NWAC is larger than that of load-free NWAC. Compaction theory is supported by some researchers [37, 88]. However, the compaction seems to have only a marginal effect on the extra increase in strength. In this thesis, a self-healing mechanism, i.e. self-healing of micro-cracks and densification of the paste adjacent to the cracks, is proposed to explain the extra increase in strength of loaded concrete. It is incorporated in the modified lattice model. The simulated results (deformation and strength) for NWAC are found to fit relatively well with the experimental data [19].

- The heterogeneity of concrete makes it prone to micro-cracking under sustained load, even at low stress levels. Although the crack width at low stress levels is very small (a few micro-meters), it increases with time, decreases strength and results

in an additional deformation in the long term. According to the simulations in this thesis, the additional deformation can reach values around 10% of the total deformation after 30 years for concrete with a low water-cement ratio (w/c=0.50 and 0.54) under a stress of 30% of the 14-day compressive strength (if no self-healing is considered). This percentage will be doubled for concrete with a high water-cement ratio (w/c=0.67 and 0.80). Self-healing can prevent the occurrence of the additional deformation caused by micro-cracking. However, if the self-healing efficiency is lower (e.g. insufficient water supply, concrete with a high water-cement ratio or loaded at high stress level) than the effect of micro-cracking, the additional deformation will still appear. Ignoring the effect of micro-cracking in cementitious materials with low self-healing efficiency could lead to the underestimation of long-term creep.

- Under sustained load micro-cracks in LWAC appear not only in the paste and ITZ (i.e. matrix), but also in the aggregates. Self-healing occurs in the matrix, but not in the aggregates. Self-healing then increases the heterogeneity between the matrix and the aggregate phase, which exacerbates the stress concentration phenomenon. Therefore, the creep strain becomes even larger when self-healing is considered and the strength of LWAC will not be recovered. Hence, self-healing might be not beneficial to LWAC in the same way as it does to NWAC. If self-healing takes place in LWAC under sustained load, the aggregate cracks should be healed as well. Self-healing should aim at making materials more homogeneous in order to mitigate the stress concentration problem.

6.4. FURTHER RESEARCH

BASED on this research, several aspects regarding further experiments and numerical simulations are recommended:

- Experimental data show that the strength of loaded concrete stored in air or sealed concrete is also larger than that of the load-free concrete stored in the same conditions [19, 24, 37, 88]. In Brooks' 30-year creep test [19] the extra increase in strength of some loaded concretes stored in air (relative humidity 60%) after 30 years is even larger than that of loaded concrete stored in water. The water content in concrete stored in air or in sealed condition is limited. The self-healing as proposed for the extra increase in strength of loaded concrete in this research might not occur or only play a minor role since, it requires sufficient water to initiate the self-healing (or further hydration)[2]. Some reasons have been proposed to explain the extra increase in strength of loaded concrete stored in air or sealed condition:

  (1) The formation of a denser gel under pressure [99];

  (2) The effective prestress against tensile stresses due to drying [99][3];

[2] Theoretically complete reaction of cement requires a water-cement ratio of 0.4. This means that a certain amount of water is left unused for concrete/cement paste with a water-cement ratio higher than 0.4. This amount of water is available for self-healing in *sealed* concrete/paste. Then, the self-healing as proposed in this thesis may still take place, if the water in pores flows to the cracks (which needs further study).

[3] No further explanation about this reason in [99]. The statement in [223] might be a possible explanation for

(3) The redistribution of internal stress concentrations around the crack tips due to creep [12].

It is still unclear which one is mainly responsible for the extra strength increase in loaded concrete stored in air or sealed condition. Experiments to analyse the microstructural changes of concrete or cement paste under sustained load (such as porosity, void ratio or gel structure [99]) would be helpful.

- The long-term evolution of strength and elastic modulus influences the shape of the creep curve. A proper evaluation of the long-term evolution of strength and elastic modulus would be necessary for a more reliable prediction of the long-term creep.
- There is a need to study the behaviour of concrete (both the material performance and properties) stored in drying-wetting or freeze-thaw conditions under sustained load. These conditions better meet the real conditions in many countries. This will help to make more accurate predictions of the long-term creep deformation of real structures in practice.
- Recovery degree of strength after self-healing of cracks depends on many factors, e.g. crack width, water-cement ratio, age of concrete and healing time. Experiments, which have been carried out to study this, are relatively scarce. More experiments are needed to investigate the effect of self-healing of cracks on the mechanical properties of concrete/paste and to quantify the relationship between the strength recovery and these factors. It is also necessary to study self-healing of cracks and strength recovery in new or blended mixtures.
- Although densification of the paste adjacent to cracks has been observed in the experiments of Huang [14], more experiments and/or simulations are needed to study the diffusion of water and ions to help us to understand how this process happens. How much additional strength will be gained due to densification of the paste adjacent to a crack in mixtures (NWAC and LWAC) with different water-cement ratios should be further investigated.
- It is expected by Hughes and Ash [37] that factors which increase creep deformation would also enlarge the extra gain in strength of concrete under sustained load. Davis and Davis [224–226] observed that the extra gain in strength becomes larger with increasing cement content. Although these data are very old, they are still valid and not well understood yet. More experiments and simulations are needed to study the effect of cement content and volume, size and stiffness of aggregate on the strength development of concrete under sustained load.
- When concrete is loaded at high stress levels, the rate of micro-cracking and strain rate will be higher than of concrete loaded at low stress levels. Failure will occur much earlier and faster. Self-healing (and also continuous hydration) could reduce the rate of micro-cracking and strain rate and thus postpones failure. By making

this: capillary pressure, disjoining pressure and surface tension lead to mean compressive stresses in the solid skeleton, which can increase the strength of concrete.

use of this, favourable conditions can be created or special agents can be added to concrete so as to effectuate the self-healing. In this way, the additional deformation and the reduction in strength caused by micro-cracking can be reduced and failure can be postponed. Some preliminary attempts, regarding the effect of self-healing on the creep deformation and failure of concrete loaded at high stress levels, have been made using the modified lattice model, which is shown in Appendix B. More experiments are needed to investigate the effect of self-healing on the creep deformation and failure behaviour of concrete loaded at high stress levels.

APPENDIX

A

THE COMPACTION THEORY

A.1. GENERAL CONCEPT

CONCRETE under sustained compressive load continuously deforms and the capillary pores are compressed. As a consequence, the volume of concrete becomes smaller and the material becomes denser and stiffer. This is known as the compaction theory. This theory implies that the extra strength increase comes from the reduction of capillary porosity resulting from the compressive loading.

In load-free concrete the capillary porosity decreases and the strength increases due to ongoing hydration of cement. In loaded concrete the strength increase is supposed to consist of two parts: the increase due to the reduction of capillary porosity resulting from the hydration of cement, $\triangle f_{c,hydr}$, and the increase due to the reduction of capillary porosity resulting from compressive loading, $\triangle f_{c,compr}$. The latter is supposed to cause the extra increase in strength. The evolution of capillary porosity and compressive strength of loaded and load-free concrete over time is illustrated in Fig. A.1.

It is assumed that concrete is loaded at t_0. During the loading period $t - t_0$, the total reduction of capillary porosity of loaded concrete, $\triangle p_{l,tot}$, consists of two parts:

$$\triangle p_{l,tot} = p(t_0) - p_{l,tot}(t) = \triangle p_{compr} + \triangle p_{hydr} \tag{A.1}$$

where $\triangle p_{hydr}$ is the reduction of capillary porosity due to hydration and $\triangle p_{compr}$ is the reduction of capillary porosity due to compressive loading. The reduction of capillary porosity due to hydration $\triangle p_{hydr}$ can be calculated with Eq. A.2, viz.:

$$\triangle p_{hydr} = p(t_0) - p_{lf,tot}(t) \tag{A.2}$$

The reduction of capillary porosity due to compressive loading $\triangle p_{compr}$ is

$$\triangle p_{compr} = p_{lf,tot}(t) - p_{l,tot}(t) \tag{A.3}$$

where $p(t_0)$ is the capillary porosity in concrete at age at loading t_0; $p_{lf,tot}$ is the total capillary porosity of load-free concrete and $p_{l,tot}$ is the total capillary porosity of loaded

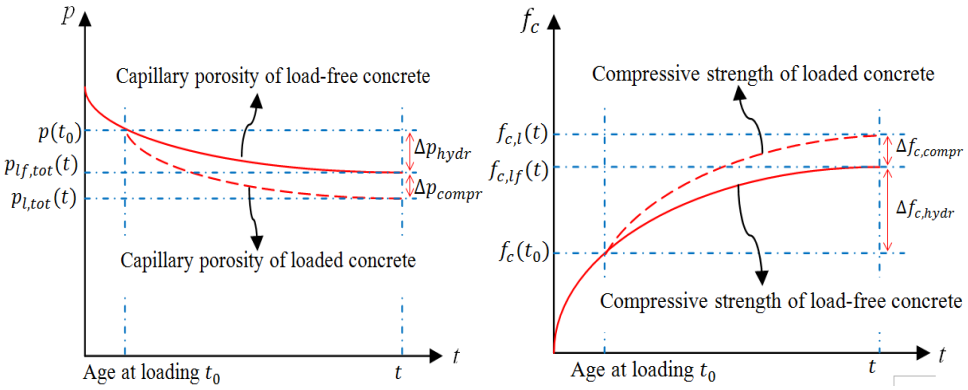

(a) Capillary porosity (b) Compressive strength

Figure A.1: The evolution of capillary porosity and compressive strength of loaded and load-free concrete over time: schematic diagram

concrete. The reduction of capillary porosity due to compressive loading, $\triangle p_{compr}$, leads to the extra increase in strength of loaded concrete $\triangle f_{c,compr}$. In order to generate the extra strength increase $\triangle f_{c,compr}$, the reduction of capillary porosity due to compressive loading is supposed to reach $\triangle p_{compr}$. Therefore, $\triangle p_{compr}$ calculated with Eq. A.3 can be called the *required* reduction of capillary porosity resulting from the compressive loading.

A.2. EFFECTIVE REDUCTION OF CAPILLARY POROSITY DUE TO COMPRESSIVE LOADING

CONCRETE continues to deform under sustained compressive loading and its volume decreases (see Fig. A.2). According to the compaction theory, the volume reduction of concrete under compressive loading is solely assigned to the reduction of the capillary porosity resulting from the compressive loading. Then, the reduction of capillary porosity due to compressive loading $\triangle p_{compr}$ during the loading period $t - t_0$ can also be calculated as (assuming creep poisson's ratio is not changing too much over time when concrete is loaded at low stress levels [38]):

$$\triangle p_{compr} = \frac{\triangle V_{p,compr}}{V_0} = \frac{\triangle V}{V_0} = \frac{A_0 \cdot \triangle l}{A_0 \cdot l_0} = \frac{\triangle l}{l_0} = \epsilon_{cr}(t) - \epsilon_{cr}(t_0) = \epsilon_{cr}(t) \tag{A.4}$$

where A_0 is the cross section of concrete; V_0 is the volume of concrete at age at loading t_0; $\triangle V_{p,compr}$ is the reduction of the volume of the capillary pores due to compressive loading and $\triangle p_{compr}$ is the reduction of capillary porosity due to compressive loading. With this equation the *effective* reduction of the capillary porosity due to compressive loading is calculated.

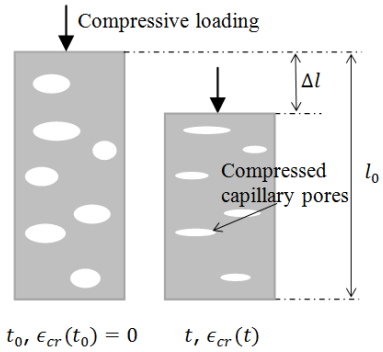

Figure A.2: Reduction of volume and capillary porosity of concrete under sustained compressive loading: schematic diagram

A.3. EVALUATION OF THE COMPACTION THEORY USING THE EXPERIMENTAL DATA

NOW a calculation will be made using the experimental data from Brooks' test (Section 3.2) to study whether the compaction theory can explain the extra increase in strength of concrete under sustained load. According to Eq. A.4, the effective reduction of the capillary porosity due to compressive loading from 14 days to 30 years equals the 30-year creep strain. According to the data in Table 3.2 the 30-year creep strain holds:

$$\epsilon_{cr}(t = 30y) = 11.12 \times 10^{-4} - 3.71 \times 10^{-4} = 7.41 \times 10^{-4}$$

So the *effective* reduction of the capillary porosity due to compressive loading is:

$$\triangle p_{compr} = \epsilon_{cr}(t = 30y) = 7.41 \times 10^{-4} \tag{A.5}$$

The 30-year compressive strength of loaded and load-free concrete is 61.6MPa and 50.6MPa (see Table 3.1), respectively. The extra increase in strength of the loaded concrete specimen is 11MPa. Based on existing relationships between capillary porosity and strength, i.e. $f_c = f_c(p)$, the 30-year capillary porosity can be calculated through back calculation. Three empirical equations describing the relationship between capillary porosity and strength are used here (see first column in Table A.1). The 30-year capillary porosity of loaded ($p_{l,tot}$) and load-free ($p_{lf,tot}$) concrete after 30 years are shown in Table A.1. With the values of $p_{l,tot}$ and $p_{lf,tot}$ and Eq. A.3, the *required* reduction of

Table A.1: Reduction of capillary porosity due to compressive loading (30-year compressive strength of load-free and loaded concrete is 50.6 and 61.2MPa respectively)

Equation	30-year $p_{lf,tot}$ (back calculated)	30-year $p_{l,tot}$ (back calculated)	30-year $\triangle p_{compr}$ (Eq. A.3)
$f_c = 37.1\ln(0.284/p)$ [227]	0.073	0.055	0.018
$f_c = 74.4\exp(-8.96p)$ [228]	0.043	0.022	0.021
$f_c = 68.74(1-p)^{8.15}$ [229]	0.037	0.014	0.023

capillary porosity after 30 years due to compressive loading, $\triangle p_{compr}$, is calculated and shown in the fourth column in Table A.1. It can be seen that the capillary porosity should decrease by 0.018 to 0.023 by the compressive loading in order to generate the 11MPa extra strength increase. However, the *effective* (actual) reduction of capillary porosity due to compressive loading is only 7.41×10^{-4} (Eq. A.5). It appears that the actual change in porosity is very small and cannot explain the extra increase in strength of concrete under sustained load. In conclusion, the compaction theory alone cannot explain the entire extra increase in strength of concrete under sustained load. There must be an other mechanism which can explain the extra strength increase.

B

EFFECT OF CONTINUOUS HYDRATION AND SELF-HEALING ON CREEP DEFORMATION AND FAILURE TIME OF CONCRETE LOADED AT HIGH STRESS LEVELS

B.1. INTRODUCTION

THE effect of continuous hydration and self-healing on the creep deformation and failure time of concrete loaded at high stress levels is simulated with modified lattice model. Concrete specimens with a water-cement ratio of 0.50 presented in Chapter 3 is used as a virtual specimen for numerical analysis[1]. The concrete specimens are loaded at 14 days at high stress levels (60%-100%). Here, only the simulations are performed and no experimental data are available to validate the simulation results.

B.2. SIMULATION RESULTS

B.2.1. ROLE OF CONTINUOUS HYDRATION

Fig. B.1 show the simulated creep strains with and without the effect of continuous hydration. The number of micro-cracks during the creep process is shown in Fig. B.2. The failure time is listed in Table B.1 and compared to that in case no continuous hydration occurs. When continuous hydration is taken into account, no failure is found within 100

[1]The input parameters, i.e. the empirical ageing factor a (Eq. 3.17), the evolution of strength $f_c[\alpha(t)]$ and elastic modulus $E[\alpha(t)]$ of the mortar and bond beams with time resulting from the continuous hydration (Eq. 3.18 and 3.19) and the additional degree of hydration of the paste adjacent to any crack, $\Delta\alpha_{add,j}$ ($\Delta\alpha_{add,j}$ = 0.21 in Eq. 3.27 to 3.30), have been calculated in Chapter 3.

years for concrete loaded at 14 days at a stress level lower than 75%. Without considering continuous hydration, concrete fails at a stress level of about 60% (see Fig. B.1 and Table B.1). The rate of micro-cracking is reduced (Fig. B.2) and the failure of concrete is postponed when concrete, loaded up to a stress level of 80%, continues to hydrate. When the stress level is higher than 80%, continuous hydration hardly has any effect on the failure time of concrete (Table B.1).

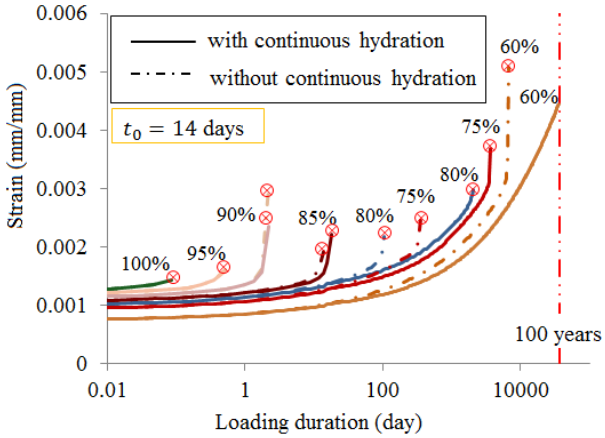

Figure B.1: Simulated creep strains of the concrete specimen with a water-cement ratio of 0.50 loaded at 14 days at different stress levels: the role of continuous hydration

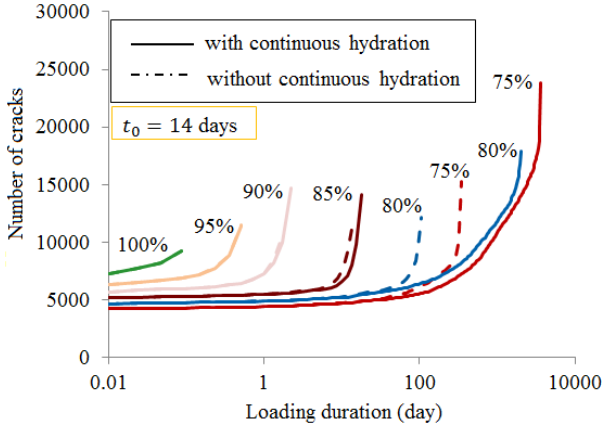

Figure B.2: Number of cracks in the concrete specimen with a water-cement ratio of 0.50 loaded at 14 days at different stress levels

B.2.2. ROLE OF SELF-HEALING

When self-healing is considered, the simulated creep strains are shown in Fig. B.3. The failure time is listed in Table B.2 and compared to that in case no self-healing occurs.

Table B.1: Failure time of the concrete specimen with a water-cement ratio of 0.50 loaded at 14 days at different stress levels: the role of continuous hydration

Situations	Failure time (day)								
	Stress level (%)								
	60	65	70	75	80	85	90	95	100
Without continuous hydration	6757	2176	1048	349	105	14	1.7	0.5	0.08
With continuous hydration	-	-	-	3616	2036	17	2.2	0.5	0.08

"-" means no failure within 100 years.

For concrete, loaded at stress levels lower than 90%, the strain rate is reduced and the failure is postponed due to the self-healing of micro-cracks (Fig. B.3). When concrete is loaded at stress levels higher than 90%, self-healing hardly has any effect on the creep deformation and failure time (Table B.2).

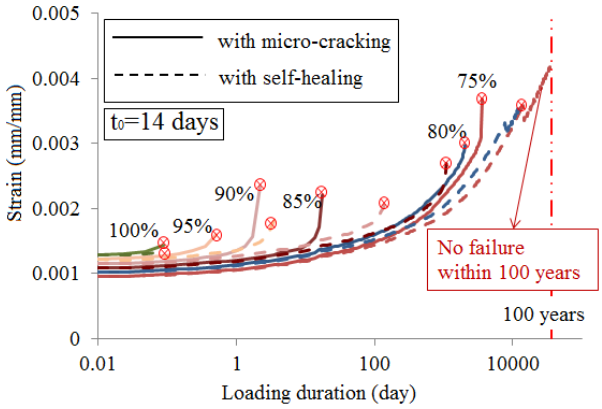

Figure B.3: Simulated creep strains of the concrete specimen with a water-cement ratio of 0.50 loaded at 14 days at stress levels 75%-100%: with and without the effect of self-healing

Table B.2: Failure time of the concrete specimen with a water-cement ratio of 0.50 loaded at 14 days at different stress levels

Simulations	Failure time (day)					
	Stress level (%)					
	75	80	85	90	95	100
Without the effect of self-healing	3616	2036	17	2.2	0.5	0.08
With the effect of self-healing	-	12687	1101	145	3.5	0.08

"-" means no failure within 100 years.

REFERENCES

REFERENCES

[1] The 10 best concrete buildings, https://theguardian.com/artanddesign/2016/jan/08/10-best-concrete-buildings-architecture-pantheon-gaudi-corbusier, accessed: 2018-09-04.

[2] Z. P. Bažant, Q. Yu, G.-H. Li, Excessive long-time deflections of prestressed box girders. i: Record-span bridge in palau and other paradigms, Journal of Structural Engineering 138 (6) (2012) 676–686.

[3] K. M. Nemati, Lecture notes in concrete technology: Volume changes and creep of concrete, university of washington (Winter Quarter 2015).

[4] L. W. McKeen, The effect of long term thermal exposure on plastics and elastomers, William Andrew, 2013.

[5] Z. P. Bažant, X. Yunping, Drying creep of concrete: constitutive model and new experiments separating its mechanisms, Materials and structures 27 (1) (1994) 3–14.

[6] Z. P. Bažant, W. J. Raftshol, Effect of cracking in drying and shrinkage specimens, Cement and Concrete Research 12 (2) (1982) 209–226.

[7] Z. P. Bažant, F. H. Wittmann, Creep and shrinkage in concrete structures, Wiley New York, 1982.

[8] P. Acker, M. Reymond, L'apport des moyens non destructifs l'interprétation du comportement instantané et différé du béton durci, in: Colloque international "Liaison pâte de ciment-matériaux associés", 1982.

[9] P. Rossi, J.-L. Tailhan, F. Le Maou, L. Gaillet, E. Martin, Basic creep behavior of concretes investigation of the physical mechanisms by using acoustic emission, Cement and concrete research 42 (1) (2012) 61–73.

[10] J. Saliba, A. Loukili, F. Grondin, Acoustic emission monitoring and quantitative evaluation of damage in concrete beams under creep, in: Acoustic Emission and Related Non-Destructive Evaluation Techniques in the Fracture Mechanics of Concrete, Elsevier, 2015, pp. 113–136.

[11] N. Burlion, G. Pijaudier-Cabot, N. Dahan, Experimental analysis of compaction of concrete and mortar, International journal for numerical and analytical methods in geomechanics 25 (15) (2001) 1467–1486.

[12] F. H. Wittmann, J. Zaitsev, Behaviour of hardened cement paste and concrete under sustained load, in: Proceedings of the Society of Materials Science Conference on the Mechanical Behavior of Materials., no. Conf Paper, 1972.

[13] E. Schlangen, Ct5146 lecture notes fracture mechanics, delft university of technology (2007).

[14] H. Huang, Thermodynamics of autogenous self-healing in cementitious materials, Delft University of Technology, 2014.

[15] H. Huang, G. Ye, L. Pel, New insights into autogenous self-healing in cement paste based on nuclear magnetic resonance (nmr) tests, Materials and Structures 49 (7) (2016) 2509–2524.

[16] J. Chen, G. Ye, A lattice boltzmann single component model for simulation of the autogenous self-healing caused by further hydration in cementitious material at mesoscale, Cement and Concrete Research 123 (2019) 105782.

[17] E. Schlangen, Experimental and numerical analysis of fracture processes in concrete, Ph.D. thesis, Delft University of Technology (1993).

[18] L. P. Granger, Z. P. Bažant, Effect of composition on basic creep of concrete and cement paste, Journal of engineering mechanics 121 (11) (1995) 1261–1270.

[19] J. J. Brooks, 30-year creep and shrinkage of concrete, Magazine of concrete research 57 (9) (2005) 545–556.

[20] F. H. Wittmann, Bestimmung physikalischer Eigenschaften des Zementsteins, no. 232, Wilhelm Ernst & Sohn, 1974.

[21] K. van Breugel, Relaxation of young concrete. department of structural concrete, faculty of civil engineering, Delft University of Technology, Research Report (5-80) (1980).

[22] J. J. Brooks, Accuracy of estimating long-term strains in concrete, Magazine of Concrete Research 36 (128) (1984) 131–145.

[23] H. R. Hardy, et al., Time-dependent deformation and failure of geologic materials, in: The 3rd US Symposium on Rock Mechanics (USRMS), American Rock Mechanics Association, 1959.

[24] A. S. Coutinho, A contribution to the mechanism of concrete creep, Matériaux et Construction 10 (1) (1977) 3–16.

[25] J. J. Brooks, A. M. Neville, Estimating long-term creep and shrinkage from short-term tests, Magazine of Concrete Research 27 (90) (1975) 3–12.

[26] J. Torrenti, Basic creep of concrete-coupling between high stresses and elevated temperatures, European Journal of Environmental and Civil Engineering 22 (12) (2018) 1419–1428.

[27] Z. P. Bažant, Q. Yu, G.-H. Li, Excessive long-time deflections of prestressed box girders. ii: Numerical analysis and lessons learned, Journal of Structural Engineering 138 (6) (2012) 687–696.

[28] M.-C. Tang, The Story of the Koror Bridge, International Association for Bridge and Structural Engineering (IABSE), 2014.

[29] P. Rossi, N. Godart, J. Robert, J. Gervais, D. Bruhat, Investigation of the basic creep of concrete by acoustic emission, Materials and Structures 27 (9) (1994) 510.

[30] P. Rossi, P. Acker, A new approach to the basic creep and relaxation of concrete, Cement and Concrete Research 18 (5) (1988) 799–803.

[31] A. Carpinteri, A. R. Ingraffea, Fracture mechanics of concrete: Material characterization and testing, Vol. 3, Springer Science & Business Media, 2012.

[32] W.-F. Chen, Plasticity in reinforced concrete, J. Ross Publishing, 2007.

[33] A. Freudenthal, F. Roll, Creep and creep recovery of concrete under high compressive stress, in: Journal Proceedings, Vol. 54, 1958, pp. 1111–1142.

[34] G. W. Washa, P. G. Fluck, Effect of sustained loading on compressive strength and modulus of elasticity of concrete, in: Journal Proceedings, Vol. 46, 1950, pp. 693–700.

[35] Z. Qian, Multiscale modeling of fracture processes in cementitious materials, Ph.D. thesis, Delft University of Technology (2012).

[36] Z. P. Bažant, G.-H. Li, Comprehensive database on concrete creep and shrinkage, ACI Materials Journal 105 (6) (2008) 635–637.

[37] B. Hughes, J. Ash, Some factors influencing the long term strength of concrete, Matériaux et Construction 3 (2) (1970) 81–84.

[38] A. M. Neville, Creep of Concrete: Plain, Reinforced, and Prestressed, North Holland Pub. Co., 1970.

[39] W. Hatt, Notes on the effect of time element in loading reinforced concrete beams, in: Proc. ASTM, Vol. 7, 1907, pp. 421–433.

[40] Z. P. Bažant, Prediction of concrete creep and shrinkage: past, present and future, Nuclear Engineering and Design 203 (1) (2001) 27–38.

[41] N. K. Arutyunyan, Some problems in the theory of creep, International series of monographs in civil engineering 1 (1966).

[42] Z. P. Bažant, Mathematical modeling of creep and shrinkage of concrete, John Wiley and Sons, 1988.

[43] F. H. Wittmann, Creep and shrinkage mechanisms, Creep and shrinkage in concrete structures (1982) 129–161.

[44] S. J. Lokhorst, Deformational Behaviour of Concrete Influenced by Hydration Related Changes of the Microstructure, Delft University of Technology, 2001.

[45] H. Ye, Creep mechanisms of calcium–silicate–hydrate: an overview of recent advances and challenges, International Journal of Concrete Structures and Materials 9 (4) (2015) 453–462.

[46] Z. P. Bažant, Constitutive equation for concrete creep and shrinkage based on thermodynamics of multiphase systems, Matériaux et Construction 3 (1) (1970) 3–36.

[47] R. F. Feldman, Mechanism of creep of hydrated portland cement paste, Cement and concrete research 2 (5) (1972) 521–540.

[48] P. Klug, F. H. Wittmann, Activation energy of creep of hardened cement paste, Matériaux et Construction 2 (1) (1969) 11–16.

[49] M. Vandamme, F.-J. Ulm, Nanogranular origin of concrete creep, Proceedings of the National Academy of Sciences 106 (26) (2009) 10552–10557.

[50] G. Pickett, The effect of change in moisture-content on the crepe of concrete under a sustained load, in: Journal Proceedings, Vol. 38, 1942, pp. 333–356.

[51] S. A. Altoubat, D. A. Lange, The pickett effect at early age and experiment separating its mechanisms in tension, Materials and Structures 35 (4) (2002) 211–218.

[52] F. H. Wittmann, P. E. Roelfstra, Total deformation of loaded drying concrete, Cement and Concrete Research 10 (5) (1980) 601–610.

[53] B. Gamble, L. Parrott, Creep of concrete in compression during drying and wetting, Magazine of concrete research 30 (104) (1978) 129–138.

[54] Z. P. Bažant, A. B. Hauggaard, S. Baweja, F.-J. Ulm, Microprestress-solidification theory for concrete creep. i: Aging and drying effects, Journal of Engineering Mechanics 123 (11) (1997) 1188–1194.

[55] Z. P. Bažant, A. B. Hauggaard, S. Baweja, Microprestress-solidification theory for concrete creep. ii: Algorithm and verification, Journal of Engineering Mechanics 123 (11) (1997) 1195–1201.

[56] R. Sinko, M. Vandamme, Z. P. Bažant, S. Keten, Transient effects of drying creep in nanoporous solids: understanding the effects of nanoscale energy barriers, Proc. R. Soc. A 472 (2191) (2016) 20160490.

[57] Z. P. Bažant, S. Prasannan, Solidification theory for aging creep, Cement and Concrete Research 18 (6) (1988) 923–932.

[58] Z. P. Bažant, S. Prasannan, Solidification theory for concrete creep. ii: Verification and application, Journal of engineering mechanics 115 (8) (1989) 1704–1725.

[59] L. Parrott, Basic creep, drying creep and shrinkage of a mature cement paste after a heat cycle, Cement and Concrete Research 7 (5) (1977) 597–604.

[60] E. A. Pachon-Rodriguez, E. Guillon, G. Houvenaghel, J. Colombani, Wet creep of hardened hydraulic cements-example of gypsum plaster and implication for hydrated portland cement, Cement and Concrete Research 63 (2014) 67–74.

[61] X. Li, Z. Grasley, E. J. Garboczi, J. W. Bullard, Modeling the apparent and intrinsic viscoelastic relaxation of hydrating cement paste, Cement and Concrete Composites 55 (2015) 322–330.

[62] I. Pignatelli, A. Kumar, R. Alizadeh, Y. Le Pape, M. Bauchy, G. Sant, A dissolution-precipitation mechanism is at the origin of concrete creep in moist environments, The Journal of chemical physics 145 (5) (2016) 054701.

[63] B. L. Meyers, Time-dependent strains and microcracking of plain concrete, Ph.D. thesis, Cornell University.

[64] B. L. Meyers, G. Winter, et al., Relationship between time-dependent deformationand microcracking of plain concrete, in: Journal Proceedings, Vol. 66, 1969, pp. 60–68.

[65] J. Saliba, A. Loukili, F. Grondin, J. Regoin, Identification of damage mechanisms in concrete under high level creep by the acoustic emission technique, Materials and structures 47 (6) (2014) 1041–1053.

[66] P. Rossi, J. Tailhan, F. Le Maou, Creep strain versus residual strain of a concrete loaded under various levels of compressive stress, Cement and concrete research 51 (2013) 32–37.

[67] Z. P. Bažant, E. Osman, Double power law for basic creep of concrete, Matériaux et Construction 9 (1) (1976) 3–11.

[68] Z. P. Bažant, J.-C. Chern, Double-power logarithmic law for concrete creep, Cement and Concrete Research 14 (6) (1984) 793–806.

[69] R. Wendner, M. Hubler, Z. P. Bažant, The b4 model for multi-decade creep and shrinkage prediction, in: Mechanics and Physics of Creep, Shrinkage, and Durability of Concrete: A Tribute to Zdeňk P. Bažant, 2013, pp. 429–436.

[70] J. A. Rhodes, D. J. Carreira+, Prediction of creep, shrinkage, and temperature effects in concrete structures, Hills, Unite States: American Concrete Institue, 1982.

[71] C. Videla, D. J. Carreira, N. Garner, et al., Guide for modeling and calculating shrinkage and creep in hardened concrete, ACI report 209 (2008).

[72] CEB-FIP, Model code for concrete structures [comite euro-international du beton–federation internationale de la precontrainte (ceb-fip)], London, UK (1993).

[73] N. Gardner, M. Lockman, Design provisions for drying shrinkage and creep of normal-strength concrete, Materials journal 98 (2) (2001) 159–167.

[74] L. Taerwe, S. Matthys, et al., fib model code for concrete structures 2010, Ernst & Sohn, Wiley, 2013.

[75] Z. P. Bažant, S. Baweja, Creep and shrinkage prediction model for analysis and design of concrete structures: Model b3, ACI Special Publications 194 (2000) 1–84.

[76] Z. P. Bažant, M. Jirásek, M. Hubler, I. Carol, Rilem draft recommendation: Tc-242-mdc multi-decade creep and shrinkage of concrete: material model and structural analysis. model b4 for creep, drying shrinkage and autogenous shrinkage of normal and high-strength concretes with multi-decade applicability, Materials and structures 48 (4) (2015) 753–770.

[77] M. Mazloom, Estimating long-term creep and shrinkage of high-strength concrete, Cement and Concrete Composites 30 (4) (2008) 316–326.

[78] R. P. Ojdrovic, M. S. Zarghamee, Concrete creep and shrinkage prediction from short-term tests, Materials Journal 93 (2) (1996) 169–177.

[79] Z. P. Bažant, L. Panula, Practical prediction of time-dependent deformations of concrete: part 2 basic creep, Matériaux et Construction 11 (5) (1978) 317–328.

[80] Z. P. Bažant, L. Panula, Practical prediction of time-dependent deformations of concrete: part 3 drying creep, Materials and Structures 11 (1980).

[81] Z. P. Bažant, Y. Xi, Continuous retardation spectrum for solidification theory of concrete creep, Journal of Engineering Mechanics 121 (2) (1995) 281–288.

[82] M. Briffaut, F. Benboudjema, J.-M. Torrenti, G. Nahas, Concrete early age basic creep: Experiments and test of rheological modelling approaches, Construction and Building Materials 36 (2012) 373–380.

[83] A. Hilaire, F. Benboudjema, A. Darquennes, Y. Berthaud, G. Nahas, Modeling basic creep in concrete at early-age under compressive and tensile loading, Nuclear Engineering and Design 269 (2014) 222–230.

[84] D. Gawin, F. Pesavento, B. A. Schrefler, Hygro-thermo-chemo-mechanical modelling of concrete at early ages and beyond. part i: hydration and hygro-thermal phenomena, International Journal for Numerical Methods in Engineering 67 (3) (2006) 299–331.

[85] D. Gawin, F. Pesavento, B. A. Schrefler, Hygro-thermo-chemo-mechanical modelling of concrete at early ages and beyond. part ii: shrinkage and creep of concrete, International Journal for Numerical Methods in Engineering 67 (3) (2006) 332–363.

[86] M. Jirásek, P. Havlásek, Microprestress–solidification theory of concrete creep: Reformulation and improvement, Cement and Concrete Research 60 (2014) 51–62.

[87] K. Maekawa, T. Ishida, T. Kishi, Multi-scale modeling of concrete performance, Journal of Advanced Concrete Technology 1 (2) (2003) 91–126.

[88] J. Bisschop, Does applied stress affect portland cement hydration, in: Submitted to 13th international congress chemistry cement, 2011, pp. 3–8.

[89] T. Tamboue, The role of CSH microstructure and calcium hydroxide on creep and shrinkage of hardened portland cement paste, University of Ottawa (Canada), 2001.

[90] J. Bisschop, D. K. Dysthe, Instabilities and coarsening of stressed crystal surfaces in aqueous solution, Physical review letters 96 (14) (2006) 146103.

[91] A. G. Shtukenberg, J. M. Astilleros, A. Putnis, Nanoscale observations of the epitaxial growth of hashemite on barite (0 0 1), Surface Science 590 (2-3) (2005) 212–223.

[92] J. N. Sherwood, R. I. Ristic, The influence of mechanical stress on the growth and dissolution of crystals, Chemical Engineering Science 56 (7) (2001) 2267–2280.

[93] J. Saliba, A. Loukili, F. Grondin, J.-P. Regoin, Experimental study of creep-damage coupling in concrete by acoustic emission technique, Materials and structures 45 (9) (2012) 1389–1401.

[94] Compaction of concrete-purpose, process and effect, https://civilblog.org/2016/02/17/compaction-of-concrete-purpose-process-effect/, accessed: 2018-09-13.

[95] D. Bonikowsky, R. Minnich, N. Cumming, M. Olsen, T. Dolen, L. Olson, J. Ford, S. Popovics, S. Gebler, S. Ragan, Guide for consolidation of concrete, ACI 309R 96 (1996).

[96] D. Cook, P. Chindaprasirt, Influence of loading history upon the compressive properties of concrete, Magazine of Concrete Research 32 (111) (1980) 89–100.

[97] T. C. Hansen, Creep and stress relaxation of concrete: a theoretical and experimental investigation, Svenska forskningsinstitutet för cement och betong vid Kungl. Tekniska högskolan, 1960.

[98] T. C. Hansen, Creep of concrete. the influence of variations in the humidity of the ambient atmosphere, in: 6th Congress of the IABSE, Preliminary Publication, 1960, pp. 57–65.

[99] A. M. Neville, Current problems regarding concrete under sustained loading, Intern. Ass. for Bridge and Structural Engineering 26 (1966) 337–343.

[100] K. van Breugel, Conceptual and numerical modelling and simulation of microstructure of cement-based materials, Journal of Sustainable Cement-Based Materials 5 (1-2) (2016) 57–75.

[101] V. C. Li, E. Herbert, Robust self-healing concrete for sustainable infrastructure, Journal of Advanced Concrete Technology 10 (6) (2012) 207–218.

[102] N. Hearn, C. Morley, Self-sealing property of concrete-experimental evidence, Materials and structures 30 (7) (1997) 404–411.

[103] N. Hearn, Self-sealing, autogenous healing and continued hydration: what is the difference?, Materials and structures 31 (8) (1998) 563.

[104] G. W. Hyde, W. J. Smith, Results of experiments made to determine the permeability of cements and cement mortars, Journal of the Franklin Institute 128 (3) (1889) 199–207.

[105] W. Glanville, The Permeability of Portland Cement Concrete, Technical paper, H. M. Stationery Office, printed by Harrison and sons, Limited, 1926.

[106] V. Soroker, A. Denson, Autogenous healing of concrete, Zement 25 (30) (1926).

[107] S. Brandeis, Autogenous healing of concrete, Beton u. Eisen 36 (12) (1937).

[108] L. Turner, The autogenous healing of cement and concrete - its relation to vibrated concrete and cracked concrete, in: Proc. Int. Assoc., Testing Materials, 1937.

[109] H.-W. Reinhardt, M. Jooss, Permeability and self-healing of cracked concrete as a function of temperature and crack width, Cement and concrete research 33 (7) (2003) 981–985.

[110] C. Edvardsen, Water permeability and autogenous healing of cracks in concrete, Materials Journal 96 (4) (1999) 448–454.

[111] P. Fidjestol, N. Nilsen, Field test of reinforcement corrosion in concrete, Special Publication 65 (1980) 205–222.

[112] S. Jacobsen, J. Marchand, L. Boisvert, Effect of cracking and healing on chloride transport in opc concrete, Cement and Concrete Research 26 (6) (1996) 869–881.

[113] N. Otsuki, S.-i. Miyazato, N. B. Diola, H. Suzuki, Influences of bending crack and water-cement ratio on chloride-induced corrosion of main reinforcing bars and stirrups, Materials Journal 97 (4) (2000) 454–464.

[114] S. Jacobsen, E. J. Sellevold, Self healing of high strength concrete after deterioration by freeze/thaw, Cement and Concrete Research 26 (1) (1996) 55–62.

[115] P. Pimienta, G. Chanvillard, Retention of the mechanical performances of ductal specimens kept in various aggressive environments, in: Fib Symposium 2004, Avignon, France, Vol. 52, April 26-28, 2004, pp. 455–480.

[116] N. ter Heide, Crack healing in hydrating concrete, Master's thesis, Delft University of Technology (2005).

[117] S. Granger, A. Loukili, G. Pijaudier-Cabot, G. Chanvillard, Experimental characterization of the self-healing of cracks in an ultra high performance cementitious material: Mechanical tests and acoustic emission analysis, Cement and Concrete Research 37 (4) (2007) 519–527.

[118] K. Van Tittelboom, E. Gruyaert, H. Rahier, N. De Belie, Influence of mix composition on the extent of autogenous crack healing by continued hydration or calcium carbonate formation, Construction and Building Materials 37 (2012) 349–359.

[119] Z. Jiang, W. Li, Z. Yuan, Z. Yang, Self-healing of cracks in concrete with various crystalline mineral additives in underground environment, Journal of Wuhan University of Technology-Mater. Sci. Ed. 29 (5) (2014) 938–944.

[120] K. Shahid, M. Jaafar, F. Yahaya, Self-healing behaviour of pre-cracked pofa-concretes in different curing conditions, Journal of Mechanical Engineering and Sciences 7 (2014) 1227–35.

[121] L. Ferrara, V. Krelani, M. Carsana, A fracture testing based approach to assess crack healing of concrete with and without crystalline admixtures, Construction and Building Materials 68 (2014) 535–551.

[122] L. Ferrara, V. Krelani, F. Moretti, On the use of crystalline admixtures in cement based construction materials: from porosity reducers to promoters of self healing, Smart Materials and Structures 25 (8) (2016) 084002.

[123] L. Ferrara, V. Krelani, F. Moretti, M. R. Flores, P. S. Ros, Effects of autogenous healing on the recovery of mechanical performance of high performance fibre reinforced cementitious composites (hpfrccs): Part 1, Cement and Concrete Composites 83 (2017) 76–100.

[124] J. Pelto, M. Leivo, E. Gruyaert, B. Debbaut, D. Snoeck, N. De Belie, Application of encapsulated superabsorbent polymers in cementitious materials for stimulated autogenous healing, Smart Materials and Structures 26 (10) (2017) 105043.

[125] J. Kim, E. Schlangen, Super absorbent polymers to simulate self healing in ecc, in: 2nd International Symposium on Service Life Design for Infrastructures, RILEM Publications SARL, Delft, 2010, pp. 849–858.

[126] D. Snoeck, K. Van Tittelboom, S. Steuperaert, P. Dubruel, N. De Belie, Self-healing cementitious materials by the combination of microfibres and superabsorbent polymers, Journal of Intelligent Material Systems and Structures 25 (1) (2014) 13–24.

[127] L. Czarnecki, P. Lukowski, Polymer-cement concretes, Cement Wapno Beton 15 (5) (2010) 243–+.

[128] P. Łukowski, G. Adamczewski, Self-repairing of polymer-cement concrete, Bulletin of the Polish Academy of Sciences. Technical Sciences 61 (1) (2013) 195–200.

[129] A. R. M. Sam, N. F. Ariffin, M. W. Hussin, H. S. Lee, M. A. Ismail, N. H. A. S. Lim, N. H. A. Khalid, M. Samadi, J. Mirza, M. Z. A. Majid, Performance of epoxy resin as self-healing agent, Jurnal Teknologi 77 (16) (2015).

[130] K. Van Tittelboom, N. De Belie, D. Van Loo, P. Jacobs, Self-healing efficiency of cementitious materials containing tubular capsules filled with healing agent, Cement and Concrete Composites 33 (4) (2011) 497–505.

[131] N. De Belie, E. Gruyaert, A. Al-Tabbaa, P. Antonaci, C. Baera, D. Bajare, A. Darquennes, R. Davies, L. Ferrara, T. Jefferson, et al., A review of self-healing concrete for damage management of structures, Advanced materials interfaces 5 (17) (2018) 1800074.

[132] A. Sidiq, R. Gravina, F. Giustozzi, Is concrete healing really efficient? a review, Construction and Building Materials 205 (2019) 257–273.

[133] L. Ferrara, T. Van Mullem, M. C. Alonso, P. Antonaci, R. P. Borg, E. Cuenca, A. Jefferson, P.-L. Ng, A. Peled, M. Roig-Flores, et al., Experimental characterization of the self-healing capacity of cement based materials and its effects on the material performance: a state of the art report by cost action sarcos wg2, Construction and building materials 167 (2018) 115–142.

[134] K. van Breugel, Is there a market for self-healing cement-based materials, in: Proceedings of the first international conference on self-healing materials, 2007, pp. 1–9.

[135] J. Munday, C. Sangha, R. Dhir, Comparative study of autogenous healing of different concretes, Tech. rep., University of New South Wales (1974).

[136] C. Clear, Cement and concrete association, in: Technical Report No. 559, Cement and Concrete Association England, UK, 1985.

[137] S. Fan, M. Li, X-ray computed microtomography of three-dimensional microcracks and self-healing in engineered cementitious composites, Smart materials and structures 24 (1) (2014) 015021.

[138] H. He, Z. Guo, P. Stroeven, M. Stroeven, L. J. Sluys, Self-healing capacity of concrete-computer simulation study of unhydrated cement structure, Image Analysis & Stereology 26 (3) (2011) 137–143.

[139] H. He, Z. Guo, P. Stroeven, M. Stroeven, Numerical assessment of concrete's self-healing potential for promoting durability, International Journal of Modelling, Identification and Control 7 (2) (2009) 142–147.

[140] H. Rahmani, H. Bazrgar, Effect of coarse cement particles on the self-healing of dense concretes, Magazine of Concrete Research 67 (9) (2015) 476–486.

[141] Z. Lv, H. Chen, Self-healing efficiency of unhydrated cement nuclei for dome-like crack mode in cementitious materials, Materials and structures 46 (11) (2013) 1881–1892.

[142] Z. Lv, H. Chen, Modeling of self-healing efficiency for cracks due to unhydrated cement nuclei in hardened cement paste, Procedia Engineering 27 (2012) 281–290.

[143] M. Darabi, R. Abu Al-Rub, E. Masad, D. Little, Constitutive modeling of fatigue damage response of asphalt concrete materials, Transportation Research Record: Journal of the Transportation Research Board (2373) (2013) 11–21.

[144] M. K. Darabi, R. K. A. Al-Rub, D. N. Little, A continuum damage mechanics framework for modeling micro-damage healing, International Journal of Solids and Structures 49 (3-4) (2012) 492–513.

[145] E. J. Barbero, F. Greco, P. Lonetti, Continuum damage-healing mechanics with application to self-healing composites, International Journal of Damage Mechanics 14 (1) (2005) 51–81.

[146] E. Schimmel, J. Remmers, Development of a constitutive model for self-healing materials, Delft Aerospace Computational Science, 2006.

[147] R. K. A. Al-Rub, M. K. Darabi, D. N. Little, E. A. Masad, A micro-damage healing model that improves prediction of fatigue life in asphalt mixes, International Journal of Engineering Science 48 (11) (2010) 966–990.

[148] A. A. Alsheghri, R. K. A. Al-Rub, Thermodynamic-based cohesive zone healing model for self-healing materials, Mechanics Research Communications 70 (2015) 102–113.

[149] A. A. Alsheghri, R. K. A. Al-Rub, Finite element implementation and application of a cohesive zone damage-healing model for self-healing materials, Engineering Fracture Mechanics 163 (2016) 1–22.

[150] J. Mergheim, P. Steinmann, Phenomenological modelling of self-healing polymers based on integrated healing agents, Computational Mechanics 52 (3) (2013) 681–692.

[151] S. Zhou, H. Zhu, J. W. Ju, Z. Yan, Q. Chen, Modeling microcapsule-enabled self-healing cementitious composite materials using discrete element method, International Journal of Damage Mechanics 26 (2) (2017) 340–357.

[152] H. Zhu, S. Zhou, Z. Yan, J. W. Ju, Q. Chen, A two-dimensional micromechanical damage–healing model on microcrack-induced damage for microcapsule-enabled self-healing cementitious composites under compressive loading, International Journal of Damage Mechanics 25 (5) (2016) 727–749.

[153] R. Davies, A. Jefferson, Micromechanical modelling of self-healing cementitious materials, International Journal of Solids and Structures 113 (2017) 180–191.

[154] C. Joseph, Experimental and numerical study of the fracture and self-healing of cementitious materials, Ph.D. thesis, Cardiff University (2008).

[155] J. J. Remmers, R. de Borst, Numerical modelling of self healing mechanisms, in: Self Healing Materials, Springer, 2007, pp. 365–380.

[156] R. K. A. Al-Rub, M. K. Darabi, A thermodynamic framework for constitutive modeling of time-and rate-dependent materials. part i: Theory, International Journal of Plasticity 34 (2012) 61–92.

[157] M. K. Darabi, R. K. A. Al-Rub, E. A. Masad, D. N. Little, A thermodynamic framework for constitutive modeling of time-and rate-dependent materials. part ii: Numerical aspects and application to asphalt concrete, International Journal of Plasticity 35 (2012) 67–99.

[158] B. Hilloulin, F. Grondin, M. Matallah, A. Loukili, Modelling of autogenous healing in ultra high performance concrete, Cement and Concrete Research 61 (2014) 64–70.

[159] T. Jefferson, E. Javierre, B. Freeman, A. Zaoui, E. Koenders, L. Ferrara, Research progress on numerical models for self-healing cementitious materials, Advanced materials interfaces 5 (17) (2018) 1701378.

[160] W. Lyu, E. Schlangen, K. van Breugel, Numerical analysis of effect of microcracking and selfhealing on the long-term creep of cementitious materials, in: Proceedings of the Symposium on Concrete Modelling: CONMOD2018, Vol. PRO 127, 2018, pp. 169–178.

[161] J. J. Brooks, A. M. Neville, Predicting long-term creep and shrinkage from short-term tests, Magazine of concrete research 30 (103) (1978) 51–61.

[162] K. van Breugel, Simulation of hydration and formation of structure in hardening cement-based materials, Ph.D. thesis, Delft University of Technology (1997).

[163] K. A. Riding, J. L. Poole, K. J. Folliard, M. C. Juenger, A. K. Schindler, Modeling hydration of cementitious systems, ACI Materials Journal 109 (2) (2012) 225–234.

[164] R. H. Mills, Factors influencing cessation of hydration in water cured cement pastes, Highway Research Board Special Report (90) (1966).

[165] S. Seki, K. Kashara, T. Kuriyama, M. Kawasum, Relation between compressive strength of concrete and the effective cement-water from the hydration rate of cement ratio calculated, in: Journal Proceedings, Vol. 66, 1969, pp. 198–201.

[166] G. Parry-Jones, A. Al-Tayyib, S. Al-Dulaijan, A. Al-Mana, 29si mas-nmr hydration and compressive strength study in cement paste, Cement and Concrete Research 19 (2) (1989) 228–234.

[167] S. Oyefesobi, D. Roy, Hydrothermal studies of type v cement-quartz mixes, Cement and Concrete Research 6 (6) (1976) 803–810.

[168] D. P. Bentz, O. M. Jensen, A. Coats, F. P. Glasser, Influence of silica fume on diffusivity in cement-based materials: I. experimental and computer modeling studies on cement pastes, Cement and Concrete research 30 (6) (2000) 953–962.

[169] R. Day, B. Gamble, The effect of changes in structure on the activation energy for the creep of concrete, Cement and Concrete Research 13 (4) (1983) 529–540.

[170] P. Klug, F. Wittmann, Activation energy and activation volume of creep of hardened cement paste, Materials science and Engineering 15 (1) (1974) 63–66.

[171] G. Gibbs, The activation parameters for dislocation glide, Philosophical Magazine 16 (139) (1967) 97–102.

[172] F. H. Wittmann, Grundlagen eines modells zur beschreibung charakteristischer eigenschaften des betons, Wilhelm Ernst & Sohn, 1977.

[173] Euler method, https://en.wikipedia.org/wiki/Euler_method, accessed: 2016-02-30.

[174] L. Stefan, F. Benboudjema, J.-M. Torrenti, B. Bissonnette, Prediction of elastic properties of cement pastes at early ages, Computational Materials Science 47 (3) (2010) 775–784.

[175] G. De Schutter, L. Taerwe, Degree of hydration-based description of mechanical properties of early age concrete, Materials and structures 29 (6) (1996) 335.

[176] N. Challamel, C. Lanos, C. Casandjian, Creep failure in concrete as a bifurcation phenomenon, International Journal of Damage Mechanics 14 (1) (2005) 5–24.

[177] D. Liu, H. Li, Y. Liu, Numerical simulation of creep damage and life prediction of superalloy turbine blade, Mathematical Problems in Engineering 2015 (2015).

[178] T. T. C. Hsu, Mathematical analysis of shrinkage stresses in a model of hardened concrete, in: Journal Proceedings, Vol. 60, 1963, pp. 371–390.

[179] H. Zhang, Y. Gan, Y. Xu, S. Zhang, E. Schlangen, B. Šavija, Experimentally informed fracture modelling of interfacial transition zone at micro-scale, Cement and Concrete Composites 104 (2019) 103383.

[180] A. Vervuurt, Interface fracture in concrete, Ph.D. thesis, Delft University of Technology (1997).

[181] G. Lilliu, J. G. van Mier, 3d lattice type fracture model for concrete, Engineering Fracture Mechanics 70 (7-8) (2003) 927–941.

[182] G. Lilliu, 3d analysis of fracture processes in concrete, Ph.D. thesis, Delft University of Technology (2007).

[183] Timoshenko beam theory, https://https://en.wikipedia.org/wiki/Timoshenko_beam_theory, accessed: 2020-01-06.

[184] S. P. Timoshenko, On the correction for shear of the differential equation for transverse vibrations of prismatic bars, The London, Edinburgh, and Dublin Philosophical Magazine and Journal of Science 41 (245) (1921) 744–746.

[185] H. Zhang, B. Šavija, Y. Xu, E. Schlangen, Size effect on splitting strength of hardened cement paste: Experimental and numerical study, Cement and Concrete Composites 94 (2018) 264–276.

[186] N. L. Tran, C.-A. Graubner, Uncertainties of concrete parameters in shear capacity calculation of rc members without shear reinforcement, in: Beton-und Stahlbetonbau, 16th International Probabilistic Workshop, 2018.

[187] Y. Zhu, S. Xu, Fracture properties of cement paste and mortar: an experimental investigation, Proceedings of the International Association of Fracture Mechanics for Concrete and Concrete Structures, FRAMCOS-6, Catania, Italy (2007) 17–22.

[188] A. M. Neville, Properties of concrete, 5th Edition, Pearson Education Limited, 2011.

[189] K. Vishalakshi, V. Revathi, S. S. Reddy, Effect of type of coarse aggregate on the strength properties and fracture energy of normal and high strength concrete, Engineering Fracture Mechanics 194 (2018) 52–60.

[190] Q. how does the strength of the aggregate particles affect the strength of the concrete?, https://concrete.org/tools/frequentlyaskedquestions.aspx?faqid=718, accessed: 2018-08-30.

[191] The effect of aggregate properties on concrete, https://www.engr.psu.edu/ce/courses/ce584/concrete/library/materials/aggregate/aggregatesmain.htm, accessed: 2018-08-30.

[192] R. M. Christensen, Mechanics of composite materials, Courier Corporation, 2005.

[193] M. Abreu, J. Lemos, J. Carmeliet, E. Schlangen, Modelling compressive cracking in concrete by a modified lattice model, in: Proceedings of the 6th International Conference on Fracture Mechanics of Concrete and Concrete Structures, New trends in Fracture Mechanics of Concrete, Vol. 1, 2007, pp. 453–460.

[194] W. Liao, X. Sun, A. Kumar, H. Sun, H. Ma, Hydration of binary portland cement blends containing silica fume: A decoupling method to estimate degrees of hydration and pozzolanic reaction, Frontiers in Materials 6 (2019) 78.

[195] H. Dong, P. Gao, G. Ye, Characterization and comparison of capillary pore structures of digital cement pastes, Materials and Structures 50 (2) (2017) 154.

[196] W. D. Lindquist, D. Darwin, J. Browning, Cracking and chloride contents in reinforced concrete bridge decks, Tech. rep., University of Kansas Center for Research, Inc. (2005).

[197] W. Zhong, W. Yao, Influence of damage degree on self-healing of concrete, Construction and building materials 22 (6) (2008) 1137–1142.

[198] B. Haranki, Strength, modulus of elasticity, creep and shrinkage of concrete used in florida, Master's thesis, University of Florida Gainesville (2009).

[199] G. Bouquet, Effect of relaxation on eigenstresses and microcracking in concrete under imposed deformation, Ph.D. thesis, Delft University of Technology (2019).

[200] G. C. Fanourakis, Y. Ballim, The influence of aggregate stiffness on the creep of concrete, Concrete Beton 112 (2006) 5–12.

[201] Y. Ke, A. Beaucour, S. Ortola, H. Dumontet, R. Cabrillac, Influence of volume fraction and characteristics of lightweight aggregates on the mechanical properties of concrete, Construction and Building Materials 23 (8) (2009) 2821–2828.

[202] J. Chi, R. Huang, C. Yang, J. Chang, Effect of aggregate properties on the strength and stiffness of lightweight concrete, Cement and Concrete Composites 25 (2) (2003) 197–205.

[203] M. Lopez, L. F. Kahn, K. E. Kurtis, Characterization of elastic and time-dependent deformations in high performance lightweight concrete by image analysis, Cement and Concrete Research 39 (7) (2009) 610–619.

[204] N. U. Kockal, T. Ozturan, Durability of lightweight concretes with lightweight fly ash aggregates, Construction and Building Materials 25 (3) (2011) 1430–1438.

[205] N. U. Kockal, T. Ozturan, Effects of lightweight fly ash aggregate properties on the behavior of lightweight concretes, Journal of hazardous materials 179 (1-3) (2010) 954–965.

[206] O. Ünal, T. Uygunoğlu, A. Yildiz, Investigation of properties of low-strength lightweight concrete for thermal insulation, Building and Environment 42 (2) (2007) 584–590.

[207] T. Y. Lo, H. Cui, W. Tang, W. M. Leung, The effect of aggregate absorption on pore area at interfacial zone of lightweight concrete, Construction and Building Materials 22 (4) (2008) 623–628.

[208] T. Y. Lo, W. C. Tang, H. Z. Cui, The effects of aggregate properties on lightweight concrete, Building and Environment 42 (8) (2007) 3025–3029.

[209] G. E. Troxell, Long-time creep and shrinkage tests of plain and reinforced concrete, in: ASTM, Vol. 58, 1958, pp. 1101–1120.

[210] R. S. Jensen, F. E. Richart, Short:, time creep tests of concrete in compression, in: Proc. ASTM, Vol. 38, 1938, p. 410.

[211] K. Kordina, Experiments of the Influence of the Mineralogical Character of Aggregates on the Creep of Concrete, 1958.

[212] J. J. Shideler, Lightweight-aggregate concrete for structural use, in: Journal Proceedings, Vol. 54, 1957, pp. 299–328.

[213] C. H. Best, M. Polivka, Creep of lightweight concrete, Magazine of Concrete Research 11 (33) (1959) 129–134.

[214] Z. Guo, Principles of reinforced concrete, Butterworth-Heinemann, 2014.

[215] P. Morlier, Le fluage des roches, in: Annales de l'Institut Technique du Bâtiment et des Travaux Publics, Vol. 217, 1966, pp. 90–112.

[216] D. Griggs, Creep of rocks, The Journal of Geology 47 (3) (1939) 225–251.

[217] R. N. Swamy, G. H. Lambert, The microstructure of lytag aggregate, International Journal of Cement Composites and Lightweight Concrete 3 (4) (1981) 273–282.

[218] EN206-1, European Standard. Concrete–Part 1 Specification, performance, production and conformity, 2008.

[219] EN1097-6, European standard. Tests for Mechanical and Physical Properties of Aggregates: Part 6 Determination of Particle Density and Water Absorption, British Standards Institution, 2000.

[220] L. Domagała, The effect of lightweight aggregate water absorption on the reduction of water-cement ratio in fresh concrete, Procedia Engineering 108 (2015) 206–213.

[221] S. Ahmad, Y. Sallam, I. Al-Hashmi, Optimising dosage of lytag used as coarse aggregate in lightweight aggregate concretes, Journal of the South African Institution of Civil Engineering 55 (1) (2013) 80–84.

[222] Technical Manual - Section 2 Introduction to Lytag lightweight aggregate concrete - LWAC, Lytag lightweight solutions, Lytag Ltd, 2016.

[223] F. Benboudjema, F. Soleilhet, X. Jourdain, F. Gatuingt, Effect of drying on the mechanical performances of concrete, in: Computational Modelling of Concrete Structures: Proceedings of the Conference on Computational Modelling of Concrete and Concrete Structures (EURO-C 2018), February 26-March 1, 2018, Bad Hofgastein, Austria, CRC Press, 2018, p. 209.

[224] R. E. Davis, Flow of concrete under sustained compressive stress, in: Journal Proceedings, Vol. 24, 1928, pp. 303–326.

[225] R. E. Davis, H. E. Davis, Flow of concrete under the action of sustained loads, in: Journal Proceedings, Vol. 27, 1931, pp. 837–901.

[226] R. E. Davis, H. E. Davis, J. Hamilton, Plastic flow of concrete under sustained stress, in: Proc. ASTM, Vol. 34, 1934, pp. 354–386.

[227] K. Schiller, Strength of porous materials, Cement and Concrete Research 1 (4) (1971) 419–422.

[228] E. Ryshkewitch, Compression strength of porous sintered alumina and zirconia: 9th communication to ceramography, Journal of the American Ceramic Society 36 (2) (1953) 65–68.

[229] M. Balshin, Relation of mechanical properties of powder metals and their porosity and the ultimate properties of porous-metal ceramic materials, Dokl Askd SSSR 67 (5) (1949) 831–834.

ACKNOWLEDGEMENTS

The PhD journey has come to an end, which makes me both nostalgic and happy. I still remember the first day I came to the Netherlands. I was so excited, but, at the same time, also overwhelmed by the fear of not knowing whether I could overcome the forthcoming challenges and succeed in both work and life in this alien country. Until now, I still don't know whether I have made it or not. The only thing I am sure about is that I am quite happy to have chosen to pursue this journey, from which I have learned a lot. At the end of this thesis I would like to express my appreciation to those people who have helped and supported me during the past four years.

First of all, a special gratitude goes to China Scholarship Council for offering me a scholarship for my PhD at Microlab, Section of Materials and Environment, Faculty of Civil Engineering and Geosciences, Delft University of Technology.

I would like to express my sincere gratitude to my promotor and supervisor Prof. Klaas van Breugel who has always trusted that I could do this PhD project. His patience, support, and encouragement have soothed and reassured me from all the struggles that I came across during this doctoral research. He has taught me how to think/write critically and logically and how to become an patient and independent researcher. This thesis would not have been accomplished without his guidance.

Besides my supervisor, I also want to take a moment to thank the other members of my PhD committee, Dr. Ton van Beek, Prof. Erik Schlangen, Dr. Guang Ye, Prof. Farid Benboudjema, Prof. Eddie Koenders, Prof. Tony Jefferson and Prof. Bert Sluys, for taking time and effort to read my work, for their insightful comments and valuable questions which have improved this thesis and widen my research.

I would like to express my deep appreciation to Dr. Ton van Beek for supervising me at the first one and half years. Frequent meetings and talks with him have inspired and helped me a lot, which makes the start of my PhD much easier. Thanks for reading my first thesis draft and giving me many valuable comments which have helped me improve this thesis. Thanks also for inviting me to his company and the interesting tour through his laboratory.

Great thanks go to Prof. Erik Schlangen, Dr. Mladena Luković and Dr. Zhiwei Qian for helping me with my questions about lattice model as well as their interesting ideas for creep modelling. I would like to thank Prof. Farid Benboudjema and Prof. Ningxu Han for the valuable discussions and suggestions regarding my work during Rilem Week 2018. Special thanks go to Prof. Bert Sluys, Dr. Angelo Simone and Dr. Frans van der Meer for allowing me to participate in their group meetings where I have learned a lot about computational modelling. Thanks also go to Dr. Jorge Sánchez Dolado for the inspiring discussion about creep at nano-scale. I would like to thank Prof. Folker Wittmann for spending an entire day discussing creep and shrinkage with me and the nice excursion to ETH Zürich. I also would like to give my special gratitude to Dr. Guang Ye and Ms. Lei Zhang for their kindness, support and invitations.

The start of the modelling was difficult, but some people made it easier for me. I would like to express my great appreciation to Yaolu Liu who has always been patient to guide me through my modelling problems and help to broaden my knowledge on finite element method. I would like to thank Jiayi Chen for helping me with my questions about coding and debugging. Although we are working on completely different topics, he has always been so kind to answer my research questions and make suggestions. Thanks also for cooperating with me and providing me simulations of self-healing (Section 3.4.2) to strengthen my research story. Many thanks also go to Mingzhao Zhuo, Dr. Branko Šavija and Dr. Yuguang Yang for their kind help with my questions.

I would like to warmly acknowledge all my colleagues at Microlab. It was a great privilege to be a part of the group with so many nice people and great minds. I would like to thank our secretaries, Jacqueline van Unen-Bergenhenegouwen, Iris Batterham, Claire de Bruin, Nynke Verhulst, Claudia Baltussen, for their support and assistance during my stay at Microlab. I would like to give my special thanks to my officemates: Shi Xu (Qilin Wang), Hongzhi Zhang, Xuhui Liang, Zhi Wan, Xingliang Yao, Zainab Aldin and Kamel Arbi. It was my great pleasure to share these four years with all of you. I would like to express my gratitude to Prof. Rob Polder, Prof. Jiangxiong Wei, Prof. Yingzi Yang, Dr. Henk Jonkers, Dr. Oguzhan Copuroglu, Dr. Dessi Koleva, Dr. Marc Ottele, Dr. Fuhai Li, Dr. Yun Huang, Dr. Damian Palin, Dr. Amir Tabakovic, Dr. Bahman Ghiassi, Dr. Farhad Pargar, Dr. Amir Zomorodian, Stefan Chaves Figueiredo, Claudia Romero Rodríguez, Fernando Franca de Mendonca Filho, Martin Megalla, Yask Kulshreshtha, Jakub Pawłowicz, Luiz Lima, Clarissa Justino de Lima, Jeannette van den Bos, Albina Kostiuchenko, Agus Susanto, Emanuele Rossi, Bart Hendrix, Maiko van Leeuwen, Arjan Thijssen, Ton Blom and John van den Berg for their support. Many thanks go to Renée Mors, Dr. Marija Nedeljković and Patrick Holthuizen for their valuable suggestions on my career. I would like to give my great appreciation to my Chinese colleagues: Dr. Yong Zhang, Dr. Hua Dong, Dr. Tianshi Lu, Dr. Peng Gao, Hao Huang (Niha), Bei Wu, Jiayi Chen (Dr. Wenqin Shi), Xuliang Hou (Dr. Ying Yang), Dr. Xu Ma, Jiahua Liu, Dr. Leyang Lu, Zhipei Chen, Dr. Xiaowei Ouyang (Cui Wei), Dr. Yibing Zuo, Zhenming Li, Shizhe Zhang (Kelly Mao), Ze Chang, Yidong Gan, Yading Xu, Boyu Chen, Yun Chen, Zhiyuan Xu, Yu Chen, Shan He and Yu Zhang. All the lunches, dinners, parties and trips that we have spent together are memorable. My PhD journey would not be complete without any of them.

I would like to thank my supervisors, professors and instructors from my home universities, Prof. Baodong Liu from Beijing Jiaotong University, Prof. Peng Zhang, Dr. Liang Li and Ms. Xuesong Chu from Qingdao University of Technology, for their kind support. I also want to express my gratitude to Ms. Franca Post from Valorisation Centre for her support and help with my stay in the Netherlands. Many thanks also go to Tom Petersen and Linda Cornelissen from Witteveen+Bos for their kind support and encouragement, and patiently waiting for me to start my new job.

Completion of this PhD research would not be possible without the love and support of all my dearest friends. I would like to thank my sportsmates and food-adventure partners, Mingjuan Zhao, Juan Tang and Zi Wang, with whom I have had a lot of fun; my travel buddy, Liting Qiu, a tough lady always with smile on her face, from whom I have learned a lot about life; my "5-minute walking-mate", Selin, for her support and interesting conversations; my alumni from Beijing Jiaotong University, Tao Lu and Lizuo

Xin, for their kind attention and help; my fellow townsfolks, Zilong Wei (Yan Zhou) and Hong Zhang, for their concern and support; my dearest neighbours, Bianca, Stefan, Sotia, Faymaa, Hitham, Cristina, Maya, Afshin, for all the wonderful brunches and parties; also my friends in China, Yaowei Wu, Huanhuan Chen, Qingwei Zhang, Wenting Li, Lili Xing, Zhichao Zhang, Zhaojie Wang and Xiangfei Kong, for their support and always taking care of me when I was in China. Special thanks go to Paula van Osch for being my taalcoach and helping me with my Dutch, along with delicious tea/soup and interesting talks about Dutch politics, history and culture.

I owe lots of "thank you" to my aunts, uncles and cousins, Minglan Li, Zhongqian Dong, Hui Dong (Xinghao Wang), Yuanzhen Zhang, Dengping Lyu, Jian Lyu (Xueyan Zhang), Dengsheng Lyu (Menggai Dong), Mingying Li, Qingyu Wang, Shuxin Wang and Guangpeng Wang (Weina Li) for always caring about me, taking care of me and supporting me along the way.

I want to express my deepest and greatest thanks to my parents, Mingfen Li and Denggang Lyu, for their endless and unconditional love and support. Pale words cannot express my gratitude for everything they have done for me. Mom and dad, thanks! May you have a life full of health and happiness, love and joy! I love you! 爸爸妈妈，谢谢你们的爱和支持！祝你们永远健康、快乐、平安！我爱你们！

In the end, my greatest appreciation goes to all the health care workers and all the people who are trying their best to keep our life running during COVID-19 crisis. These heroes deserve our recognition, and our deepest gratitude and respect!

May the world have no more wars and diseases!

Wenjuan Lyu
Delft, March 2020

CURRICULUM VITÆ

Wenjuan LYU

19-02-1990 Born in Shandong Province, P.R.China.

EDUCATION

September 2008 - June 2012	BSc student Civil Engineering Qingdao University of Technology, P.R.China
September 2012 - June 2015	MSc student Bridge and Tunnel Engineering Beijing Jiaotong University, P.R.China
October 2015 - September 2020	PhD researcher Faculty of Civil Engineering and Geosciences Delft University of Technology, The Netherlands
Email	wenjuanlv1990@outlook.com